



National Library
of Canada

Acquisitions and
Bibliographic Services Branch

395 Wellington Street
Ottawa, Ontario
K1A 0N4

Bibliothèque nationale
du Canada

Direction des acquisitions et
des services bibliographiques

395, rue Wellington
Ottawa (Ontario)
K1A 0N4

Acquisitions and Bibliographic Services Branch

Direction des acquisitions et des services bibliographiques

NOTICE

The quality of this microform is heavily dependent upon the quality of the original thesis submitted for microfilming. Every effort has been made to ensure the highest quality of reproduction possible.

If pages are missing, contact the university which granted the degree.

Some pages may have indistinct print especially if the original pages were typed with a poor typewriter ribbon or if the university sent us an inferior photocopy.

Reproduction in full or in part of this microform is governed by the Canadian Copyright Act, R.S.C. 1970, c. C-30, and subsequent amendments.

AVIS

La qualité de cette microforme dépend grandement de la qualité de la thèse soumise au microfilmage. Nous avons tout fait pour assurer une qualité supérieure de reproduction.

S'il manque des pages, veuillez communiquer avec l'université qui a conféré le grade.

La qualité d'impression de certaines pages peut laisser à désirer, surtout si les pages originales ont été dactylographiées à l'aide d'un ruban usé ou si l'université nous a fait parvenir une photocopie de qualité inférieure.

La reproduction, même partielle, de cette microforme est soumise à la Loi canadienne sur le droit d'auteur, SRC 1970, c. C-30, et ses amendements subséquents.

University of Alberta

INTERFACE MODELING OF GEOSYNTHETICS REINFORCEMENT

BY

CHANG-TOK YI

A thesis submitted to the Faculty of Graduate Studies and Research in partial fulfillment of
the requirements for the degree of Doctor of Philosophy

in

GEOTECHNICAL ENGINEERING

DEPARTMENT OF CIVIL ENGINEERING

Edmonton, Alberta

Spring 1995



National Library
of Canada

Acquisitions and
Bibliographic Services Branch

395 Wellington Street
Ottawa, Ontario
K1A 0N4

Bibliothèque nationale
du Canada

Direction des acquisitions et
des services bibliographiques

395, rue Wellington
Ottawa (Ontario)
K1A 0N4

Exemplaire - Votre référence

Copie - Notre référence

THE AUTHOR HAS GRANTED AN IRREVOCABLE NON-EXCLUSIVE LICENCE ALLOWING THE NATIONAL LIBRARY OF CANADA TO REPRODUCE, LOAN, DISTRIBUTE OR SELL COPIES OF HIS/HER THESIS BY ANY MEANS AND IN ANY FORM OR FORMAT, MAKING THIS THESIS AVAILABLE TO INTERESTED PERSONS.

L'AUTEUR A ACCORDE UNE LICENCE IRREVOCABLE ET NON EXCLUSIVE PERMETTANT A LA BIBLIOTHEQUE NATIONALE DU CANADA DE REPRODUIRE, PRETER, DISTRIBUER OU VENDRE DES COPIES DE SA THESE DE QUELQUE MANIERE ET SOUS QUELQUE FORME QUE CE SOIT POUR METTRE DES EXEMPLAIRES DE CETTE THESE A LA DISPOSITION DE PERSONNE INTERESSEES.

THE AUTHOR RETAINS OWNERSHIP OF THE COPYRIGHT IN HIS/HER THESIS. NEITHER THE THESIS NOR SUBSTANTIAL EXTRACTS FROM IT MAY BE PRINTED OR OTHERWISE REPRODUCED WITHOUT HIS/HER PERMISSION.

L'AUTEUR CONSERVE LA PROPRIETE DU DROIT D'AUTEUR QUI PROTEGE SA THESE. NI LA THESE NI DES EXTRAITS SUBSTANTIELS DE CELLE CI NE DOIVENT ETRE IMPRIMES OU AUTREMENT REPRODUITS SANS SON AUTORISATION.

ISBN 0-612-01781-8

Canada

University of Alberta

Library Release Form

Name of Author: Chang-Tok Yi

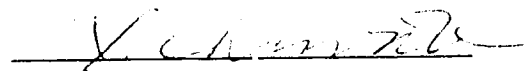
Title of Thesis: Interface Modeling of Geosynthetics Reinforcement

Degree: Doctor of Philosophy

Year this Degree Granted: Spring 1995

Permission is hereby granted to The University of Alberta Library to reproduce single copies of this thesis and to lend or sell such copies for private, scholarly or scientific research purposes only.

The author reserves all other publication and other rights in associate with the copyright in the thesis, and except as hereinbefore provided, neither the thesis nor any substantial portion thereof may be printed or otherwise reproduced in any material form whatever without the author's prior written permission.



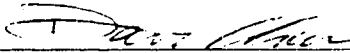
580 Dal Dong Me kpo, Chennam
Korea

Date April 13, 1995


University of Alberta

Faculty of Graduate Studies and Research

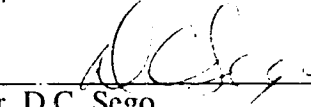
The undersigned certify that they have read, and recommend to the Faculty of Graduate Studies and Research for acceptance, a thesis entitled **Interface Modeling of Geosynthetics Reinforcement** submitted by **Chang-Tok Yi** in partial fulfillment of the requirements for the degree of Doctor of Philosophy in Geotechnical Engineering.



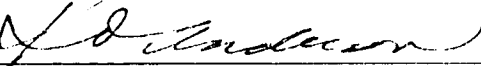
Dr. D. Chan (Supervisor)



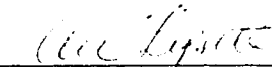
Dr. J.D. Scott (Co-Supervisor)



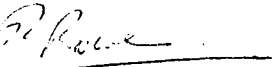
Dr. D.C. Segor



Dr. K.O. Anderson



Dr. A.W. Lipsett



Dr. R.K. Rowe

Date..... April 12, 1995

ABSTRACT

In the last two decades a wide variety of reinforcement has been used for geotechnical engineering applications. The economical and safe design of reinforced soil structures requires knowledge of both the mechanical behavior of the composite material and the behavior at the soil-reinforcement interface. The interaction behavior at the soil-reinforcement interface has been investigated extensively using various types of geosynthetics by conducting large scale laboratory pull-out and direct shear tests.

To understand the interface behavior between the soil and the reinforcement, the pull-out and the direct shear tests were analyzed using the finite element method. The elongation of the reinforcement during the pull-out test results in a non-uniform shear stress distribution along the reinforcement. This progressive shearing at the soil-reinforcement interface was considered in this analysis. The direct shear test, using ribbed reinforcement, was also analyzed to evaluate the passive resistance of the ribs. The failure mode of the interface between the cohesive soil and the reinforcement was predicted.

The conventional finite element method for modeling the soil-reinforcement interface uses a zero thickness joint element with normal and shear stiffness and can only accommodate a small amount of deformation. When large slippage occurs, the model provides an incorrect mechanism of deformation. A new interface finite element model is developed which is able to simulate large amounts of slippage between soil and reinforcement. The formulation of the model is presented and the capability of the model is demonstrated using illustrative examples.

The behavior of a Tensar reinforced test fill was analyzed using the finite element method. The results of the finite element method were compared with field measurements in terms of settlements, lateral deflections and soil strains. The strains along the reinforcement were also compared with the calculated strains to understand the soil-reinforcement interface behavior.

Acknowledgments

I wish to express my deepest appreciation to Dr. D. Chan for his continued guidance and generous encouragement during the preparation of this thesis.

Sincere appreciation is expressed to Dr. J.D. Scott for his invaluable guidance and support. Thanks are also extended to the members of the examining committee for their advice and patience.

The contributions made by B.A. Hofmann and Dr. Bill Liu who worked on the Devon test fill are appreciated.

I wish to thank SNC Inc. and Tensar Earth Technologies Inc. for donating an Award from the North American Geosynthetics Society in support of this research.

I wish to thank to my wife Chung-sun, whose patience and encouragement have been invaluable during my graduate studies.

Finally, my deepest gratitude to my parents for their love and encouragement for a further education. To my late mother, I dedicate this thesis.

Table of Contents

Chapter	page
1. Introduction	1
1.1 General	1
1.2 Objectives of Thesis	3
1.3 Scope and Organization	4
1.4 Reference	5
2. Literature review	6
2.1 Introduction	6
2.2 Factors Affecting the Interface Properties between Soil and Reinforcement	8
2.2.1 Confining Pressure	8
2.2.2 Stiffness of Reinforcement	12
2.2.3 Geometry of Reinforcement	15
2.2.4 Soil Type and Density	21
2.2.5 Effect of Fine Grained Portion of the Soil	23
2.2.6 Boundary Condition and Scale Effect	26
2.2.7 Pull-out and Direct Shear Test.	29
2.2.8 Confined and Unconfined Tensile Test Methods for Reinforcement	32
2.3 Summary	35
2.4 References	37
3. An Interpretation of the Pull-out Test	55
3.1 Introduction	55
3.2 Pull-out Test Mechanism	57
3.3 Shear Stiffness	59
3.4 Finite Element Modeling of the Pull-out Test	61
3.5 Connection of Interface Element	63
3.6 Results of Finite Element Analysis	64
3.7 Conclusion	66
3.8 References	66
4. Finite Element Analysis of the Direct Shear Test	80

4.1 Introduction	81
4.2 Experimental Configuration	82
4.2.1 Soil Properties	83
4.2.2 Finite Element Modeling	84
4.3 Numerical Results and Discussion	86
4.3.1 Shearing Resistance versus Relative Displacement	86
4.3.2 Shear Failure Surface	89
4.3.3 Grain Movement and Shear Zone	94
4.4 Prediction Cohesive Soil Behavior	96
4.5 Conclusion	97
4.6 References	98
5. A Large Slipping Finite Element Model for Geosynthetics Interface Modeling	126
5.1 Introduction	126
5.2 Model Formulation	130
5.2.1 Imposition of Constraints	130
5.2.2 Horizontal Constraints	132
5.3 Solution Strategy	134
5.4 Application	135
5.5 Conclusion	137
5.6 References	138
6. Finite Element Analysis of the Devon Test Fill	150
6.1 Introduction	150
6.2 Material Properties for the Finite Element Analysis	152
6.2.1 Foundation Soil	152
6.2.2 Test Fill Soil	154
6.2.3 Geogrid	155
6.3 Unreinforced Slope Analysis	157
6.4 Reinforced Slope Analysis	161
6.4.1 Strain Distribution along the SR-2 Reinforcement	163
6.4.1.1 SR-2 Reinforcement Bottom Layer	164

6.4.1.2 SR-2 Reinforcement Middle Layer	165
6.4.1.3 SR-2 Reinforcement Top Layer	166
6.4.2 Vertical Settlement of Fill and Foundation Soils	166
6.4.2.1 Ground Level in Tensar Section	167
6.4.2.2 2m Level in Tensar Section	170
6.4.2.3 4m Level in Tensar Section	171
6.4.3 Horizontal Deflection of Soils beneath Toe of Reinforced Section	171
6.4.4 Settlement beneath Crest of the Slope in Reinforced Section	172
6.4.5 Horizontal Soil Strain in Reinforced Section	173
6.5 Conclusion	174
6.6 References	174
7. Summary and Conclusions	214
7.1 General	214
7.2 Summary of Results	214
7.3 Conclusions	216
7.4 Recommendations for Further Research	218
Appendix A. Material Properties of the Devon Test Fill	219
Appendix B. Finite Element Analysis of the Devon Test Fill	230

List of Figures

Figure	Page
2.1 Behavior of a Reinforced Slope	44
2.2 Dilatancy Effect on Normal Stress along Reinforcement (after Schlosser, 1980)	45
2.3 Mobilization of Pull-out Resistance (after Bauer and Shang, 1993)	46
2.4 Pull-out Instrumented Testing Device (after Juran, 1989)	47
2.5 Passive Soil Resistance of Grid Reinforcement During Pull-out Test (after Jewell, 1984)	48
2.6 Effect of Interference between Grid Transverse Members (modified from Kitamoto, 1992)	49
2.7 Effect of Spacing between Bearing Members on Pull-out Resistance (after Palmerira and Milligan, 1989)	50
2.8 Influence of Particle Size on Soil-Reinforcement Interaction (modified from Sarsby, 1985)	51
2.9 Comparison of Field Laboratory Pull-out Resistance for Clayed Sand Backfill (after Bergado, 1992)	52
2.10 Comparison between Measured Pattern of Displacement in Sand (after Jewell, 1980)	53
2.11 Comparison of Direct Shear and Pull-out Tests (after Fouries et al., 1990)	54
3.1 Finite Element Idealization of Soil and Reinforcement for Pull-out Test	70
3.2 Load-strain Response of Tensar SR-2 Used in the Simulation (strain rate, 2% /min.)	71
3.3 Methods of Connecting Interface Element to the Soil Element	72
3.4 Comparison of the Connection Methods (Displacement of 0.5 cm)	73
3.5 Calculated and Observed Force-displacement Response of Reinforcement	74
3.6 Mobilized Shear Stress along the Reinforcement	75

Figure	Page
3.7 Relationship between the Apparent and Shear Stiffness	76
3.8 Calculated and Observed Force-displacement Response of the Reinforcement in the Pull-out Test	77
3.9 Mobilized Shear Stresses along the Reinforcement	78
3.10 Comparison of Horizontal Displacement along the Reinforcement	79
4.1 Direct Shear Device for Ribbed Reinforcement Testing (after Irsyam, 1991)	101
4.2 Hyperbolic Model Analyses Compared with Experimental Results	102
4.3 Finite Element Idealization of Shear Box	103
4.4 Observed Shearing Resistance versus Relative Displacement, 3.3 cm Rib Spacing (after Irsyam, 1991)	104
4.5 Observed Shearing Resistance versus Relative Displacement Compared with Calculated Response (Rib Spacing, 3.3 cm)	105
4.6 Shear Strain Distribution for Plate without Ribs	106
4.7 Mohr Circle for State of Stress at Nodal Point 294 for Ribbed Plate	107
4.8 Mohr Circle for State of Stress at Nodal Point 294 for Plate without Ribs	108
4.9 Effect of Rib Spacing on Failure Surfaces	109
4.10 Calculated Shear Failure Surface Compared with Observed Failure Surface, 3.3 cm Rib Spacing	110
11 Calculated Shear Failure Surface for 1.5 cm Rib Spacing, 0.3 cm displacement	111
4.12 Shear Strain Distributions for 1.5 cm rib Spacing, 0.3 cm Displacement	112
4.13 Shear Strain Distributions for 3.3 cm rib Spacing, 0.3 cm Displacement	113
4.14 Shear Stress Distributions for 1.5 cm rib Spacing, 0.3 cm Displacement	114
4.15 Shear Stress Distributions for 3.3 cm rib Spacing, 0.3 cm Displacement	115
4.16 Effect of Rib Spacing on Shearing Resistance	116

Figure	Page
4.17 Comparison of Failure Modes	117
4.18 Observed Soil Grains Movement for 3.3 cm Rib Spacing	118
4.19 Calculated Nodal Displacement Arrows for 3.3 cm Rib Spacing (displacement 0.3 cm)	119
4.20 Calculated Nodal Displacement Arrows for 1.5 cm Rib Spacing (displacement 0.3 cm)	120
4.21 Calculated Nodal Displacement Arrows for No Ribs (displacement 0.3 cm)	121
4.22 Calculated Nodal Displacement Arrows for 3.3 cm Rib Spacing, Cohesive Soil.	122
4.23 Shear Strain Distributions for 3.3 cm Rib Spacing, 0.3 cm Displacement, Cohesive Soil	123
4.24 Shear Stress Distributions for 3.3 cm Rib Spacing, 0.3 cm Displacement, Cohesive Soil	124
4.25 Calculated Shear Failure Surface for Cohesive Soil	125
5.1 Constitutive Law for Shear-displacement Behavior	141
5.2 Flow Chart for Application Horizontal Resistance on Reinforcement	142
5.3 Reinforced Soil Structure	143
5.4 Tensile Force Distribution along the Reinforcement	144
5.5 Displacement Distribution along the Reinforcement	145
5.6 Finite Element Idealization of Soil and Reinforcement for the Pull-out Test	146
5.7 Force-Displacement Response of the Reinforcement in the Pull-out Test.	147
5.8 Tensile Force Distribution along the Reinforcement.	148
5.9 Shear Stress Distribution along the Reinforcement	149
6.1 Consolidated Undrained Triaxial Tests on Foundation Soil (after Hofmann, 1989)	177
6.2 Predicted Stress-Strain Curves Compared with the Observed Stress-Strain Curves.	178
6.3 Predicted Volume Change Curves Compared with the Observed Volume Change Curves.	179

Figure	Page
6.4 Effect of Modulus Number(K) on Stress-Strain Curves (Confining Pressure=40kPa, n=0.23, Rf=0.84)	180
6.5 Isochronous Load-strain Curves for SR-2	181
6.6 Tensile Test of Tensar SR-2 Compared with Predicted Response	182
6.7 Two Dimensional Plane Strain Idealization of Unreinforced Section.	183
6.8 Embankment Construction Sequences.	184
6.9 Settlement at Ground Level in Unreinforced Section at 6m Fill	185
6.10 Settlement at Ground Level in Unreinforced Section at 12m Fill.	186
6.11 Settlement at 2 m Level in Unreinforced Section at 6 m Fill.	187
6.12 Settlement at 4 m Level in Unreinforced Section at 6m Fill.	188
6.13 Horizontal Deflection of Soil beneath Toe of Slope in Unreinforced Section at 3m Fill.	189
6.14 Horizontal Deflection of Soil beneath Toe of Slope in Unreinforced Section at 6m Fill.	190
6.15 Two Dimensional Plane Strain Idealization of Reinforced Section.	191
6.16 Observed Strain Distribution in Tensar Bottom Layer (modified from Liu, 1992)	192
6.17 Calculated Strain Distribution in Tensar Bottom Layer.	193
6.18 Strain Distribution along Tensar Reinforcement of Bottom Layer at 6m Fill.	194
6.19 Measured Strain Distribution in Tensar Middle Layer (modified from Liu, 1992).	195
6.20 Strain Distribution in Tensar Middle Layer at 6m Fill.	196
6.21 Strain Distribution in Tensar Middle Layer at 12m Fill	197
6.22 Measured Strain Distribution in Tensar Top Layer (modified from Liu, 1992)	198
6.23 Strain Distribution in Tensar Top Layer at 6m Fill.	199
6.24 Strain Distribution in Tensar Top Layer at 12m Fill	200
6.25 Settlement at Ground Level in Tensar Section at 3 m Fill.	201

Figure	Page
6.26 Settlement at Ground Level in Tensar Section at 6 m Fill.	202
6.27 Settlement at Ground Level in Tensar Section at 12 m Fill.	203
6.28 Settlement at Ground Level in Unreinforced Section Compared with Signode Section (modified from Liu, 1992).	204
6.29 Settlement at Ground Level in Unreinforced Section Compared with Tensar Section (modified from Liu, 1992)	205
6.30 Settlement at 2 m Level in Tensar Section at 3 m Fill.	206
6.31 Settlement at 2 m Level in Tensar Section at 6 m Fill.	207
6.32 Settlement at 4 m Level in Tensar Section at 6 m Fill	208
6.33 Horizontal Deflection of Soils beneath Toe of Slope in Tensar Section at 12m Fill	209
6.34 Settlement beneath Crest of Slope in Tensar Section at 6m Fill.	210
6.35 Distribution of Horizontal Soil Strain at Ground Level in Tensar Section at 6m Fill.	211
6.36 Comparison of Calculated Horizontal Soil Strain at Ground Level between Unreinforced and Reinforced Section.	212
6.37 Distribution of Horizontal Soil Strain at 4m Level in Tensar Section at 12m Fill.	213
A1 Plane View of Devon Test Fill	220
A2 Soil Profile of the Fill Foundation (modified from Hofmann, 1989).	221
A3 Cross Section and Reinforcement Layout of Reinforced Slope.	222
A4 Layout of Soil Instrumentation in Test Fill.	223
A5 UU Triaxial Tests on Fill Soil (modified from Hofmann, 1989).	224
A6 CU Triaxial Tests on Fill Soil (modified from Hofmann, 1989)	225
A7 Effective Stress p-q Plot for Fill Soil (modified from Hofmann, 1989)	226
A8 Total Stress p-q Plot for Foundation Soil (modified from Hofmann, 1989)	227
A9 Pull-out Tests for Tensar SR-2 Geogrid (after Costalonga, 1988)	228
B1 Settlement at Ground Level in Unreinforced Section at 3m Fill.	230

Figure		Page
B2	Horizontal Deflection of Soil beneath Crest of Slope in Unreinforced Section at 3m Fill.	231
B3	Horizontal Deflection of Soil beneath Crest of Slope in Unreinforced Section at 6m Fill.	232
B4	Settlement beneath Crest of Slope in Unreinforced Section at 3m Fill.	233
B5	Settlement beneath Crest of Slope in Unreinforced Section at 6m Fill	234
B6	Settlement beneath Crest of Slope in Unreinforced Section at 12m Fill.	235
B7	Horizontal Deflection of Soils beneath Toe of Slope in Tensar Section at 3m Fill	236
B8	Calculated Horizontal Deflection of Soils beneath Toe of Slope in Tensar Section	237
B9	Settlement beneath Crest of Slope in Unreinforced Section at 3m Fill.	238
B10	Settlement beneath Crest of Slope in Unreinforced Section at 12m Fill.	239
B11	Distribution of Horizontal Soil Strain at Ground Level in Unreinforced Section at 3m Fill.	240
B12	Distribution of Horizontal Soil Strain at Ground Level in Unreinforced Section at 12m Fill.	241
B13	Distribution of Horizontal Soil Strain at Ground Level in Tensar Section at 3m Fill.	242
B14	Comparison of Calculated Horizontal Soil Strain at Ground Level between Tensar and Unreinforced Section.	243

List of Tables

Table		Pages
3.1	Summary of Material Properties Used in the Finite Element Analysis	69
4.1	Soil and Steel Reinforcement Parameters Used in Analysis.	100
5.1	Vertical Displacement at Step 3 (1m horizontal displacement).	140
6.1	Material Parameters Used in Devon Test Fill Analysis.	176

List of Symbols

A	One side surface area of reinforcement
α	Interfacial efficiency factor
B	Thickness of transverse members of grid reinforcement
C	cohesion between soil and reinforcement
CU	Consolidated undrained triaxial test
C_u	Coefficient of uniformity
C_v	Coefficient of consolidation
D	Diameter of transverse member of reinforcement
Δd	Change in relative displacement between soil and reinforcement
D_i	Initial load modulus
Δp	Change in axial force along reinforcement
$\Delta \tau$	Change in shear stress
D_{50}	Particle size of soil corresponding to 50 % finer
E	Young's Modulus
ϵ_a	Axial strain
ϵ_f	Axial strain at failure
F	Tensile force of reinforcement
f	Real friction coefficient
f^*	Apparent friction coefficient
ϕ'	Friction angle between soil and reinforcement
ϕ	Internal friction angle of soil
[K]	Stiffness matrix
K_c	Rectangular matrix containing constraint conditions
K_f	Lateral stress ratio at failure
K_n	Normal stiffness
K_o	Coefficient of lateral earth pressure at rest
k_{ri}	Initial stiffness of interface
K_s	Shear stiffness
k_{sa}	Apparent stiffness of interface
K_{sf}	Stiffness from friction resistance
K_{sp}	Stiffness from passive soil resistance
k_{st}	True stiffness of interface
λ	Lagrange multiplier
Nq	Bearing capacity factor
Π	Functional
{R}	Vector of forces
r	True stiffness ratio
Rf	Failure Ratio
S	Spacing of transverse members of grid reinforcement
SDR	Ratio grid spacing to average grain size
σ_o	Normal stress at rest
σ_n	Normal stress on reinforcement
τ_f	Shear stress on reinforcement
τ_r	Residual shear stress
τ_{max}	Maximum shear stress
τ_p	Peak shear stress

$\{U\}$ Vector of global displacement

CHAPTER 1. INTRODUCTION

1.1 General

The basic concept of reinforced earth has been demonstrated abundantly in nature by animals and the action of tree roots. Primitive people used sticks and branches for the reinforcement of mud dwellings. The first record of reinforced soil structures is found in the Bible, describing the reinforcement of clay or bricks with reeds or straw for the construction of houses. Construction using these techniques is believed to have existed in the 5th and 4th millenniums B.C., with some of these earth reinforcement structures still standing today.

Modern earth reinforcement techniques were pioneered in 1966 by Henri Vidal, a French architect and inventor who found that roughly formed mounds of dry sand could be made to stand at a steeper angle after the addition of horizontal layers of needles. The basic conclusion reached by Vidal was that when dry granular soil is combined with a rough material having a tensile strength, the resulting composite material is stronger than the soil alone. The introduction of Vidal's idea led to the rapid development of soil reinforcement and improved forms of this type of reinforcement.

Initially, metallic strips, granular fill, and concrete panels were commonly used in reinforced soil structures. Polymer reinforcements have been introduced in an effort to avoid the problem of metal corrosion on long term durability. Koerner (1986) called these polymer materials 'geosynthetics', because the materials were used in soil and were synthetics. He classified them into four groups depending on the geometry and the function of the geosynthetics: geotextiles, geogrids, geomembranes, and geocomposites. Polymer materials can be produced in two basic forms for reinforcing elements as either geotextiles or geogrids.

The use of new polymer materials as reinforcement also led to a diverse range of applications for reinforced soil structures in geotechnical engineering: reinforced retaining walls, slopes, and embankments on soft foundations. Reinforced retaining walls generally consist of three elements: reinforcement, backfill materials, and facing panels. The reinforcement is attached to a rigid facing panel and, thus, the maximum tensile stress of the reinforcement will occur very near the facing panel. For a reinforced slope, the facing of the slope is usually treated by vegetation or wrapping the compacted backfill by the reinforcement, therefore, the tensile forces mobilized along the reinforcement are a maximum at a certain distance from the facing of the slopes within the embankment. Other than the geometrical differences, these two types of reinforced structures can be distinguished by the distribution of tensile stresses in the reinforcement. For a reinforced embankment on a soft foundation, the reinforcement will be placed at the base of the embankment to prevent failure in the foundation and to constrain the horizontal movement of the embankment .

The advantages of reinforced soil structures include the fact that they provide a technically attractive solution on poor foundation soils because they are extremely tolerant of large lateral and vertical deformations. Reinforced soil structures provide ease of forming, handling and quick construction using a diverse range of backfill materials. Usually granular and cohesionless soils have been used as backfill materials. However, clayey and silty soils have only been used successfully in a few applications. Reinforced soil structures are suited for construction in seismically active regions because of their gravity mass, flexibility, and high degree of structural damping. Consequently, reinforced soil structures have emerged over the last two decades as a technically attractive and cost-effective construction.

Theoretical developments associated with reinforced soil have grown considerably in the past two decades. However, a complete understanding of every aspect has not yet been developed, especially the interaction mechanism between soil and reinforcement. The

design methodology still uses limit equilibrium methods and semi-empirical methods based on measurements of prototype and model reinforced soil structures. During the last two decades the finite element method of has rapidly become a popular technique for the analysis of complex problems in geotechnical engineering. Application of this method to reinforced soil structures has some limitations because the interaction between soil and reinforcement is one of the most complex mechanisms in soil-structure interaction problems. Presently this method of analysis is being used mainly to verify existing semi-empirical design methods.

Case histories of reinforced soil structures indicate that current design methods are conservative. Liu (1992) suggested that the uncertainty of stress-deformation characteristics of reinforced soil and of load distributions within the reinforced soil and the reinforcement were the main reasons for conservatism. These uncertainties could be overcome by using finite element methods including a proper simulation of the interaction between soil and reinforcement. Proper account of strain compatibility between soil and reinforcement, and stress-deformation characteristics of the reinforced soil can only be made by using finite element methods. Mobilization of tensile strength in the reinforcement and load distribution within the soil are also provided by these methods. Undoubtedly, the finite element methods with proper geometry and material simulation are superior to the limit equilibrium methods.

1.2 Objective of Thesis

The main objective of this research is to apply the finite element method in modeling the interaction of soil and reinforcement and to explore new techniques in simulating the mechanism of load transfer between the soil and the reinforcement. To examine the interaction between the soil and the reinforcement, a review was made of the failure mechanism and the failure shape during the shearing process in the pull-out test and

direct shear test. These tests were analyzed using finite element methods which included a conventional interface element and a new interface element.

The second objective of this study is to investigate the behavior of reinforced slopes with cohesive backfill. To achieve this objective a comparison was made between the predicted behavior using the finite element method incorporating the interface element, and the observed behavior in a well instrument full scale test fill built near Devon, Alberta. The reinforced test fill, 12m high with 1:1 side slopes was designed with a low factor of safety in order to mobilize a large strain and tensile resistance in the soil and the reinforcement, respectively.

1.3 Scope and Organization

Reinforced soil technology has developed rapidly over the last two decades which has led to an increase in the volume of literature dealing with reinforced soil. Chapter 2 presents a literature review which deals extensively with factors affecting the interaction mechanisms between the soil and the reinforcement. There is an emphasis on the pull-out test which has been recognized as a good simulation of the interface behavior between the soil and the reinforcement. The differences between pull-out and direct shear tests are compared to obtain the interface parameters to understand the interaction mechanisms.

The thesis is organized in paper format. Each chapter is a self contained study and, therefore, there may be some repetition among chapters. Although each chapter is distinct, they are all related to the modeling of the soil-reinforcement interface.

Chapter 3 contains the analysis of pull-out tests on a geogrid in cohesive soil. The interface behavior between the soil and the reinforcement were simulated using a zero thickness interface element, which can consider the progressive shearing at the interface. In this chapter the method which considers the progressive shearing characteristics of the interface elements is discussed.

Ribbed steel reinforcement was used in the direct shear test to evaluate the passive resistance of the rib reinforcement. The analysis of the results of the direct shear test is compared with the observed values in Chapter 4. The shear zone which developed from the large shear strain around the reinforcement during the shearing process is discussed. The failure modes of the interface between the soil and the reinforcement are given.

A new interface element is proposed in Chapter 5. The background theory and illustrative examples of the new interface element are presented. A pull-out test analysis using the new interface element is also presented.

Chapter 6 presents the summary of the Devon test fill and the analyses of the test fill using the finite element method. A detailed comparative study between the calculated values and observed values is carried out to assess the reliability of the finite element analysis for use in the design of reinforced slopes and to determine the deformation pattern.

Based on the analyses, recommendations and practical conclusions are made in Chapter 7.

1.4 References

- Koerner, R.M. (1990), **Designing with Geosynthetics**, 2nd Ed., Prentice Hall, New York, 652p.
- Liu, Y. (1992), **Performance of Geogrid Reinforced Clay Slopes**, Ph.D. thesis, Department of Civil Engineering, University of Alberta, Edmonton, Alberta, 406p.

CHAPTER 2. LITERATURE REVIEW

2.1 Introduction

In the last two decades a wide variety of reinforcement has been used for geotechnical engineering applications. In selecting a specific reinforcement for an embankment or a wall, the interface behavior between the soil and the reinforcement needs to be assessed for design purposes. Current design methods for reinforced soil structures are based on limit equilibrium analysis which postulates different failure mechanisms and requires input parameters to characterize the bond resistance at the soil-reinforcement interface. The bond resistance includes two factors: direct shearing along the soil and reinforcement interface and anchorage shearing within the stable soil mass.

The internal failure of a reinforced soil structure can be caused either by a progressive breaking of the reinforcement or by slippage of the reinforcement within the soil. These factors could be evaluated through laboratory testings using direct shear or pull-out tests. Resistance to sliding is a function of the interaction mechanisms between the soil and the reinforcement. Design consideration of frictional mechanisms requires the knowledge of the soil and reinforcement interfacial shear strength. The magnitude of the interfacial strength is primarily a function of the physical properties of the soil, the normal stress acting on the reinforcement, and the geometry of the reinforcement.

In the mechanism of soil-reinforcement interaction for a reinforced soil slope, there is an active zone where the shear stresses are directed outwards. These stresses are restrained by the reinforcement that transfers the load to a resistance zone. In the passive zone, shear stresses are mobilized to prevent the sliding of the reinforcement. Maximum tensile forces in the reinforcement occur between the active and the passive zones. The mechanism simulated at the interface in a direct shear test is likely to occur at the boundary of the active zone and passive zone as shown in Figure 2.1. The reinforcement must be

capable of resisting pull-out from the passive zone. The transfer of load in the soil mass to the reinforcement in the passive zone can be described by the pull-out test.

Milligan et al. (1990) stated that the pull-out resistance of smooth reinforcements can be measured directly by interface tests using a suitably modified shear box. However, the passive soil resistance can only be simulated by the pull-out test. In the direct shear test the soil moves relative to the reinforcement and this movement is constant along the reinforcement. In the pull-out test, the reinforcement is in tension and therefore the relative movement between the reinforcement and the soil is not constant along the interface and depends on the distance from the point of the tensile load in the reinforcement. The contribution of passive resistance is greatly affected by the geometry and the stiffness of the reinforcement; about 20 to 60% of pull-out forces could be transferred by the passive soil resistance (Wilson-Fahmy and Koerner, 1993).

The interaction between the soil and the reinforcement have been considered a critical subject to study by researchers. A number of studies have been carried out to understand the interaction characteristics of reinforced soils using different reinforcement such as woven and nonwoven geotextiles, geogrids, metallic bars and mesh (Jewell, 1980; Costalonga, 1988). The results are usually represented in terms of an apparent interface friction angle compared with the friction angle of the unreinforced soil.

The development of computer systems and constitutive laws for soil have led to the application of finite element methods to analyze soil structures. In designing reinforced soil structures using limit equilibrium methods the reinforcing members are incorporated into the analysis either as a resisting force, or by an overall improvement of the shear strength of the soil. However, when deformation of a reinforced soil structure is of concern, limit equilibrium methods can not provide satisfactory predictions. To overcome the drawbacks of the current limit equilibrium design methods, the finite element method with a proper soil-reinforcement interaction model may be used.

In order to adequately model the stress-strain behavior of a reinforced soil

structure, the soil-reinforcement interaction must be included in the analysis. The complex phenomenon of stress transfer between soil and the reinforcement is dependent on the soil-reinforcement characteristics. When using the finite element method it is necessary that the behavior of the interaction between the soil and the reinforcement be understood for proper modeling.

A comprehensive literature review on the interaction between the soil and the reinforcement will be provided to understand the mechanisms of reinforcement and to develop a proper interface simulation. In operational circumstances reinforcing can only occur if the reinforcement can transfer the tensile forces, which develop within itself, to a stable soil mass. This indicates that the pull-out test is a more realistic model for soil-reinforcement interaction than the direct shear test. The pull-out test has been commonly accepted as an effective method to evaluate the pull-out resistance of an embedded reinforcement (Holtz, 1977; Ingersoll 1983; Garbulewski, 1990; Venkatappa and Kate, 1990). This literature review is focused on evaluating various factors affecting the interface properties between soil and reinforcement, and pull-out resistance.

2.2 Factors Affecting the Interface Properties between Soil and Reinforcement

2.2.1 Confining Pressure

The shear strength at the soil-reinforcement interface as measured in the direct shear test or the pull-out test is a function of the normal stress at the interface. The relationship between the interface shear strength and normal stress is often considered to be linear up to a limiting value. However, Giroud et al. (1993) stated that the relationship between the interface shear strength and normal stress is not linear. He proposed an equation to represent the interfacial shear strength using a hyperbola function based on experimental data. Where the portion of the slip surface along the reinforcement is

subjected to a high normal stress, the proposed equation would give a reasonable assessment.

The granular soil in the vicinity of the reinforcement tends to dilate during the shearing process. Juran et al. (1988) suggested that the restrained dilatancy by the surrounding volume of soil results in a normal stress concentration at the soil-reinforcement interfaces, thereby increasing the pull-out resistance of the reinforcement as shown Figure 2.2. The dilatancy of the soil is highly dependent on confining stress, type of soil and geometry of the reinforcement. The overburden pressure can significantly affect the mobilized frictional resistance in dense soils by restraining soil expansion. Schlosser and Elias (1978) showed that soil dilatancy has a significant influence on the apparent friction coefficient (f^*) defined as:

$$f^* = \tau_{\max.} / \sigma_0$$

where $\tau_{\max.}$ is the shear stress along the reinforcement and σ_0 is the normal stress at rest. The soil dilatancy occurring around the reinforcement causes an increase in the overburden pressure as shown in Figure 2.2. Thus values of f^* is much higher than the coefficient of real friction, f .

Bergado et al.(1992) carried out both laboratory and field pull-out tests using steel grid reinforcements in cohesive-frictional backfill soils. It was observed that the overburden pressure, bar sizes, and number of transverse bars definitely affected the total pull-out resistance. The pull-out force was increased almost linearly with the increase in the overburden pressures. In another case of lateritic back fill soil in field tests, there was a decrease in the maximum pull-out resistance with the increase in the overburden pressures; this was explained by arching effects in the middle section of the reinforced soil structure and by the particle-crushing phenomenon of the lateritic soils under a high normal stress. The arching effects must have drastically reduced the overburden

pressures. However, the dilatancy around the reinforcement during the shearing process resulted in an increase in the overburden pressures. Thus, the boundary conditions of the test apparatus would cause an error in predicting the pull-out resistance. The effect of the boundary conditions will be discussed in detail in section 2.7.

Athanasopoulos (1993) using sand with different particle sizes and a woven geotextile conducted direct shear tests to study the effect of the confining stress and the particle size on the mechanical behavior at the interface. It was concluded that the magnitude of the confining stress determined the mode of failure of the reinforced soil. Two different modes may be manifested by a bilinear failure envelope: a slippage of the reinforcement and a progressive breaking of the reinforcement. In breakage of the reinforcement, the reinforcement deforms uniformly within the soil. The position of the break point on the bilinear envelope is usually dependent on the aperture size of the woven geotextile. If short reinforcements were used or when the frictional resistance developed along the reinforcement was smaller than the strength of the reinforcement, the slippage failure mode will occur. The frictional resistance is a function of the confining pressure on the reinforcement.

Farrag (1993) examined the effect of confining pressure on the frictional resistance of a reinforcement for geogrid SR-2 during the pull-out test. The geogrid reinforcement, during the pull-out test is restrained by the passive soil resistance and particle interlocking within the transversal reinforcement elements. An increase in the confining pressure results in a significant increase of the pull-out resistance of the geogrid. The soil-geogrid interface shear stress is more uniformly mobilized along the geogrid under low confining pressures. The increase in the confining pressure restrains the geogrid displacement and results in a higher mobilization of shear stress near the pull-out box slot.

Palmeira and Milligan (1989) carried out pull-out tests using stiff and extensible geotextiles, geogrids, and steel grids under different normal stresses. The steel grids gave a very stiff response under both low and high stresses, while the stiff geotextile reached

its limiting bond stress at a displacement of about 15 mm. The weak and extensible geotextile could only be tested at low confining stresses without failing in tension, and the polymer grid exhibited a stiff response at low confining stress level.

Jewell (1980) carried out pull-out tests using a single stiff, rough reinforcement bar in dense sand under different applied normal stress. As expected, the peak pull-out force increased with the applied stress level. Surprisingly, the pull-out displacement required to mobilize the peak pull-out force remained approximately constant and was independent of stress level.

Fainnin and Raju (1991) carried out pull-out tests using geosynthetics in a relatively dense sandy soil. It was concluded that pull-out failure alone, rather than some combination of pull-out and tensile failure, was controlled by the mean shear stress acting on the specimen and required selection of an embedded length taken into account the normal stress applied during testing. Usually the embedded length of the reinforcement needed to prevent slippage failure of the reinforcement is determined by checking the pull-out resistance of the reinforcement.

Holtz (1977) carried out pull-out tests at a constant strain rate and relatively low normal stresses. It was observed that the relationship between the developed frictional stress and the applied normal stress is slightly curved. A straight line envelope through the points was approximately the same as the angle of internal friction when measured in the triaxial test at the same relative density.

Therefore, it could be concluded that the total pull-out resistance increased linearly with the confining stress in stiff reinforcements such as metallic sheets or grids where failure modes were governed by the pull-out of the reinforcement. The relationship between the total pull-out resistance and normal stress has a bilinear form for extensible reinforcements such as geotextile fabrics which show the progressive failure of the reinforcement and the breakage of the reinforcement. In addition, the embedded length of the reinforcement and the soil type would affect the relationship between the pull-out

resistance and the normal stress.

2.2.2 Stiffness of Reinforcement

Reinforcements presently used can be classified into two different types, namely 'extensible' and 'inextensible' reinforcements (McGown et al., 1978; Bonaparate and Berg, 1987). The steel reinforcement meets the criterion for inextensible reinforcement, whereas geogrid and geotextiles belong to the first category.

The extensibility of the reinforcement influences the load transfer mechanisms, thereby affecting the pull-out response of the soil-reinforcement system. With inextensible reinforcements, the shear stress and shear displacement along the reinforcement are practically constant. As a result, limit equilibrium methods considering a uniformly mobilized shear stress have been developed for the design of the earth structures reinforced with metallic reinforcements.

Extensible reinforcements develop a non-uniform shear stress and relative displacement distribution along the reinforcement. A large portion of the shear stress is mobilized at the front of the reinforcement. The distribution of shear stress along the geosynthetics in the direction of the pull-out force is not uniform since the tensile strain decreases away from the point of application of the pull-out forces (Chan et al., 1993). This progressive shearing at the soil-reinforcement interface during the pull-out testing was observed by Costalonga (1988) and Fannin and Raju (1991). Fannin and Raju used strain gauges mounted at a constant spacing along the embedded geogrid reinforcement. All curves of strains in the geogrid specimen showed the greatest measured strain at a location nearest to the pull-out slot and smallest strain at a location nearest the embedded end of the reinforcement for all geogrid specimen.

A similar pull-out study was done by Costalonga (1988) using LVDTs on three types of geosynthetics: SR-2, TNX5001, and Paragrid reinforcement. It was observed

that the TNX5001 geogrid mobilizes higher tensile force than SR-2 for the same displacement because the TNX5001 has a higher tensile module than the SR-2 geogrid. The difference in the distribution of tensile force is larger for small pull-out displacement because the difference in initial tensile modulus is also larger.

The progressive shearing can be explained in four steps of stress transfer mechanism of the pull-out test as shown in Figure 2.3 (Bauer and Shang, 1993).

Stage 1. No pull-out force is applied to the grid. The only stress acting on the grid is the vertical or normal stress from the soil overburden and surcharge loading. No shear stress or grid displacement have occurred.

Stage 2. The applied pull-out force causes tensile straining in the geogrid. The tensile force is resisted by shear stresses mobilized at the soil and geogrid interface. During this stage shear stresses are mobilized along the free end part of the geogrid. The free end of the geogrid is displaced but the embedded end has not yet moved.

Stage 3. As the free end of the geogrid is further displaced the pull-out resistance increases. Eventually the embedded end of the geogrid is also displaced but at a smaller rate than the front end.

Stage 4. As the geogrid is further pulled through the soil, a maximum pull-out resistance is reached and the two ends of the geogrid are displaced at the same rate.

Jones (1988) presented the stress-strain behavior of the reinforced soil in the triaxial test. If the reinforcement is extensible, the maximum force in the reinforcement will not be generated before the soil has passed the point of maximum shear strength. In these cases the maximum force in the reinforcement is controlled by the displacement of the soil. As strains develop beyond the peak strength of the soil alone, although the soil may be losing strength, the reinforcement would be gaining strength. Thus, the reinforced soil may exhibit a peak load-carrying capacity relating to the peak shear strength of the soil, or it may exhibit an enhanced strength at strains beyond the point of peak shear strength of the soil alone.

Bergado et al. (1992) carried out the pull-out test using a welded steel geogrid reinforcement embedded in weathered clay. The maximum strain in the longitudinal members of the reinforcement amounted to about 0.01 to 0.2%. This indicated that the front and rear displacements of the metallic reinforcement are approximately equal, and therefore the reinforcement moves as a rigid body within the soil.

Typical variations of the displacement along a woven polyester strip were measured in the pull-out instrumented test device by Juran and Christopher (1989) as shown in Figure 2.4. Experimental results indicated that the elongation of the reinforcement during the pull-out test can significantly affect its pull-out response and the non-uniform shear stress distribution.

Kharchafi and Dysli (1993) carried out pull-out tests on three different types of nonwoven geotextiles of varying rigidities to study the effects of geotextile stiffness. It was concluded that two reinforcements with different rigidities gave the same friction angle with the soil. However, the more rigid geotextile distributed the friction over a larger surface area which gave improved soil-geotextile adherence.

Pull-out tests on geogrid (Juran et al., 1991; Hanna and Touahmia, 1991; Bauer et al., 1991; Farrag et al., 1993) and geotextile (Leshchinsky and Field, 1987; Milligan et al., 1990) have demonstrated that the reinforcement between the soil and extensible reinforcement results in a non-uniform shear stress distribution along the reinforcement. It is affected by the stiffness of the reinforcement and more importantly the tensile strength of the reinforcement (Fourie and Fabian, 1987).

In conclusion, reinforcement extensibility significantly affects the load transfer mechanism. Reinforcement extensibility results in a decreasing shear displacement distribution along the reinforcement length. The interface shear stress is not uniformly mobilized along the total reinforcement length. The pull-out resistance becomes a function of the specimen length. Therefore, the concept of a uniformly mobilized shear stress is not appropriate for interpretation of the pull-out test results on extensible reinforcements.

An appropriate load transfer model for extensible reinforcement is needed to determine the relevant interaction design parameters.

2.2.3 Geometry of Reinforcement

The shearing resistance of reinforcements are basically mobilized by three interaction mechanisms: frictional resistance, passive resistance on the transverse elements, and particle interlocking in the geofabric. Reinforcement pull-out resistance is mobilized through one or a combination of two basic soil-reinforcement interaction mechanisms: frictional and passive resistance. These mechanisms depend primarily upon the geometry of the reinforcement, grid or fiber spacing of the reinforcement, and the grain size of the soil. When the grain size of the soil is significantly smaller than the fiber or grid spacing, the grains cannot effectively interlock within the geosynthetic apertures and frictional resistance is reduced (Jewell et al., 1984). Passive soil resistance in the pull-out tests develops at the transverse elements of the reinforcement.

The transverse members of a grid reinforcement can be assumed to be a series of strip footings in succession which have been rotated through 90 degrees to the horizontal and pulled through the soil as shown in Figure 2.5. This assumes that the transverse member is much larger than the particle size of the soil. Two types of failure mechanisms were proposed: general bearing failure and punching shear failure in front of the transverse members of the grid reinforcement. Therefore, the passive soil resistance on the transverse members is a function of the soil cohesion, friction angle and bearing capacity factors (N_q) based on the Terzaghi bearing capacity equation (Jewell et al., 1984). Bergado et al. (1993) observed that the pull-out failure mechanism of the grid reinforcement is a function of the geometry of the transverse bars, the compaction moisture content of the soil, and the stiffness of the soil as compared with that of the transverse member.

In reinforced soil systems the maximum frictional resistance would be mobilized at small deformations (Holtz, 1977). For grid reinforcement, the frictional resistance is relatively small and needs a small relative displacement to be fully mobilized. This explains why a small deformation of the reinforced soil mass can mobilize large tensile forces in the reinforcement. The displacement required to mobilize the passive soil resistance is much greater (Schlosser and Elias, 1978; Alimi et al., 1977). When both mechanisms are active, it is not clear that the frictional resistance is always completely mobilized before the mobilization of the passive soil resistance.

A load transfer method in soil reinforcement developed by Beech (1987) was based on the concept of pile foundation. Pile foundation may be considered as a widely used inclusion in which the development of the maximum load capacity consists of two mechanisms: skin friction and end bearing. From the fundamental function of piles, the displacement needed to mobilize the skin frictional resistance is small compared to that for the end bearing resistance. Thus, the ultimate skin frictional resistance is reached much sooner than the end bearing resistance. The portion of the load carried by the end bearing resistance is smaller in the working conditions than at failure (Vesic, 1977).

The load transfer mechanism of piles is as complicated as that of reinforced soil structures. Both the pile point and all points on the pile shaft must move sufficiently with respect to adjacent soil to simultaneously develop the ultimate end bearing and the skin friction resistance as in stage 4 in Figure 2.3. The displacement of the pile head can be considerably greater than that of the pile tip. The skin frictional resistance in the upper part of the pile can be mobilized much earlier than that at the lower part of the pile. This load transfer stage could correspond with stage 2 in Figure 2.3. Therefore, the relative contribution of each mechanism in a pile will strongly depend on its strain level.

Bergado et al.(1992) stated that the frictional component of the pull-out resistance can be mobilized with a small displacement, but the displacement necessary to completely mobilize the passive soil resistance is of the order of 10 times larger than that required to

generate the frictional resistance. The determination of the relative contribution of each mechanism is quite difficult and a general solution is not available, at least on the basis of the present knowledge (Mitchell and Villet, 1987). Chang et al.(1977) observed that for a mesh reinforcement in sandy gravel, the passive resistance contributed about 90% of the total pull-out resistance. Irsyam and Hryciw (1991) performed the direct shear test using two types of reinforcement with ribs and without ribs to investigate the relative portion of the passive soil resistance. It was found that the passive resistance was only about 10 to 20% of the total pull-out resistance. But Bergado et al.(1993) observed that the frictional resistance of the longitudinal members in welded steel geogrid was found to contribute only about 5 to 15% of the total pull-out resistance.

Wilson-Fahmy and Koerner (1993) illustrated the relative portion of each mechanism in a geogrid using finite element modeling of the soil-geogrid interaction. The three components of the pull-out resistance of a stiff geogrid were expressed as a percentage of the ultimate pull-out load. The relative contributions in friction of both longitudinal and transverse ribs decrease with the increase in the pull-out force. However, the relative contribution of passive soil resistance on the ribs is increased. This indicated that the displacement required to mobilize the bearing resistance is greater than those required to mobilize frictional resistance. For an extensible geogrid, the transverse ribs offer practically no resistance in frictional resistance or in passive resistance up to about 25% of the total pull-out force.

Farrag et al.(1993) carried out a pull-out test on Conwed geogrids with and without transverse ribs. It was noted that the frictional resistance along the longitudinal ribs constitutes an average of 75% of the total pull-out resistance for this specific geogrid. The passive soil resistance on the transverse ribs is mobilized at higher levels of strain resulting in a higher post-peak pull-out resistance. The strain level required to mobilize the passive soil resistance on the transverse elements will vary with the types of geogrid and the soil. The relative proportions of the total pull-out resistance that are contributed by

each mechanism depend on the reinforcing material including its surface characteristics and geometry, especially the strain levels of the reinforcement.

Rib size and spacing of the reinforcement play an important role in developing the passive soil resistance along the reinforcement. Irsyam and Hryciw (1992) carried out shear box tests using rigid ribbed steel reinforcement with various rib spacings in Ottawa sand. It was found that the shearing resistance was entirely due to the frictional resistance for a small rib spacing of 5 mm, and partial development of the passive resistance was observed for a rib spacing of 15 mm. Therefore a large rib spacing is desirable for full development of the passive resistance. A similar study was carried out in the pull-out test by Srinivasa Murthy et al.(1993). When the spacing of transverse elements is too close, the passive zones overlap resulting in a reduced passive resistance. However, for a large spacing of transverse elements, complete mobilization of the failure plane results in the full mobilization of the passive resistance.

Kitamoto and Abe (1991) demonstrated that the pull-out resistance of geogrids was greatly affected by the thickness (B) and the spacing (S) of the transverse ribs of the reinforcement. It was observed that when S/B was smaller than 20 to 30, the measured soil passive resistance by the pull-out test was approaching zero as shown in Figure 2.6. More detailed results were investigated by Palmeria and Milligan (1989). It was observed that the difference between the normalized friction coefficient at peak and the large pull-out resistance displacement was dependent on the S/B ratio. For low S/B values, a more severe drop in shear stress occurred after peak, whereas for the rear part of the grid junction no peak was observed owing to its large S/B values ($S/B=31$). Based on the Kitamoto and Abe's results it was suggested that for large values of S/B the bearing resistance is a small portion of the pull-out resistance.

Similar results could be found in Bergado et al.(1992). The pull-out passive soil resistance ratio refers to the pull-out resistance on the transversal element of the grid divided by the pull-out resistance of an isolated single transversal element in the same

condition. It was observed that pull-out resistance was increased with an increase of the S/B ratio. However, interference between the passive resistance zones of the transverse member became negligible for S/B values beyond about 50. Milligan and Palmeria (1987) also suggested that for most grids in use at present, which have S/B much less than 50, the predicted interface behavior will be markedly affected by the geometry of the reinforcement.

Palmeria and Milligan (1989) performed pull-out tests to investigate the pull-out behavior of two or more ribs as the spacings, S, between them were varied. The results are presented in Figure 2.7. It was observed that as the spacing between ribs decreases, a corresponding loss in pull-out resistance occurs because of the increase in interference between ribs. It can therefore be concluded that an increase in mesh opening of the reinforcement will substantially reduce the pull-out resistance of the bar mesh reinforcement. The main factors controlling the interface between the ribs of a grid are likely to be the soil properties, the thickness and the spacing of ribs, and the number of ribs of the reinforcement.

Sridharan et al.(1991) carried out pull-out tests using several types of the steel reinforcements to investigate the influence of shape, size, and surface characteristics of the reinforcement on the pull-out resistance. Pronounced peak is seen for tor-steel reinforcement, while no peak is observed for mild-steel round bars and flats which have almost the same pull-out resistance. However, the pull-out resistance of tor-steel bars is significantly higher than those for mild steel reinforcement. This indicated that the surface roughness of the reinforcement significantly affects the total pull-out resistance.

Jones (1985) stated that the surface properties of the grid reinforcement have little or no effect on the pull-out resistance if soil particles penetrate through the grid between the transverse members of the grid. The frictional adherence between the longitudinal members of a grid and the soil is influenced by the surface properties and the coefficient of friction between the longitudinal members and the soil.

The effect of reinforcement layout in the pull-out tests was investigated by Arenicz (1992) who carried out large shear box tests using two types of strips; smooth and ribbed strips. If the same quantity and type reinforcement was placed, (1) along the direction of shear, (2) across the direction of shear, or (3) uniformly spread along and across the direction of shear, the third configuration was found to be consistently most efficient regardless of type and width of the strips used. Conversely, the strips placed along the direction of shear were found to be least effective. The recorded difference between the first and third configurations, in terms of relative soil strength enhancement, was between 30 and 50%, depending on the strip width.

Geometry of reinforcement has a significant influence on soil dilatancy as illustrated by Schlosser and Elias (1978). It was shown that the dilatancy effect can be associated with a passive soil resistance, as in the case of wire-mesh grids. It is possible to obtain a higher pull-out resistance through mobilizing higher frictional resistance by having a bar with asperities rather than a smooth bar. However, a large displacement is needed to reach the peak pull-out resistance.

Geometry of reinforcement has a strong influence on the pull-out resistance due to the passive soil resistance as well as dilation of the soil during pull-out test. Fourie and Fabian (1987) performed pull-out tests on woven and nonwoven geotextiles in a clay soil. It was observed that the pull-out resistance of the woven geotextile was not limited by its tensile strength, and the woven geotextiles did not show any greater pull-out resistance than the nonwoven geotextile.

In summary the best geometry of reinforcement was found to be the grid or bar mat which provides a large pull-out resistance due to the passive resistance on the transversal element of the reinforcement. However, compared with the pure frictional interaction reinforcement such as nonwoven geotextile and strips, the grid reinforcements require a large displacement to fully mobilize the pull-out resistance.

2.2.4 Soil Type and Density

Typically, granular materials such as clean sand and gravel have been used as backfill materials in reinforced soil structures. Normally cohesive backfill materials have been excluded for use in reinforced soil structures regardless of whether the reinforcement is metallic or polymer fabric. The maximum adhesion strength between the reinforcement and clay is normally not expected to be more than the undrained strength of the clay. Additionally, the fine-grained portion of the backfill material and the excess moisture content above the optimum moisture content cause creeping of the reinforced soil structure. Nevertheless, cohesive backfill materials have been used successfully in a few applications. As performance experience is gained use of these soil types may become more frequent.

The frictional resistance is a function of soil density, the frictional characteristics of the soil, surface roughness of the reinforcement, stiffness of the reinforcement, the amount of fines in the backfill, angularity of grains, confining pressure, and soil type. Dense soils, under moderate confining pressures, tend to dilate when shear stresses are mobilized along the reinforcement interface. The soil surrounding the soil-reinforcement interface develops a condition of restrained dilatancy as the reinforcement is pulled out. The magnitude of this restraint depends on the soil density and the confining stress. Several researches (Elias, 1979 ; Schlosser and Elias, 1978; Guillois and Schlosser, 1979) have demonstrated that the dilatancy behavior of dense sands can significantly influence the results of the pull-out test.

An apparent friction coefficient, f^* which is defined as the ratio of the applied pull-out force to the overburden pressure, can be obtained from the pull-out test results. Alimi et al. (1977) investigated the influence of the soil density on the apparent friction coefficient in pull-out tests. It was observed that the value of f^* was increased very substantially with the increase in sand density. It was also noted that much larger

displacements were needed to reach the peak value of f^* in dense sand. A similar study can be found in Schlosser and Elias (1978). The peak pull-out resistance was obtained at small displacements in loose sand.

Sridharan et al.(1991) carried out pull-out tests, using steel bars in a good quality of cohesionless sand and kaolin clay, to investigate the effect of soil type on the pull-out resistance. It was observed that residual pull-out resistance in kaolin clay was very much less than the peak value which was developed at very small displacements. However, the cohesion could be overcome under small displacements, and the residual pull-out resistance was almost constant. The residual pull-out resistance of the sand was almost equal to its peak value.

Farrag et al.(1993) stated that increased densities lead to mobilization of the interlocking mechanism and result in a higher concentration of the passive resistance extruded on the traverse ribs. At higher densities pull-out resistance increased and displacements moved closer to the point of application of the pull-out load.

When cohesive soil is used as backfill material in reinforced soil structures the drainage condition may affect the interaction mechanism. Fourie and Fabian (1987) carried out a number of pull-out and direct shear tests on geotextiles and geogrids in a silty clay to investigate the clay-reinforcement interaction in both drained and undrained conditions. The main factors affecting the undrained clay-geotextile interaction were identified to be the stiffness, the surface roughness, and the transmissivity of the geotextile. The pull-out resistance was strongly related to the interaction mechanism which was also affected by the stiffness and the tensile strength of the geotextile. In drained conditions the clay-geotextile interaction was similar to sand-geotextile interaction. However, the pull-out resistance was found to be dependent on the relaxation of the geotextile during long-term testing. This reduced the tensile strength of the geotextile, producing a lower ultimate pull-out resistance than in the undrained tests. The drained pull-out resistance developed in a way similar to the undrained resistance, reaching a

maximum value which was proportional to but substantially lower than the tensile strength of the geotextile.

The shear stress distribution along the geogrids during pull-out tests is not uniform as discussed in section 2.3. In addition, the distribution of shear stress varies with the type of soil. Bauer and Shang (1993) carried out large pull-out test using Tensar UX 160 in different soils. It was also observed that tensile forces are not uniform along the geogrid. The tensile forces were the highest at the leading end of the embedded geogrid with a rapid decrease towards the rear part of the geogrid. This can be attributed to the relatively low stiffness of the geogrid which reduces the efficiency of load transfer in the soil. High interlock in the geogrid spacing of aggregate soil provided high non-linear tensile stress distribution. Fine soil particles of silty clay provided little interlock with the geogrid apertures and there were less tensile forces at free end of the geogrid.

Soil compaction, carried out by means of an electric jack hammer, standard proctor hammer, hand tamping devices, mechanical tamping, and hopper with flexible tube to insure uniform soil density, may also affect the interaction mechanism. It mobilizes the lateral earth pressure resistance on the reinforcement and increases the frictional resistance at the interface. The restraint on the geogrid movement and the slippage by soil compaction increases the peak pull-out resistance.

In summary dense soils tend to dilate during shearing and cause the normal stress to increase stress at the interface of the reinforcement. Thus the pull-out resistance increases as the normal stress on the reinforcement increases.

2.2.5 Effect of Fine Grained Portion of the Soil

The effect of the fine-grain portion of the soil on the pull-out resistance depends mainly on the ratio between the grid opening size of the geogrid or the yarn spacing of the geotextile and the average particle size of the soil. Jewell et al.(1984) studied the

relationship between the efficiency factor and the ratio of the yarn or grid spacing to the average grain size (SDR). SDR is defined as relative size of geogrid opening or of yarn spacing for woven geotextiles, compared to the particle size of soil. When the particles are significantly smaller than the yarn or grid spacing, the grains cannot effectively interlock within the geosynthetics apertures and the sliding resistance is low. As the grain size of the soil increases, the particles can more efficiently interlock in the fabric, thereby increasing the frictional resistance. When the grain size approaches the opening size (SDR=1), the soil particles become embedded in the apertures. Therefore, the failure zone is forced away from the interface into the soil mass, mobilizing the shearing resistance of the soil. In this case the efficiency factor is approximately equal to 1 and the pull-out resistance attains its maximum value.

Occasionally, a reinforcement can be placed in a soil where the grains are significantly larger than the fabric openings (SDR \ll 1). For this case, the particles are too large to penetrate the geofabric apertures. Since the grains can not efficiently interlock within the reinforcement, a low pull-out resistance is mobilized which is generated primarily by skin friction at the soil -reinforcement interface.

A similar study was done by Sarsby (1985) as shown in Figure 2.8. The data lies on a curve with the peak value of α occurring at a S/D_{50} value of about 3.5, where D_{50} is the particle size of the backfill soil corresponding to 50% finer and S is the spacing between the transverse members. Efficiency factor, α , can be defined as $\tan\phi' / \tan\phi$ where ϕ' is the friction angle between the soil and the reinforcement; and ϕ is the angle of internal friction of the soil. Below this optimum value the coefficient of interaction falls rapidly as S/D_{50} decreases, i.e. the grid apertures become narrower or the grains become larger. This is obviously due to the loss of interlocking between the grains and grid and also between the soil grains on either side of the grid.

Pull-out tests using different grid openings in granular backfill material were carried out to investigate the shearing resistance of the soil particles which have

interlocked through the apertures of the geogrid (Bauer and Shang, 1993). It was found that the maximum pull-out resistance was achieved when the soil particle diameter was in the order of 0.25 to 0.35 of the aperture dimension.

Athanasopoulos et al.(1993) carried out direct shear tests on sand of different particle sizes with woven geotextiles embedded normal to the shear plane. It was observed that the dilatancy behavior of the composite material was affected by the aperture ratio. For fine sands (high values of aperture ratio) the reinforcement increased the volume expansion of the composite material whereas the opposite behavior was verified for coarser sands(low values of aperture ratio). For aperture ratios close to unity no effect of the reinforcement was found on the dilatancy behavior of the reinforced sand. The test results also indicated that the dilatancy of the composite material does not depend on the confining stress.

Mowafy (1986) carried out pull-out tests on steel meshes, plastic geogrids and glass grid to study the pull-out resistance mechanisms of mesh immersed in sand. The mechanism of interaction between the soil and the reinforcement were separated into two mechanisms: interlocking between the mesh and the soil, and the interface friction between the mesh and the soil. In order to evaluate the different pull-out resistance components pull-out tests were also executed on Tensar geogrids. Approximately 70% of the total maximum pull-out resistance was due to interlocking and confinement while the other 30% was due to friction only. In the case of mesh reinforcement 93% of the total pull-out resistance was due to the interlocking and only 7% was due to the frictional resistance. The interlocking resistance component depended on the mesh opening and soil particle size. It was recommended that the soil particle size be equal to one quarter to one third of the smallest mesh dimension of the reinforcement.

Many important factors affect both the overall behavior of the reinforced soil structure and interaction at the soil-geosynthetics interface such as the aperture ratio, S/D_{50} , and the ratio of the yarn or grid spacing to the average grain size of the soil.

2.2.6 Boundary Conditions and Scale Effects

The pull-out test has been commonly accepted as an effective method to evaluate the pull-out resistance or bond resistance of an embedded reinforcement because there are some limitations to model the real situation. These include different boundary conditions and scale effects, testing procedures and apparatus need to be standardized. As the reinforcement is pulled through the soil lateral pressure will develop against the rigid front wall. This leads to arching of the soil over the reinforcement which reduces the local vertical stress on the reinforcement. This reduction in vertical stress results in a decrease of the pull-out resistance of the reinforcement. The size of the box governs the boundary conditions which have an influence on the test results. Test results from a small test apparatus are probably too limited to provide information for the interpretation of the load transfer mechanisms. Coarse granular soils can be compacted to field specifications in a large apparatus which can minimize the influence from boundary conditions. To totally eliminate boundary conditions and to obtain proper design parameters it is recommended that field tests be conducted.

Bergado et al.(1992) conducted field pull-out tests to investigate the pull-out resistance of reinforcements embedded at representative overburden, field moisture, and density conditions. In the laboratory, pull-out tests were also carried out using a 1300 mm x 800 mm x 500 mm pull-out box using steel grid reinforcements with different opening sizes to compare with the field tests. Three types of backfill materials were used: weathered clay, lateritic soil, and clayey sand. In the laboratory the backfill materials were compacted to 95% standard Proctor density and well monitored to simulate the field conditions. A reinforcement grid having 0.15 m x 0.23 m openings with 5 transverse bars was used in the laboratory and field pull-out tests. The length of the longitudinal bars in the laboratory tests was about 1.0 m, while in the field tests it was about 2.0 m. Some

of the transverse bars were cut off with only the ribbed longitudinal bars remained. In order to compare the field and laboratory peak pull-out resistance, two assumptions were made : 1) the frictional and passive resistance were linearly proportional to the surface area and, 2) there was a constant value for the apparent frictional coefficient between soil and reinforcement. Figure 2.9 shows the comparison between field and laboratory pull-out test results in terms of maximum pull-out resistance plotted against normal stress. For weathered clay and clayey sand, it was observed that the field tests in all cases provided a higher pull-out resistance than in the laboratory tests. The arching effect of the embankment must have increased the vertical stresses on the two end sections of the embankment. This phenomenon resulted in increased pull-out resistance at the end sections of the embankment where the pull-out tests were carried out. At the 50 kPa of normal stress, the field test had nearly the same pull-out resistance as the corresponding laboratory tests. However, at the 66 kPa of normal stress, the field test provided much lower pull-out resistance than that of the laboratory tests. This indicated that the arching effect was dominant at the lower portion of the wall.

Palmeira and Milligan (1989) carried out pull-out tests using two different sizes of box, 253 x 150 x 200 mm and 1000 x 1000 x 1000 mm to extensively investigate the scale effect and boundary conditions affecting the results of the pull-out tests. The vertical load was applied by the two methods: a rubber bag filled with water and a rigid rough plate. The conclusions on the boundary conditions can be summarized as follows:

(1) A slight decrease in peak resistance value in the pull-out force-displacement curve was obtained with the use of a flexible boundary although the initial slope of the pull-out forces-displacement curve was identical in both tests.

(2) The dilatancy of the soil adjacent to the reinforcement during the shearing process will tend to increase the vertical stress on the reinforcement. As the lateral stresses against the front wall of the box will be very much higher than against the other three sides, the magnitude of the down drag will be controlled by the frictional

characteristics of the front wall.

(3) Pull-out test results using the various roughness of the front wall showed that the friction coefficient between the soil and the reinforcement can be severely overestimated due to friction on the internal side of the front wall in small scale tests. By increasing the size of front wall, the influence is minimized. This effect can be minimized by lubricating the front face and by increasing the size of the specimens.

If the thickness of the soil above and below the reinforcement is small, the interaction between the soil and the reinforcement and boundaries will significantly influence the shearing resistance along the interface. Brand and Duffy (1987) studied the relationship between the clay shear strength and the stress transfer zone thickness around the SR-2 geogrid in a pull-out test. They carried out pull-out tests varying the thickness of clay on one side of the geogrid. As the thickness of clay increased the pull-out force necessary to pull the geogrid through the clay decreased until a minimum force was reached. The rigid boundaries above and below the reinforcement can lead to increases in the normal stresses in the vicinity of the geogrid surface, especially when the soil thickness is small and soil dilatancy is restrained.

Johnston and Romstad (1989) executed twenty-four large scale pull-out tests (1300 x 910 x 510 mm) on a high density polyethylene grid embedded in a granular soil. The results indicated that the maximum pull-out load was influenced by dilation of the soil in the vicinity of the grid and by the boundary conditions of the pull-out apparatus.

Large scale pull-out tests on sand reinforced with Tensar SR-2 were carried out by the Department of Civil Engineering at the University of California (1984). The inside dimensions of the pull-out box were 137 cm long, 91 cm wide and 51 cm deep. One test was carried out without the front end of the pull-out box. The maximum pull-out force was increased by 40% . This increase of pull-out resistance was thought to be due to lack of soil confinement which caused the transmission of the total normal pressure to the full length of the reinforcement.

2.2.7 Pull-out and Direct Shear Tests

Whatever reinforcement and backfill materials are used for the design of reinforced soil structures, the reinforcement and the backfill soil interaction properties play an important role. The interaction mechanism between the soil and the reinforcement can be simulated by two types of test: the pull-out test and the direct shear test. These two fundamentally different testing methods are associated with different boundary conditions and loading paths, which lead to significantly different design parameters. The relationship between local shear stress and shear displacement can be obtained from the direct shear test. The pull-out test provides the relationship between pull-out force and displacement at the pull-out slot. Pull-out tests would normally yield results different from those obtained through direct shear tests. Figure 2.10 illustrates the displacement patterns of each type of test.

Generally the direct shear resistance between the grid reinforcement and the soil has three components: (1) the shearing resistance between the soil and the reinforcement plane surface area; (2) the soil to soil shearing resistance at the grid opening; and (3) the resistance from soil bearing on the reinforcement apertures (Jewell et al., 1984). Pull-out resistance has two components: the passive soil resistance and the frictional resistance as described in section 2.4. There is no soil to soil shearing resistance as there is no relative movement of the soil on either sides of the reinforcement.

There are several differences between a direct shear and a pull-out test. In a direct shear test after normal loads are applied to the soil, a shear force is mobilized until sliding occurs between the reinforcement and the soil with no further increase in the required shear force for continuing deformation. In a pull-out test, although the normal load is exerted to the soil, the pull-out force is applied directly to the reinforcement. In a direct shear test shearing occurs at a pre-defined shear plane and the whole composite fails by

shear. In a pull-out test shearing occurs at the two interfaces between the reinforcement and the soil. In a direct shear test the soil volume changes due to dilatancy which plays an important role in the mobilization of tensile force in the geogrid since the whole soil and reinforcement composite is involved. However, in a pull-out test the dilatancy of the soil occurs only in the vicinity of the reinforcement and is restrained by the surrounding soil. In the direct shear test the boundary conditions limit dilatancy of the interface soil layer and thereby reduce the effect of the restrained sample expansion on the interface shear resistance. In a pull-out test as the confining stress increases, the amount of soil dilation decreases and the apparent interface bonding angle approaches a limiting value, which is smaller than those obtained from the direct shear test.

Ingold (1983) carried out pull-out and direct shear tests in both sand and clay. The reinforcements used in these tests were polymer net, polymer fabrics, mild steel sheet, and steel rod mesh. The results from both direct shear and pull-out tests were compared. The apparent coefficient of friction measured in the direct shear test for sand reinforced with polymer nets, steel sheet and steel rod mesh ranged from 0.6 to 1.0, with a mean value of 0.95. The same value was found to be about 0.86 when measured in a pull-out test.

Jewell (1980) stated that the most important difference between a direct shear and a pull-out test resides in the stress level experienced by the soil. In a direct shear test the reinforcement improves the strength of the sand by modifying the strains which develop as the sand deforms plastically under an applied load. The sequence is as follows: (1) an increment of shear stress causes the soil to undergo strain hardening; (2) the strains cause displacements in the sand adjacent to the reinforcement due to compatibility conditions between the reinforcement and the soil; (3) this displacement induces straining in the reinforcement due to friction and bearing of the reinforcement elements; and (4) the mobilized tensile strain and tensile force in the reinforcement changes the strains and stresses in the soil. In a pull-out test the soil is "at rest" and experiences a relatively low stress level. As the pull-out force is applied to displace the reinforcement, the soil

immediately adjacent to the reinforcement experiences a high stress ratio. Once this stress ratio exceeds a critical value significant straining will occur in the soil immediately adjacent to the reinforcement which is constrained by the surrounding soil. It was concluded that the pull-out test would normally yield different results from those obtained from the direct shear test. This was due to differences in the state of stress and displacement in the two tests.

Collios et al.(1980) compared pull-out test results with direct shear test results for geotextiles. If the soil particles were smaller than the fabric openings of the geotextiles, the efficiencies (α), defined earlier, were higher; if not, they could be lower. In all cases, however, the pull-out resistance was less than the direct shear resistance. The deformation of the geotextiles was large during the shearing process which caused the soil particles to reorient themselves. This reduced the shearing resistance at the soil-reinforcement interface in the pull-out test. However, it was very interesting to note that the shearing resistance of the direct shear test was not always greater than that of the pull-out tests.

Juran et al. (1988) compiled the results of the pull-out and the direct shear tests using the same reinforcement and backfill materials. It was demonstrated that the difference in the maximum soil-reinforcement interface resistance determined from the direct shear and the pull-out test can be expressed by comparing the bond coefficient which was defined as the ratio of soil friction to soil-reinforcement friction. Although the reinforcement has different geometry, the direct shear test generally yielded a higher bond coefficient than that of pull-out test, except for the case of a grid placed in coarse dense sands under low confining pressures. The higher bond coefficient may be attributed to the relatively low degree of soil dilation generated in the direct shear test. In loose fine grained soils, the direct shear test and the pull-out test generally produced approximately equal values of interface shear strength.

Bonaparte et al. (1987) suggested that the direct shear test was suitable to

determine the required reinforcement embedment length and interfacial characteristics between the soil and the reinforcement. They also suggested that for the same vertical effective stress and length of the reinforcement the ultimate pull-out resistance may be equal to approximately twice the equivalent direct shear strength.

Fourie et al.(1990) carried out direct shear and pull-out tests using a low plasticity clay reinforced with various types of geosynthetics. Figure 2.11 shows that the ultimate pull-out resistance is not twice as large as the equivalent direct shear value for all the reinforcement tested. The pull-out resistance of the geogrid was unexpectedly low because the geogrid and adjacent soil became so effectively interlocked that failure of the grid in tension occurred adjacent to the point of load application. The maximum pull-out resistance for the woven and nonwoven geotextiles was at best 50% larger than that of direct shear. Using this value would result in severe overestimates of the pull-out resistance, and, therefore, the required embedment length of the reinforcement would be underestimated.

Rowe et al.(1985) carried out pull-out and direct shear test using SR-2 reinforcement in a conventional granular fill. It was found that because the soil did not dilate, the efficiency factor obtained from pull-out tests and direct shear tests, with reinforcement oriented in the transversal direction, were equal. It was also found that the pull-out resistance of the geogrid was a function of the orientation of the geogrid. The orientation of the grid reinforcement governs the number and the available bearing contact length of the transversal elements and could therefore significantly affect the mobilized passive resistance.

2.2.8 Confined and Unconfined Tensile Test Methods for Reinforcement

In the conventional methods for determining the strength and deformation properties of reinforcement, the operational conditions of the reinforcement are not fully

considered. The load-extension properties, including the stiffness and the ultimate strength have commonly been obtained from unconfined tests such as the grab tensile test, the strip tensile test (ASTM D4632, ASTM D4595), or the wide grip tensile test (ASTM61-2101). Field experience of soil structures, reinforced with nonwoven geotextiles, has also suggested that the results obtained from unconfined tests may be overly conservative if soil-geotextile interface slippage does occur (Wu, 1991). The confinement of the geosynthetic reinforcement has a major effect on the performance of the reinforced soil structure. The confinement effect will increase the specimen resistance by minimizing necking which reduces the effect of the width / length ratio on the observed material behavior in laboratory tests.

For nonwoven geotextiles, in which the load-extension properties are dominated by the internal structure of the fibers, it has been recognized that soil confinement can affect the load-extension properties of such geotextiles in the design of a reinforced soil structure (McGown et al., 1982 ; Juran & Christopher, 1989 ; Wu, 1991). Therefore, an apparatus is required to measure the load elongation relationship for the reinforcement in air and in-soil conditions. The work of McGown et al.(1982) has led many researchers to propose various test methods for the reinforcement under the soil confinement conditions. However, it is believed that McGown's test methods failed to simulate the actual field conditions. In his work, the frictional resistance between the reinforcement and the soil has to be overcome before tensile strain in the reinforcement can be developed. The test was a model test in which the stress distribution was non uniform, therefore, the test results may be strongly subjected to boundary effects. The principle of the test arrangement should ensure that the reinforcement is confined by normal stress, keeping the shear stress zero when it is being extended.

Raguiet et al.(1993) carried out confined and unconfined wide width tests on various geosynthetics using the confined, wide-width test apparatus developed by McGown (1982). It was found that heat bonded and needle-punched nonwoven

geotextiles exhibited a positive effect of confinement, which was already shown by McGown (1982). The confinement modulus of a needle-punched geotextile was found to be as high as 1.8 to 4.8 times that under no confinement. However, the effect of confinement on the ultimate strength was negligible. With the heat bonded geotextile, the effect of confinement was mainly to improve the ultimate strength. However, all other types of geosynthetics tested, the stress-strain characteristics were essentially the same when tested with and without confinement.

Juran et al.(1989) carried out confined extension tests in a wooden pull-out box under a confining pressure. The front edge of the strip sample was subjected to successive load increments, while the rear edge was either fixed or simultaneously subjected to the same load increments. Figure 2.4 shows the confined and unconfined stress-strain relationships obtained for the geotextiles. It was observed that the confinement effect was particularly significant in the case of the nonwoven geotextile strips where the confined elastic modulus is about 20 times the unconfined modulus and the confined tensile strength is about four times the unconfined one.

Wu (1991) proposed a new confined method which has the following three distinct characteristics: (1) it was an element test, thus the load-extension properties determined from the test were the inherent properties of geotextile; (2) the test measured the confined stiffness and strength of the geotextiles without mobilizing the soil-geotextile interface adhesion; and (3) the stiffness and strength obtained from the test were conservative values. The conclusion drawn from the observations was that the properties measured by the confined test can be used in design specifications of geotextile-reinforced structure in a more unified and rational manner. However, to date, no standardized testing procedure has yet been established with regard to the confined test method for the design of reinforced soil structures.

Juran et al (1992) developed testing equipment to establish the in-soil confined load-extension behavior and interface properties of geotextiles. This modified biaxial

compression cell permitted both load and displacement controlled extension tests to be conducted on geotextile specimens 20 cm. wide and 10 cm. long under both drained and undrained conditions. The soil was placed and compacted to the required relative density using the conventional triaxial test preparation procedure. The geotextile specimen was attached at its two extremities to load cells in order to monitor both the applied force and its variation along the specimen during the extension test. The tensile force variation along the specimen corresponded to the sum of the interface shear stresses mobilized under the applied extension loading. The measurements permit the decoupling of the effects of confined stiffness and interface shear on the observed material behavior. However, further research is required to establish a standard testing procedure and carefully evaluate the application of laboratory test results to the design of actual reinforced soil structures.

2.3 Summary

From the preceding discussion it can be concluded that a number of factors have influence on the measurement of the soil-reinforcement interface shear resistance. These factors can be briefly summarized as follows:

a) Confining pressure: the tendency of dense sands to dilate causes an increase in confining pressure and, therefore, the pull-out resistance increases. The total pull-out resistance increases linearly with the normal pressure in a stiff reinforcement. However, the relationship between the pull-out resistance and the normal pressure has a bilinear form in the extensible reinforcement which indicates progressive failure along the reinforcement.

b) Stiffness of reinforcement: reinforcement extensibility significantly affects the load transfer mechanism. The elongation of the reinforcement during the pull-out test affects its pull-out response and the non-uniform shear stress distribution along the reinforcement. Therefore, the concept of a uniformly mobilized limit interface shear stress

for extensible reinforcement is not appropriate for interpreting the results of the pull-out tests. Furthermore, as a consequence of the elongation effect, the specimen size becomes an important parameter. The related scale effects also makes it difficult to extrapolate pull-out test results of selected specimens to reinforcement of different dimensions.

c) Geometry of reinforcement: the passive soil resistance contributed up to 90% of the total pull-out resistance depending on the geometry of the reinforcement and the type of soil. Specifically, the geometry of the reinforcement governs the number and the passive resistance contact length of the transversal elements, and it can significantly affect the mobilized passive soil resistance.

d) Soil type and density of soil: the pull-out test in a highly frictional and well graded coarse grained soil shows higher fractional resistance. Dense and coarse sand tend to dilate during shearing, and restraining soil dilation causes an increase of normal pressure at the interface, thereby increasing the total pull-out resistance. On the other hand, a loose sand tends to contract and the apparent friction coefficient, f^* , obtained from the pull-out test is practically equal to that obtained from the direct shear test.

e) Fine grained portion of soil: for geotextile and geogrids the effect of the fine grained portion of soil is related to the ratio between the grid opening or yarn spacing and the average soil particle size, D_{50} . As the grain size of the soil increases, the particle can more efficiently interlock in the fabric, thereby increasing the pull-out resistance. As the grain size approaches the opening size of the grids, the particle become embedded within the apertures, and the pull-out resistance of the reinforcement increases.

f) Boundary condition and scale effect: interaction between the soil-reinforcement system and rigid front face of the testing apparatus may result in an arching effect which reduces the normal stress on the reinforcement and consequently, a decrease in the pull-out resistance. The size of the testing apparatus box governs the boundary conditions and also has an influence on the test results. Therefore, it is required that testing procedure and apparatus be standardized.

g) Pull-out and direct shear test: These two fundamentally different testing methods are associated with different boundary conditions and loading paths, which lead to significantly different design parameters. For dense coarse soils under low confining stresses, the pull-out test usually generates higher interface shear strengths than the direct shear tests. This may be attributed to the relatively low degree of soil dilation generated in the direct shear test. In loose fine grained soils, the direct shear and pull-out tests will generally produce approximately equal interface shear strength values. The frictional resistance observed for the stiffer reinforcement in the direct shear test is lower than in the pull-out test. For more extensible fabrics, while the pull-out resistance presents a pronounced leveling of pull-out resistance with increasing normal stress levels, the values of the angle of bond stress remained constant and independent of the normal stress level.

h) Confined and unconfined test method: comparative data from unconfined in-soil tests on geotextiles showed that highly structured nonwoven and composite geotextiles significantly change the shape of their load-strain curves when tested in-soil. Estimating tension forces in geosynthetic reinforcement requires appropriate testing procedures and interpretation methods to adequately determine the in-soil confined material properties and relevant soil-reinforcement interaction parameters. It is believed that the soil confinement can affect the load-extension properties of geotextiles in the design of a reinforced soil structure. Therefore further research should be conducted to establish reliable testing procedures and interpretation methods.

2.11 References

- Alimi, I. J., Lareal, P., Long, N.T., and Schlosser, F. (1977) "Etude del' Adherence Sols-armatures", Pro. 9th Inter. Confer. on Soil Mechanics and Foundation Engineering, Tokyo, Vol.1, pp.11-14.
- Arenicz, R.M. (1992) "Effect of Reinforcement Layout on soil Strength", Geotechnical

- Testing Journal, Vol.15, No.2 , pp. 158-165.
- Athanasopoulos, G.A. (1993) " Effect of Particle Size on the Mechanical Behavior of Sand-Geotextile Composites", *Geotextiles and Geomembranes* 12, pp.255-273.
- Bauer, G.E., Halim, A.O.A. and Shang, Q.(1991) " Large -Scale Pull-out Tests : Assessment of Procedure and Results," *Proceeding of Geosynthetics'91, Atlanta*, pp. 615-627.
- Bauer, G.E. and Shang, Q. (1993) " Pull-out Resistance of Large Geogrid Specimens in Site Specific Soils," *Journal of Southeast Asian Geotechnical Society*, Vol. 24 , No.1, pp.17-37.
- Beech, J.F. (1987) "Importance of Stress-Strain Relationship in Reinforced Soil System Designs", *Geosynthetics'87 Conference Proceedings*, Vol 1, pp.133-144.
- Bergado, D.T., Hardiyatimo, H.C., Cisneros, C.B., Chai, J.C., Alfaro, M.C., Balasubranim, A.S., Anderson, L.R. (1992) " Pull-out Resistance of Steel Geogrids with Weathered Clay as Backfill Material ", *Geotechnical Testing Journal*, Vol.15. No.1, pp.33-46.
- Bergado, D.T., Lo, K.H., Chai, J.C., Shivashankar, R., Alfaro, M.C., Anderson, L.R. (1992) "Pull-out Test Using Steel Grid Reinforcements with Low-Quality Backfill", *Journal of Geotechnical Engineering*, Vol.118, No.7 , pp.1047-1063.
- Bergado, D.T., Shivashankar, R., Alfaro, M.C., Chai, J.H and Balasubranim, A.S., (1993) " Interaction Behavior of Steel Grid Reinforcements in a Clayey Sand" , *Geotechnique* Vol.43, No.4, pp.589-603.
- Bonaparate, G.E. and Berg, R. (1987) "Long-term Allowable Tension for Geosynthetics Reinforcement ", *Geosynthetics'87 Conference, New Orleans*, pp.181-192.
- Brand, S.R.and Duffy, D.M. (1987) "Strength and Pull-out Testing of Geogrids ", *Geosynthetics'87 Conference, New Orleans*, Vol.1, pp. 226-236.
- Chan, D.H, Yi, C.T. and Scott, J.D. (1993) "An Interpretation of the Pull-Out Test", *Proc. Geosynthetic '93 Conference, Vancouver, Canada*, Vol.2, pp.593-605.

- Chang, J.C., Hannon, J.B., and Forsyth, R.A.(1977) "Pull-out Resistance and Interaction of Earthwork Reinforcement and Soil", Transportation Research Board Record 640, National Research Council.
- Collios, A. , Delmas, P. and Giroud, J.P.(1980) " Experiments on Soil Reinforcement with Geotextiles" the Use of Geotextiles for Soil Improvement, ASCE, National Convention, Portland, Oregon , pp.80-117.
- Costalonga, M.A.R. (1988), **Geogrid Pull-out Tests in Clay**, M.sc Thesis, University of Alberta. Edmonton, Alberta, 211p.
- Department of Civil Engineering, University of California, Davis (1984) " Large Scale Pull-out Tests on Tensar SR-2 Geogrids", Report for the Tensar Corp.
- Elias, V.(1979) " Friction in reinforced Earth Utilizing Fine Grained Backfills ", International Conference of Soil Reinforcement, Paris, France, pp. 435-438.
- Fannin, R.J. and Raju, D.M. (1991) " Pull-out Resistance of Geosynthetics," 44 th Canadian Geotechnical Conference , Calgary, Alberta pp. 81/1-8.
- Farrag, K., Acar, Y.B.and Juran, I. (1993) 'Pull-out Resistance of Geogrid Reinforcements, " Geotextiles and Geomembrans No.12, pp.133-159.
- Fourie, A.B. and Fabian, K.J. (1987) "Laboratory Determination of Clay -Geotextile Interaction", Geotextile and Geomembranes, No 6, pp. 275-294.
- Fourie, A.B., Bentley, N.G. and Fabian, K. (1990) "Improving Design through the Use of In-soil Testing", 4th International Conference on Geotextiles Geomembranes and Related Products, Hague, pp. 753-758.
- Garbulewski, K. (1990) "Direct Shear and Pull-out Frictional Resistance at the Geotextile-mud Interface", 4th International Conference on Geotextiles Geomembranes and Related Products, Hague, pp. 737-742.
- Giroud, J.P., Darrasse, J. and Bachus, R.C. (1993) " Hyperbolic Expression for Soil-Geosynthetic or Geosynthetics-Geosynthetic Interface Shear Strength ", Geotextiles and Geomembranes 12, pp.275-286.

- Guilloux, A., Schlosser, F., and Long, N.T. (1979) " Etude du frottement sable-armature en laboratoire ", International Conference of Soil Reinforcement, Paris, France, pp.35-40.
- Hanna, T.H. and Toumbinia, M.(1991) " Comparative Behavior of Metal and Tensar Geogrid Strips under Static and Repeated Loading," Proceeding of Geosynthetics'91, Atlanta, Vol.2, pp. 575-586.
- Holtz, R.D. (1977) "Laboratory Studies of Soil Reinforced Earth using a Woven Polyester Fabric " , Proceedings of the International Conference on the Use of fabrics in Geotechnics, Paris, Vol.3, PP. 149-154.
- Ingold, T.S. (1983) " Laboratory Pull-out Testing of Grid Reinforcements in Sand", Geotechnical Testing Journal , Vol.6, No.13, pp.101-111.
- Irsyam, M. and Hryciw, R.D.(1991)"Friction and Passive Resistance in Soil Reinforced by Plane Ribbed Inclusion", Geotechnique 41, No.4, pp. 485-498.
- Jewell, R.A. (1980) **Some effects of Reinforcement on the Mechanical Behavior of Soil**, Ph.D. Thesis Cambridge University
- Jewell, R.A., Milligan, G.W.E., Sarsby, R.W. and Dubois, D.(1984) " Interaction Between Soil and Geogrids, " Proceedings of Symposium on Polymer Grid Reinforcement in Civil Engineering, London, England, pp.18-30.
- Johnston, R.S. and Romstad, K.M. (1989) "Dilation and Boundary Effects in Large Scale Pull-out Tests", Proceedings of 12th International Conference on Soil Mechanics and Foundation Engineering, Rio de Janeiro, 1989, Vol., pp.1263-1266.
- Jones, C.J.F.P.(1985) **Earth Reinforcement and Soil Structures**, Butterworths, London, UK, 183p.
- Jones, C.J.F.P.(1988) "Predicting the Behavior of Reinforced Soil Structures", International Symposium on theory of Practice of Earth Reinforcement, pp. 535-590.

- Juran, I., Farrag, K.H. and Richmond, L. (1991) "Short and Long Term Performance of Polymeric Geogrids," Proceeding of Geosynthetics'91, Atlanta, Vol.2, pp. 587-599.
- Juran, I., Knochenmus, G., Acar, Y.B. and Arman, A.(1988) "Pull-out Response of Geotextiles and Geogrids," Pro. of Symp. on Geotextiles for Soil Improvement, ASCE, Geotechnical Special Publication 18, pp 92-111.
- Juran, I. and Christopher, B.(1989) "Laboratory Model Study on Geosynthetic Reinforced Soil Retaining Walls," Journal of Geotechnical Engineering, ASCE, Vol.115, No.7, pp.905-926.
- Kharchafi, M. and Dysli, M. (1993) "Study of Soil-Geotextile Interaction by an X-Ray Method", Geotextiles and Geomembranes 12, pp.307-325.
- Kitamoto, Y. and Abe, H. (1992) "Stability Evaluation of Geogrid Reinforced Embankments on Soft ground ", IX Asian Regional Conference on Soil Mechanics and Foundation Engineering, Bangkok, Thailand, Vol.1, pp.327-330.
- Leshchinsky, D., Field, D.A.(1987) "In-soil Load, Elongation, Tensile Strength and Interface Friction of Nonwoven Geotextiles", Geosynthetics Conference, New Orleans, Vol.1, pp. 238-249.
- McGown, A., Adraws, K.Z. and Kabir, M.H.(1982) "Load-Extension Testing of Geotextiles Confined In-soil," 2nd International Conference on Geotextiles, Las Vegas Vol.3, pp.793-798.
- McGown, A., Andrawes, K.Z. and Al-hasani, M.M. (1978) "Effect of Inclusion Properties on the Behavior of Sand", Geotechnique 28, No 3, pp.327-346.
- Milligan, G.W.E., Earl, R.F. and Bush, D.I.(1990) "Observations of Photo-elastic Pull-out Tests on Geotextiles and Geogrids", 4th International Conference on Geotextiles Geomembranes and Related Products, Hague, Vol.2, pp747-751.
- Milligan, G.W.E. and Palmeira, E.P. (1987) "Prediction of Bond between Soil and Reinforcement ", Prediction and Performance in Geotechnical Engineering,

Calgary, Alberta, pp. 147-153.

Mitchell, J.K. and Villet, W.C.B.(1987) **Reinforcement of Earth Slopes and Embankments**, NCHRP Report 290, Transportation Research Board, 323pp.

Mowafy, Y.M.M.(1986) **Analysis of Grid Reinforced Earth Structures**, Ph.D. thesis, Carleton University, Ottawa, 384 p.

Palmeira, E.M., Milligan, G.W.E. (1989) "Scale and other Factors Affecting the Results of Pull-out Tests of Grids Buried in Sand," *Geotechnique* 39, No. 5, pp.511-524.

Rowe, R.K. Ho, S.K. and Fisher, D.G. (1985) "Determination of Soil-Geotextile Interface Strength Properties," 2nd Canadian Symposium on Geotextiles, pp.25-34.

Sarsby, R.W. (1985)"The Influence of Aperture Size/Particle Size on the Efficiency of Grid Reinforcement", *Proceeding of 2nd Canadian Symposium on Geotextiles and Geomembranes*, Edmonton ,Alberta, pp7-12.

Schlosser, F.S., Elias, V. (1978) " Friction in Reinforced Earth", *Proceedings of a Symposium on Earth Reinforcement* , Pittsburgh, pp.735-763.

Schlosser, F., and Delage, P. (1987)"Reinforced Soil Retaining Structures and Polymeric Materials", *The Application of Polymeric Reinforcement in Soil Retaining Structures*, NATO ASI Series: Applied Sciences Vol.147, pp3-65.

Sridharan, A., Srinivasa Murthy, B.R., Bindumadhava, R. K.(1991)" Technique for Using Fine -Grained Soil in Reinforced Earth", *Journal of Geotechnical Engineering*, ASCE, Vol.117, No.8, pp.1174-1190.

Srinivasa Murthy, B.R Sridharan, A., Bindumadhava, R.K. (1993) " Evaluation of Interfacial Frictional Resistance", *Geotextiles and Geomembranes* 12, pp.235-253.

Venkatappa, G. Kate, J.M.(1990) " Interface Friction Evaluation of Some Indian Geotextiles",4th International Conference on Geotextiles Geomembranes and

Related Products, Hague, pp.793.

Vesic, A.S.(1977) **Design of Pile Foundation**, National Cooperative Highway
Research Program Synthesis of Highway Practice 42.

Wilson-Fahmy, R.F., Koerner, R.M. (1993) "Finite element Modeling of Soil-Geogrid
Interaction with Application to the behavior of Geogrid in a Pull-out Loading
Condition," *Geotextiles and Geomembrans* No.12, pp.479-501.

Wu, J.T.H.(1991) " Measuring Inherent Load-Extension Properties of Geotextiles for
Design of Reinforced Structures," *Geotechnical Testing Journal*, Vol.14, No.2,
pp.157-165.

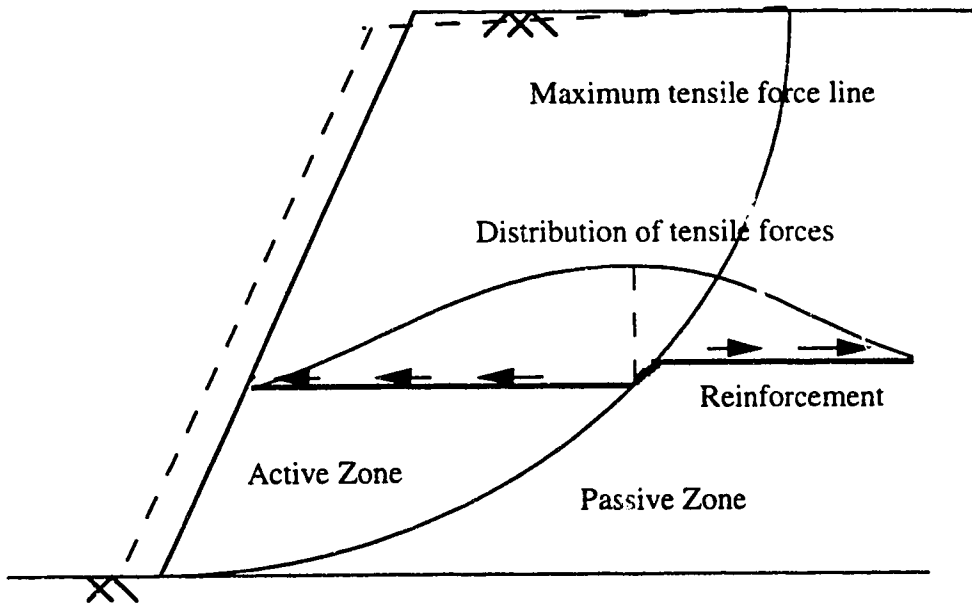


Figure 2.1 Behaviour of Reinforced Slope

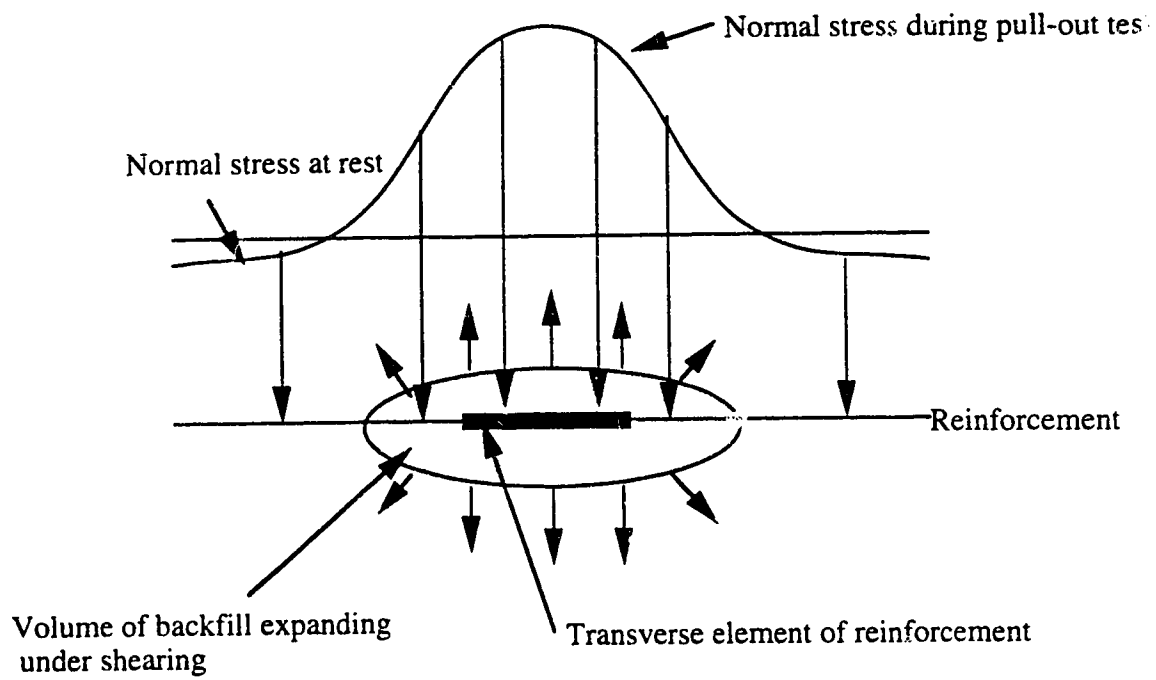


Figure 2.2 Dilatancy Effect on Normal Stress along Reinforcement
(after Schlosser and Elias,1978)

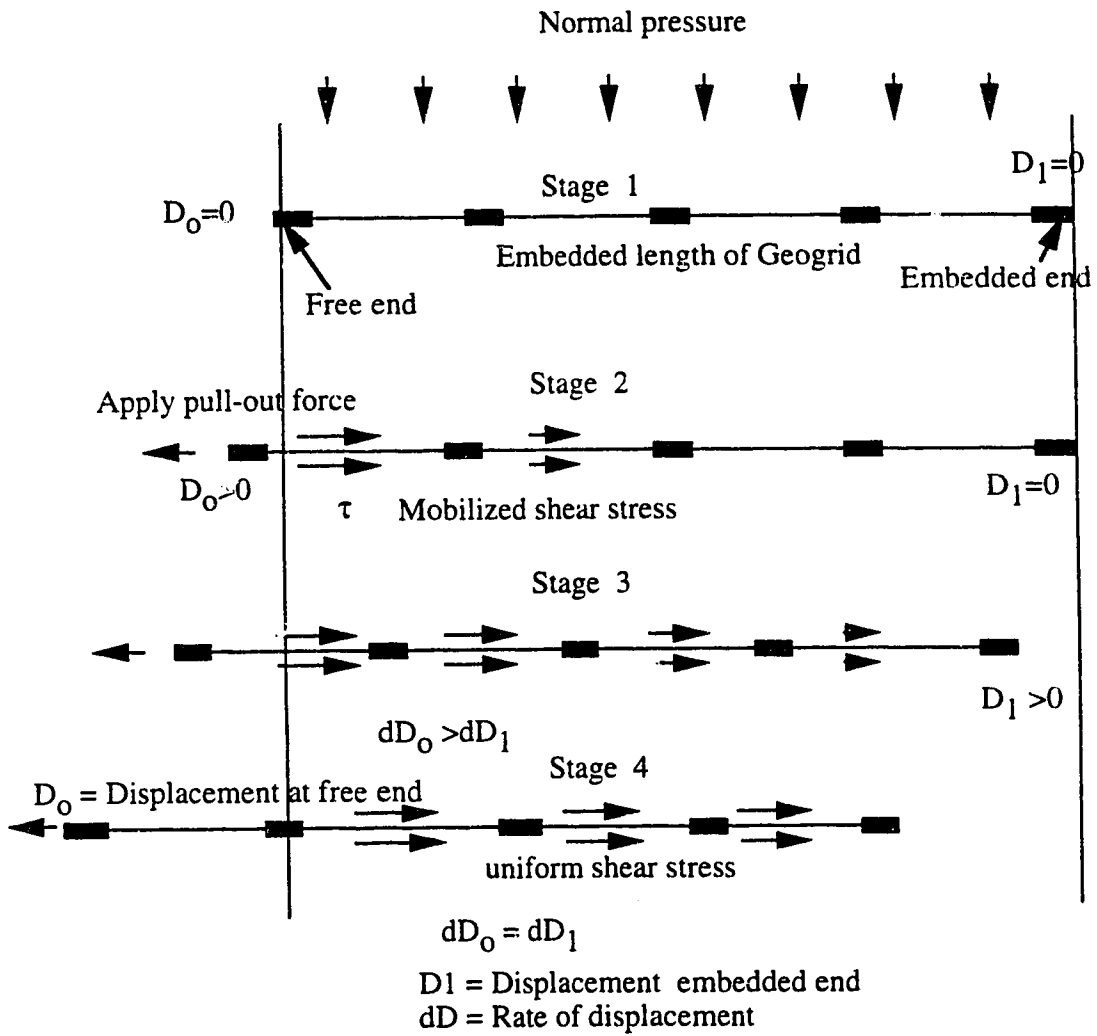


Figure 2.3 Mobilization of Pull-out Resistance (after Bauer and Shang, 1993)

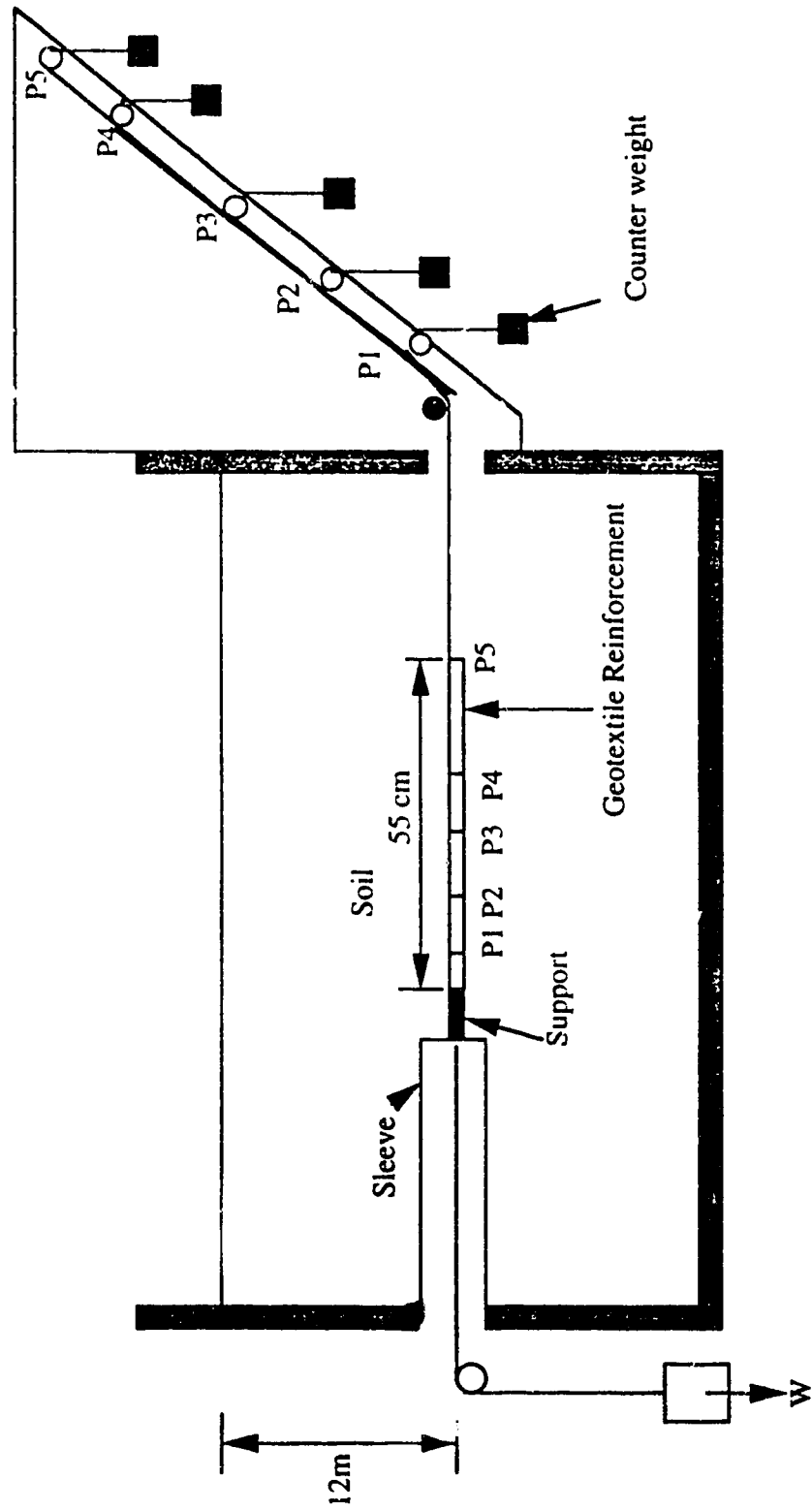


Figure 2.4 Pull-out Instrumented Test Device (after Juran and Christopher, 1989)

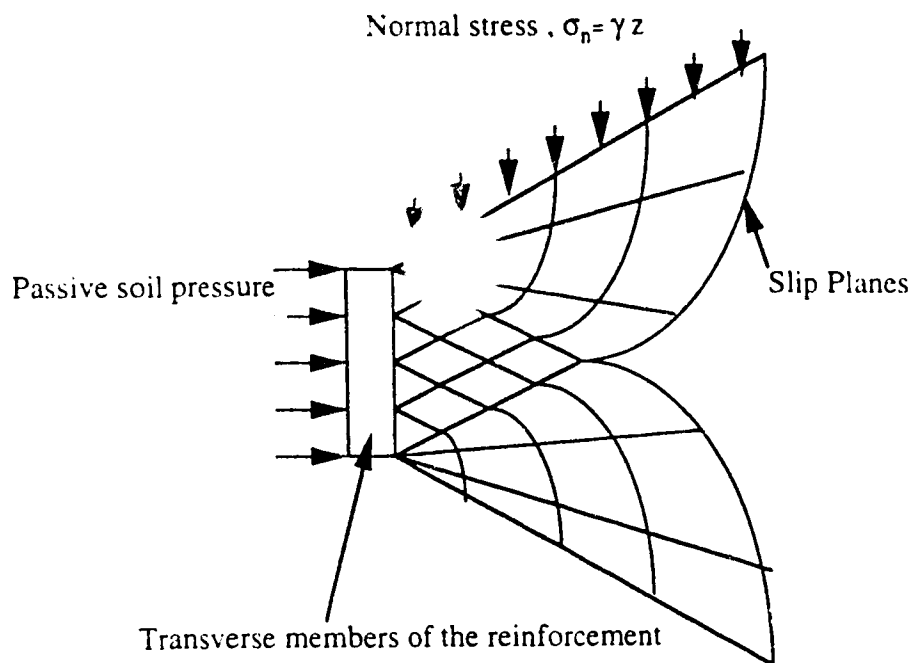


Figure 2.5 Passive Soil Resistance of Grid Reinforcement during Pull-out Test (after Jewell et al., 1984)

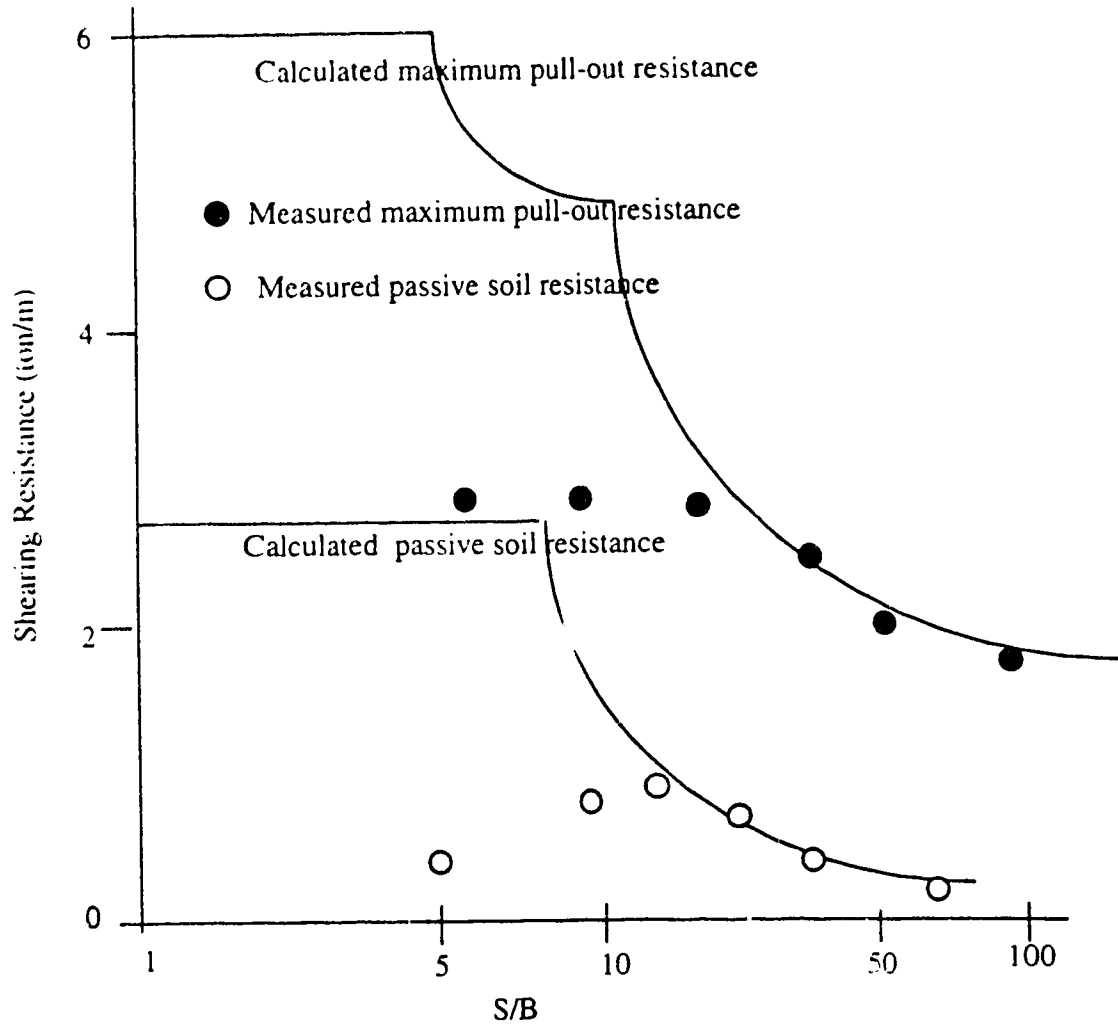


Figure 2.6 Effect of Interference between Grid Transverse Members
(modified from Kitamoto and Abe, 1992)

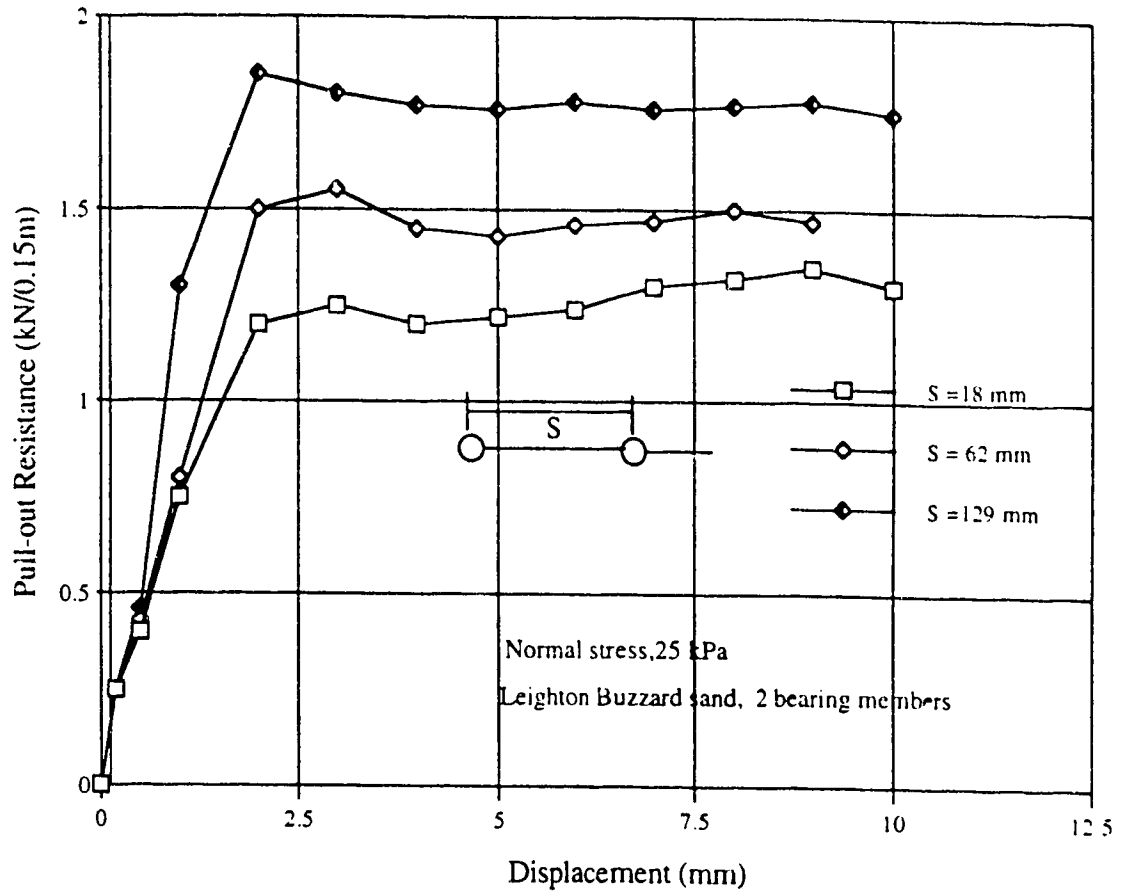


Figure 2.7 Effect of Spacing between Bearing Members on Pull-out Resistance (after Palmeira and Milligan, 1989)

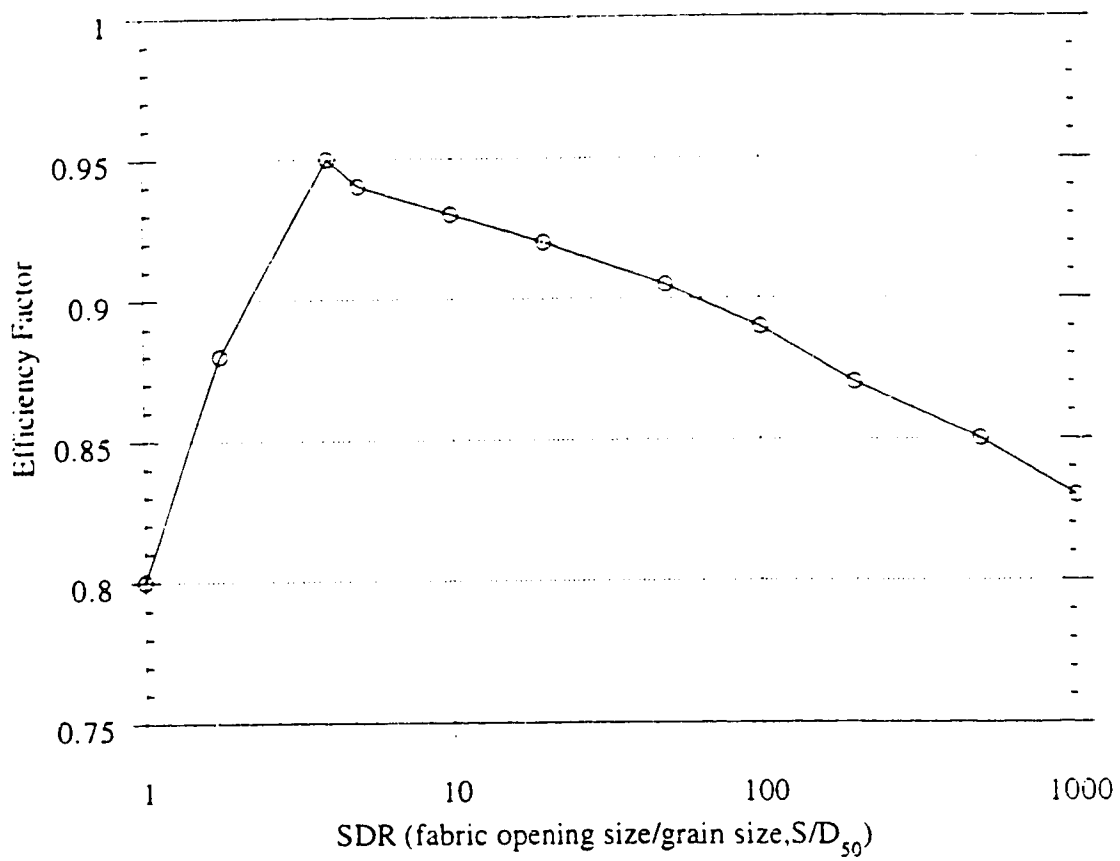


Figure 2.8 Influence of Particle Size on Soil-Reinforcement Interaction (modified from Sarsby, 1985)

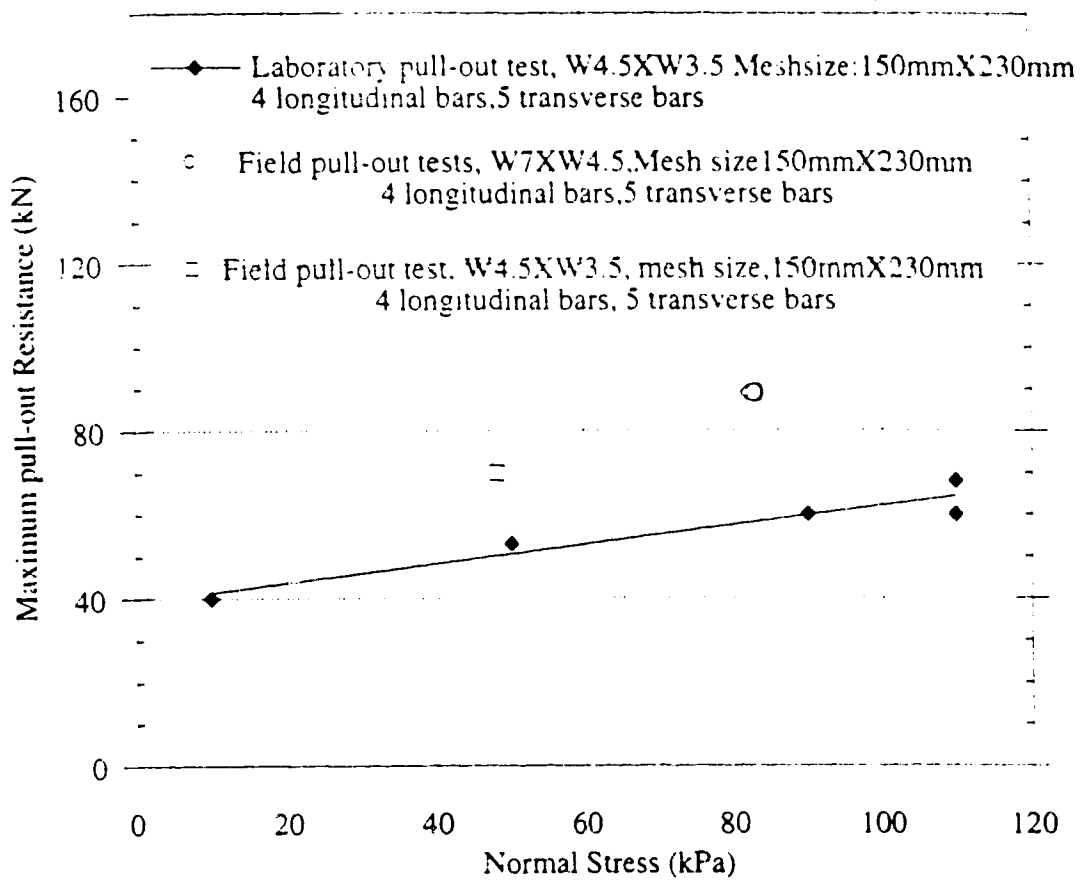
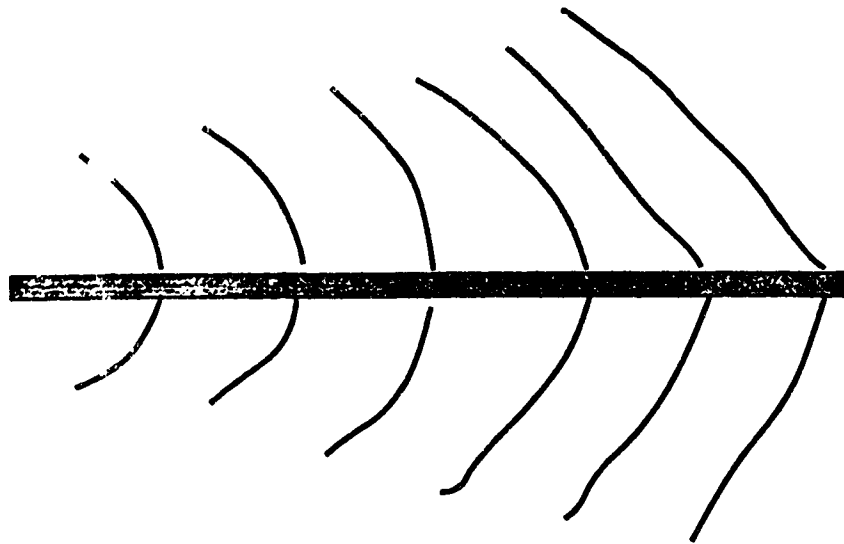
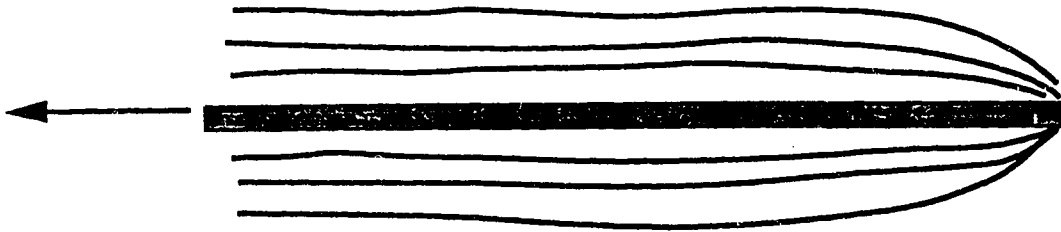


Figure 2.9 Comparison of Field and Laboratory Pull-out Resistances for Clayey sand Backfill (after Bergado et al., 1992)



(a) Direct shear test



(b) Pull-out test

Figure 2.10 Comparison between Measured Pattern of Displacement in Sand (after Jewell, 1980)

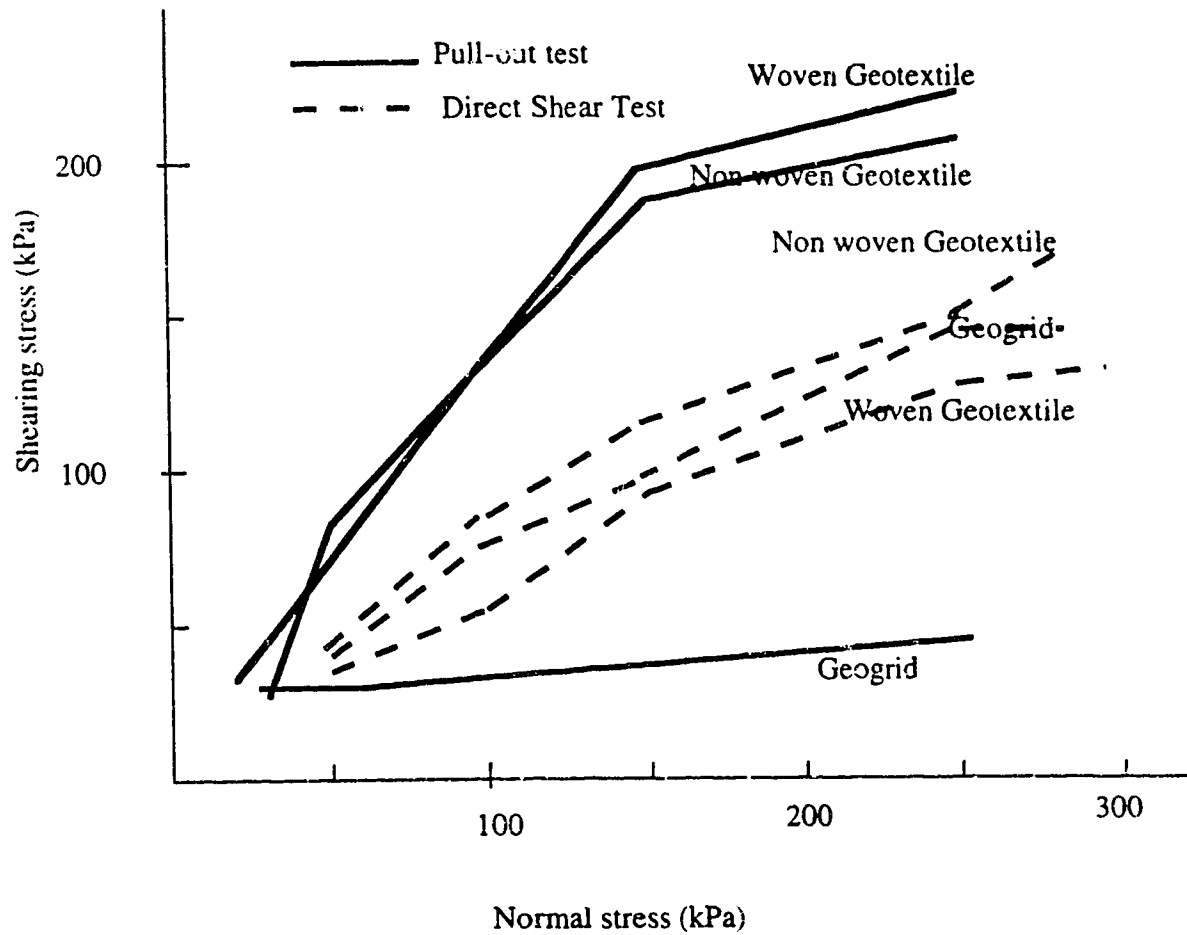


Figure 2.11 Comparison of Direct Shear and Pull-out Tests (after Fourie et al., 1990)

CHAPTER 3. AN INTERPRETATION OF THE PULL-OUT TEST

3.1 Introduction

Design of reinforced soil using geosynthetics currently adopts a limit equilibrium approach. In this approach the stability of the structure is evaluated at a limiting state of incipient failure satisfying force equilibrium but not strain compatibility. A satisfactory design emerges from the analysis by ensuring an adequate factor of safety for the structure. Although this current procedure is a logical extension of the well established method of designing and analyzing unreinforced soil, there is one basic difference between the reinforced and unreinforced structures; namely, the unreinforced structure usually consists of one material while the reinforced structure has at least two materials. The calculation of one factor of safety for the reinforced soil assumes the same degree of mobilization of shearing resistance for the soil and the reinforcement, which obviously is not true for most serviceability conditions except at the state of incipient failure. The use of partial factors of safety is an attempt to account for such discrepancies in mobilized resistance. Thus, reinforced soil structures are a composite material and the deformation in the backfill soil and the reinforcement must satisfy compatibility. However, it is well recognized that the calculation of mobilized resistance should account for strain compatibility. The importance of strain compatibility in a reinforced soil analysis has been discussed by Beech (1987). Procedures have been proposed to incorporate strain compatibility in conventional methods of design (Rowe and Mylleville, 1989). Proper account of strain compatibility can only be made using a deformation analysis. The finite element method is well suited for this purpose.

Numerous studies have been carried out to use the finite element method in analyzing reinforced soils (Schaefer and Duncan, 1988). In most finite element analysis, the soil is modeled using conventional solid elements. The reinforcement is generally

modeled using flexible beam elements incapable of providing bending or compressive resistance. The connection of the reinforcement and the soil can be modeled in two ways. The first approach assumes that the reinforcement is firmly bonded to the soil, allowing no slip until the shear stress between the two materials reaches a critical value. This critical value is often determined using the Mohr-Coulomb failure criterion modified to account for the reduced resistance at the interface. Once slip occurs at the interface, a limiting shear stress is applied on the reinforcement and the soil. This approach requires no special treatment at the interface between the soil and reinforcement.

The second approach is to model the soil and reinforcement interface using an interface element such as that proposed by Goodman et al.(1968) or Carol and Alonso (1988). Movement, or partial slip, is allowed between the soil and the reinforcement. This relative movement is controlled by a shear stiffness, k_s , until the shear stress is sufficiently high to cause slippage. To assess the soil-reinforcement interface characteristics such as interface friction angle and the shear stiffness, pull-out tests and/or shear box tests are commonly employed. Although the choice of test to obtain the relevant characteristics is a matter of debate, pull-out tests have been generally acknowledged to provide a better simulation of the behavior of reinforcement in reinforced soil structures (Garbulewski, 1990; Venkatappa and Kate, 1990).

The numerical modeling and the mechanism of the pull-out test are described in this chapter. Numerical modeling of the pull-out test was carried out by applying a corrected shear stiffness which was considered the progressive development of stress and strain in the reinforcement. The implication of assuming uniform shear stress in calculating the shear stiffness from the results of the pull-out test were examined in detail. Comparison of results were then made to examine the effect of progressive deformation on the pull-out test and to understand the pull-out resistance mobilization process.

3.2 Pull-out Test Mechanism

The mobilization of a pull-out resistance is a complicated process. The pull out resistance of the geogrid reinforcement is basically mobilized by three interaction mechanisms: soil friction on the longitudinal member of the reinforcement, soil passive resistance on the transverse elements and particle interlocking in the apertures in the reinforcement. The mechanisms by which the reinforcement develops depend on the size of the apertures, stiffness, geometry, roughness of the surface of the reinforcement, and the grain size of the soil. For small soil-reinforcement displacement there is initially a mobilization of the friction along the longitudinal element of the reinforcement. The soil passive resistance on the transverse element is mobilized under a larger displacement which is influenced by the stiffness, structure, and geometry of the reinforcement (Schlosser and Delage, 1987). However, friction and passive soil resistance were not necessarily completely additive and some relative reinforcement and soil displacement occurs for either friction and/or passive soil resistance to mobilize. Irsyam and Hryciw (1991) showed experimentally that shear surfaces develop around the ribs of the reinforcement during the shearing process. The particle interlocking resistance is often neglected because the particles of the soil are significantly smaller than the fiber or grid spacing and the grains cannot effectively interlock within the geosynthetics apertures (Sarsby, 1985). The soil passive resistance on the transverse elements plays an important role on the total pullout resistance. It is a function of soil cohesion, friction angle, and the bearing capacity factor (N_q) in the Terzaghi bearing-capacity equation. The expression for N_q depends on the assumed failure mechanisms such as the general shear failure mode and the punching failure mode, which provide apparent upper and lower bounds of actual pull-out test results (Jewell et al. 1984).

When a load is applied to the front end of the reinforcement, shear stresses at the soil-reinforcement interface are developed as the reinforcement is strained. Load is then

transferred progressively along the entire length of the reinforcement. For extensible grid reinforcement under the influence of pull-out force, considerable elongation of grid longitudinal members will occur. The magnitude of the mobilized resistance of each bearing member varies along the pull-out direction. The maximum resistance occurs at the front bearing member. In addition, under an applied pull-out force and a certain confining pressure, only a certain portion of the grid reinforcement has a relative displacement with the backfill soil. Therefore, the mobilized shear stress along the reinforcement during the pull-out test might have a highly non-uniform distribution. It is possible that the shearing process might not occur at the rear part of the reinforcement. However, for inextensible reinforcement the pull-out resistance might mobilize the entire length of the reinforcement under a small relative displacement, and a uniform shear stress distribution along the entire length of the reinforcement.

When the load at the pull-out slot is applied and the mobilized frictional resistance is greater than the rupture strength of the reinforcement, the reinforcement ruptures. On the other hand, if a shorter length of reinforcement is used, the frictional resistance along the reinforcement is lower, thus allowing displacement to occur over the entire length of the reinforcement. If the load generated is higher than the frictional resistance developed along the entire length of the reinforcement, slippage of the reinforcement will occur. Frictional resistance can be assessed based on the normal stress on the reinforcement and the friction angle, which is dependent on the soil and properties of the reinforcement. To prevent the slippage failure of the reinforcement in reinforced soil structures the use of a higher confining stress or granular materials are needed as backfill materials. Understanding the pull-out resistance mobilization process is important because the reinforced soil structure does not always work at a limit equilibrium condition. Thus, the designed pull-out resistance should be compatible with the deformation condition of the structure, i.e., the deformation in the backfill soil and in the reinforcement must be compatible.

3.3 Shear Stiffness

The interaction between the grid reinforcement and the soil has two components: the passive soil resistance and the frictional resistance. The contribution of the soil passive resistance to the interaction between the reinforcement and the soil was considered high. The passive soil resistance is usually expressed as effective bearing resistance which can be developed on the transverse members, and is a function of the vertical effective stress. A definition of shear stiffness used to simulate the interface behavior between the soil and the reinforcement is:

$$K_s = \frac{D_t}{D_d} \quad (3.1)$$

where D_t is the change in shear stress and D_d is the corresponding change in relative displacement between the soil and reinforcement.

The shear stiffness expressed in equation (3.1) depends on the soil and type of reinforcement and it is often determined experimentally for use in finite element analysis. The direct shear and the pull out tests are commonly used to determine the interaction properties between the soil and the reinforcement. In particular the pull-out test simulates the anchorage condition of the reinforcement and provides an estimation of the pull-out resistance for design. It is also used to provide an estimate of the shear deformation between the reinforcement and soil (Katagiri et al., 1990). In calculating the shear stiffness using equation (3.1), it is necessary to calculate the shear stress acting on the reinforcing material. In calculating the shear stress it is assumed that the mobilization of shear stress is uniform along the reinforcement and the change in shear stress is given by:

$$D_t = \frac{D_p}{2A} \quad (3.2)$$

where DP is the measured change in axial force and A is the one sided surface area of the reinforcement. Therefore equation (3.1) becomes:

$$K_s = \frac{DP}{2A \Delta d} \quad (3.3)$$

The change in displacement in equation (3.3) is often taken as the displacement measured on the reinforcement at the pull-out slot. However, the shear stiffness value is clearly a function of the specimen size.

Shear stiffness was also expressed as a non-linear form, stress-dependent and inelastic which is represented by a hyperbolic model similar to that for soil. The shear stiffness, K_s , would be expected to decrease with increasing shear stress and displacement, as the applied shear stress approaches the shear strength of the interface. In other words, there could be nonlinear behavior of the variation of shear stiffness with respect to shear stress level. If the interface element is in tension or has a shear stress above the failure level then the shear stiffness is reduced to a very small value.

It is recognized that the mobilization of shear stress is non-uniform along the extensible reinforcement as discussed in Section 3.2, pull-out mechanism. At failure, that is the fully slipping condition, the mobilization of shear strength is approximately uniform if the interface does not possess a strain weakening characteristic. Most granular material used in reinforced soil structures does not exhibit strain weakening behavior. For clayey soil, the strain weakening behavior results in non-uniform mobilization of shear strength.

It is possible to account for the non-linear characteristic of K_s with respect to displacement as well as normal stress (Katagiri et al., 1990). However, the assumption of uniform shear stress can result in serious error in obtaining K_s . The mobilization of shear stress is highly non-uniform along the reinforcement during the loading process. Although the shear stress can be estimated using the load transfer approach proposed by

Coyle and Reese (1966) the corresponding relative displacement cannot be determined easily.

3.4 Finite Element Modeling of the Pull-out Test

The pull-out test was simulated using the finite element method. An interface element was used which was capable of sustaining tensile stress but not bending or compressive stress. A description of the formulation of the joint element can be found in Chalaturnyk (1988).

A two dimensional plane strain idealization of the pull-out specimen is shown in Figure 3.1. A total of 170 elements, including 17 reinforcing and 34 interface elements, with 636 nodes was used in the simulation. The reinforcing elements are three node element capable of sustaining only tensile stress. The interface was modeled by a 6 node element. An eight node isoparametric element was used to simulate the soil.

An actual experimental set-up carried out at the University of Alberta was used for modeling (Costalonga, 1988). The reinforcement was extended from one side of the box to the other side. The advantage of this arrangement is that the area of contact between the reinforcement and soil remained constant throughout the experiment. Also the displacement of the reinforcement at the opposite end of the pull-out slot could be monitored to determine the load at which movement occurred.

The reinforcement was modeled using a non-linear force-strain relationship. The tensile force in the reinforcement can be expressed as:

$$F = D_i \left(\epsilon_a - \frac{\epsilon_a^2}{2\epsilon_f} \right) \quad (3.4)$$

where F , D_i , ϵ_a and ϵ_f are the tensile force, initial load modulus, axial strain and axial strain at failure respectively.

Equation (3.4) is based on a parabolic relationship between stress and strain developed in the reinforcement. This is found to be a good approximation for polymeric geogrid within the range of strains of interest in this study (Chalaturnyk, 1988). The reinforcement which is studied was Tensar SR-2 geogrid. The force vs. strain relationship used in the present modeling is shown in Figure 3.2. The force-strain relationship was considered not to be time-dependent.

The shear behavior of the interface between the soil and the reinforcement was modeled using an elastic-plastic model. The shear modulus remained constant until a failure condition was reached along the interface. The failure condition is defined by the Mohr-Coulomb relationship :

$$\tau_f = c + \sigma_n \tan \delta \quad (3.5)$$

where c and δ are the cohesion and frictional resistance between the soil and the reinforcement and;
 σ_n and τ_f are the normal and shear stress on the reinforcement respectively.

In the finite element analysis the shear stress at each integration point was checked with the failure criterion. If failure was reached, a constant shear stress was applied and maintained at the integration point throughout the remainder of the analysis.

A linear elastic model was used to model the behavior of the soil. Since it was expected that the amount of straining in the soil be smaller than the strain in the interface and reinforcement, the initial tangent modulus, based on triaxial testing of the soil, was used to calculate the elastic parameters for the model. A summary of the material parameters used in the analysis is given in Table 3.1. The shear stiffness for the interface was calculated based on the pull-out test conducted by Costalonga (1988). The normal stiffness, K_n , was assigned a very high value to prevent incompatibility in the normal direction.

In simulating the pull-out experiment, a vertical uniform pressure of 51 kPa and the weight of the soil were applied prior to imposing force on the reinforcement located at the mid-height of the apparatus. The pull-out forces acting on the reinforcement during the test were calculated from prescribed displacements specified on the reinforcement at the pull-out slot. The reinforcement was extended to the back of the apparatus which gives a constantly embedded length during the entire shearing process.

3.5 Connection of Interface Element

Interface elements are formulated as a zero-thickness element with normal shear springs at each end of the element. Bar elements representing reinforcement are included in the mesh associated interface element. The methods of connecting the interface elements to the soil and reinforcement element is very important, especially at the reinforcement ends. When finite element methods are used to analyze the reinforced soil wall, the connection of the wall facing elements with the reinforcement or soil element could cause errors. It was found in this analysis that the methods connecting the interface element to soil at end of the reinforcement have a marked influence on the analysis results.

Two types of connection methods are used to evaluate the effect of the end connection as shown in Figure 3.3. Figure 3.4 presents the tensile forces along the reinforcement at a displacement of 5 mm at the pull-out slot during the pull-out test. As shown in Figure 3.4, method B gives a smooth curve, the tensile force decreases smoothly along the reinforcement as expected, while in method A the tensile force on the reinforcement drops down at 30 cm from the pull-out slot. The reasons for the drop in tensile force could not be explained. Thus, method B was chosen for use in further analysis.

3.6 Results of Finite Element Analysis

The force-displacement response calculated from the finite element analysis is shown in Figure 3.5. It is seen that the finite element model underestimated the force required for a certain displacement. For the analysis shear stiffness was calculated based on the observed load-displacement response from the pull-out test. It is clear that the assumption of uniform mobilized shear stress along the reinforcement used in calculating the shear stiffness underestimated the actual shear stiffness. Katagiri et al. (1990) also simulated the pull-out test and the calculated response was lower than the experimental observations.

The mobilized shear stress along the reinforcement is shown in Figure 3.6. As a result of the progressive shearing along the interface between the soil and reinforcement, the mobilized shear stress is highly non-uniform. The calculated shear stress decreases along the reinforcement. The mobilized shear stress remains relatively constant over the portion of the reinforcement where slip has occurred.

In order to calculate the "true" stiffness for use in a finite element analysis, it is required to perform a series of simulations of the pull-out test and determine the apparent stiffness, using Equation (3.3) from the finite element results. A relationship between the apparent stiffness and the true stiffness can be determined.

It is observed that the stiffness of the reinforcement influences the load transfer mechanism. The degree of progressive deformation will depend on the relative stiffness between the reinforcement and the interface. It is therefore appropriate to introduce a quantity called the true stiffness ratio, r . The true stiffness ratio is defined as the ratio of the true stiffness of the interface, k_{st} , over the initial stiffness of the reinforcement, k_{ri} ;

$$r = \frac{k_{st}}{k_{ri}} \quad (3.6)$$

For very stiff reinforcement, such as metallic strips, the value of r is relatively small and the mobilized shear stress and displacements along the reinforcement are uniform. Very soft reinforcement, such as a nonwoven geotextile, develops non-uniform shear stress and displacements along the reinforcement. The value of r will be relatively high for this material. It is expected that a higher value of r will result in a larger error when calculating the shear stiffness from the pull-out test results. A series of numerical simulations of the pull-out test was carried out for different values of the stiffness ratio. In each analysis, a shear stiffness, K_{st} , was specified for the interface between the solid and reinforcement. The apparent stiffness, K_{sa} , was calculated from the load-displacement response. The result of the analysis is shown in Figure 3.7. As r increases, i.e. the stiffness of the reinforcement decreases, progressive shearing becomes more significant and the discrepancy between the apparent shear stiffness and true shear stiffness increases.

Based on an apparent shear stiffness of $1.24 \times 10^3 \text{ kN/m}^3$, a true shear stiffness value was found to be $2.0 \times 10^4 \text{ kN/m}^3$ for use in the finite element analysis. Figure 3.8 shows the observed and calculated load-displacement response using both the apparent and true stiffnesses. It is seen that the corrected stiffness provides better agreement between calculated and observed values. The mobilized shear stress along the reinforcement at different stages of the test is shown in Figure 3.9. Since the true stiffness is higher than the apparent stiffness, the mobilized shear stress using the true stiffness is higher than that calculated using the apparent stiffness for a given displacement of the reinforcement. The mobilized shear stress is the same for both cases when slipping occurs.

The calculated displacement along the reinforcement is also compared with the experimental results at a displacement of 37 mm. The results shown in Figure 3.10 indicate that the finite element solution slightly overestimated the displacement along the reinforcement. It is interesting to note that the difference between the calculated and

observed displacements remains relatively constant along the entire length of the reinforcement.

3.7 Conclusion

The pull-out test was simulated numerically using the finite element method. It was found that the mobilization of shear stress along a reinforcement is highly non-uniform during the initial stage of the test. If the force-displacement response of the pull-out test was used to obtain a shear stiffness for modeling the interface between the soil and reinforcement, the assumption of uniform stress distribution can result in considerable error between the apparent shear stiffness and the true shear stiffness values. This discrepancy depends on the relative stiffness between the interface and the reinforcement. It was illustrated that stiffer reinforcement results in less degree of progressive shearing and, therefore, results in less discrepancy between the true and apparent stiffness values. The true stiffness can be estimated from the results of the pull-out test by using an appropriate stiffness correction. The calculated force-displacement response using true stiffness value gives better agreement with the experimental observations.

3.8 References

- Beech, J.F. (1987) "Importance of Stress-Strain Relationship in Reinforced Soil System Designs", Geosynthetics'87 Conference Proceedings, Vol. 1, pp.133-144.
- Carol, A.G. and Alonso, E.E. (1988) "An Interface Element Formulation for the Analysis of Soil-Reinforcement Interaction", Computer and Geotechnics, Vol. 7, pp. 131-151.
- Chalaturnyk, R. (1988), **The Behavior of a Reinforced Soil Slope**, M.Sc. Thesis, The University of Alberta, Edmonton Alberta, Canada

- Christopher, B.R. and Berg, R.R. (1990) "Pullout Evaluation of Geosynthetics in Cohesive Soils", 4th International Conference on Geotextiles, Geomembrances and Related Products Proceedings, Vol. 1, pp. 731-736.
- Costalonga, M.A.R. (1988), **Geogrid Pull-out Tests in Clay**, M.Sc Thesis, University of Alberta. Edmonton, Alberta, 211p.
- Coyle, H.M. and Reese, L.C. (1966) "Load Transfer for Axially Loaded Piles in Clay", Journal of Soil Mechanics and Foundation Engineering Division, Vol. 92, No. SM 2, pp. 1-26.
- Garbulewski, K. (1990) "Direct Shear and Pull-out Frictional Resistance at the Geotextile-Mud Interface", 4th International Conference on Geotextiles Geomembranes and Related Products, Hague, pp.737-742.
- Goodman, R.E., Taylor, R.L. and Brekke, T.L. (1968) "A Model for the Mechanics of Jointed Rock", Journal of Soil Mechanics and Foundation Engineering Division, Vol. 94, No. SM 3, pp. 637-659.
- Irsyam, M. and Hryciw, R. D. (1991) "Friction and Passive Resistance in Soil Reinforced by Plane Ribbed Inclusions", Geotechnique, Vol. 41, No. 4, pp. 485-498.
- Jewell, R.A., Milligan, G.W.E., Sarsby, R.W. and Dubois, D.(1984), "Interaction Between Soil and Geogrids ", Proceeding from the Symposium on Polymer Grid Reinforcement in Civil Engineering, London, England, pp.18-30.
- Katagiri, T., Haneda, H., Moriyama, M., Tsuruoka, T., Toriumi, S., Takaoka, K., Yahaba, T. (1990) "Steep Reinforced Embankment using Geogrid - Laboratory Pull-out Test of Geogrid and its Finite Element Analysis, 4th International Conference on Geotextiles, Geomembrances and Related Products Proceedings, Vol. 1, pp. 45-51.

- Palmeira, E.M. and Milligan, G.W. (1990) "Large Scale Pull-Out Tests on Geotextiles and Geogrids", 4th International Conference on Geotextiles, Geomembrances and Related Products Proceedings, Vol. 2, pp. 743-746.
- Rowe, R.K. and Mylleville, B.L.J. (1990) "Implications of Adopting an Allowable Geosynthetic Strain in Estimating Stability", 4th International Conference on Geotextiles, Geomembrances and Related Products Proceedings, Vol. 1, pp. 131-136.
- Rowe, R.K. and Mylleville, B.L.J. (1989) "Consideration of Strain in the Design of Reinforced Embankments", Geosynthetics'89 Conference, San Diego, pp. 124-35.
- Sarsby, R.W. (1985) "The Influence of Aperture Size/Particle Size on the Efficiency of Grid Reinforcement ", Proceeding of 2nd Canadian Symposium on Geotextiles and Geomembranes, Edmonton , Alberta, pp. 7-12.
- Schaefer, V.R. and Duncan, J.M.(1988) "Finite Element Analysis of the St. Alban Test Embankments", ASCE ,Geotechnical Special Publication No. 13, pp.158-177.
- Schlosser, F. and Delage, P.(1987) "Reinforced Soil Retaining Structures and Polymeric Materials", The Application of Polymeric Reinforcement in Soil Retaining Structures, NATO ASI Series: Applied Sciences, Vol.147, pp.3-65.
- Venkatappa, G. and Kate, J.M.(1990) " Interface Friction Evaluation of Some Indian Geotextiles", 4th International Conference on Geotextiles Geomembranes and Related Products, Hague, pp.793.

Table 3.1 Summary of Material Properties Used in the Finite Element Analysis

Silty clay	Unit Weight (kN/m^3)	18.86
	Initial Elastic Modulus (kPa)	3600
	Poisson's Ratio	0.36
	Cohesion (kPa)	29
	Internal Friction Angle ($^\circ$)	20
Geogrid	Tensile Strength (kN/m)	78.8
	Initial Load Modulus (kN/m)	800
	Failure Strain (%) ϵ_f	16.4
Interface	Normal Stiffness (kN/m^3), K_n	1.0E17
	Shear Stiffness (kN/m^3), K_s	1240
	Cohesion (kPa), C	2
	Friction ($^\circ$)	14

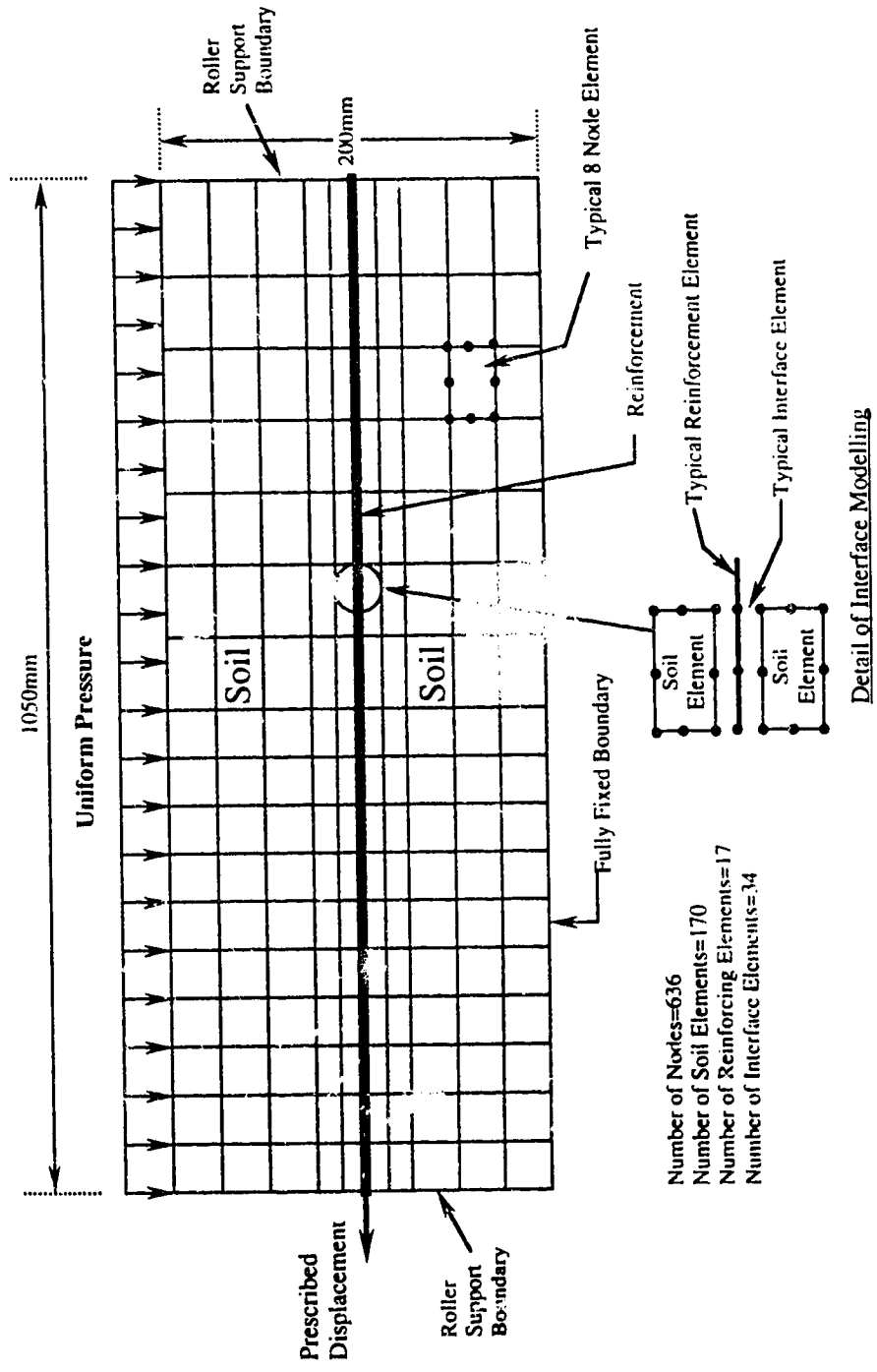


Figure 3.1 Finite Element Idealization of Soil and Reinforcement for Pull-out Test

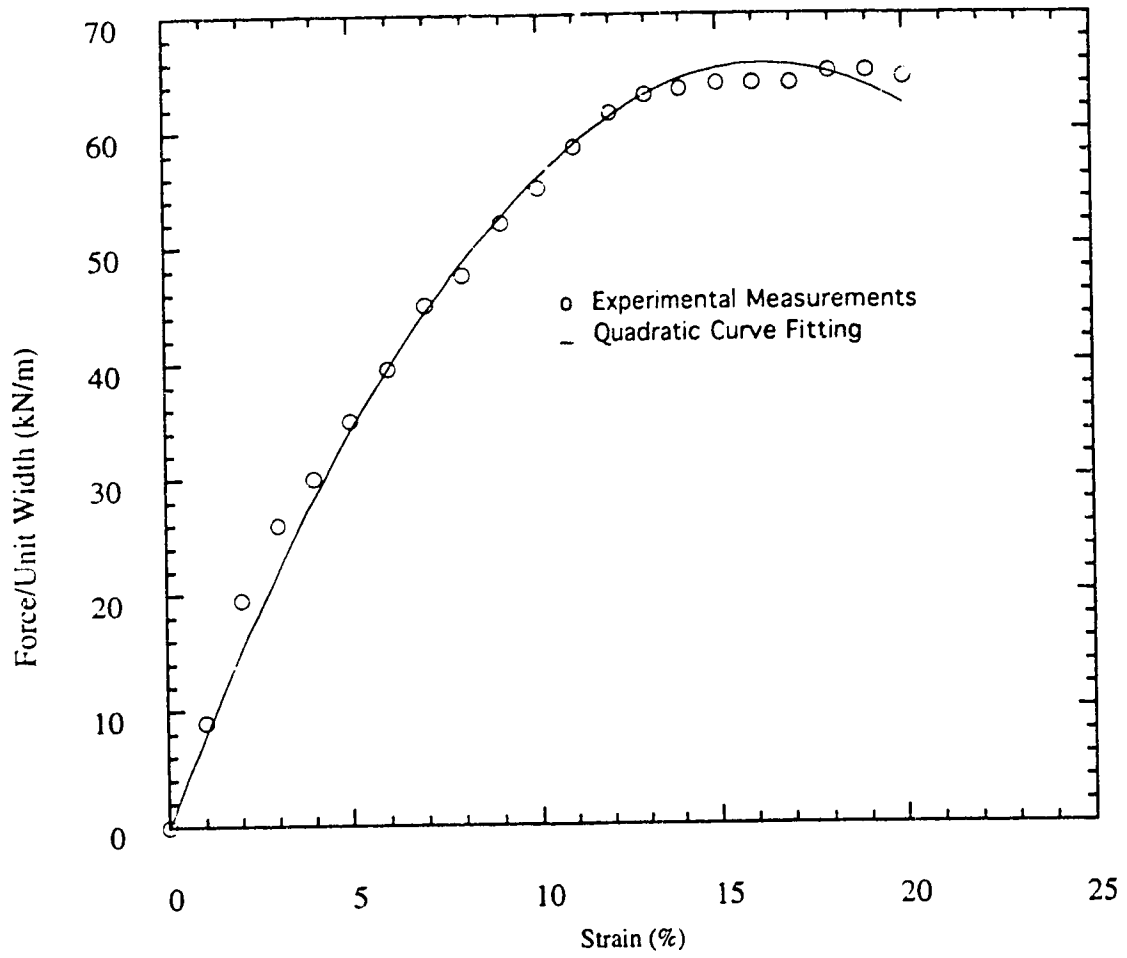
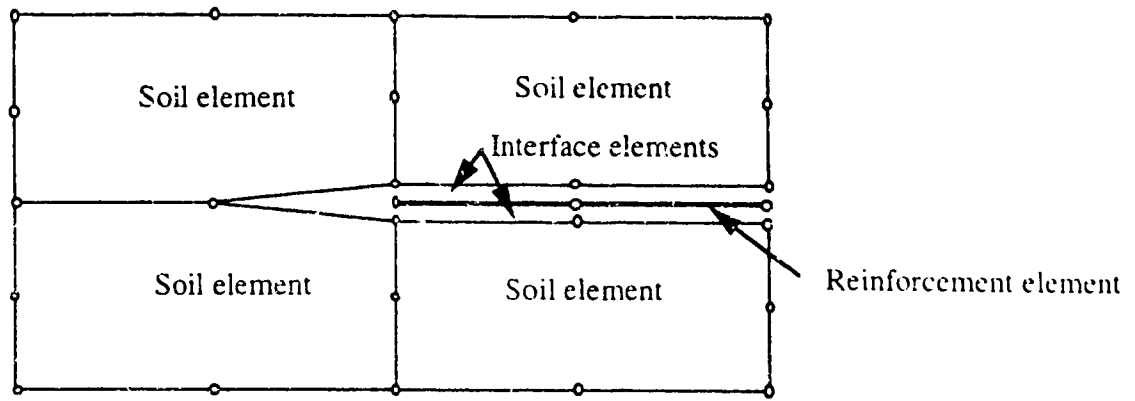
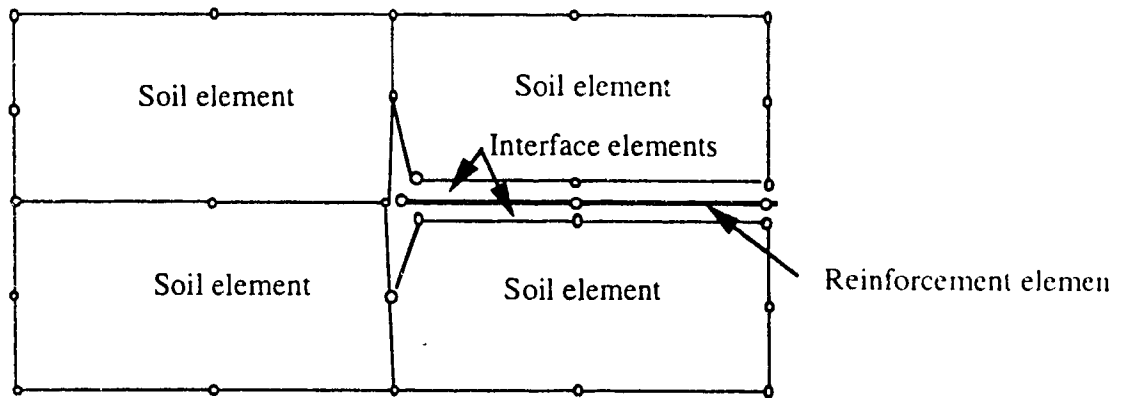


Figure 3.2 Load-strain Response of Tensar SR-2 Used in the Simulation (strain rate, 2%/min.)



(a) Connection of Interface Elements Method A



(b) Connection of Interement Method B

Figure 3.3 Method of Connecting Interface Element to Soil Element

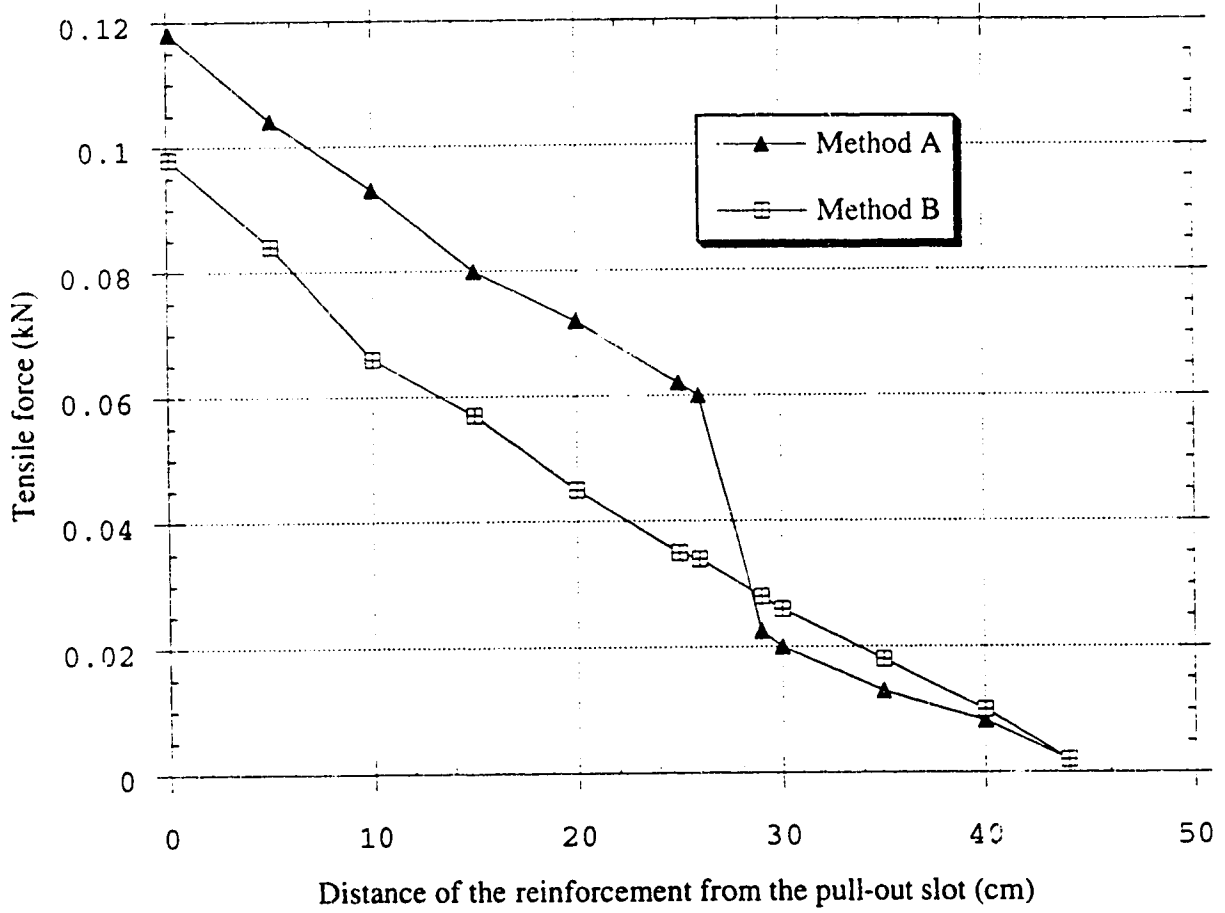


Figure 3.4 Comparison of the Connection Methods of the Interface Element at Displacement of 0.5 cm

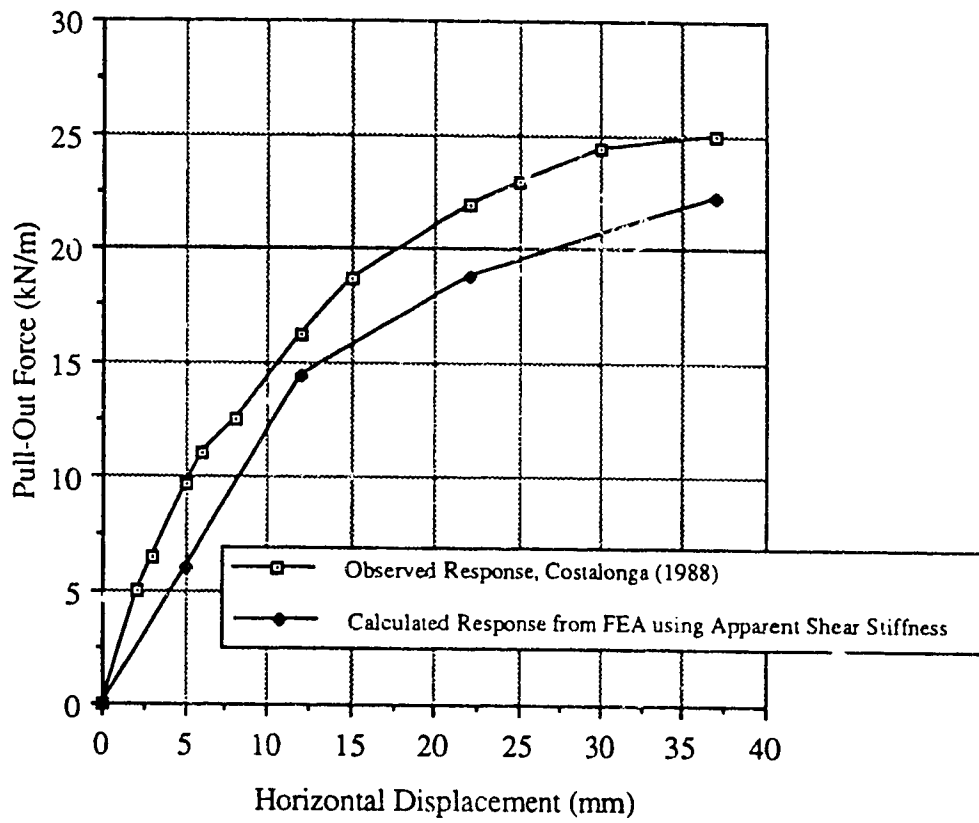


Figure 3. 5 Calculated and Observed Force-Displacement Response of Reinforcement

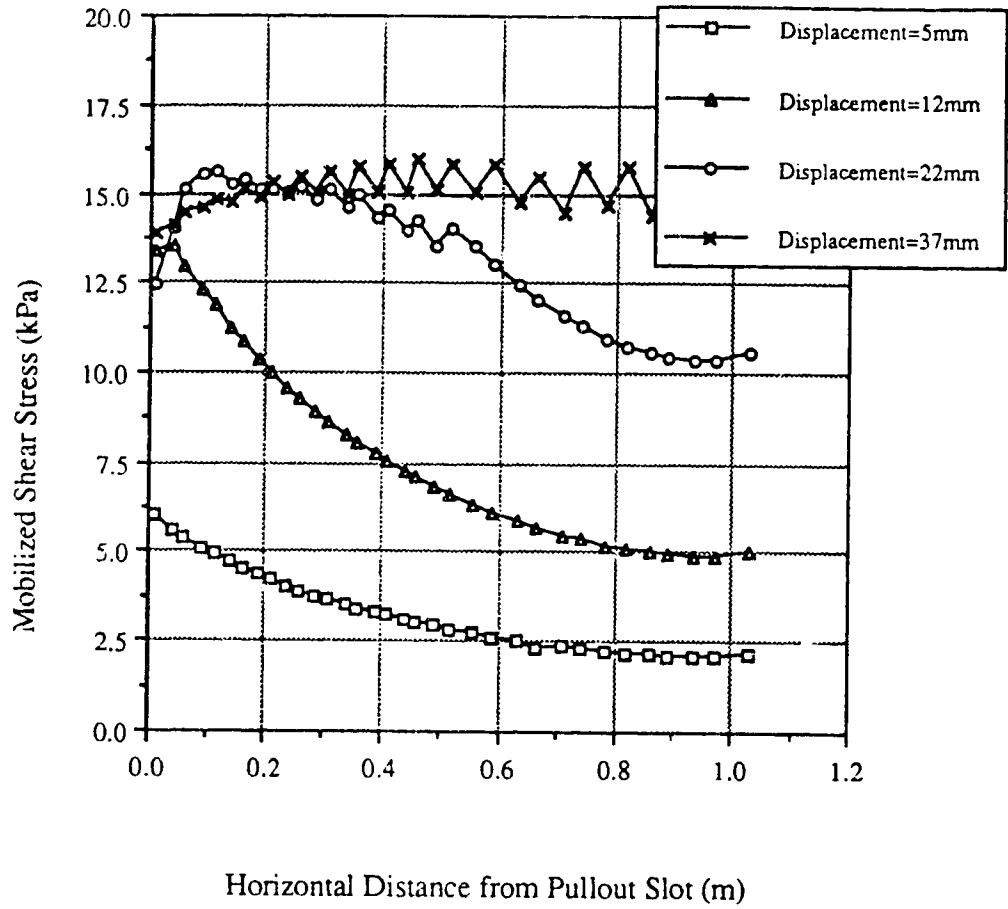


Figure 3.6 Mobilized Shear Stress along Reinforcement

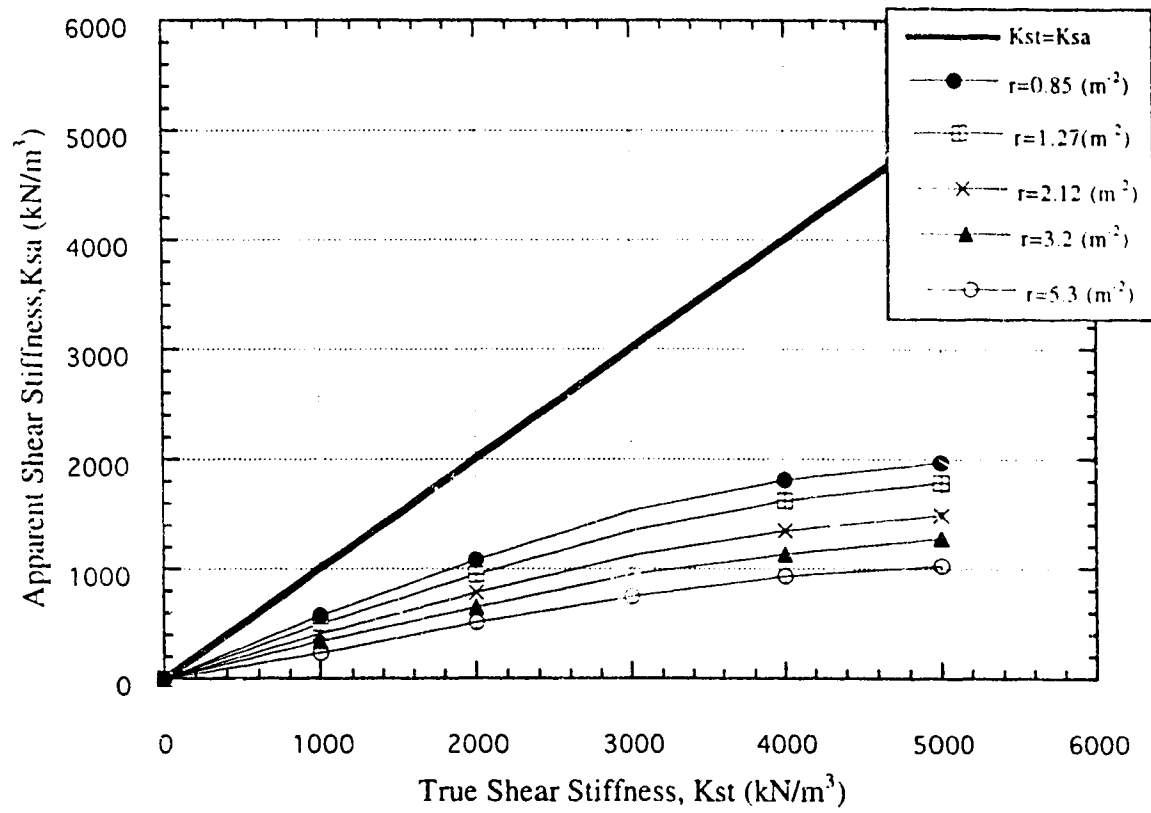


Figure 3.7 Relationship between the Apparent and Shear Stiffnesses

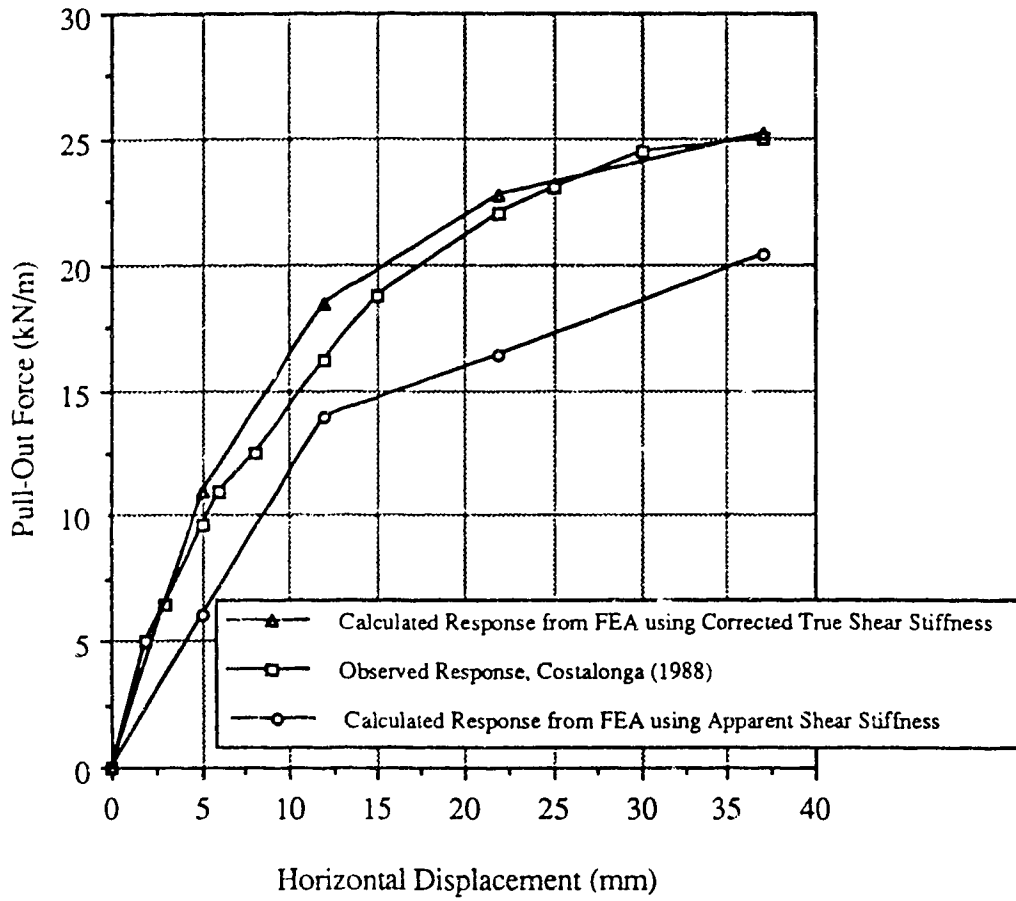


Figure 3.8 Calculated and Observed Force-Displacement Response of the Reinforcement in the Pullout Test

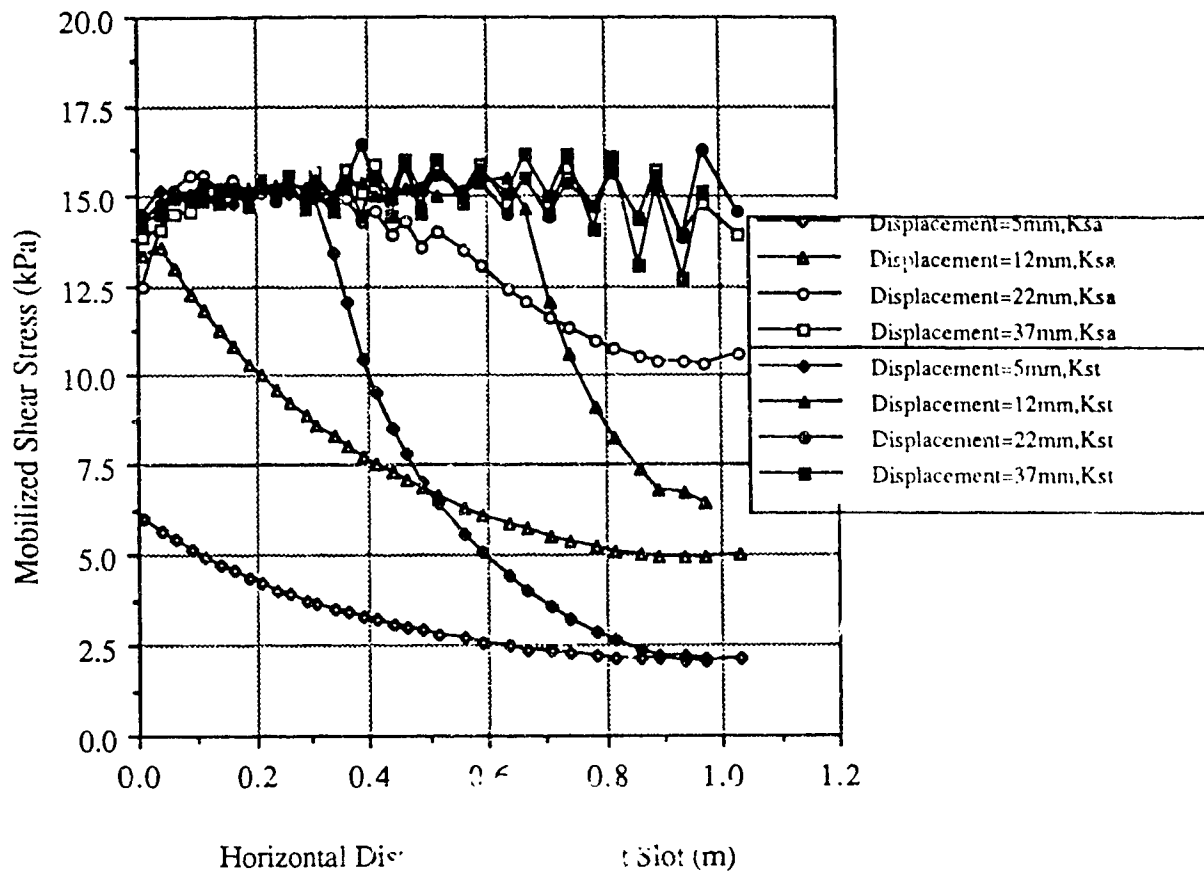


Figure 3.9 Mobilized Shear Stress vs Horizontal Displacement for Different Reinforcement

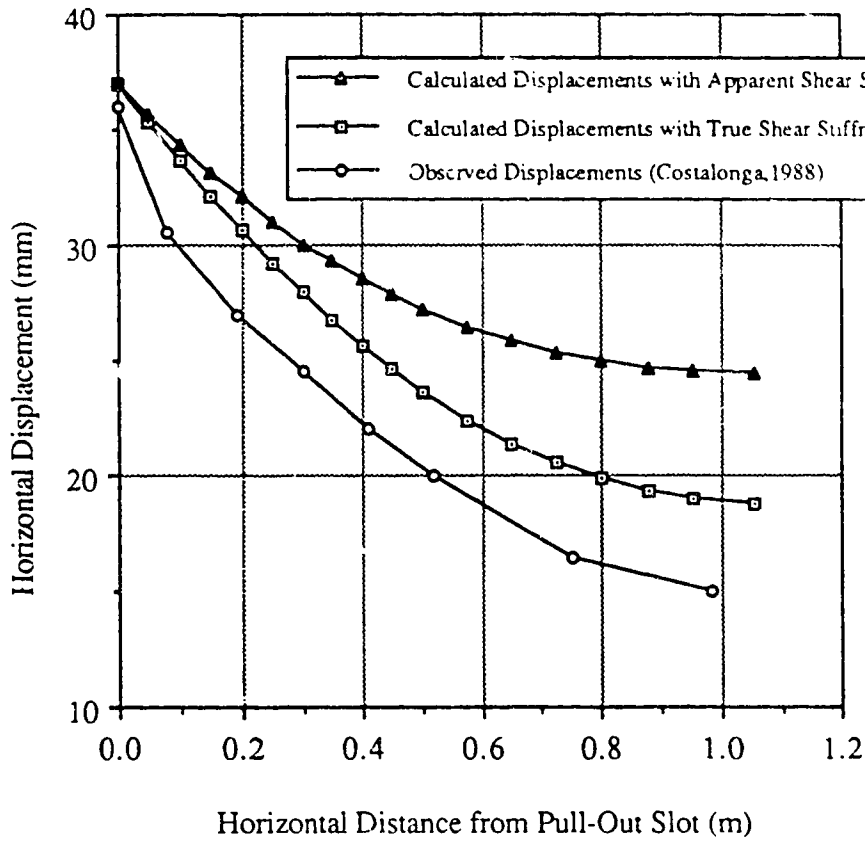


Figure 3.10 Comparison of Horizontal Displacement along Reinforcement

CHAPTER 4. FINITE ELEMENT ANALYSIS OF THE DIRECT SHEAR TEST

4.1 Introduction

In the last two decades a wide variety of reinforcement has been used for geotechnical engineering applications. The economical and safe design of reinforced soil structures requires the knowledge of both the mechanical behavior of the composite material and the behavior at the soil-reinforcement interface. The interaction behavior at the soil-reinforcement interface has been investigated extensively using various types of geosynthetics while conducting large scale laboratory pull-out and direct shear tests.

The stress transfer mechanism between soil and grid reinforcement involves two basic mechanisms: namely, lateral friction which can be active in nonwoven geotextiles and passive soil resistance on the transverse elements of geogrids. In reinforced soil structures, such as reinforced soil walls and embankments, the primary mechanism of stress transfer is frictional, with passive soil resistance playing an important role when grid reinforcement is employed. However, the relative contribution of each is indeterminate. The displacements required to generate each mechanism can be substantially different and often difficult to determine.

Load transfer between soil and reinforcement by frictional resistance depends on the interface characteristics of the soil and the reinforcement, and the normal stress between them. If the value of the normal stress on the reinforcement is known, it would be a simple matter to calculate the limiting value of the frictional resistance. However, the effective normal stress and the frictional coefficient are altered by the soil-reinforcement interaction and the influence of dilatancy, respectively. Load transfer by passive soil resistance has been considered by others to be similar to single anchored system consisting of a deadmen anchor and tie. There are a number of elements oriented transversely to the pull-out

direction in a geogrid each of which develops passive resistance along its front. An individual transverse member alters the state of stress in the region behind it and affects the stress distribution caused by the following members. Therefore, a grid reinforced soil system does not behave as a single anchor soil system. Several investigators (Jewell et al., 1984; Heucke and Kwasniewski, 1964) considered the passive resistance on the transverse element of the reinforcement similar to the bearing capacity of a deep foundation, and introduced a bearing capacity factor to calculate the ultimate passive resistance. Two types of bearing capacity failure modes in front of the transverse members have been proposed: the general bearing failure mode in which the slip plane is fully developed, and the punching shear failure mode which can occur in a shallow footing on a very loose soil or a pile foundation. Using a steel bar grid with the Leighton Buzzard sand, Palmeira and Milligan (1989) concluded from their pull-out tests that the failure mode changes from the punching shear failure to the general shear failure mode when D/D_{50} exceeds 7.5, where D is the diameter of the transverse bar and D_{50} is the particle size of the back fill soil corresponding to the 50 % finer particle size. Therefore, load transfer between soil and grid reinforcement by the passive soil depends on the geometry of the reinforcement, the type of soil and the confining pressure.

To study the failure mechanism of ribbed reinforcement, Irsyam (1991) performed a series of tests using steel ribs in Ottawa sand. In this chapter the direct shear test instrumented in the laboratory by Irsyam (1991) will be analyzed by using the finite element method to understand the soil-reinforcement interaction behavior. Irsyam's direct shear tests using the ribbed reinforcement were chosen to investigate the interface behavior between soil and ribbed steel reinforcement. The behavior of the ribbed reinforcement in the direct shear test is dominated by passive resistance. The finite element method is used to examine the effects of ribs on this passive resistance development and the mechanism of failure adjacent to the ribs. Comparisons between the measured and the simulated strain patterns, failure modes and load-displacement relationship are presented. The behavior of

the ribbed reinforcement in a cohesive soil will be predicted based on a good agreement between the measured and the predicted behavior of the Ottawa sand.

4.2 Experimental Configuration

The shear stress-strain relationship developed along the soil-reinforcement interface is commonly obtained from a direct shear box and/or a pull-out box test. However, no test method can measure the two mechanisms of the passive soil and the frictional soil resistance independently. The contribution of passive resistance may be affected by several factors: geometry of the reinforcement, stiffness of the reinforcement, density of the soil, grain size, grain shape and normal stress. The geometry of the reinforcement includes major factors such as rib geometry, rib spacing and surface roughness.

The influence of geometry of the reinforcement was reported by Chang et al.(1977) who carried out a pull-out test using a mesh steel reinforcement in sand. The passive soil resistance contributed about 90% of the total pull-out resistance measured. Therefore, it is important that the behavior of the passive resistance be understood for interface modeling in the finite element method.

The direct shear tests, using ribbed reinforcement, were executed to understand the behavior of soil particles and the load transfer mechanism between soil and steel ribs (Irsyam, 1991). The testing apparatus was a modified direct shear test device having a size of 267 mm x 140 mm x 76 mm high as shown in Figure 4.1. This system included an electronic data acquisition system and video camera to view the enlarged in-rarib zone on a large monitor. The direct shear box was constructed with Plexiglas walls to facilitate visual observation of grain structure during shearing. Grains of sand were colored to allow movements of select individual grains to be followed and tracked on a large monitor. A carbowax solidification procedure was adopted to verify visual observations, actual measurement of void ratio and identification of failure surfaces. The technique utilized hot

wax injected through a 0.12 cm hole at the base of the ribbed reinforcement. Copper tubes carried out hot water through the plate to prevent wax solidification, and cool water to rapidly solidify the wax. Total shearing resistance was measured by a load cell and the relative horizontal displacement of the plate to the box was recorded by two LVDTs attached to the reaction plate. More detailed description of the technique can be found in Irsyam (1991).

To investigate the effect of rib spacing of the reinforcement on the passive soil resistance, spacings of 0.00, 0.5, 1.52 and 3.3 cm. were used. The experimental work was performed using Ottawa sand which was categorized as a uniform sand with coefficients of uniformity, C_u between 1.10 and 1.30. More detailed soil properties will be discussed in Section 4.2.1. A normal stress of 34.4 kN/m^2 was applied at the top of the loading plate. The tests were conducted by displacement control with a constant rate of base plate displacement.

4.2.1 Soil properties

All soil samples were prepared by a raining method and the desired relative density of the soil was achieved by varying the height of the drop. To have a uniform height of drop for the dense condition, the sand was rained through a 19.05 cm high plastic pipe. For the dense condition of the Ottawa sand, the height of the drop was 21.59 cm which gave a void ratio of 0.52. Individual colored sand grain movement was traced on a large monitor to identify the failure surface during the test. D_{50} of the soil was 0.78 mm which was considered to be too small to visually observe individual particle rolling. Therefore a carbowax solidification technique was adopted to verify the visual observations.

In modeling the experiment using the finite element method, the stress-strain relationship of the Ottawa sand is required. However, this data was not published by Irsyam (1991). Triaxial compression test results of the Ottawa sand can be found in

Holubec (1968). The void ratio of 0.55 corresponds to a dense condition of the Ottawa sand. As shown in Figure 4.2, the stress-strain relationship for Ottawa sand can be simulated using the hyperbolic elastic model originally proposed by Chang and Duncan (1969). Many versions of the hyperbolic elastic model have been developed with the most common version based on Young's modulus and Poisson's ratio as the primary material parameters. Detailed procedures of the hyperbolic model for obtaining the input parameters from the triaxial test can be found in Duncan et al.(1980). Model parameters derived from undrained triaxial tests of the Ottawa sand and their particle sizes are listed in Table 4.1. The triaxial compression test is simulated by the finite element method using the model parameters listed in Table 4.1. The stress-strain curves given by the hyperbolic elastic model are compared with the experimental results as shown in Figure 4.2. Volume changes are also compared with the experimental results in Figure 4.2. Under small confining pressures, the predicted behavior of the Ottawa sand are in good agreement with the experimental results. The ribbed steel reinforcement can be modeled using an elastic model under the small strain conditions. The material properties of the steel reinforcement are also listed in Table 4.1.

4.2.2 Finite Element Modeling

Irsyam carried out direct shear tests in a 267 mm x 140 mm x 76 mm direct shear box using the ribbed steel reinforcement in Ottawa sands. For a rib height and width of 2.5 mm, the spacing was selected to be 33 mm for dense Ottawa sands which were prepared at a void ratio of 0.51. A normal stress of 34.5 kPa was applied on the top plate. Several rib spacings were tested to investigate the effect of rib spacing. If the rib spacing is small, the shear failure surface can not be completely formed and therefore reduces the overall passive resistance. The rib spacings of 33 mm, 15 mm and 0 mm are chosen for the finite element analysis.

The average grain size (D_{50}) of the Ottawa sand was 0.78 mm. When it was compared with the height of rib, 2.5 mm, only three times the grain diameter equaled the height of the rib. In practice, the effect of grain size can not be evaluated by the conventional finite element method but can be studied using the discrete element method. If the grain size is much larger than the rib size, grains will override the ribs and a passive zone on the shear failure surface will fail to develop. To investigate the behavior of the soil in detail, a fine mesh was used around the bottom of the plate as shown in Figure 4.3.

The finite element mesh for the shear box test constitutes 684 soil elements and 98 ribbed steel reinforcement elements using a total of 2274 nodes. Soil and reinforcement elements were modeled using a 8 node element. Usually the behavior of the interface between the soil and the reinforcement should be simulated using an interface element because the relative displacement or shearing would occur between the interface. According to the observed shear failure surface around the ribs after one rib spacing of relative displacement, the failure surface was fully developed immediately above the ribs. Slippage was not observed at the interface between the soil and the reinforcement. For the zero rib spacing case, slippage will be expected between soil and steel. Hence, a thin thickness interface is used to simulate the shearing in the horizontal direction between soil and steel.

In the hyperbolic model, the soil modulus is a function of the confining stress. If the confining stress becomes zero or negative, the calculated soil modulus will be incorrect. When the ribbed reinforcement was pulled out, tensile stresses developed around the ribs. In addition, tension zones were formed behind the ribs under small displacements, which gave incorrect stress values due to incorrect stiffness calculation based on the hyperbolic model. To overcome the tension zone problems soil modulus in the tension zone were assigned to a small value, set at 1% of the rebound soil modulus. To relieve the tension behind the ribs, the nodes between the soil and behind the ribs are made to move together in the vertical direction, i.e., they were constrained to have the same vertical displacement.

Because slipping was not observed between the soil and the plate, the boundary nodes between the soil and the plate moved together in the horizontal direction. Other boundary conditions can be found in Figure 4.3.

In the experiment, shear failure surfaces started to form after a relative displacement of 0.25 cm, and completely formed at a rib spacing displacement of 3.3 cm. The latter displacement is large compared with the dimensions of the experimental devices. Large displacement problems can not be dealt with using a small displacement finite element model. However, as shown in the plot of the shearing resistance against relative displacement in Figure 4.4, the relative displacement for peak shearing resistance was small, which can be analyzed using the small displacement finite element formulation. As the displacement of the reinforcement is increased, the tension zone behind the ribs extended rapidly which causes numerical difficulties. The maximum total displacement of the reinforcement in the finite element model is 0.3 cm after 6 modeling steps. Forces are applied in the numerical model by applying horizontal displacements on the right side of the steel plate.

4.3 Numerical Results and Discussions

4.3.1 Shearing Resistance versus Relative Displacement

The main objective of the direct shear test is to obtain shearing force versus relative displacement curves which can be used to evaluate the interaction between soils and reinforcement. As shown in Figure 4.4 some shearing resistance was mobilized at zero relative displacement, which is interpreted to be the frictional resistance between the direct shear box and the roller supporting the testing device. This shearing resistance acting outside of the shear box could be neglected because the analysis deals with the behavior inside the shear box and interaction behavior between the soil and the reinforcement.

Therefore, the shear force versus the relative displacement curve was moved to the origin as shown in Figure 4.5

Figure 4.5 shows the calculated and observed shearing resistance against relative displacement in the direct shear test. For this test the Ottawa sand was prepared at a void ratio of 0.51 and a normal stress of 34.4 kPa was applied. The ribs were 2.5 mm high, 2.5 mm wide and spaced 3.3 and 1.5 cm apart.

During the first 0.025 mm of relative displacement a relatively high shearing stiffness was observed when inter-granular shear stresses were developed. After some relative displacement, frictional resistance in the sand was built up as the grains hindered further movement. While the frictional resistance was building up, and the grains pushed or slid along, various magnitudes of inter-particle forces were generated at contact points within the assembly of the soil particles. Continuous shearing changed the grain position and prompted the grains to slide into a new position of equilibrium in directions offering the least resistance to shear. The least resistance to shear could be achieved through dilation of the sand or volume expansion after the relative displacement for the peak shearing resistance.

During the first initial 0.25 cm of relative displacement the observed shearing resistance has reached a peak value and, therefore, the numerical analysis was carried out for the first 0.3 cm of relative displacement. Figure 4.5 shows the comparison of the results of several analyses and the experimental observations. As expected the elastic analysis shows very stiff response. It was observed that there was a zone of relatively high dilation around the ribs and a zone of relatively high shear strain at the top of ribs in the dense sand at small displacement. These zones might be extended as the relative displacement increased; eventually they formed the shear failure surfaces at a relative displacement of 0.25 cm.

For the elastic-plastic models, the Mohr-Coulomb material with associated flow rule shows stiff response at small displacement before yielding occurs. As the relative

displacement increases, the calculated response diverges from the observed response. The force-displacement relationship using the elastic-plastic model is larger than that observed at small displacement. However, these values are much less than those observed at large displacements.

The results of the analysis using the hyperbolic model showed better agreement with the observed response. The predicted response give a good agreement until the relative displacement reaches 0.3 cm. Because the ribbed steel plate was very stiff, the shear failure surface was almost formed at a small relative displacement.

During pull out of an extensible grid reinforcement, the shearing forces were transferred to the bearing members and frictional resistance developed along the longitudinal members. Due to the elongation of the extensible grid reinforcement, the mobilization of the shearing resistance for different bearing members along the reinforcement varies. Only a certain part of the reinforcement might move relative to the backfill. Therefore, the maximum shearing forces are controlled by the strength of the reinforcement itself. However, the ribbed steel reinforcement would move the whole length of the reinforcement as a rigid body, and the maximum shearing resistance might be controlled by the soil strength or the soil and the reinforcement interface strength.

The steel plate without ribs was also analyzed to evaluate the effect of the ribs using the same input parameters as the ribbed reinforcement. Shearing occurred at the interface between the soil and the plate in this case. The frictional resistance of the steel plate without ribs can be estimated using a proper shear stiffness of the interface element based on the assumption that the shear failure surface of the steel plate without ribs will develop along the steel plate. The interface between the soil and the reinforcement was simulated using a thin interface four-node quadrilateral element which has resistance in compression and in sliding. The shear and normal stiffness for the interface element were adopted as 5000 kN/m^3 and 10^{10} kN/m^3 , respectively. Unfortunately, the shear force-displacement curves for the plate without ribs were not published by Irsyam (1991). However, the shear

force-displacement relationships without ribs in the dense sand are compared with those with ribs in Figure 4.16. The different shear force between the two curves is due to the passive soil resistance on the ribs. It is well known that the ribs of the reinforcement can significantly increase the shear resistance.

Shear forces of the steel plate without ribs contributed the frictional resistance along the reinforcement. The shear failure surfaces of the steel plate without ribs are expected to be different from those of the ribbed plate. Figure 4.6 shows the mobilized shear strain at the interface between soil and the steel plate at the relative displacement of 0.3 cm. The shear strain of soil is concentrated at the interface between soil and plate and propagated along the interface. This indicates that the sand is sheared along the plate without developing the passive zone, therefore, the shearing resistance consists of frictional resistance only.

The presence of the ribs can significantly change the soil behavior at the interface. To investigate the effect of the rib on the stress at the interface, the nodal point located behind the rib in the center of the plate is selected. Figure 4.7 and Figure 4.8 show the state of stress by the Mohr circle at soil nodal point 294 for the steel plate without ribs and with ribs at the relative displacement of 0.3 cm, respectively. For the ribbed steel plate the mobilized shear stress is less than that of the plate without ribs. It is interesting to note that the presence of the ribs can also change the normal stress as shown in Figure 4.7 and Figure 4.8. As the relative displacement is increased, the soil on the back of the ribs becomes loose which resulted in the development of a compressive soil arch between the top of the rib and the plate base. This arch effect reduced the normal stress for the ribbed steel plate. Therefore, the presence of the ribs can alter the shear failure surface and the shear resistance.

4.3.2 Shear failure surface

The observed failure surface during the shearing process was strongly dependent on the spacing of ribs for a rib height of 2.5 mm. For a larger rib spacing of 33 mm, a full passive soil wedge was developed at the face of each rib. Although the entire zone between the adjacent ribs could not be captured optically, it was evident that the failure surfaces dipped below the tops of the ribs and in some cases scraped the base of the plate. A typical failure pattern for rib spacing of 33 cm was initiated above the top of the ribs, touched the base plate, and continued to the rear face of the previous rib. For a small rib spacing of 15 mm soil grains became trapped between the ribs. The failure surface in such cases was flat, horizontal and immediately above the ribs, which means that for small rib spacing the large portion of the shearing resistance is due to frictional resistance of the soil. Small passive zones could develop for a rib spacing of 1.5 cm. The failure surfaces for the 3.3 cm and 1.5 cm rib spacing were shown in Figure 4.9. The frictional resistance developed was partially along a soil-soil interface and partially along the soil-top of the ribs interface.

These failure patterns could provide an explanation for the test conducted by Palmeira and Milligan (1989) who varied the spacing of the transverse members of reinforcement in the pull-out test. As the spacing of transverse members decreased, the maximum pull-out resistance became smaller. The contribution of passive resistance to the total shearing resistance was a function of the rib spacing. There might be an optimum spacing of the transverse members for reinforcement for which the passive resistance can be fully developed during the shearing process.

In addition to the 3.3 cm rib spacing, a 1.5 cm rib spacing was analyzed to investigate the effect of rib spacing on the failure surfaces. The predicted shear failure surface for the 3.3 cm rib spacing from the finite element analysis at the relative displacement of 1.2 mm is presented in Figure 4.10. The Mohr-Coulomb failure criterion was used to determine the failure condition of the soil. If the normal stress and the shear stress at a certain point are known, the failure condition can be evaluated by the Mohr-Coulomb failure criteria as follows:

$$\tau=c+\sigma \tan \phi \quad (4.1)$$

where τ and σ are the normal and shear stress and; c and ϕ are the cohesion and friction angle of the soil respectively.

The failure ratio is defined as the ratio of the failure shear stress to the mobilized shear stress. Shear failure surfaces could be determined by a failure ratio of 1. The predicted shear failure surface was in a good agreement with the observed shear failure surface at the rear part of the failure surface where the passive resistance was considered to be mobilized after a certain displacement. However, in the first part of the shear failure surface where the friction was the dominate resistance, the predicted failure surface formed above the observed one. According to the observed shear failure surface, the failure surfaces were completely formed at a relative displacement of 2.0 cm which corresponds to the residual shearing resistance in the shear force-displacement response. The complete formation of a failure surface might be associated with the establishment of a constant residual shear resistance. However, the shear failure surface started to form at a small relative displacement of 1.0 mm, and the peak shearing resistance was reached at a displacement of 2.5 mm. Therefore, the predicted shear failure surface at a relative displacement of 1.2 mm could reasonably predict the shear failure surfaces.

The predicted shear failure surfaces for the 1.5 cm rib spacing is presented in Figure 4.11. The predicted shear failure surfaces were in a good agreement with the observed shear failure surfaces. The predicted shear failure surfaces at the center of the ribs are adopted in order to minimize the effect of the wall boundary conditions of the shear box. To investigate the effect of the rib spacing on the soil behavior around the ribs, the mobilized shear strain is compared in Figure 4.12 and Figure 4.13. The shear strain for the 1.5 cm rib spacing is highly mobilized above the ribs which corresponds to the shear failure surface. The strain distribution between adjacent ribs is different for both cases.

For the rib 1.5 cm rib spacing, the soil between adjacent ribs is trapped and moves together as shown in Figure 4.13. However, the mobilized shear stress shows similar distributions above the 2.0 rib heights from the plate base, which is not dependent on the rib spacing as shown in Figure 4.14 and Figure 4.15. It indicates that the rib spacing can affect the stress distribution between adjacent ribs and for one height of a rib above the top of the rib.

According to the shear failure surfaces for 1.5 cm rib spacing, shear forces consist mainly of the frictional resistance due to soil-soil friction and partially of the passive soil resistance for the 1.5 cm rib spacing. For the 3.3 cm rib spacing, the passive soil resistance is mobilized at the rear part of the failure surface. Therefore, it is expected that the total shear forces for the 3.3 cm rib spacing are larger than those for the 1.5 cm rib spacing because of the passive soil resistance which can be fully developed for 3.3 cm rib spacing. Figure 4.16 shows the shearing resistance-relative displacement curves for varying the rib spacing. The contribution of the passive soil resistance to the total shear resistance is a function of rib spacing. Thus, the total shear resistance of the 3.3 cm rib spacing is expected to be larger than that of the 1.5 cm rib spacing. As shown in Figure 4.16, the total shear resistance at small displacements is identical. As the relative displacement increases, the total resistance for the 3.3 cm rib spacing is slightly larger than that of the 1.5 cm rib spacing. Usually frictional resistance needs small displacements to be fully mobilized while passive soil resistance requires much larger displacements. Therefore, the frictional resistance for both cases is mobilized at small displacement, which causes the identical shear resistance. However, Figure 4.16 shows that after 0.15 cm displacement the passive soil resistance starts to mobilize and the total shear force for the 3.3 cm rib spacing is increased. The total shear resistance for the 1.5 cm rib spacing is due to soil-soil frictional resistance and partially due to the passive soil resistance. As the rib spacing becomes even smaller, the passive soil resistance disappears and the total shear resistance becomes smaller.

When the typical shear failure surface was compared with the failure modes of the

foundation, it was interesting to note that there was much similarity between the two failure modes. When the load on a foundation is increased, an ultimate value is finally obtained under which the failure state in the soil is reached and the penetration of the foundation is occur in a constant rate. In extreme conditions this uncontrolled penetration can be caused by a lateral and upward expulsion of the soil beneath the foundation. The first extreme case corresponds to the state of general shear failure, the second is a punching shear failure, and the combination of both is a local shear failure (Vesic, 1963).

General shear failure is characterized by a well-defined pattern of failure in which the soil adjacent to the foundation tends to heave and a shear surface is developed which extends from one edge of the foundation to the surface. In the punching failure the foundation penetrates the ground immediately beneath the foundation due to soil compression. The soil outside the immediate foundation zone remains unaffected. In the case of a local shear failure, shear wedge and slip surfaces develop at edges of the foundation and some heave of the adjacent soil occurs. Vertical compression is the more significant factor, and a slip surface only reaches the ground surface after appreciable foundation penetration has taken place.

It is interesting to note that the failure mode of the ribbed reinforcement was quite similar to the local failure mode of the foundation. The comparison of the two failure modes are made in Figure 4.17. Passive soil resistance is developed at the rear part of the failure surface, while the frictional resistance is mobilized at the initial part of the failure surface under small displacements. This indicates that the shear resistance mobilized by friction has reached a maximum; however, the displacement required to mobilize passive resistance is much larger. As a consequence, when both mechanisms are activated it is assumed that the frictional resistance is mobilized at small displacements and the passive soil resistance is predominantly mobilized at large displacements. It is not possible that the frictional resistance is not always completely mobilized before mobilizing the passive soil resistance. Figure 4.17 shows that the passive soil resistance governs the failure modes in

the foundation failure surface because the rear part of failure surface of the foundation is very similar to that of the ribbed reinforcement where the passive resistance is mobilized.

4.3.3 Grain Movement and Shear Zone

The tests were conducted on square ribs with a 3.3 cm rib spacing in the dense Ottawa sand. Figure 4.18 shows the observed grain movements after a relative displacement of 2.0 mm. The calculated grain movements for the 3.0 cm rib spacing at a relative displacement of 3.0 mm is presented in Figure 4.19. The calculated soil particle movement from the finite element analysis is obtained from the nodal points and shown in Figure 4.19 as a displacement arrow. Since dilation can not be modeled properly using the hyperbolic model, the upward movement observed in the experiment is not captured by the finite element model. This may have an effect on the mean stress developed which will result in a stiffer material. Some soil moves upward between ribs, and most soil moves in horizontal directions as shown in Figure 4.19. Figure 4.20 shows the calculated displacement arrow directions for the 1.5 cm rib spacing. The displacement arrows in Figure 4.19 is magnified 15 times. It is found that the spacing of the ribs can not significantly affect the calculated displacement patterns. However, for the plate without ribs the displacement patterns are different from those of the plate with ribs; the displacement arrows moving slightly upward are not found as shown in Figure 4.21.

During the first 0.25 mm of relative displacement shearing was observed in the sample. When shearing began, some grains would be pushed into new positions with little difficulty. The normal stresses acting in the direction of movement were small and the grains eventually took up positions which made further sliding more difficult. Continued shearing beyond the peak stress resulted in continuous loosening of a dilatant soil and a narrow shear zone developed above the ribs. The shear zone thickness changed gradually and grain deformation is localized into a narrower zone after reaching the peak

displacement. The zone of limiting equilibrium had expanded to the front and back of the rib which resulted in a longer zone of relatively high shear strain increment which could be viewed as shear failure surface formation.

For a dense sand, continuous shearing changes the void ratio and the thickness of the shear zone. After 0.25 cm of relative displacement a failure surface completely formed. Roscoe (1970) stated that the shear zone thickness is a small multiple of the mean grain size. It implies that the thickness of the shear zone is not affected by geometrical dimensions of the soil body. There was ample experimental evidence that shear zones in granular materials involve a significant number of grains (Usegi et al., 1988; Mulhasus and Vardoulakis, 1987; Yoshimi and Kishida, 1981). According to Roscoe's experimental observation in direct shear tests, the thickness of the shear zone is about 10 times the average grain diameter(D_{50}).

Holtz (1977) conducted pull-out tests on polyester fabric in dry sand at a relative density of 65%, and reported that during the pull-out test high, non-uniform deformation occurred in the fabric. It was observed that the maximum influence zone of the reinforcement was about 10 cm on either side of the reinforcement and seemed to be independent of the soil type and confining pressure. Jewell (1980) carried out the pull-out tests in sand using the radiographic technique and several types of reinforcement to investigate the interaction mechanisms. It is interesting to note that the thickness of the shear zone developed adjacent to the reinforcement, as a result of the reinforcement being pulled out, is not strongly dependent on the reinforcement types even though the displacement patterns around the reinforcement varies with reinforcement types.

However, Irsyam (1991) found in this test that the geometry of the ribs has influence on the shear zone thickness. When the trapezoidal ribs were used to investigate the effect of the geometry of the reinforcement, the trapezoidal ribs allowed soil grains to override from the front to the back of the rib. Hence, the trapezoidal ribs behaved merely as a rough surface, which influenced the shear zone thickness. It was found that the shear

zone thickness varied from 12 grain diameters to 6 grain diameter at the residual state during the first 0.25 cm of a relative displacement.

According to the shear strain distribution in Figure 4.12 and Figure 4.13, high shear strain is concentrated at the top of the ribs and it will be extended to form the shear failure surface during the shearing process. Small shear strain occurs between adjacent ribs and at a height of one rib away from the top of ribs. Therefore, it is concluded from the results of the finite element analysis that the shear zone thickness can be expressed in terms of the rib height and at two times the rib height.

4.4 Prediction of Cohesive Soil Behavior

The load transfer and stress distribution between reinforcement and granular soil have been extensively studied in the last two decades. Reinforcement can be used for construction of cost-effective earth structures when poor back fill soils are used for the reinforced soil structures. Therefore, it is necessary to study the load transfer between reinforcement and cohesive soil, especially for the shearing resistance by passive soil resistance on the transverse element of the reinforcement and by combined frictional and passive soil resistance.

As discussed in section 4.3, the direct shear test using a steel plate with ribs and Ottawa sand can be simulated by the finite element analysis. The calculated shear failure surfaces and load-displacement curves give a good agreement with the observed results. Thus, the analysis can be extended to the direct shear test using cohesive soil.

The most commonly used characteristics to classify soil are particle size and plasticity. The particle size of soil can not be simulated by the finite element analysis. The frictional angle of soil is affected by the size of the particle. Generally, clay particles are plate-shaped but granular soil particles are rounded or angular shaped. Therefore, the friction angle of the soil can be used to indirectly simulate the soil particle size. It was also

found from the direct shear test that the particle size was found to have insignificant effect on the shape of the failure surface for particles smaller than Ottawa sand (Irsyam, 1991). The plasticity of soil can be simulated by providing the soil cohesion. To compare the analysis results with the calculated results in Ottawa sand, the input data listed in Table 4.1 are used with the exception of the friction angle and cohesion of the soil. The friction angle of cohesive soil of 23° and cohesion of 25 kPa are used for the total stress analysis.

The relationship between shear force and relative displacement is almost the same as the calculated response for the 3.3 cm rib spacing in Figure 4.5. Figure 4.22 shows the displacement arrows at the nodal points which are more horizontal in direction than the displacement arrows of the Ottawa sand in Figure 4.19. The soil cohesion does not significantly change the displacement patterns. The mobilized shear strain is concentrated at the top of the ribs and propagated parallel to the top of the ribs as shown in Figure 4.23. The magnitude of shear strain is smaller than that of Ottawa sand at a relative displacement of 1.3 cm. The sheared zone for the cohesive soil is narrower than that of Ottawa sand. It is found that the distributions of shear stress for the cohesive soil is different from that of the Ottawa sand as shown in Figure 4.24. This implies that the thickness of shear zone is affected by soil types. The shear zone thickness of the cohesive soil is about 1.5 times the rib height based on the shear stress and strain distributions.

For the Ottawa sand, the shear failure surfaces have close similarity with the local shear failure mode of the foundation. Figure 4.25 shows the failure surface of the cohesive soil. The shear failure surface is developed parallel to the top of the ribs. However, it is different from the shear failure surfaces for the 1.5 cm rib spacing in Ottawa sand which is formed above the ribs. A large relative displacement of 0.6 cm is needed to completely form the shear failure surface. When compared with the failure mode of the foundation, the shear failure surface is closer to the punching shear failure mode rather than the local shear failure mode.

4.5 Conclusion

The main objective of this study is to investigate soil-ribbed reinforcement interaction. The calculated behavior of the ribbed reinforcement is compared with the measured behavior. The results of the finite element analyses are found to be in good agreement with measured behavior except for soil grain movement. The presence of the ribs in the reinforcement causes shearing resistance to increase and changes the distributions of stress and strain around the ribs. The load transfer mechanism between the ribbed reinforcement and cohesive soil was also investigated. The sheared zone for the cohesive soil is narrower than that of granular soil. The failure mode of the ribbed reinforcement can be affected by soil type. A punching shear failure mode occurs with cohesive soil.

4.6 References

- Chang, J.C., Hannon, J.B. and Forsyth, R.A.(1977) "Pull-out Resistance and Interaction of Earthwork Reinforcement and Soil", Transportation Research Board Record 640, National Research Council Washington, D.C.
- Duncan, J.M. and Chang, C.Y.(1970) "Nonlinear Analysis of Stress and Strain in Soils ", Journal of the Soil Mechanics and Foundations Division, ASCE, Vol.96, No.SM5
- Duncan, J.M., Byrne, P., Wong, K. and Mabry, P. (1980) " Strength, Stress-Strain and Bulk Modulus Parameters for Finite Element Analysis of Stresses and Movements in Soil Masses", University of California, Berkeley, Report No. UCB/GT/80-01.
- Holtz, R.D. (1977) "Laboratory Studies of Reinforced Earth using a Woven Polyester Fabric," Proceedings of the International Conference on the Use of fabrics in Geotechnics, Paris, Vol.3, pp.149-154.
- Holubec, I. (1968) "Elastic Behavior of Cohesionless Soil ", Journal of the Soil

- Mechanics and Foundation Division, ASCE, Vol.94, No. SM6, pp. 1215-1231.
- Huecke, S.M. and Kwasniewski, J. (1961) "Scale Model Tests on the Anchorage Values of Various Elements Buried in Sand", Proc. 5th International Conference on Soil Mechanics and Foundation Engineering, Paris, Vol. 2, pp. 431-434.
- Irsyam, M. (1991) **The Mechanical Interaction between Cohesionless Soil and Ribbed Inclusions**, Ph. D. thesis, The University of Michigan, 195p.
- Jewell, R.A. (1980) **Some effects of Reinforcement on the Mechanical Behavior of Soil**, Ph.D. thesis Cambridge University
- Jewell, R.A., Milligan, G.W.E., Sarsby, R.W. and Dubois, D.(1984) "Interaction Between Soil and Geogrids," Proceedings of Symposium on Polymer Grid Reinforcement in Civil Engineering, London, England, pp.18-30.
- Mulhaus, H.B. and Vardoulakis, I. (1987) "The Thickness of Shear Bands in Granular Materials, Geotechnique, Vol. 37, No. 3, pp.271-283.
- Palmeira, E.M., Milligan, G.W.E. (1989) "Scale and other Factors Affecting the Results of Pull-out Tests of Grids Buried in Sand," Geotechnique 39, No.3, pp.511-524
- Roscoe, K.H. (1970) "The Influence of Strains in Soil Mechanics ", Geotechnique, Vol.20, No.2, PP.129-170.
- Uesugi, M., Kishida, H. and Tsubakihara, Y.(1988) "Behavior of Sand Particles in Sand-Steel Friction" Japanese Society of Soil Mechanics and Foundation Engineering, Vol.28, No.1, pp.107-118.
- Vesic, A.S.(1963) " Bearing Capacity of Deep Foundations in Sand", Highway Research Board Record, No.39, National Research Council Washington, D.C.
- Yoshimi, Y. and Kishida, H. (1981) " Friction between Sand and Metal Surface ", 10 th International Conference on Soil Mechanics and Foundation Engineering, Vol.1, pp.831-834.

Parameter	Symbol	Ottawa 20-30	Steel Plate	Cohesive Soil
Elastic Modulus, kPa	E		1.00E+09	
Poisson's Ratio	ν	0.31	0.28	0.41
Cohesion, kPa	C	0		25
Modulus Number	K	126		
Modulus Exponent	n	0.85		
Failure Ratio	Rf	0.85		
Bulk Modulus Number	Kb	450		
Bulk Modulus Exponent	m	0.67		
Unit weight, kN/m ³	γ	18.9		
D50, mm		0.72		
Friction Angle, degree	ϕ	34		23

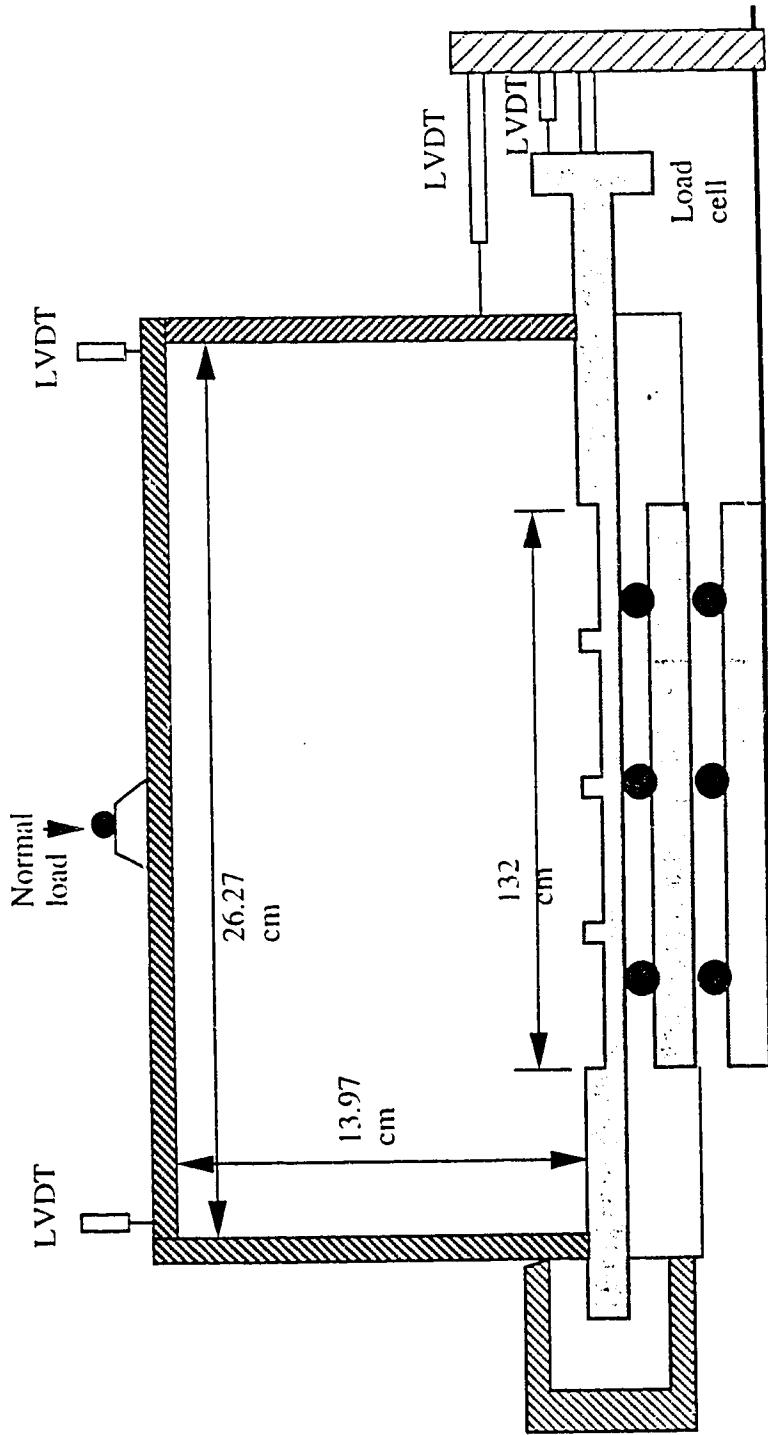
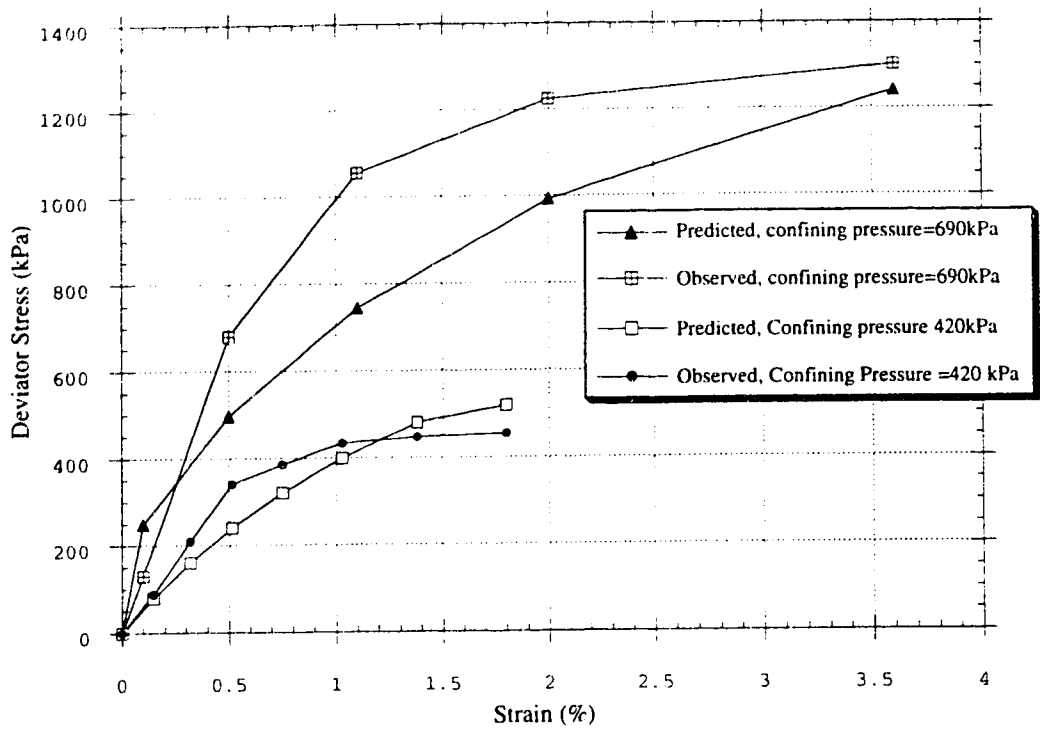
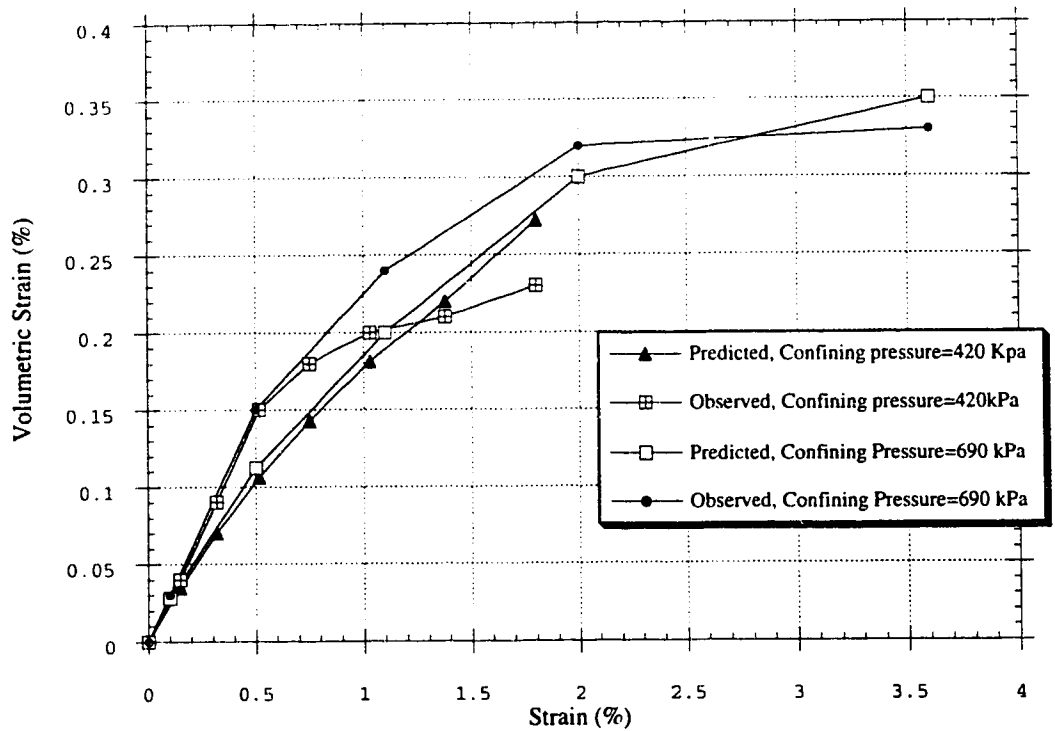


Figure 4.1 Direct Shear Device for Ribbed Reinforcement Testing (after Irsyam, 1991)



(a) Hyperbolic stress-strain curves compared with the experimental results



(b) Hyperbolic Volumetric strain curves compared with the experimental results

Figure 4.2 Hyperbolic Model Analyses Compared with Experimental Results

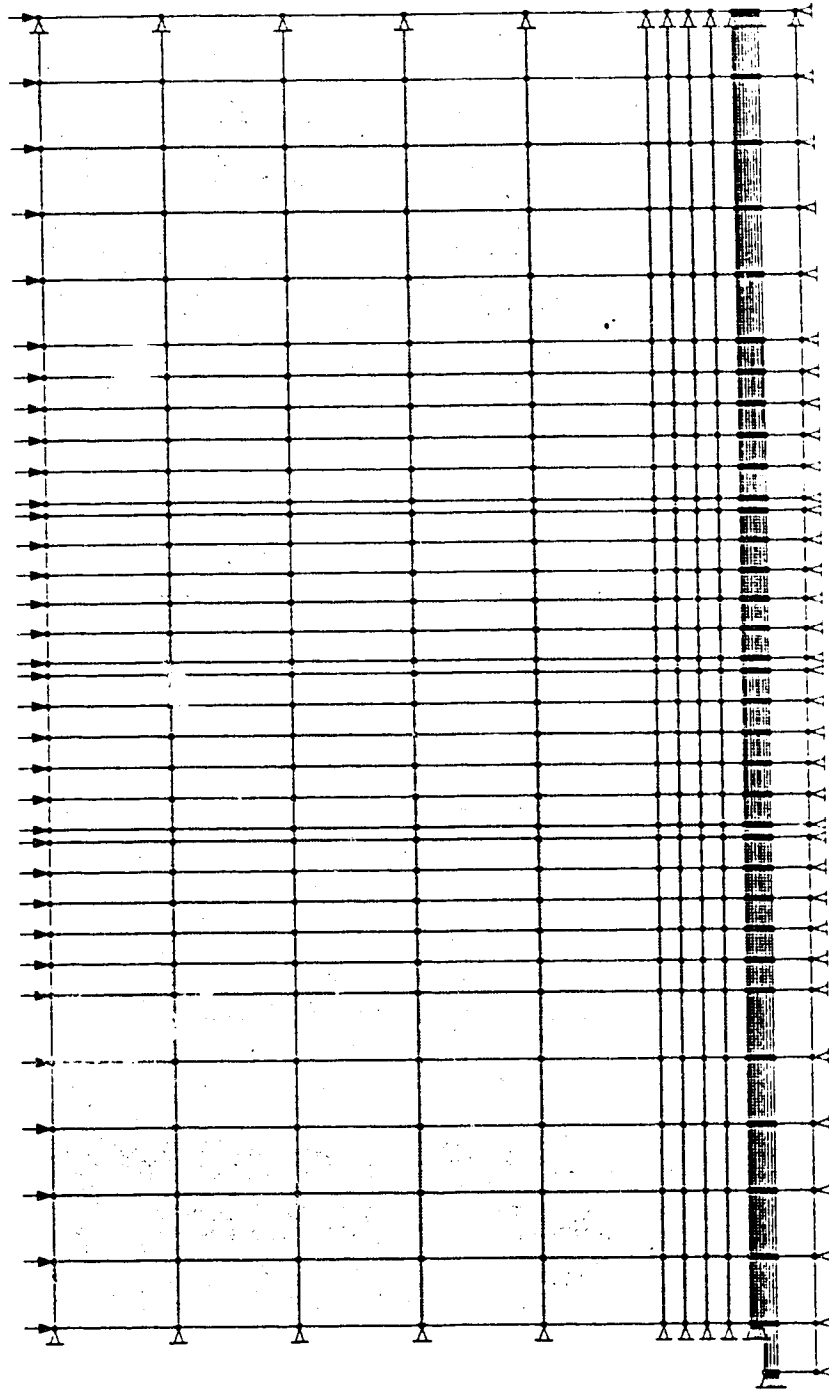


Figure 4.3 Finite Element Idealization of Shear Box

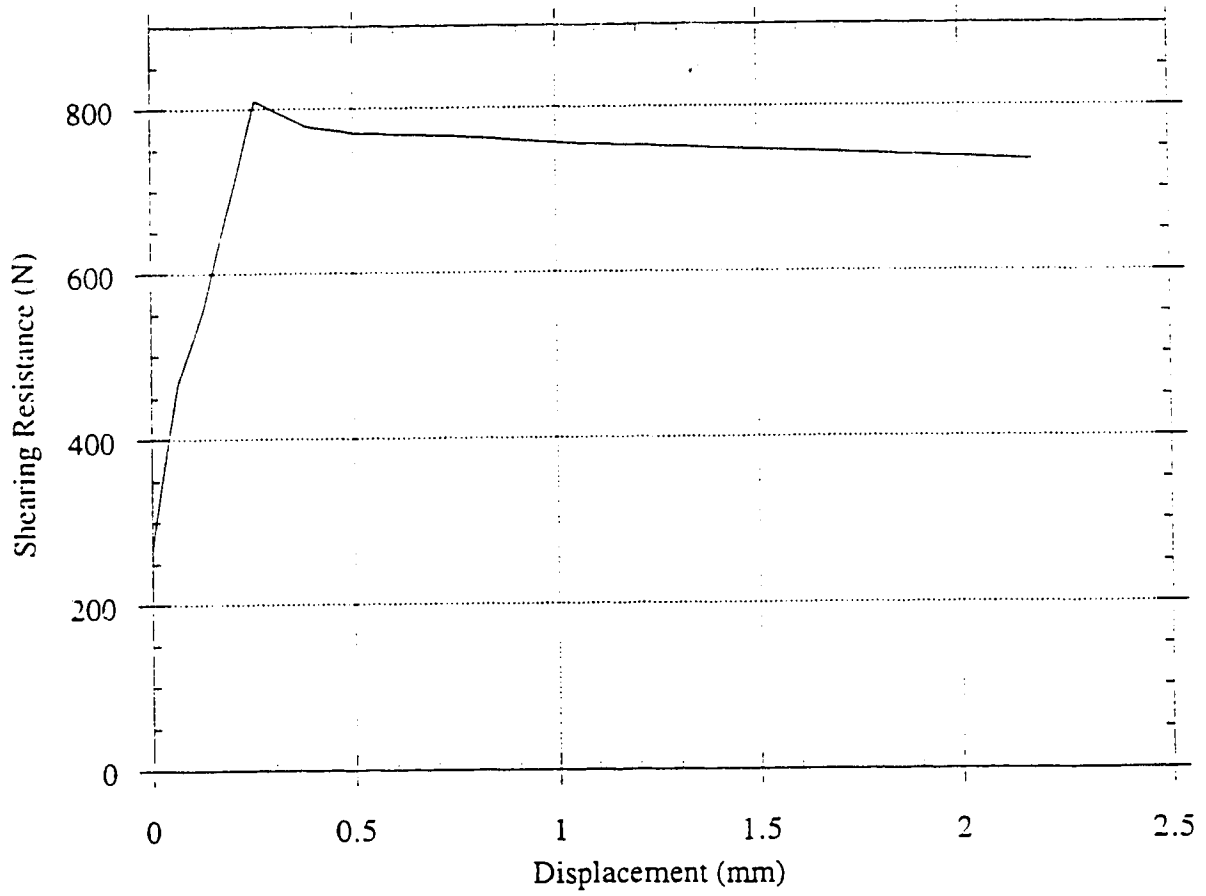


Figure 4. 4 Observed Shearing Resistance versus Relative Displacement, for 3.3 cm Rib Spacing (after Irsyam, 1991)

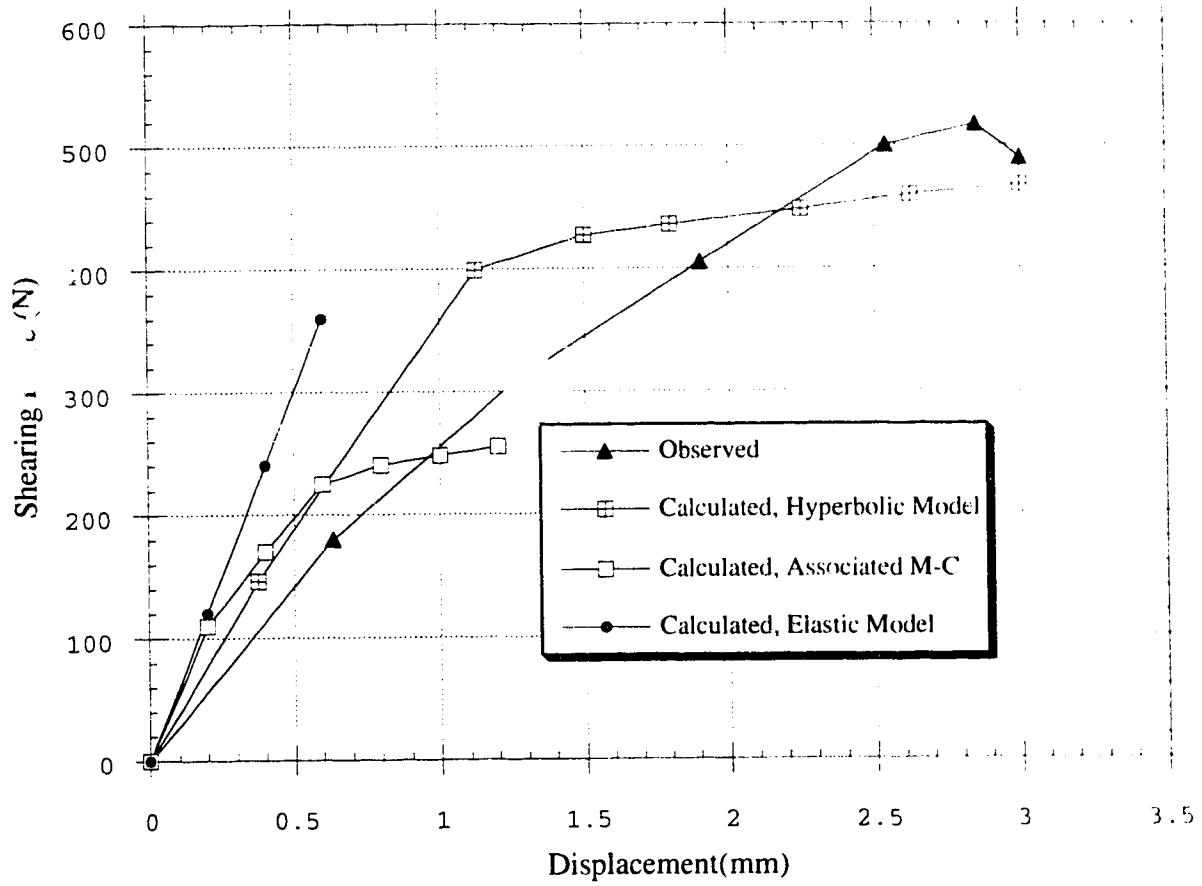
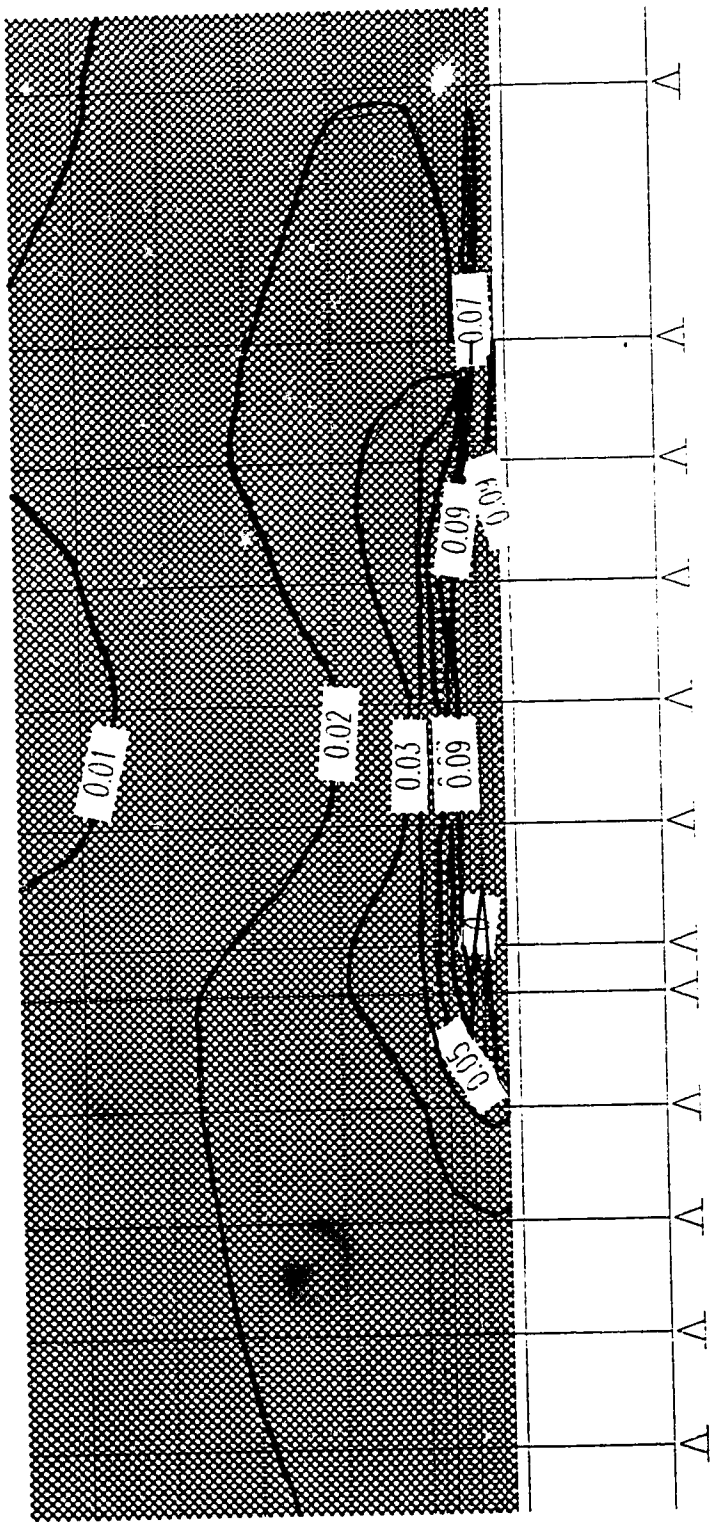


Figure 4.5 Observed Shearing Resistance versus Relative Displacement Compared with Calculated Response (Rib Spacing=3.3cm)



Shear strain (γ), $\mu\text{m/m}$, Inter

Figure 4.6 Shear Strain Distribution for Plate without Ribs

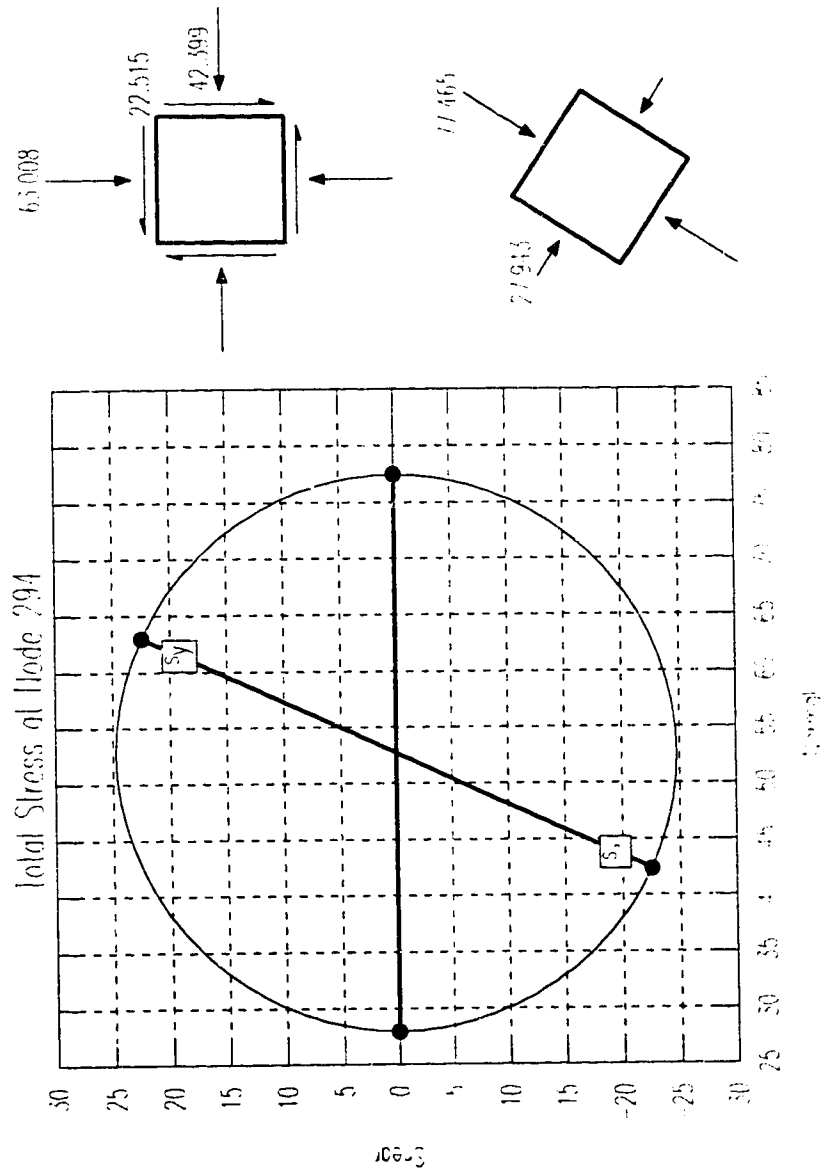


Figure 4.7 Mohr Circle for State of Stress at Nodal Point 294 for Plate without Ribs

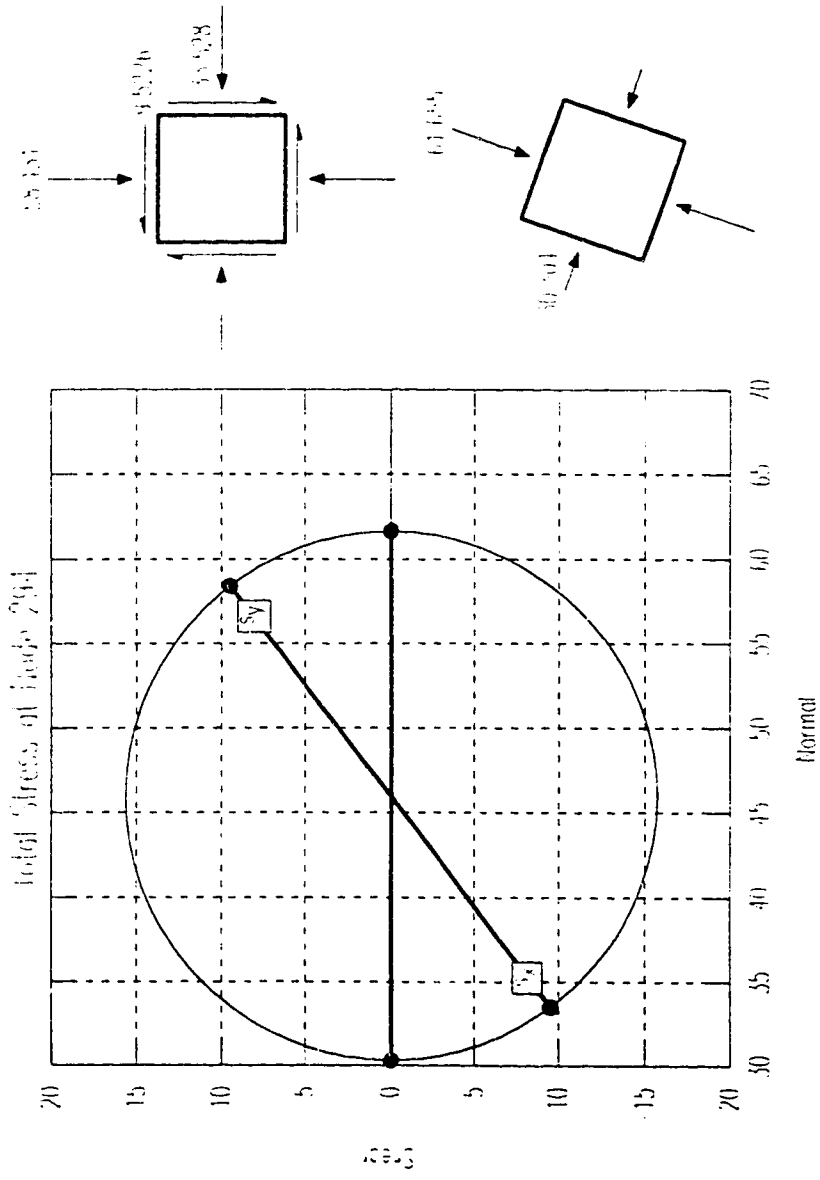


Figure 4.8 Mohr Circle for State of Stress at Nodal Point 294 for Ribbed Plate

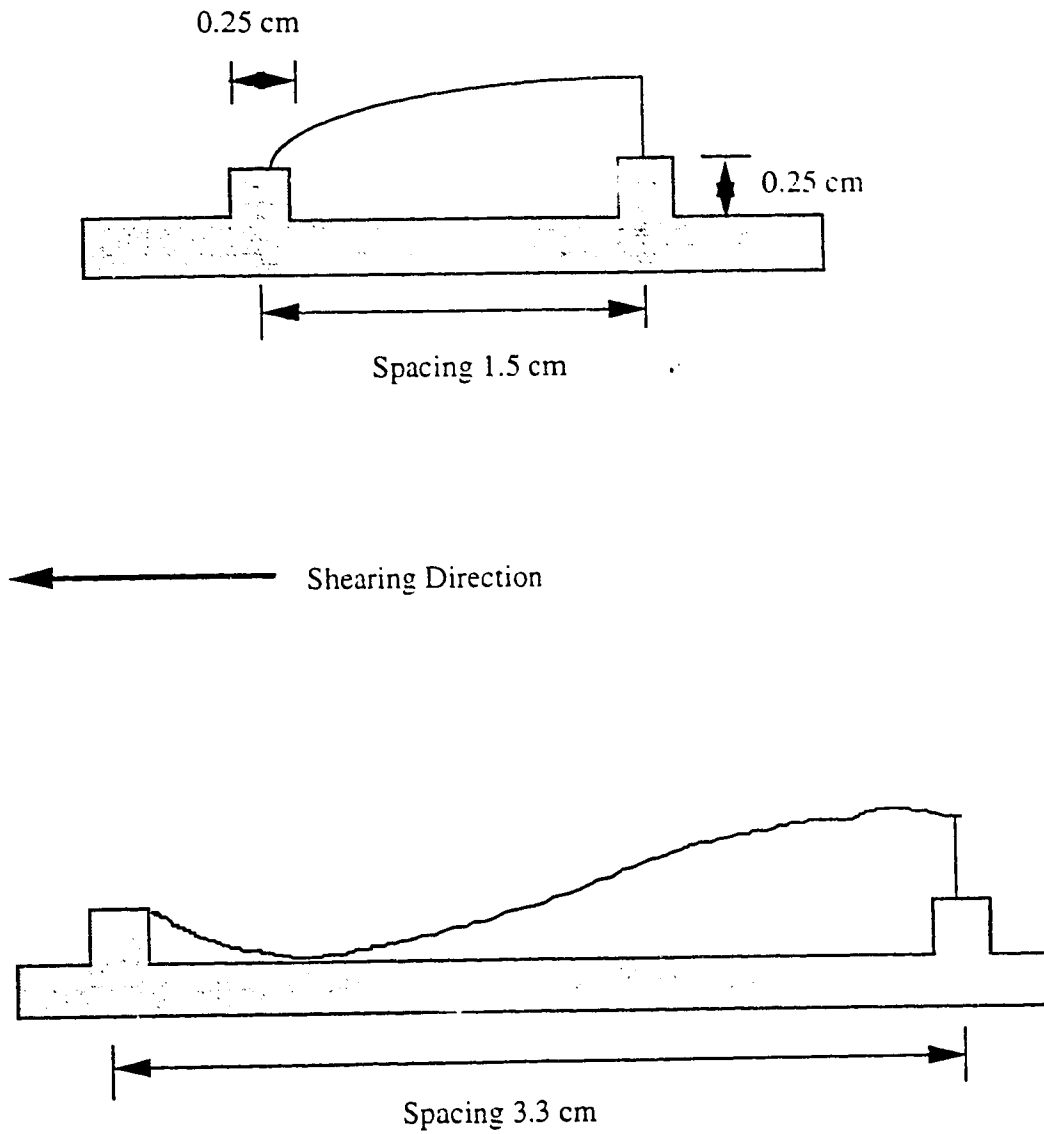
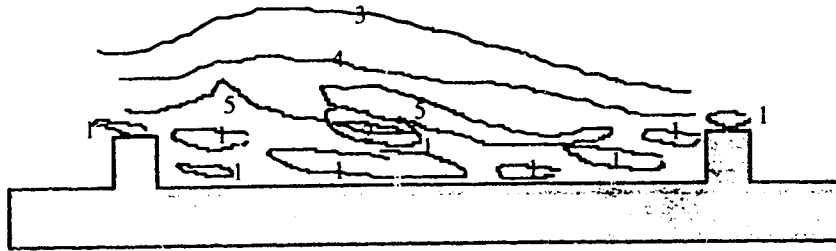


Figure 4.9 Effect of Rib Spacings on Failure Surfaces(after Irsyam,1992)

Legend

- 1 - 0.6
- 2 - 0.7
- 3 - 0.8
- 4 - 0.9
- 5 - 1.0 - Failure ratio



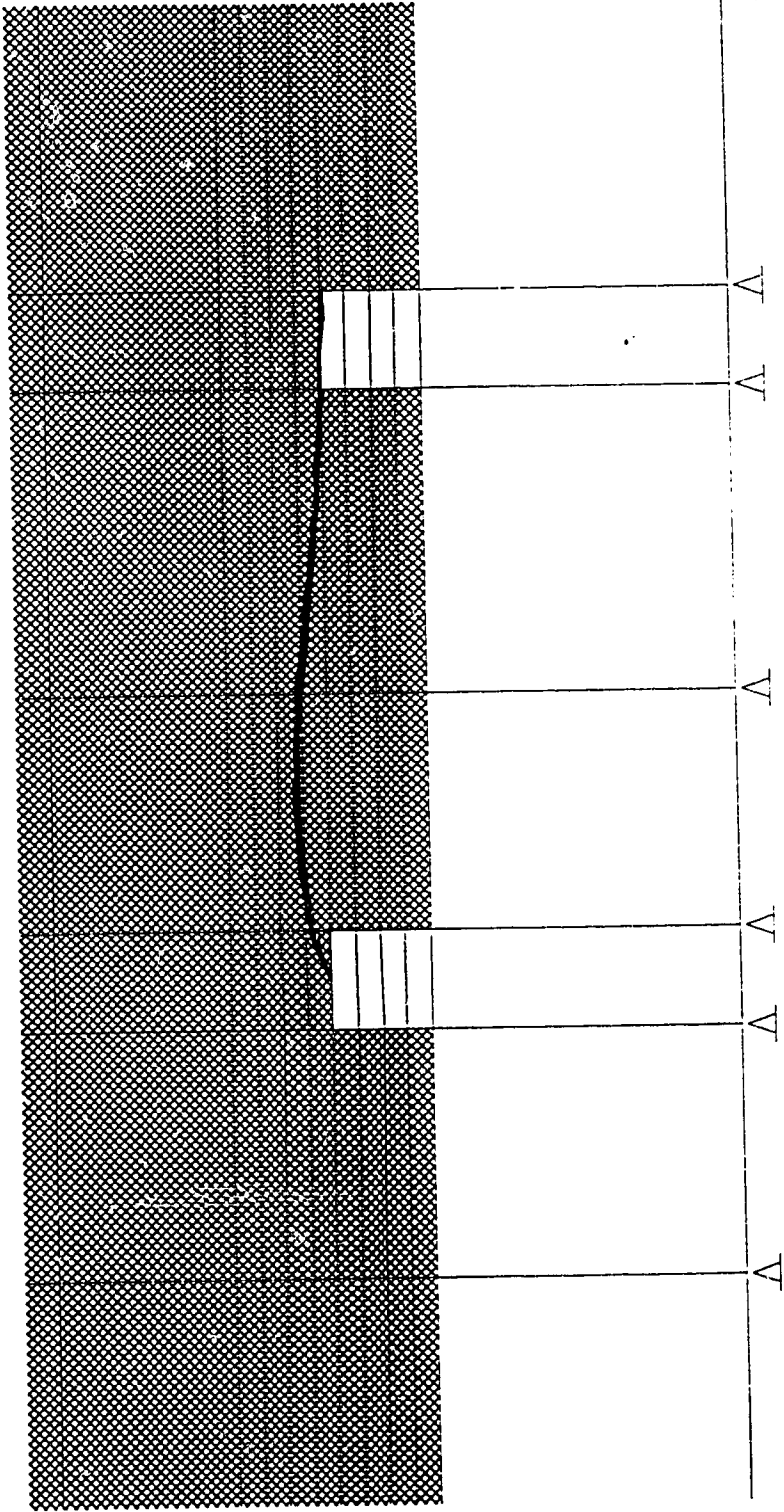
(a) Predicted failure surface, Displacement ,1.2 mm

→
Shearing Direction



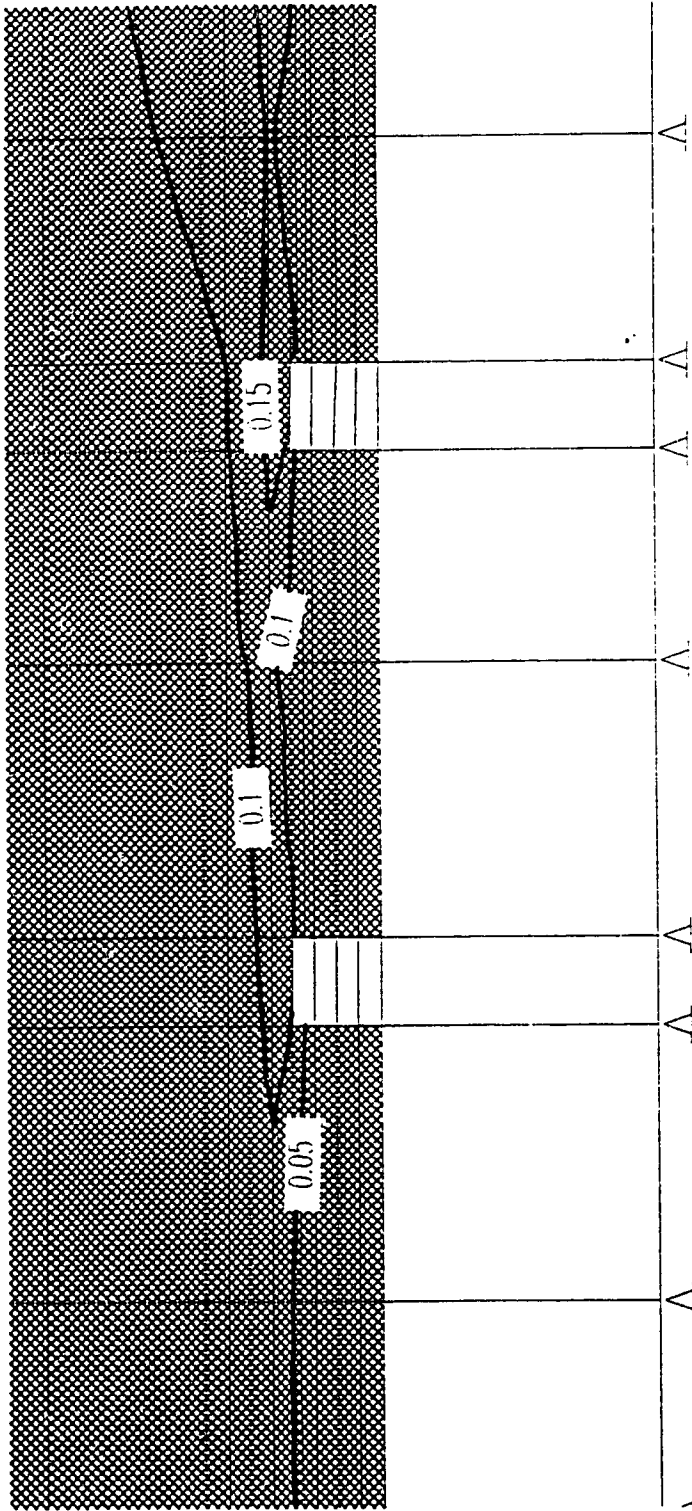
(b) Observed shear failure surface

Figure 4.10 Calculated Shear Failure Surface Compared with Observed Failure Surface (3.3 cm Rib Spacing)



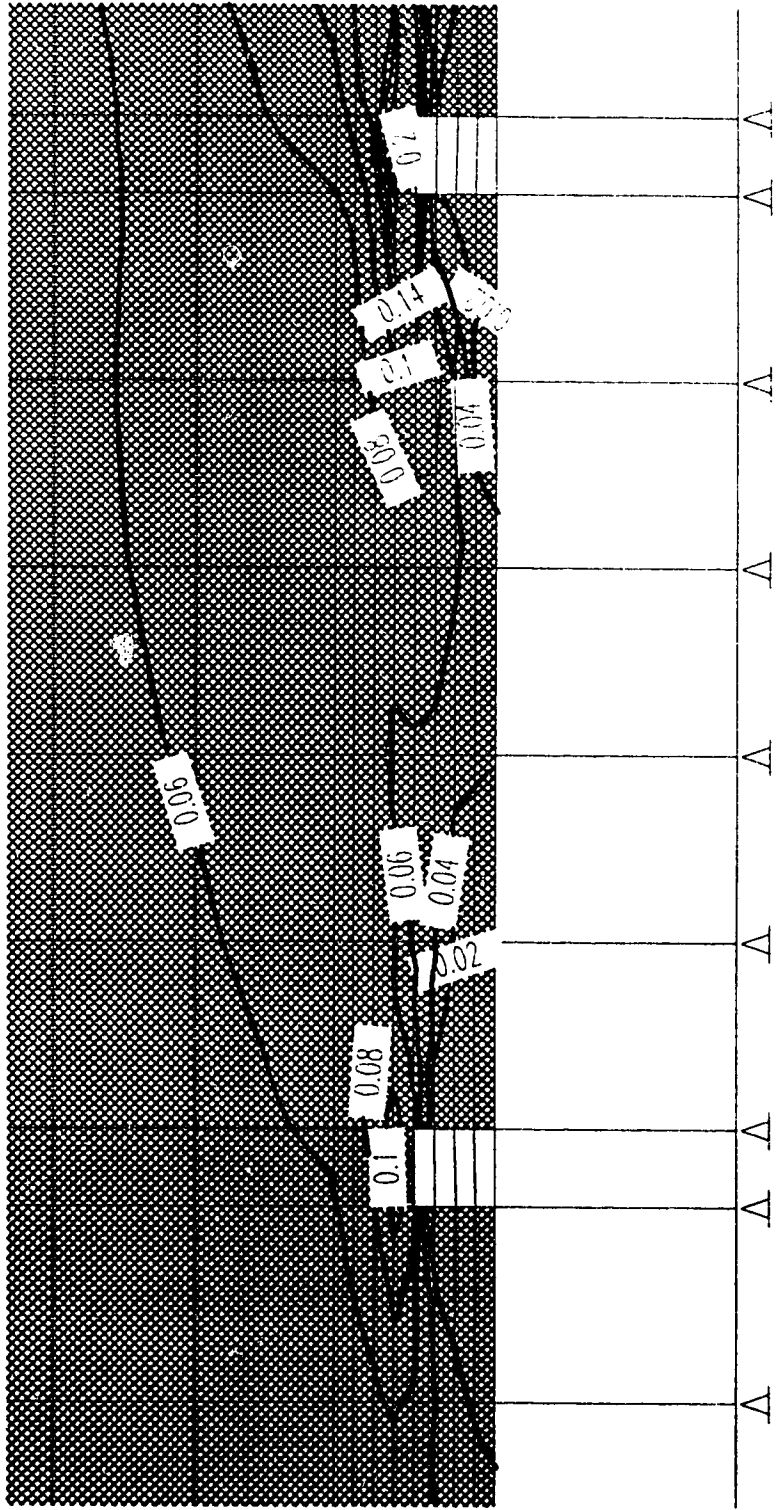
Failure Surface, Dis. = 0.3 cm, Rib Spacing = 1.5cm

Figure 4.11 Calculated Shear Failure Surface for 1.5 cm Rib Spacing (0.3 cm, Displacement)



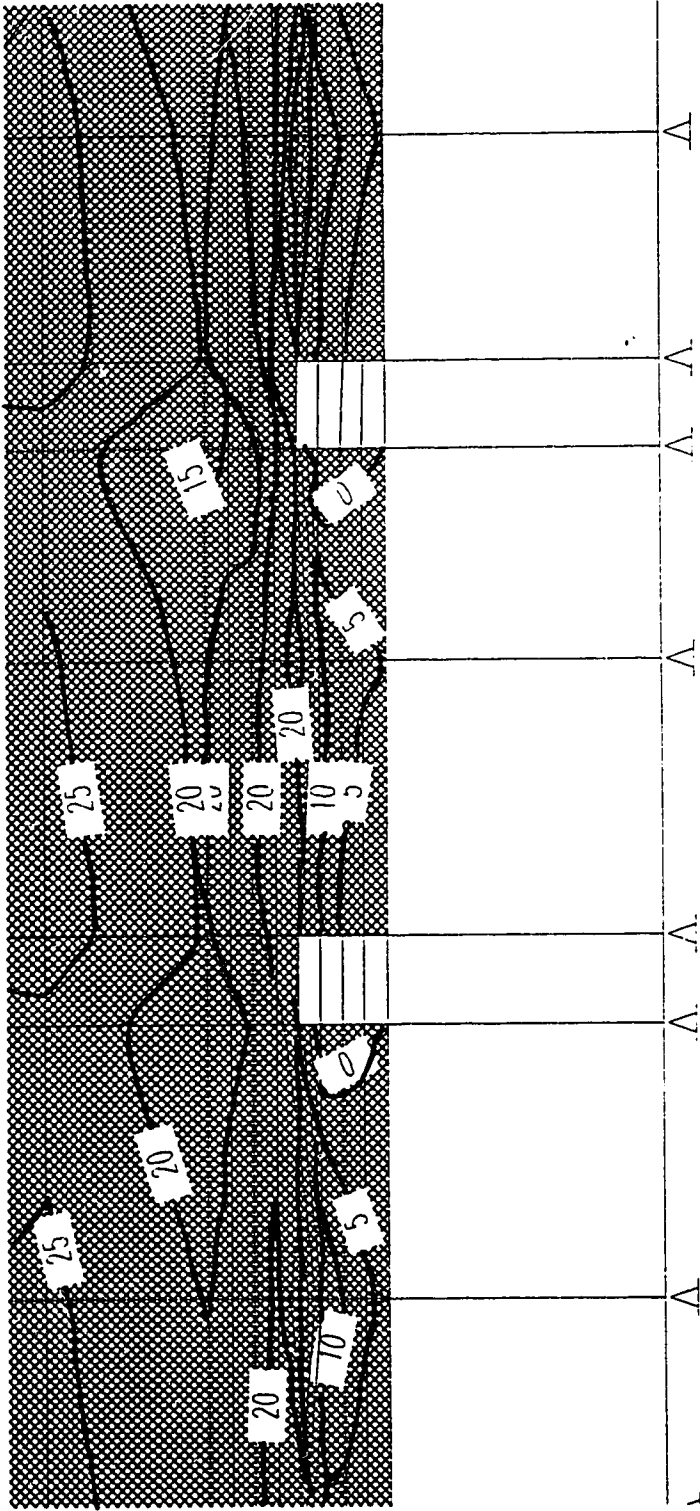
Shear strain, Dns (0.3 cm)

Figure 4.12 Shear Strain Distributions for 1.5 cm Rib Spacing (0.3 cm, Displacement)



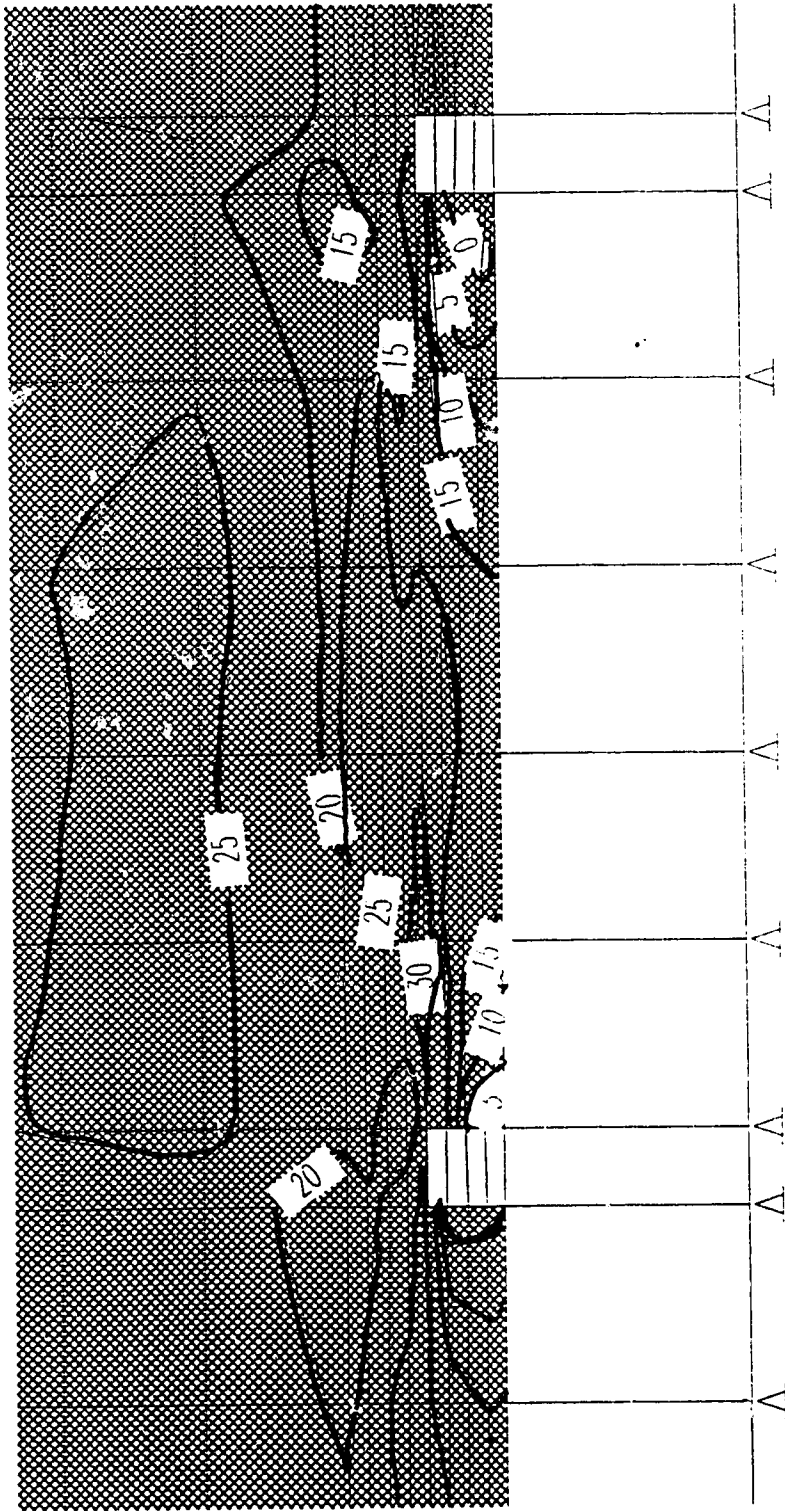
Shear strain Displ. 0.5 cm Ribspacing= 3.3 cm

Figure 4.13 Shear Strain Distributions for 3.3 cm Rib Spacing (0.3 cm, Displacement)



shear stress, Dis: 0.5 cm

Figure 4.14 Shear Stress Distributions for 1.5 cm Rib Spacing (0.3 cm, Displacement)



Shear stress, Displacement, Rib Spacing = 3.3 cm

Figure 4.15 Shear Stress Distributions for 3.3 cm Rib Spacing (0.3 cm, Displacement)

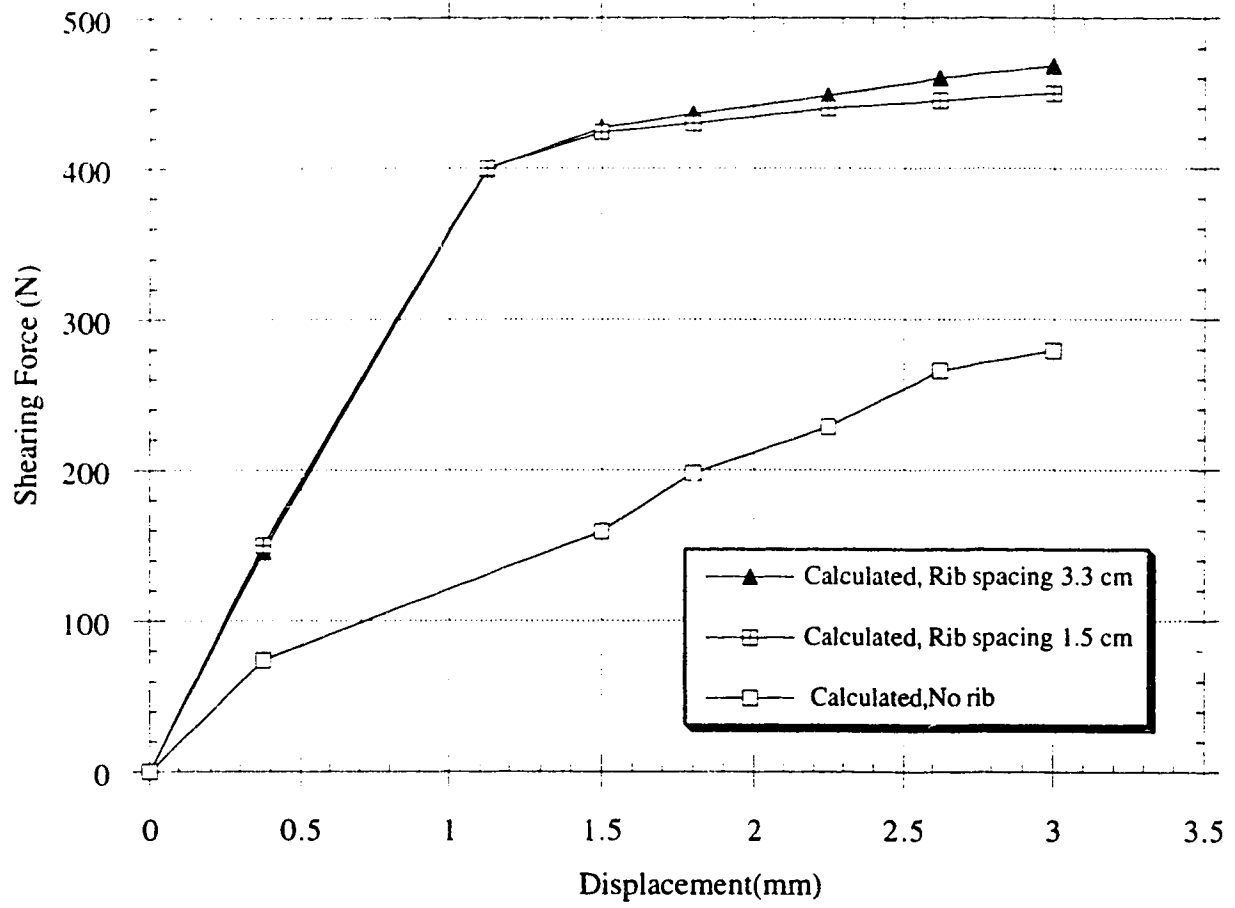


Figure 4.16 Effect of Rib Spacing on Shearing Resistance

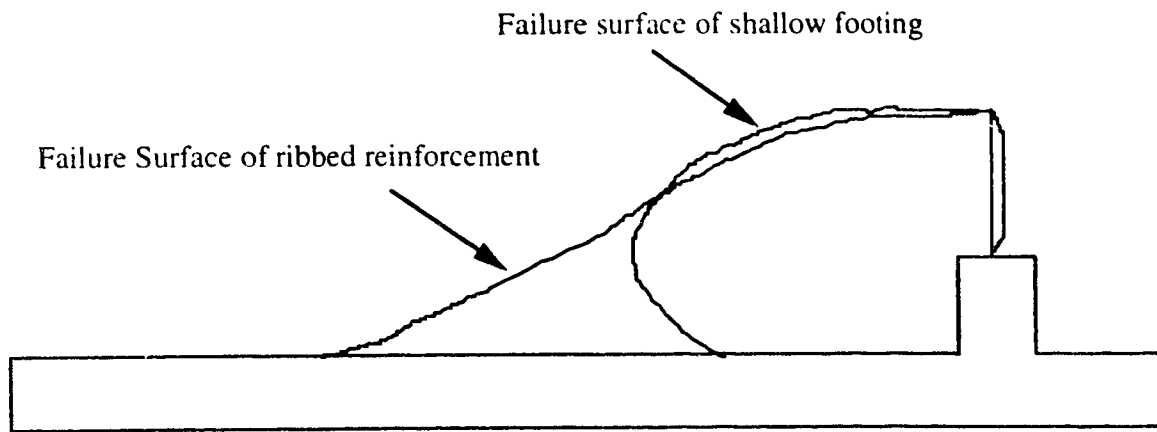


Figure 4.17 Comparison of Failure Modes

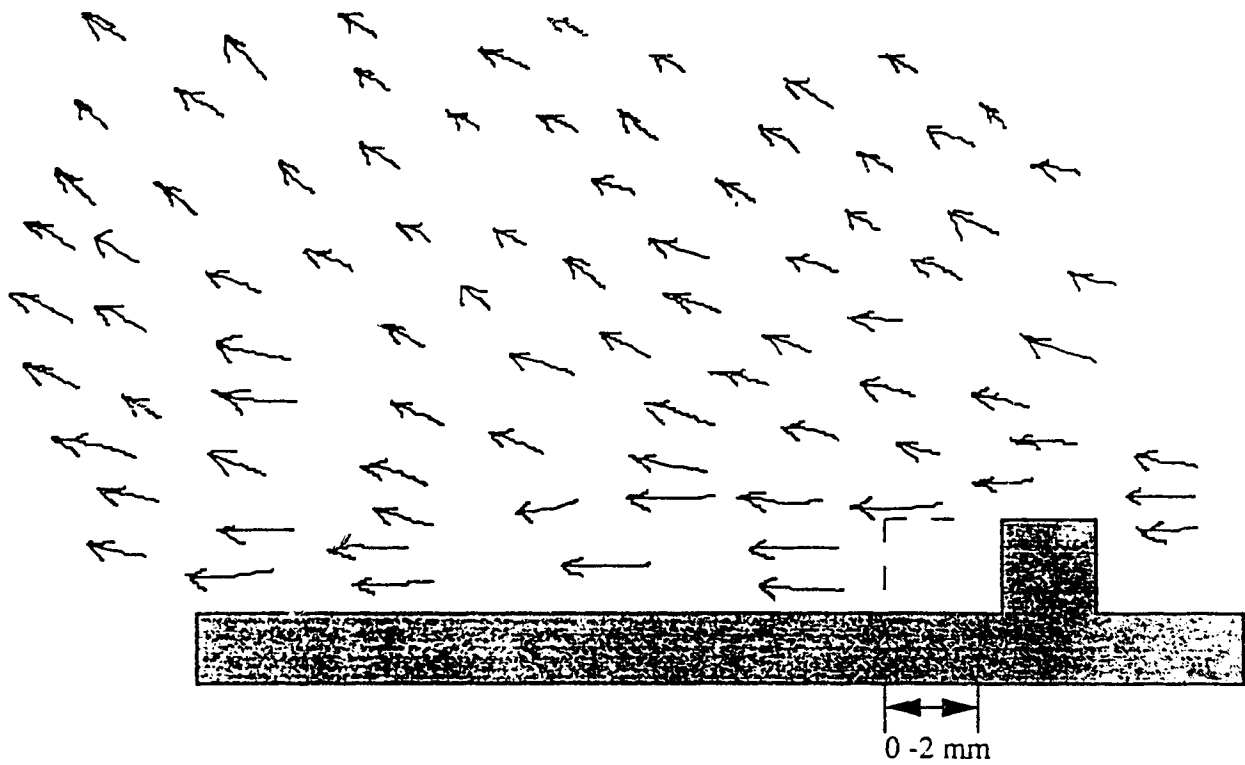


Figure 4.18 Observed Soil Grain Movement for 3.3 cm Rib Spacing
(after Irsyam,1992)

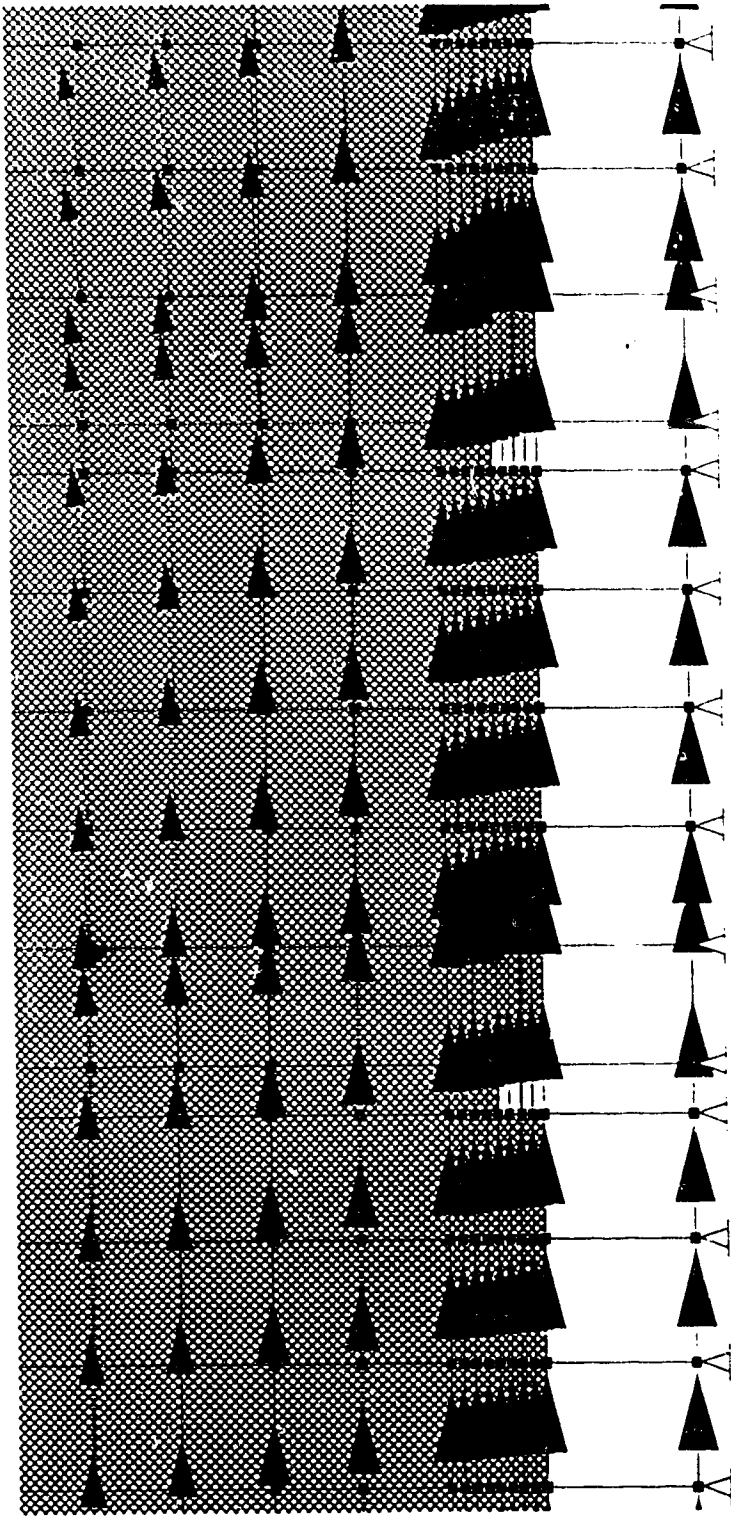
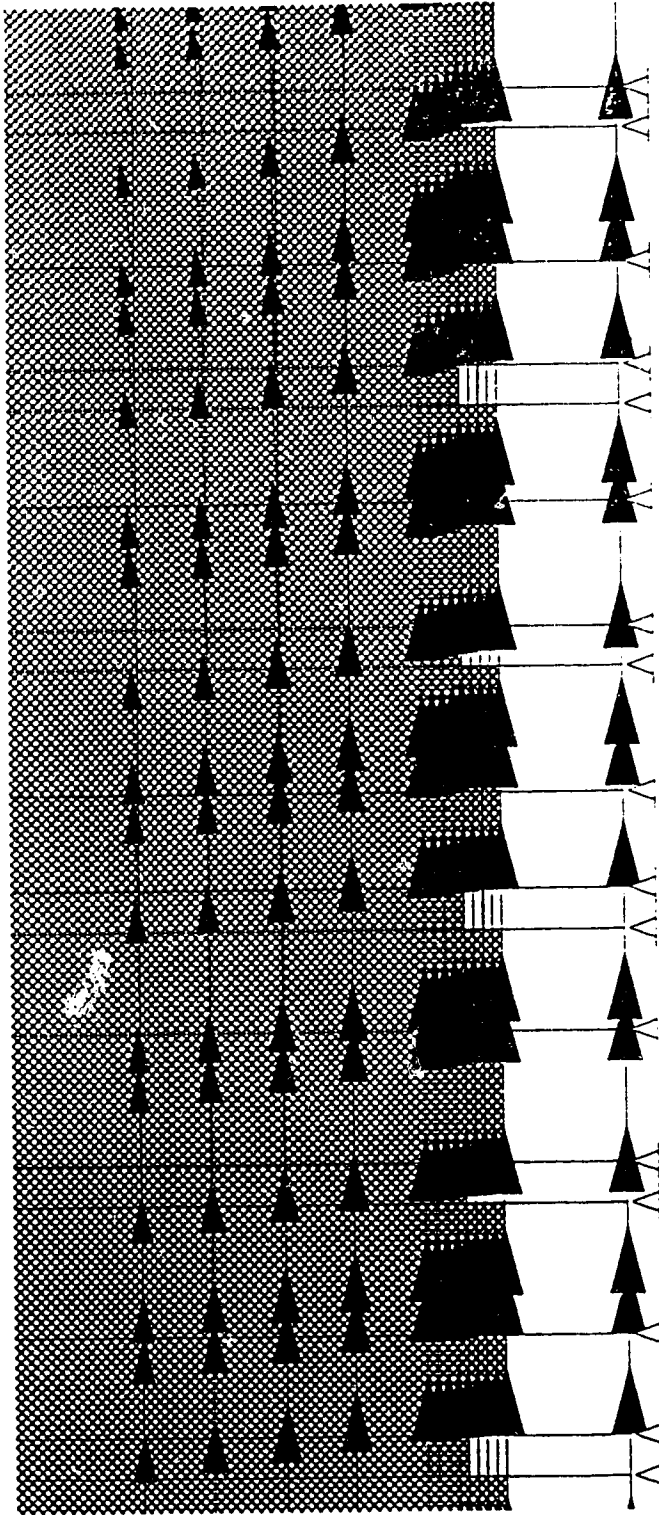
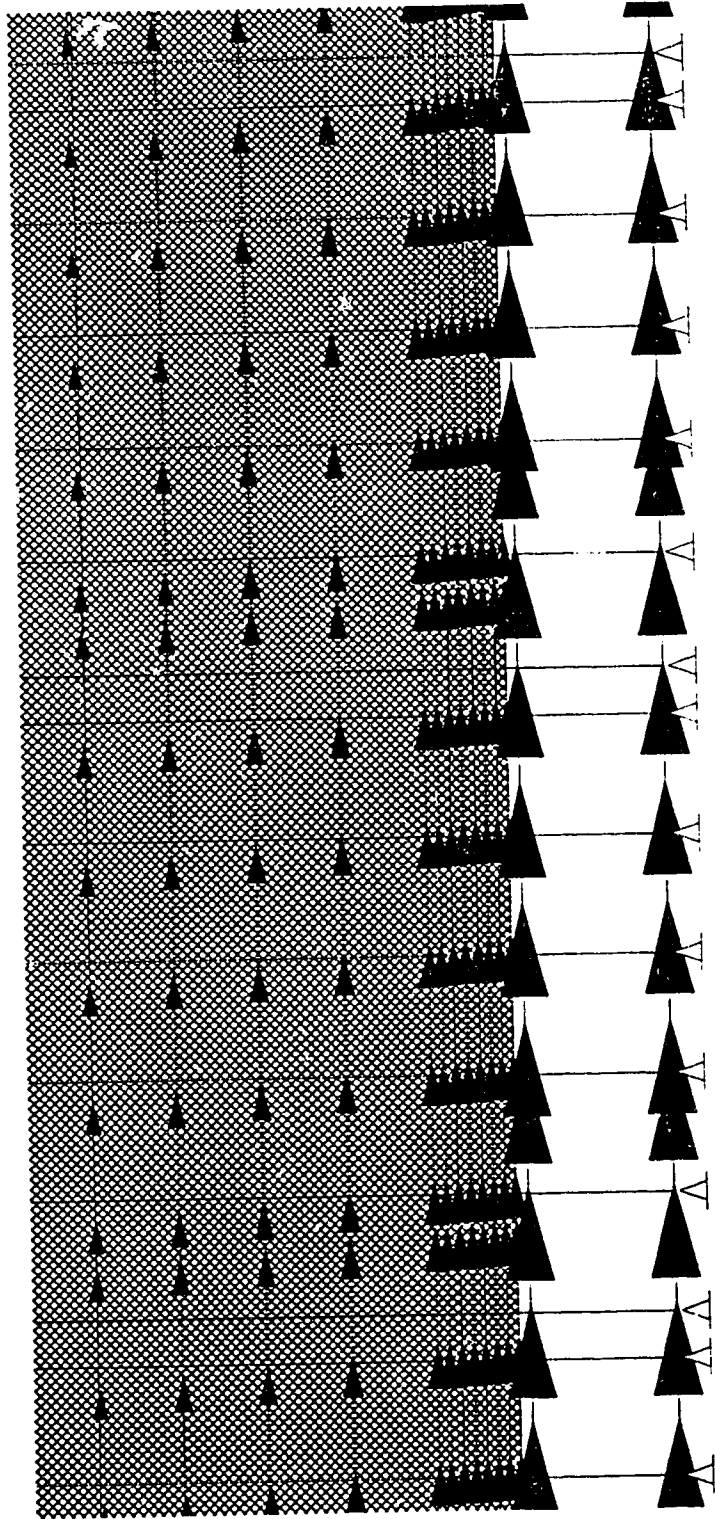


Figure 4.19 Calculated Nodal Displacement Arrows for 3.3 cm Rib Spacing (displacement 0.3 cm)



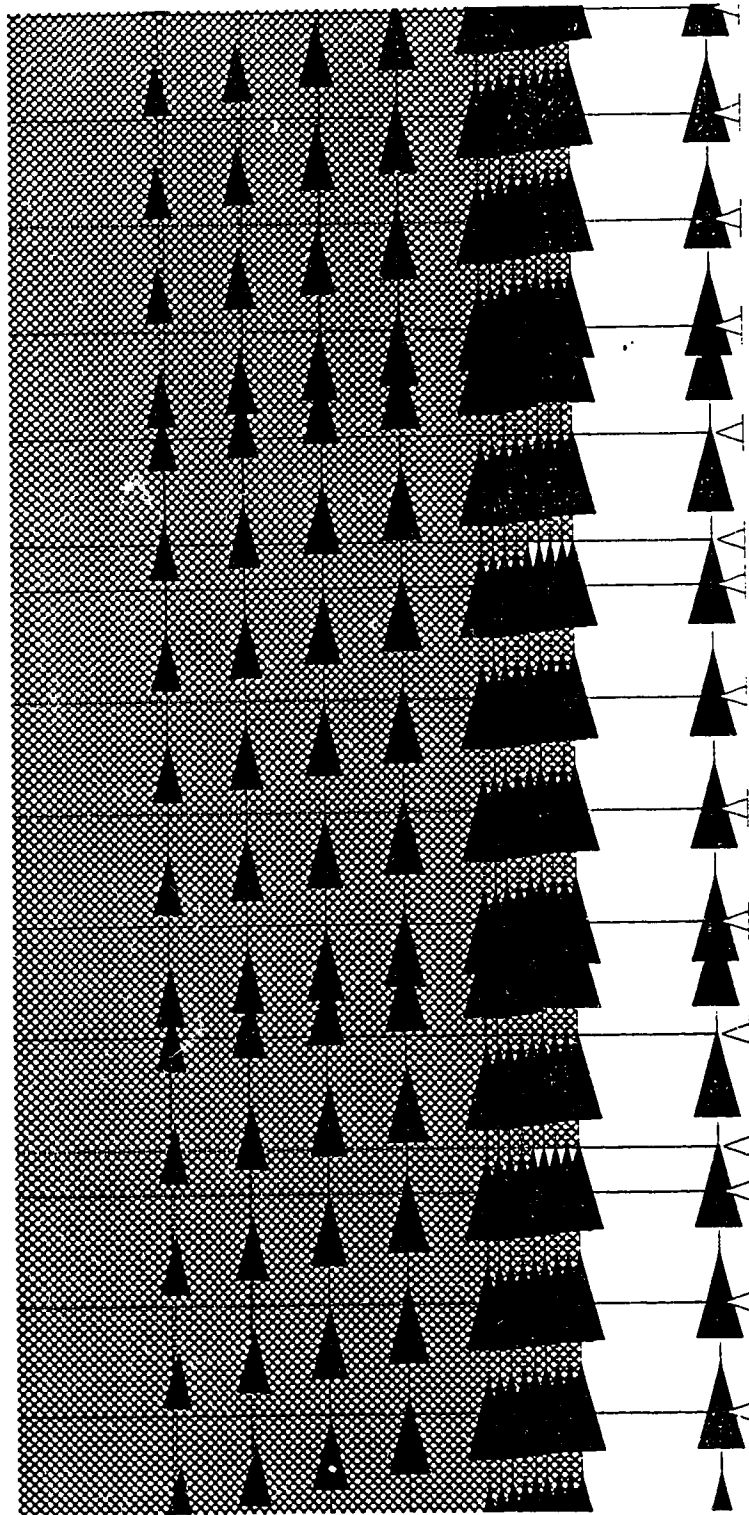
Displacement Arrow, Displacement = 0.3 cm

Figure 4.20 Calculated Nodal Displacement Arrows for 1.5 cm Rib Spacing (displacement 0.3 cm)



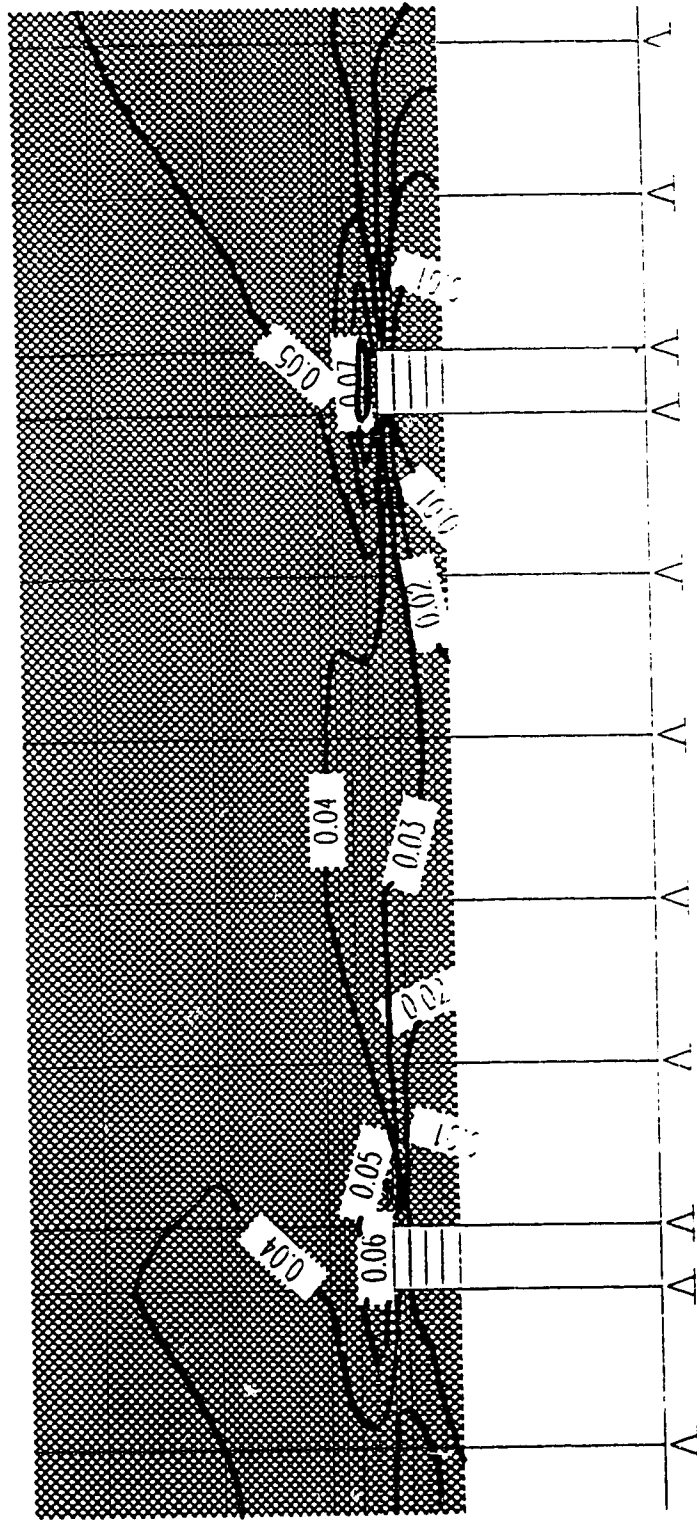
Displacement arrow: 1 cm = 0.3 cm to rib, inter

Figure 4.21 Calculated Nodal Displacement Arrows for No Ribs (displacement, 0.3 cm)



Displacement Arrow, Disp. 0.5 cm Cohesive soil

Figure 4.22 Calculated Nodal Displacement Arrows for 3.3 cm Rib Spacing, Cohesive Soil



Shear Strain(ϵ°), Displacement 0.5 cm, Cohesive

Figure 4.23 Shear Strain Distributions for 3.3 cm Rib Spacing, 0.3 cm Displacement, Cohesive Soil

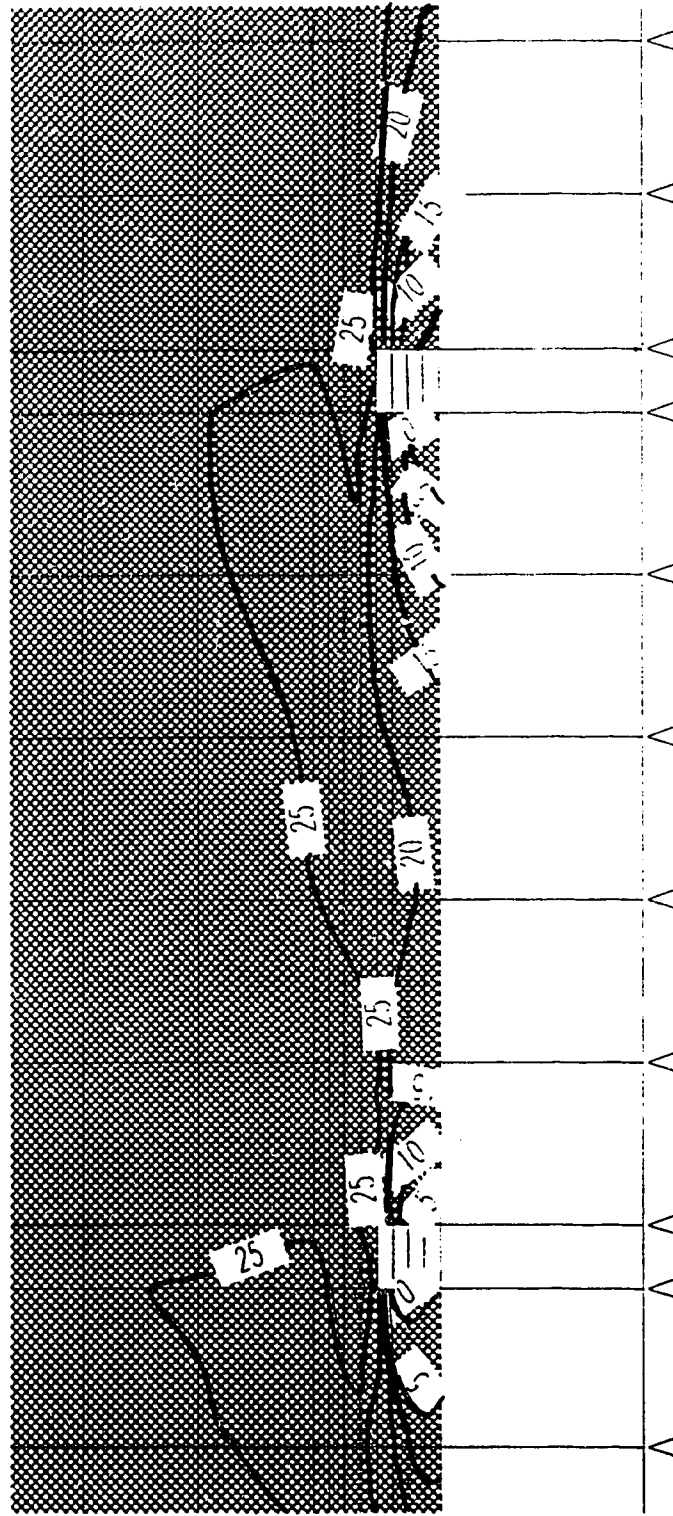
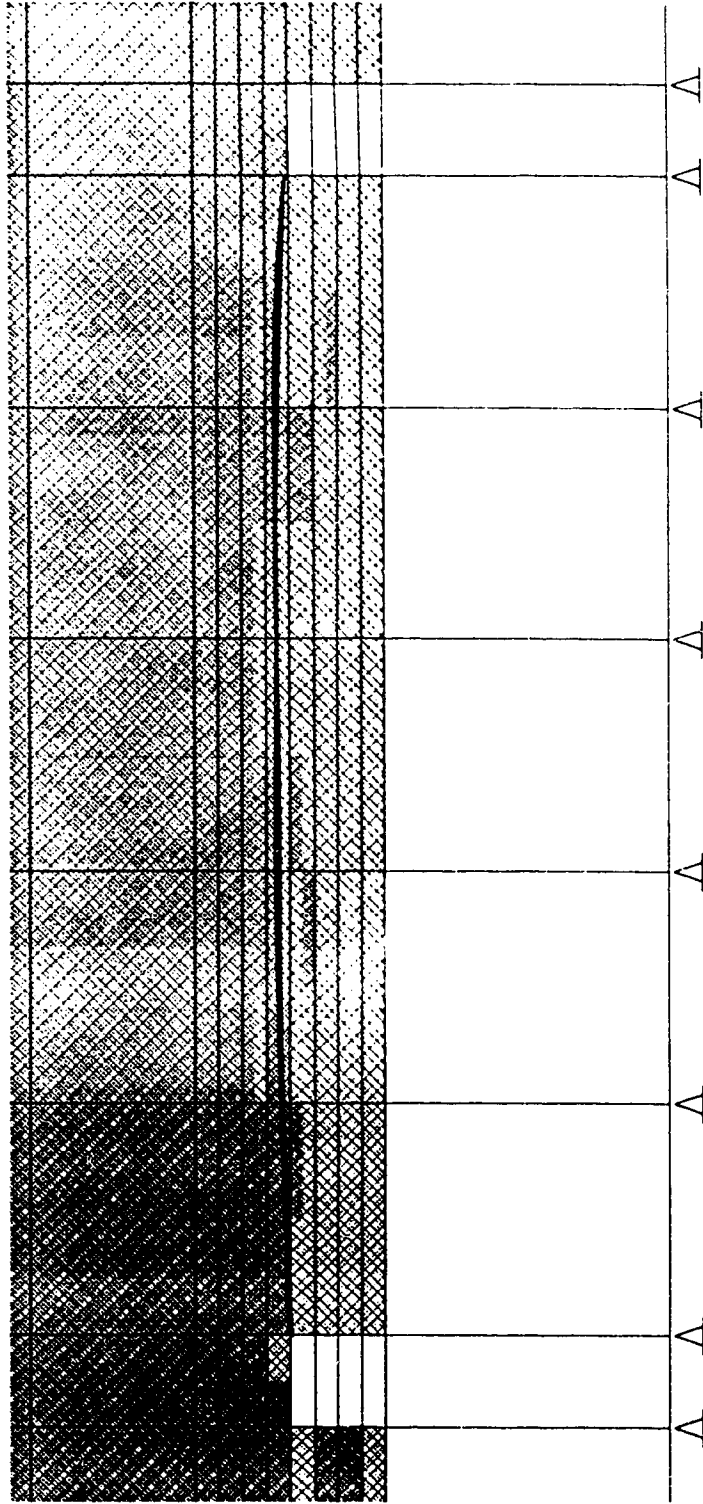


Figure 4.24 Shear Stress Distributions for 3.3 cm Rib Spacing, 0.3 cm Displacement, Cohesive Soil



Failure Surface, Cohesive Soil, Disp.cc.=0.5 cm

Figure 4.25 Calculated Shear Failure Surface for Cohesive Soil

CHAPTER 5. A LARGE SLIPPING FINITE ELEMENT MODEL FOR GEOSYNTHETICS INTERFACE MODELING

5.1 Introduction

Reinforced soil structures may experience large local movements between soil and reinforcement. Some failure modes of a reinforced structure are dependent on several factors which are governed by deformation and slipping of the reinforcement. In some cases, pulling out of the reinforcement may occur instead of rupturing. As well, the growing use of geosynthetics liner systems for storage of solid and liquid wastes has led to a number of slope instability problems. It is generally agreed that significant tensions can develop in the geosynthetics layers when they are subjected to unbalanced interface friction forces. This causes the sliding at the interfaces between the components of the liner system (Bourdeau et al., 1993). The conventional finite element method in modeling the soil-reinforcement interface uses a zero thickness joint element with normal and shear stiffnesses and can only accommodate a small amount of deformation. When large slippage occurs, this model provides an incorrect mechanism of deformation, i.e., Compatibility between the soil and the reinforcement can not be satisfied.

Several types of finite elements have been proposed for the modeling of joints and interfaces which can be classified in four categories (Gens et al., 1988). The interface element formulated based on relative displacements between opposite nodes has been widely used in finite element analysis of soil-structure interaction (Wu, 1992). This interface element can be divided into two groups; finite thickness (Sharma et al., 1992; Desai et al., 1984) and zero thickness interface element (Andrawes et al., 1982; Gens et al., 1990).

The zero thickness interface element is based on the joint element proposed by Goodman et al.(1968). The formulation of the model is derived based on the relative

displacements between surfaces of rock joints with two set of springs, one acting parallel to the interface (K_s) and the other acting perpendicular to it (K_n). The shear stiffness (K_s) representing the relationship between the shear stress and relative displacements of the solid elements surrounding the interface plays an important role in determining the interface behavior. The normal stiffness (K_n) representing the relationship between the normal stress and relative displacement is normally assumed a high value so that the interface does not overlap. However, it may not be appropriate to assign an arbitrarily high value for the normal stiffness. Because the interface is surrounded by the soil and geosynthetics, its normal properties during the deformation process must be dependent on the characteristics of the interface zone as well as the state of stress and properties of the surrounding elements. It is found that the joint element approach does not provide realistic modeling of the normal stress in soil-structure interaction, even though it provides satisfactory prediction of the shear behavior (Desai et al., 1984). It is difficult to arrive at an appropriate high value for K_n which yields reliable results.

A thin solid element to simulate the interface behavior was proposed by Desai et al.(1984) which provides satisfactory solutions for various deformation modes such as debonding when the normal stress becomes tensile. However, the element thickness can not be determined easily for soil-structure interface problems. If the thickness is too small computational difficulties may arise, and the thin layer element will behave like a solid element. The recommended solution for choosing an element thickness is based on a parametric study in which the solutions for different thicknesses are compared with observations. However, the parameters expressing the constitutive relationship of the interface element are exactly the same as the zero thickness interface element. The normal stiffness of this interface element is chosen based on the state of stress in the interface element which provides improved calculation of the interface normal stresses. However, arbitrary values of the normal stiffness are often chosen. This approach may not be realistic in soil-structure interaction problems, and can result in erratic and unrealistic

normal stress at the interface (Sharma et al., 1992).

Herrmann (1978) presented an algorithm for interface element similar to the zero thickness interface concepts with certain improvements through constraint conditions. However, the normal stiffness and shear stiffness during sliding were still chosen arbitrarily.

Rowe et al. (1978) also introduced a general method for the analysis of soil-structure interaction problems using the initial stress finite element approach. This approach avoids the computational difficulties which may arise in conventional joint elements. However, displacement compatibility at the interface was achieved by assigning the normal stiffness very large values.

In the case of reinforced soil structures, the failure mode of the reinforcement imbedded in the soil is dependent on the geometry of the reinforcement, soil type, imbedded length, normal stress, and especially the stiffness and tensile strength of the reinforcement. Costalonga (1988) has carried out pull-out tests using a HDPE geogrid and a PET geogrid in a silty clay. It was interesting to note that failure of the reinforcement occurred by slipping between soil and reinforcement rather than by rupturing the reinforcement. For geosynthetic reinforcement such as geogrids or high strength woven reinforcement, the load-strain relationship generally remains quite linear during the pull-out test, indicating that these reinforcement is stiff enough to have slippage of the reinforcement in the reinforced soil structures. Therefore it is important that, in modeling the interface of a reinforced soil, finite slippage must be simulated.

The growing use of geosynthetics liner systems for waste or liquid containment has led to a number of slope instability problems. As the waste material is dumped into the waste containment, the shear forces between soil and geosynthetics in a liner system is increased rapidly. To maximize the volume of disposal, the stability of steep side slopes is of high economic interest. The frictional properties of the system have to be examined in order to find out if there are any potential sliding surfaces under high shear stresses. In

such a case, a large amount of slipping or stretching of geosynthetics will occur along the interface between the geosynthetic and soil or between geosynthetic layers. A common failure mechanism of geomembrane lined slopes is by slippage of components within the liner system or of the cover soil due to excessive shear stresses.

Whenever a geomembrane-lined slope is covered with soil, a stability calculation for the slope should be done to assess the potential for sliding failure of the soil or tension failure of the geomembrane. A stability failure of the slope would be sliding of cover soil on the geomembrane. To increase the stability of the slope, geogrid or geotextile reinforcement is added in the liner systems. The stresses in the reinforcement are generally carried to an anchor which extended behind the geomembrane anchor trench. As the landfill was filled, the shear forces were mobilized rapidly, which could certainly trigger the sliding failure of the slope. Since, the normal forces on the reinforcement or geomembrane might be smaller than the shear forces, the frictional resistance along the reinforcement is lower, allowing displacement to occur over the entire length of the reinforcement. In this case, slippage or a large amount of relative displacement between the soil and reinforcement may occur.

The pull-out test results reported by Costalonga (1988) showed that the maximum pull-out force was mobilized during the first 20 mm to 50 mm of displacement for the PET geogrid. For the HDPE geogrid, it was mobilized between 40 mm and 60 mm of displacement in a 106 cm long x 30 cm wide x 20 cm deep pull-out box. After reaching the maximum displacement, the pull-out force of the reinforcement increased slightly or remained approximately constant as the displacement increased, indicating that the slippage of the reinforcement developed progressively from the front of the pull-out box.

These test results indicate that a large slipping finite element model should be considered for geosynthetics interface modeling. For the zero and the thin thickness interface elements, the slippage between soil and reinforcement was often assumed to occur when the induced shear stress exceeds the Mohr-Coulomb strength. After such

slippage has occurred the value of the tangential shear stiffness is arbitrarily reduced to a smaller value. In this model the value of the normal stiffness is still kept at an arbitrarily high value. However, there appears to be no physical basis for adopting these values for shear and normal stiffnesses.

In this chapter, a new interface finite element model is proposed. The constitutive law for the thin thickness interface or the zero thickness interface element is defined by expressing the constitutive matrix in terms of the normal and shear characteristics. However, in the large slippage interface model the constitutive behavior is incorporated during the solution process of the finite element scheme, and complete compatibility between the soil and the reinforcement is always satisfied without a high value of the normal stiffness which may result in erratic normal stresses at the interface. This model adopts a contact approach in which the soil and reinforcement are treated as surfaces of contact between two bodies (Bathe et al., 1985). The model can simulate a large amount of slipping between the soil and the reinforcement. The large displacement at soil-structure interface is not defined as a large amount of displacement but as the finite element mesh size. Compatibility is satisfied using a constraint approach, the Lagrange multipliers, to ensure no overlapping of material will occur. Separation of the soil and reinforcement can be modeled easily using this approach. Normal and frictional forces will be developed at the interface according to the stiffnesses of the materials. The interfacial strength between the soil and the reinforcement is assumed to be governed by the Coulomb frictional law which accounts for both frictional and passive resistance of the geogrid reinforcement.

5.2 Model Formulation

5.2.1 Imposition of Constraints

A specific constraint can be applied on the interface between the soil and

reinforcement boundary. The normal displacements along the reinforcement should be the same as those of the soil to not allow overlapping of the materials. These conditions specify the normal displacements along the soil and the reinforcement and must satisfy the compatibility condition. Therefore there is no need to adopt a high value of normal stiffness as in the thin interface model. Separation of the soil and reinforcement can be modeled easily by providing specified normal displacements at the soil-reinforcement interface.

The Lagrange multiplier method is used to incorporate constraints in the variational or weighted residual methods. The Lagrange multiplier method has been used in many fields of mathematics and physics to impose constraint conditions on algebraic or differential equations (Matthew and Walker, 1964). Considering the variational formulation of a discrete system, the functional, Π , can be expressed as follows (Bathe, 1982):

$$\Pi = 1/2 U^T K U - U^T R \quad (5.1)$$

where U is a vector of global displacement ;

K is the stiffness matrix;

R is a vector of forces acting in the direction of global displacement.

The variation with respect to displacements, U_j could be written as:

Equation (5.2) indicates that the functional Π , the total potential energy in this case, is not only stationary but is a minimum value for an approximate finite element solution. The boundary condition for equation (5.1) can be considered as a constraint on the variational formulation. If we impose a constraint U_j^* on the displacement U_j such that $U_j = U_j^*$ then we can rewrite the constraint variational Π^* ,

$$\Pi^* = 1/2 U^T K U - U^T R + \lambda(U_i - U_i^*) \quad (5.3)$$

where λ is a Lagrange multiplier.

Invoking the stationary condition, we obtain

$$\delta \Pi^* = \delta U^T K U - \delta U^T R + \lambda \delta U_i + \delta \lambda (U_i - U_i^*) \quad (5.4)$$

Since δU and $\delta \lambda$ are arbitrary values which give the following matrix form:

$$\begin{bmatrix} K & K_c^T \\ K_c & 0 \end{bmatrix} \begin{Bmatrix} U \\ \lambda \end{Bmatrix} = \begin{Bmatrix} R \\ 0 \end{Bmatrix} \quad (5.5)$$

where K_c is a rectangular matrix which contains the constraint conditions, $U_i - U_i^*$.

The size of the K_c matrix is related to the number of constraint conditions, and each row of matrix possesses two non-zero values, 1 and -1 corresponding to the constrained displacement column matrix; K is the stiffness matrix which can be easily calculated in the routine finite element procedures.

The above equation (5.5) is symmetrical if K is symmetrical. However it was observed that the diagonal elements in the coefficient matrix corresponding to the Lagrange multiplier are zero. This will cause computational difficulties unless the solution process allows for zero diagonal terms. The constraint method can be used to impose connection between any two nodes in the finite element domain. To maintain compatibility between the soil and the reinforcement the normal displacements of the corresponding nodes are connected unless tension occurs at the interface. This scheme avoids the use of the high normal stiffness in a traditional interface model.

5.2.2 Horizontal Constraints

The stress transfer mechanism between soil and grid reinforcement involves

frictional and passive soil resistance at the soil-reinforcement interface. In the reinforced soil structure the primary mechanism of stress transfer is through frictional resistance. However passive resistance plays an important role when grid reinforcement is employed.

The large slipping interface model has used the shear stiffness (K_s) in applying a horizontal resistance along the reinforcement. The shear stiffness (K_s) appears as the initial slope of the shear stress-displacement curve measured in the pull-out test or the shear box test. However, pull-out tests have been acknowledged to provide a better simulation of the interface behavior between the soil and the reinforcement (Garbulewski, 1990). Pull-out resistance includes passive and frictional resistance, i.e., the shear stiffness obtained consists of stiffness from both frictional and passive resistance components. The total equivalent initial shear stiffness (K_s) is the sum of these two components. Thus, a proper choice of shear stiffness (K_s) can make it possible to simulate the horizontal resistance of geogrid reinforcement (Chan et al., 1993). Pull-out tests provide the relationship between the shearing resistance and displacement at the pull-out slot, therefore it is necessary to calculate the shear stress in order to obtain the shear stiffness.

In a small displacement problem, the shear stiffness is assumed to be linear and is equal to the initial slope of the shear stress-displacement curve. A hyperbolic formula can be used for the shear stress-displacement relationship. However, the variation of peak and residual shear strengths with the relative displacement should be used for a large slippage model. An idealization constitutive law for the shear stress-displacement behavior is shown in Figure 5.1. The limiting shear stress, τ_p , is assumed to be governed by the Coulomb frictional law. If τ_p is exceeded, the shear stress falls to a residual value τ_r and the mobilized shear stress on the reinforcement becomes constant.

The procedure for implementing the frictional resistance on the reinforcement is explained in Figure 5.2. First nodes displacements are calculated by imposing the displacement constraints at the interface using the Lagrange multiplier. Relative

displacements are calculated between the soil and the reinforcement and the shear stresses developed are determined. The failure criteria is checked for possible slippage at the interface. Additional nodal forces are imposed due to the changes in stresses at the interface and further displacements are calculated until the system has reached an equilibrium state.

5.3. Solution Strategy

The use of the finite element method requires the solution of simultaneous algebraic equation of (5.6). Each diagonal coefficient of the stiffness matrix is always positive definite, and the stiffness matrix is banded and symmetric. The skyline method (Felippa, 1975) utilizes the concept of variable bandwidth in which only non-zero elements under skyline are stored and used in calculation. Many solution schemes have been proposed using the above properties of stiffness matrix.

Each diagonal coefficient of the stiffness matrix in equation (5.5) is no longer positive definite, many diagonal coefficients of stiffness matrix are zero. A solution to equation (5.5) can be obtained by using the Gauss-Elimination method.

The overall Gauss elimination procedure applied on the $n \times (n+1)$ augmented matrix is condensed into a three-part mathematical formula for initialization, elimination, and back substitution. Elimination formula can be expressed as follows:

$$\{R\} = [K] \{U\} \quad (5.6)$$

Where $\{R\}$ is a vector of global displacement ;

$[K]$ is the stiffness matrix

$\{U\}$ is a vector of forces acting in the direction of global displacement

$$K_{i,j}^{(k)} = K_{i,j}^{(k-1)} - \frac{K_{i,k}^{(k-1)}}{K_{k,k}^{(k-1)}} K_{k,j}^{(k-1)} \quad (5.7)$$

where $j = n+1, n, \dots, k$; $k = 1, 2, \dots, n-1$

$$i=k+1, k+2, \dots, n$$

where the counter k is the iteration counter of the outside loop in a set of nested loops that perform the elimination. It should be noted that the element K_{ii} in the denominator of equation (5.7) is always the diagonal element. It is called the pivot element. The pivot element must not be zero; otherwise the computer program will result in overflow. The computer program can be written so that it rearranges the equations at each step to attain diagonal dominance in the coefficient matrix, i.e., the row with the largest pivot element is chosen. This strategy is called partial pivoting, and it serves two purposes in the Gaussian elimination procedure: it reduces the possibility of division by zero and it increases the accuracy of the Gauss elimination method using the largest pivot element. If, in addition to row, the column is also searched for the maximum available pivot element, then the strategy is called complete pivoting. If pivoting cannot locate a non-zero element to place on the diagonal, the matrix must be singular. When two columns are interchanged, the corresponding variable must also be interchanged. A program which performed complete pivoting must keep track of the column interchanges in order to interchange the corresponding variable.

5.4 Application

To illustrate the effectiveness of the model, a simple reinforced soil sample under plane strain condition is shown in Figure 5.3. A surface traction of 2.0 kPa was applied at the top of the soil element in the first loading step of the simulation. Then a prescribed 1m horizontal displacement was imposed on the free end of the reinforcement to simulate the pull-out test. The prescribed displacement was applied in two loading steps to ensure that a large displacement or slipping of the reinforcement can be simulated properly in the large slipping interface model. The material properties are shown in Figure 5.3.

The vertical displacements of nodes 3, 4 and 5 should be equal to prevent

overlapping of the materials. The same condition applies on all other nodes along the reinforcement. A total of 10 constraints were imposed on the stiffness matrix as displacement constraint conditions. The shear stiffness, K_s , was assigned 10 kN/m^3 for the horizontal constraints. When slipping occurred, the mobilized shear stress remained relatively constant over a portion of the reinforcement. However, the mobilized shear stress on the reinforcement was assumed to increase linearly with the relative displacement between the soil and the reinforcement to ensure that the horizontal constraint works properly. Without any horizontal constraint, it was found that the mobilized shear stress along the reinforcement was zero.

Figure 5.4 shows the tensile stress along the reinforcement at 1m displacement under both constraint conditions. The vertical displacement constraints and compatibility conditions between the soil and the reinforcement were always satisfied at any loading step as shown in Table 5.1. Figure 5.5 shows the distribution of nodal horizontal displacements along the reinforcement

The simulation of the slippage of reinforcement is a main concern in this interface element. When the horizontal displacement of the reinforcement was increased, node 4 would be located between node 5 and node 11 after several steps (Figure 5.3). In this case, the constraint conditions for compatibility between the soil and reinforcement should be considered to simulate the slippage of reinforcement. The element interpolation functions can be used to calculate the normal displacement of the reinforcement at any point between two nodal points which correspond to the soil nodal points. However, an approximate method was used in this case. After calculating the horizontal relative displacement between the soil and the reinforcement, the reinforcement node was associated with the nearest soil node. For instance, if node 4 was located between node 5 and node 11, the constraint conditions would be applied based on nodes 5 or 11 depending on the proximity of the nodes to satisfy compatibility conditions. A stretching strain mode of the reinforcement, i.e., the horizontal displacement of the reinforcement in Figure 5.3

would be expected. Therefore this approximate method will not cause any calculation error.

To illustrate the capacity of the model for practical applications, the pull-out test conducted by Costalonga (1988) was analyzed. A two dimensional plane strain finite element mesh is shown in Figure 5.6. The material properties can be found in Chan et al. (1993). A shear stiffness of 540 kN/m^3 calculated from the conventional method without any correction was used for the horizontal construction. The calculated force-displacement response is compared with the pull-out test as shown in Figure 5.7. It is seen that a maximum pull-out resistance was reached at a displacement of 3.7 cm when the full length of the reinforcement was displacing at the same rate. Figure 5.8 shows that the mobilized tensile stresses on the reinforcement at a displacement of 3.7 cm increased linearly along the entire length of the reinforcement, i.e., the mobilized shear stresses were constant, indicating that the total length of the reinforcement was slipping. It was illustrated that the slippage of the reinforcement was developed at the front part of the reinforcement at a displacement of 1.2 cm. The distribution of shear stress along the reinforcement at a displacement of 1.2 cm is not uniform since the tensile force in the reinforcement decreases away from the point of application of the pull-out forces. As the reinforcement is further pulled through the soil, a maximum shear stress is reached along the entire length of the reinforcement as shown in Figure 5.9. This progressive shearing is shown by Figure 5.10.

5.5 Conclusion

A new large slipping finite element model for geosynthetic interface models has been introduced. The Lagrange multiplier method is used to satisfy compatibility between the soil and the reinforcement, and the shear stiffness (K_s) is used to apply horizontal resistance along the reinforcement which is able to account for both frictional and passive

soil resistance of geogrid reinforcement. It was demonstrated using a simple reinforced soil structure example and the analysis of a pull-out test that this model can easily simulate a large amount of slipping between the soil and the reinforcement. It is also expected that the new model can deal with any soil-structure interaction problem which involves a small displacement analysis as well as a large amount of slipping.

5.6 References

- Andrawes, K.Z., McGown, A., Wilson-Fahmy, R.F. and Mashhour, M.M.(1982) "The Finite Element Method of Analysis Applied to Soil-geotextile Systems", Proc. 2nd Int. Conf. on Geotextiles, Vol.3, pp. 695-700.
- Bathe, K.J.(1982) **Finite Element Procedures in Engineering Analysis** , Prentice-Hall, Inc., 735 p.
- Bathe, K.J. and Chaudhary, A.(1985) "A Solution Method for Planar and Axisymmetric Contact Problems ", Journal for Numerical Methods in Engineering, Vol.21, pp. 65-88.
- Bourdeau, P.L., Ludlow, S.J. and Simpson, B.E. (1993) " Stability of Soil-covered Geosynthetic-lined Slopes: A Parametric Study ", Proc.Geosynthetics '93 Conference, Vancouver, Canada, Vol.3, pp.1511-1521.
- Chan, D.H, Yi, C.T. and Scott, J.D. (1993) "An Interpretation of the Pull-Out Test", Proc.Geosynthetics '93 Conference, Vancouver, Canada, Vol.2, pp.593-605.
- Costalonga, M.A.R. (1988) **Geogrid Pull-Out test in Clay**, M.Sc Thesis , The University of Alberta, Edmonton Alberta, Canada, 211 p.
- Desai, C.S., and Zaman, M.M. (1984) "Thin -layer Element for Interfaces and Joints" , International Journal for Numerical and Analytical Methods in Geomechanics, Vol.8, pp.19 -43.
- Garbalewski, K. (1990)" Direct Shear and Pull-Out Resistance at the Geotextile

- Interface", Proceeding of the Fourth International Conference on Geotextiles Geomembrane and Related Product, Hague, Netherlands, pp.737-742.
- Gens, A., Caro, I. and Alonso, E.E.(1988) "An Interface Element Formulation for The Analysis of Soil Reinforcement Interaction", Com. and Geotech. Vol.7, pp.133-151.
- Goodman, R.E., Taylor, R.L. and Brekke, T.L. (1968) " A Model for the Mechanics of Jointed Rock", Journal of Soil Mechanics and Foundation Engineering Division, ASCE, Vol.94 No.SM 3, pp. 637-659.
- Herrmann, L.R.(1978) " Finite Element Analysis of Contact Problems", J. Eng. Mech., ASCE, Vol.104, pp.1043-1059.
- Matthew, J. and Walker, R.L.(1964) **Mathematical Methods of Physics**, New York, Benjamin, 475pp.
- Rowe, R.K., Booker, J.R. and Balaam, N.P. (1978) " Application of the initial stress method to soil -structure interaction", International Journal for Numerical Methods in Engineering, Vol.12, pp. 873-880.
- Sharma, K.G. and Desai, C.S.(1992) "Analysis and Implementation of Thin-layer Element for Interface and Joints ", Journal of Engineering Mech., ASCE, Vol.118, No.12, pp. 2442-2462.
- Wu, J.T.H.(1992) "Discussions: Embankment", Pro.Int.Sympo.on Earth Reinforcement Practice, Kyushu, Japan, Vol.2, pp. 928-929.

Table 5.1 Vertical Displacement at Step 3 (1m horizontal displacement)

Node	3, 4 & 5	9,10 &11	15,16 &17	21, 22 &23	27, 28 &29
Displacement(m)	-0.03593	-0.03617	-0.03585	-0.0362	-0.03577

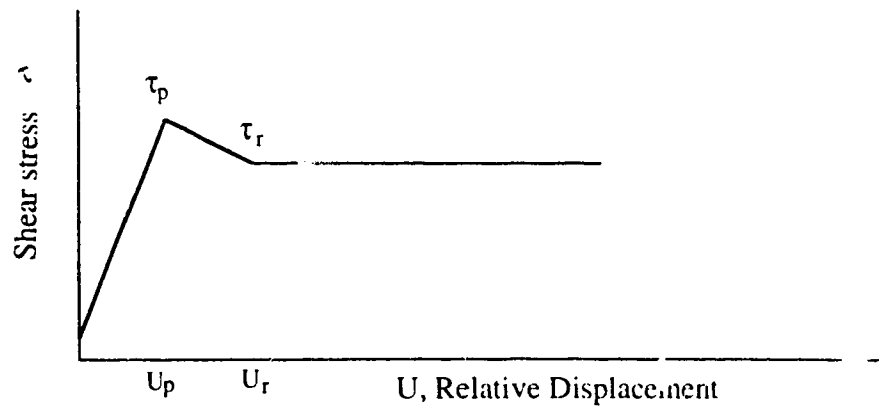


Figure 5.1 Constitutive Law for Shear-displacement Behaviour

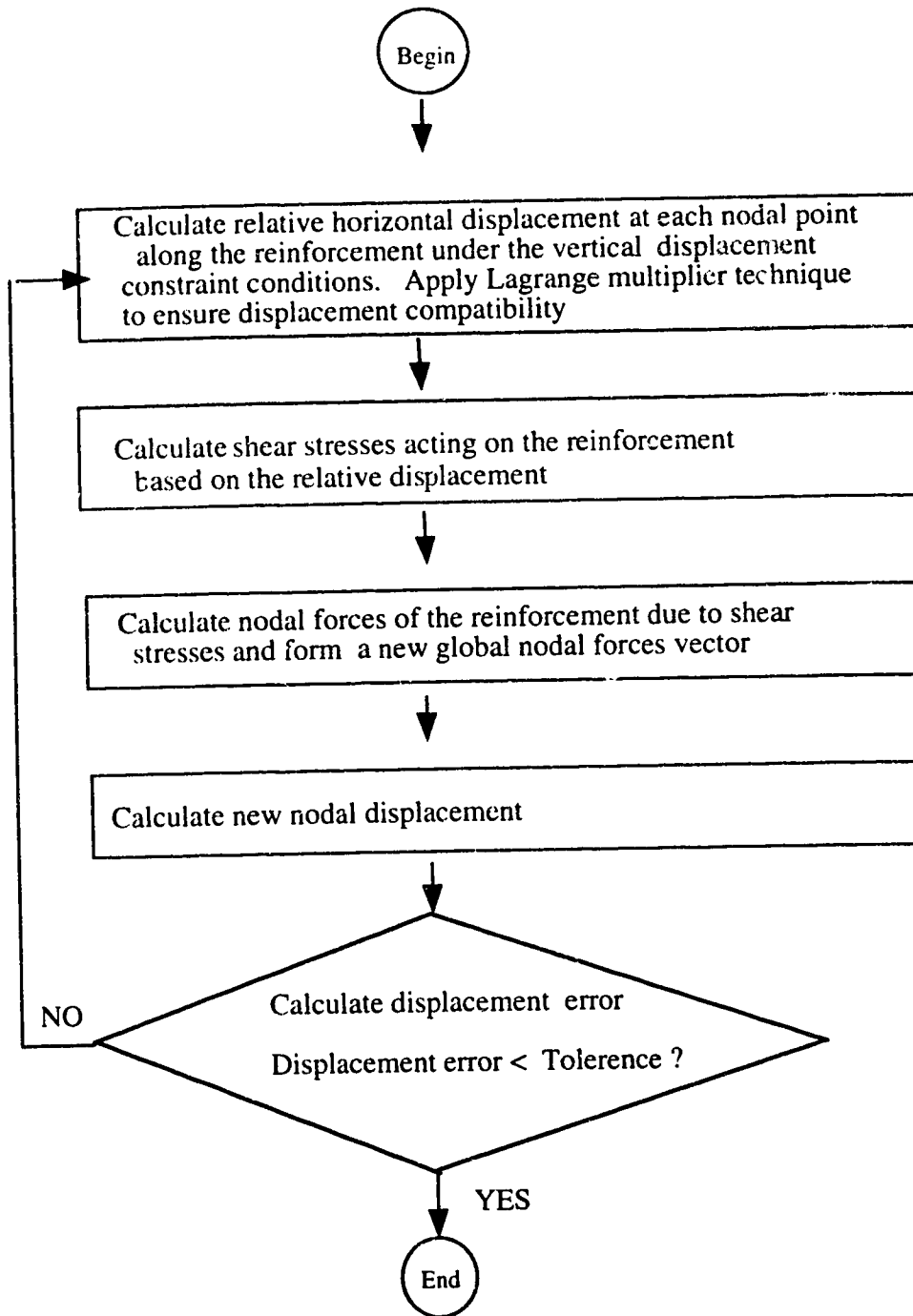


Figure 5.2 Flow Chart for Application Horizontal Resistance on Reinforcement

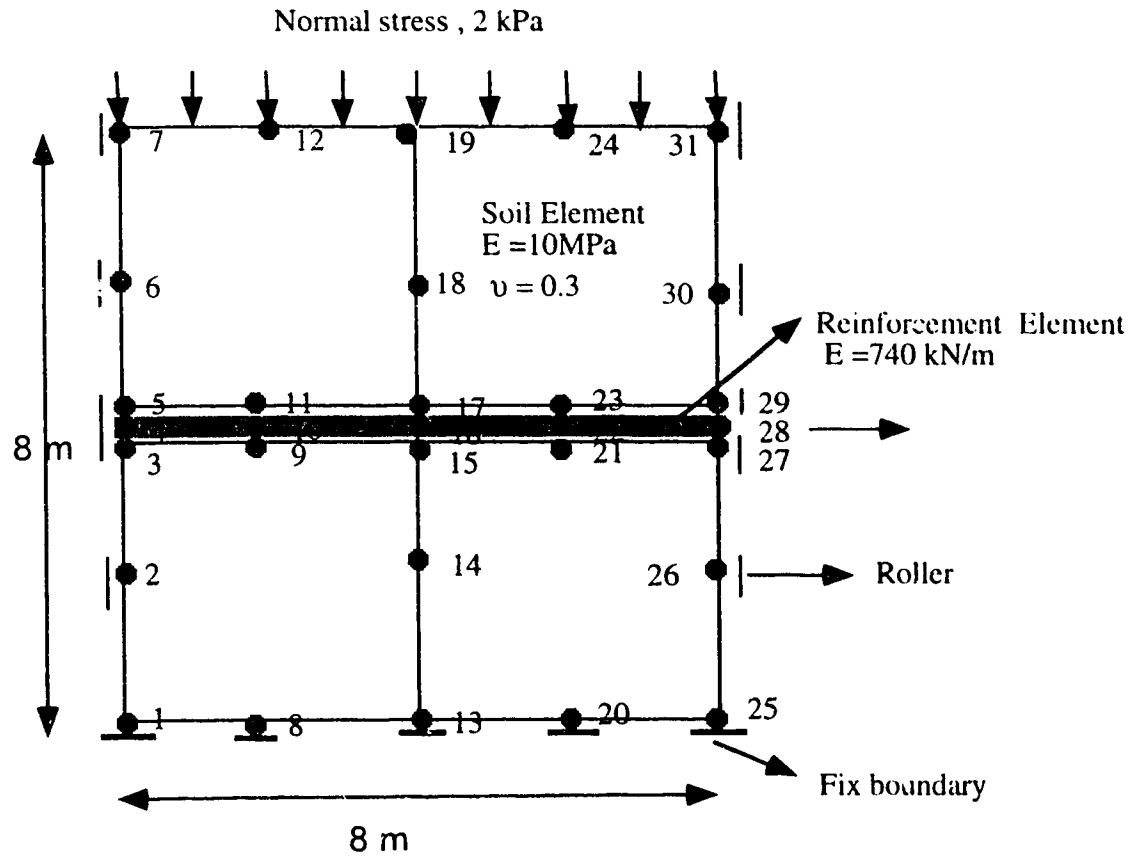


Figure 5.3 Reinforced Soil Structure

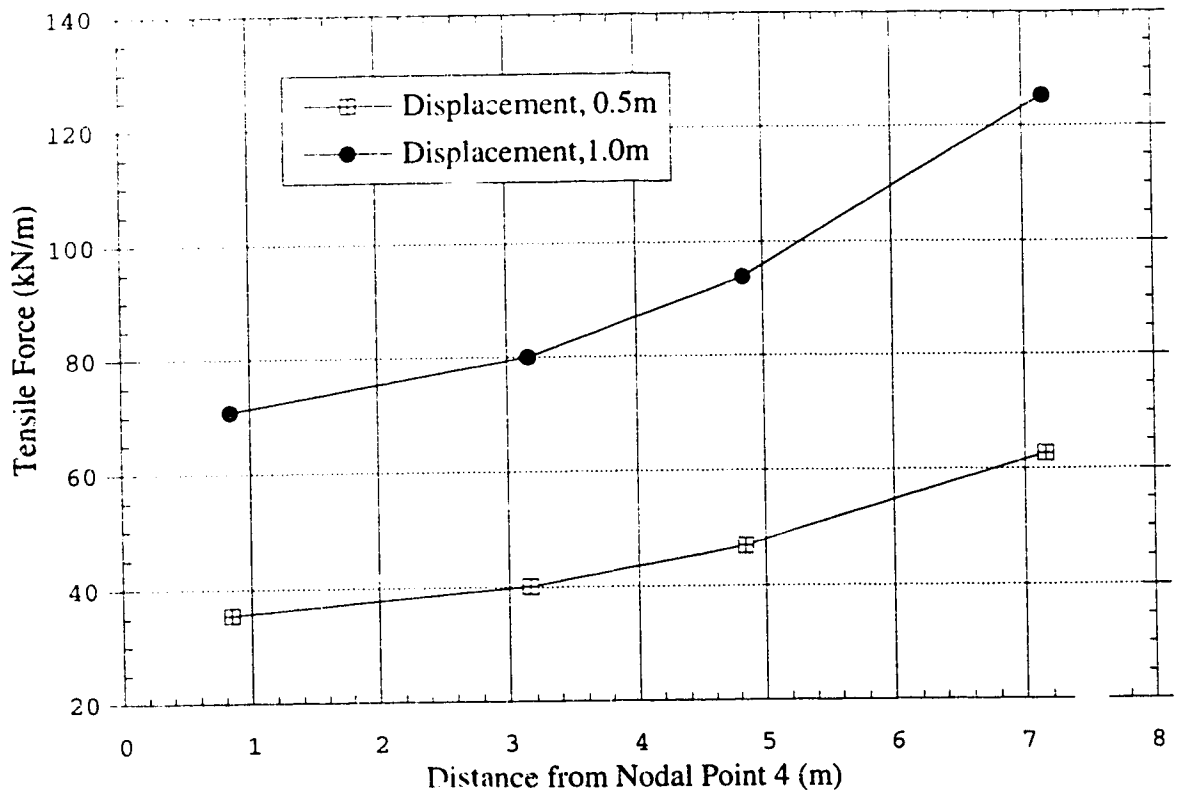


Figure 5.4 Tensile Force Distribution along the Reinforcement

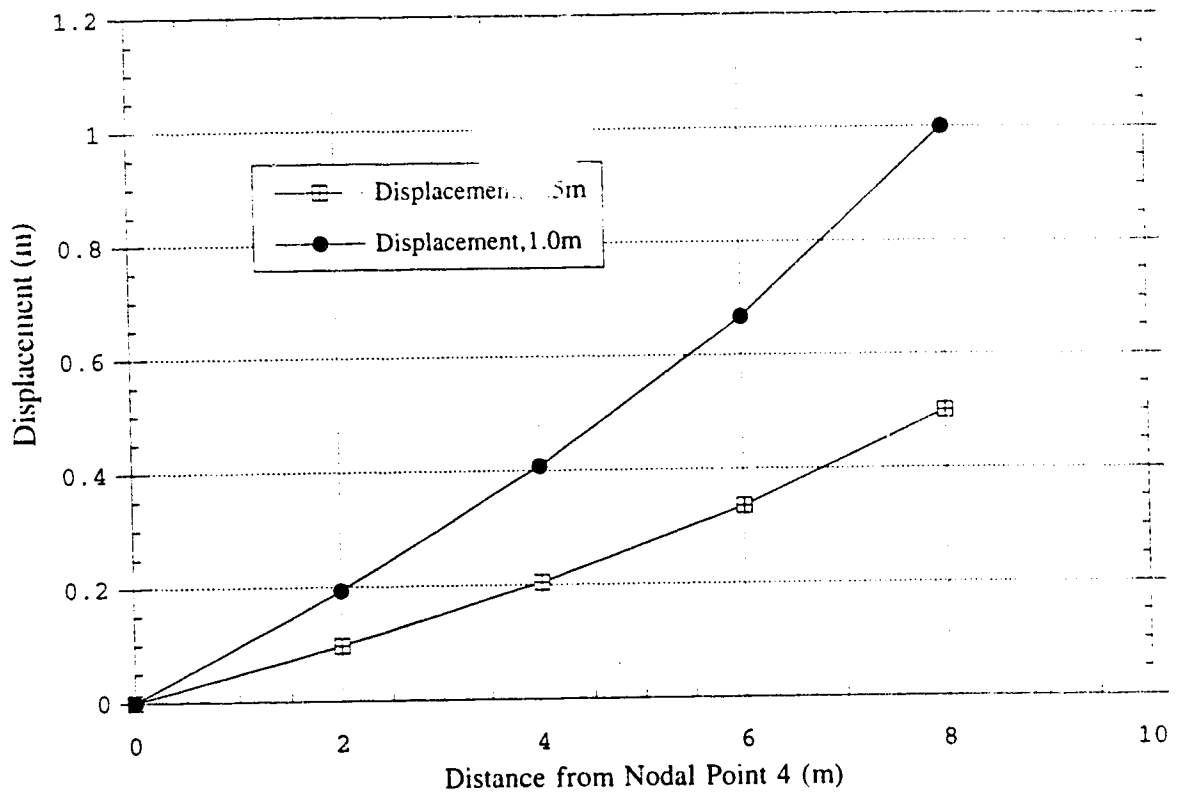


Figure 5.5 Displacement Distribution along the Reinforcement

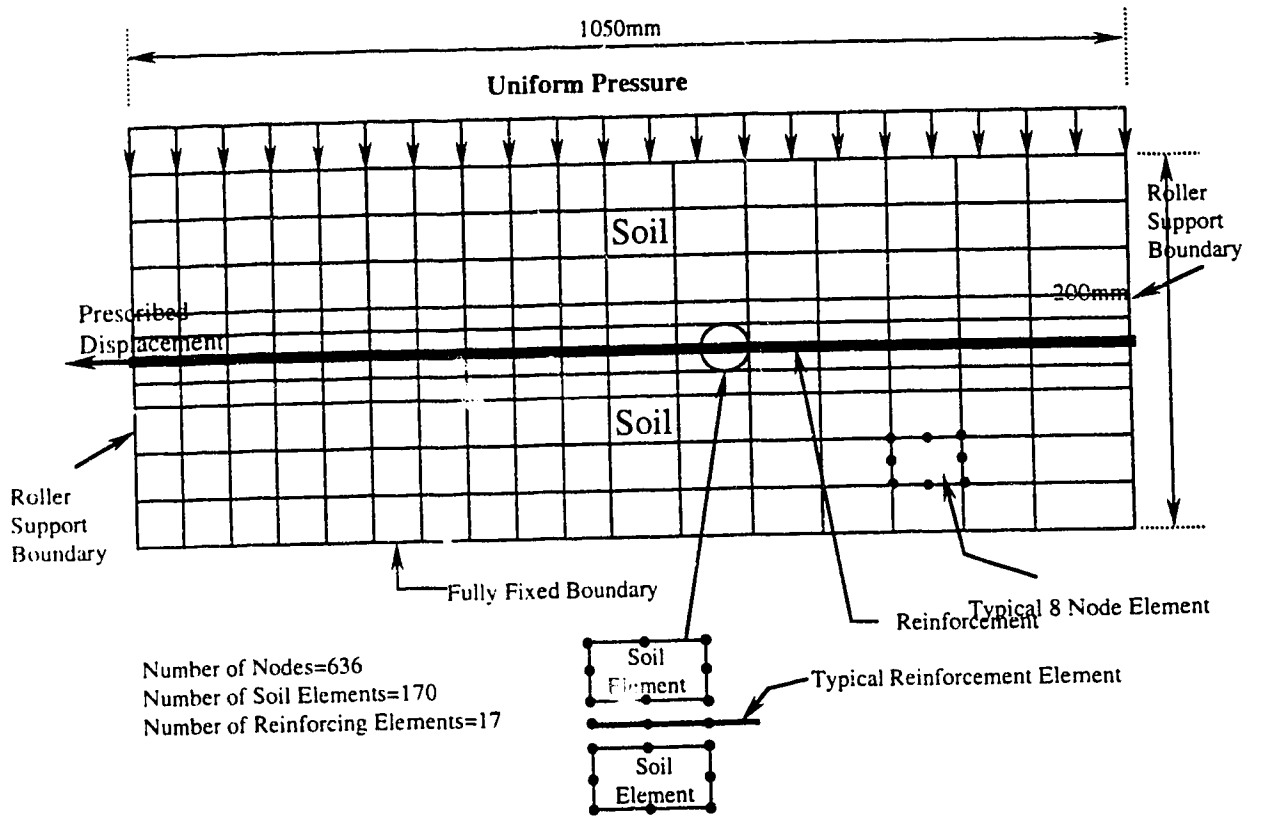


Figure 5.6 Finite Element Idealization of Soil and Reinforcement for the Pull-out Test

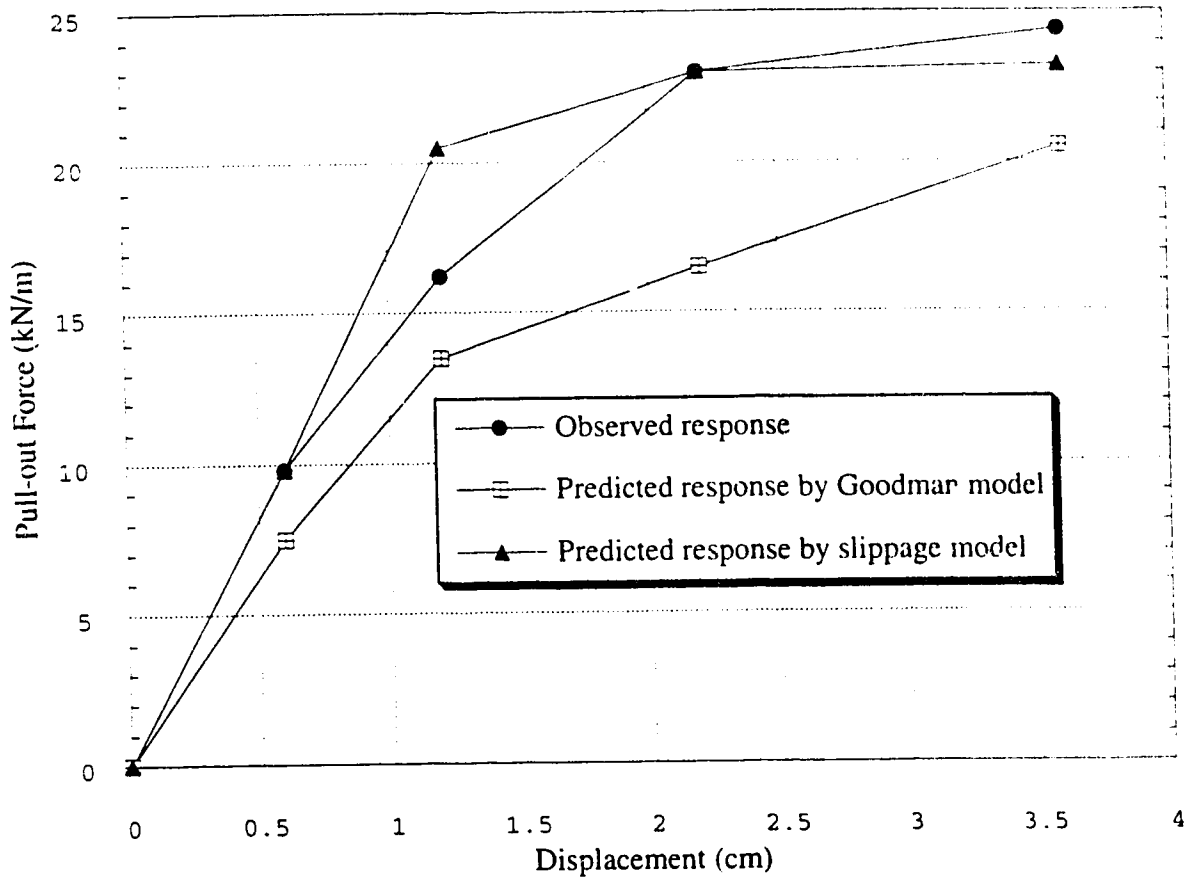


Figure 5.7 Force-Displacement Responses of the Reinforcement in the Pull-out Test

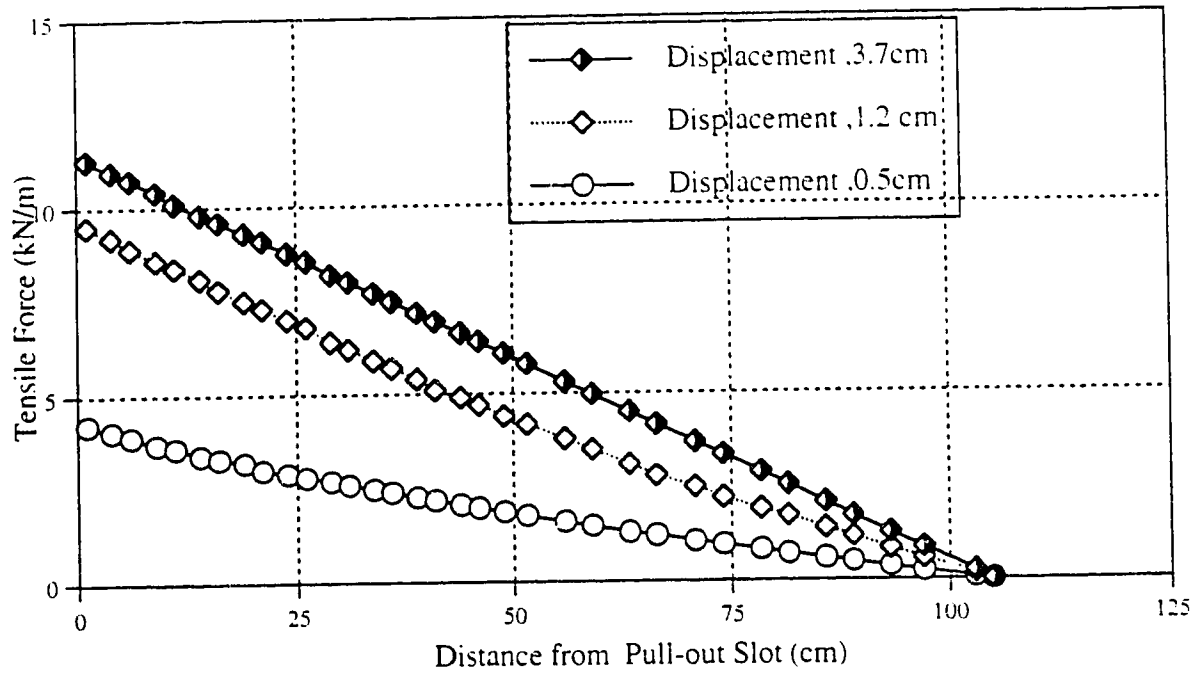


Figure 5.8 Tensile Force Distribution along the Reinforcement

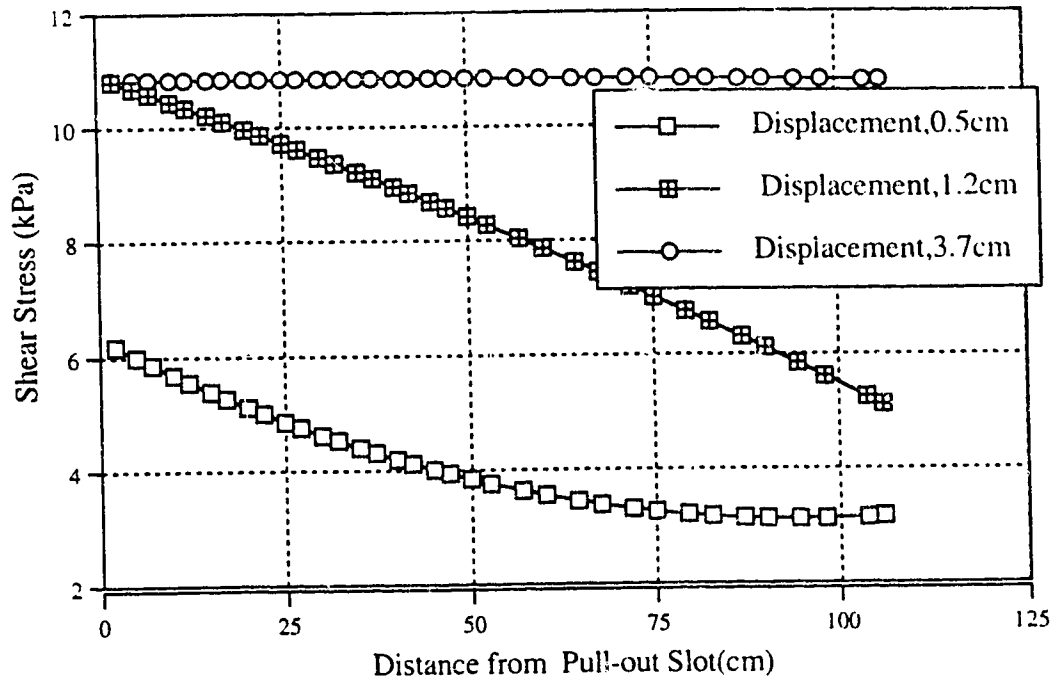


Figure 5. 9 Shear Stress Distribution along the Reinforcement

CHAPTER 6. FINITE ELEMENT ANALYSIS OF THE DEVON TEST FILL

6.1 Introduction

In the last two decades finite element methods have experienced tremendous growth, in both theoretical developments and applications. The method has gained popularity in obtaining solutions for complex problems in geotechnical engineering. However, the application of the finite element methods for analysis of reinforced soil have not been widely used for the design of reinforced soil structures. Finite element methods have been mainly used in research to verify existing semiempirical design methods and back analysis of reinforced soil structures, as these methods can provide working stresses and displacements in a reinforced soil structure. Because of the complexity of the finite element technique and the difficulties to simulate realistic soil-reinforcement interface behavior, they are not yet well-suited at present for routine design purposes.

The main concerns for a reinforced soil structure are deformation, working stress and stability. A reinforced soil structure can only perform satisfactorily if the magnitude of soil strain required to mobilize the reinforcing mechanism is acceptable. With extensible reinforcement, several percent strain may be required before sufficient forces in the reinforcement are developed to mobilize the necessary restraint. The acceptable magnitude of strain and the associated reinforcement forces mobilized should be used as a design criterion rather than using the rupture stress. This strain compatibility can only be achieved through a stress-deformation analysis such as the finite element analysis.

Stability of the reinforced structure can be evaluated using either a limit equilibrium analysis or a finite element analysis. Limit equilibrium analysis deals with the stability of the reinforced soil structures at incipient failure. Limit equilibrium methods can not provide internal stress and strain distributions within the reinforced soil structure under working

stress conditions. However, limit equilibrium methods are still the most common analytical approaches in recent design practices for the reinforced soil structure. Liu (1992) suggested that the current design methods are conservative, and the conservatism comes from the uncertainty of the stress-deformation characteristics of the reinforced soil structure and load distribution within the soil and the reinforcement.

The test fill, 12 m high with 1:1 side slope was built near Devon, Alberta to achieve a good understanding of the reinforcement mechanism in a geogrid reinforced cohesive soil slope (Liu, 1992). Finite element analyses were carried out to understand the behavior of the reinforced slope and to compare it with observations from field instrumentation. The unreinforced slope was analyzed first using the finite element method, and the result was compared with field measurements. The prediction is a class C1 prediction (Lambe, 1973). Therefore, the input parameters for the finite element analysis was determined based on the laboratory test results. Input parameters for the foundation soil and the fill could be confirmed by a comparison between the calculated and the observed behavior of the unreinforced slope.

One of the difficulties of finite element analysis of a reinforced soil system is to simulate the soil-reinforcement interaction properly. Although, the relative displacement between the soil and reinforcement was small based on the measured test fill behavior, the interface behavior was simulated by the stiffness associated with two set of springs: one in the direction normal to the interface and the other in the tangent direction (Goodman et al., 1968). These input parameters were obtained from the pull-out or direct shear tests. The method to calculate the shear stiffness of the interface element from pull-out test results can be found in Chan et al. (1993). A large slipping interface model is not considered to simulate the soil-reinforcement interaction in this analysis because the relative displacement between the soil and the reinforcement is expected to be small with maximum reinforcement strain about 2.5 %.

A parameter study of the soil input parameters was carried out until the calculated

values were in good agreement with the observed values in the unreinforced soil section. This ensured that the soil input parameters for the foundation and the fill soil were chosen properly. According to the field measurements no significant time-dependent strains were measured in the soil during the four year period following completion of the fill. It was also found that no obvious creep strains along the reinforcement were observed in the reinforced section. Therefore, long-term finite element analysis was not carried out.

In this chapter, the material properties of the test fill will be briefly described. Then, SR-2 geogrid reinforced and unreinforced sections of the test fill will be analyzed by the finite element method. Comprehensive comparison is made between the calculated values and the measured values. Favorable agreement between the calculations and field measurements will provide not only confidence to understand the load transfer between cohesive soil and geogrid reinforcement but useful information regarding the use of finite element methods to predict the behavior of reinforced embankments.

6.2 Material Properties for the Finite Element Analysis

Proper constitutive models of the test fill and their material parameters should be used in the finite element analysis. Nonlinear stress-strain relationships were used for modeling the behavior of the soil, and the model parameters were derived based on triaxial tests results. The load-strain behavior of geosynthetics under unconfined test conditions of 20°C and a strain rate 2% per minute were used to model the reinforcement. More detailed properties of the fill and foundation soils can be found in Hofmann (1989).

6.2.1 Foundation Soil

According to the borehole information of the foundation soil, it was estimated that only the top 6 m of foundation soil would compress significantly under the weight of the

test fill. A large undisturbed block sample of clayey silt was removed from the floor test pit at a depth of 4.5 m below the ground surface. The average permeability of the block samples determined from consolidation tests was 1.32×10^{-7} cm/sec. According to Holtz and Kovacs (1981), a silty clay with a permeability of 10^{-7} cm/sec would be classified as practically impervious. The top 6m of compressible foundation soil was completely saturated (Hofmann, 1989). The site and foundation preparation started on June 8, 1986 with grading of the site to a ground surface elevation, 702 m, and construction of test fill had proceeded slowly. However, the last 6m of fill soil was placed quickly.

According to the pore pressure measurements in the foundation soils of the test fill during construction, the magnitude of the pore pressures in the foundation soils were small (Liu, 1992). Therefore, the volume change of the foundation soils would also be small. Consequently, the stress-strain and settlement characteristics of the foundation soil determined by laboratory test with undrained conditions could be used to derive the material properties for the finite element analysis. The material parameters obtained from the laboratory testings are presented in Table 6.1

The stress-strain curves derived from consolidated undrained triaxial test results on the tube specimens appear to exhibit hyperbolic shapes but the stress-strain curves on block specimens rose steeply in a straight line up to about 2 % strain and then broke sharply to continue straining under a constant stress. This can be idealized as a elastic-perfectly-plastic material. If the structure of the soil is disturbed during sampling, the true stress-strain behavior of the in situ soil may not be obtained from laboratory testing. The tube specimens were considered to be disturbed considerably during the sampling process. It was therefore decided that the effective stress strength parameters obtained from block specimens were more representative of the field strength and these parameters were selected for the finite element analysis.

According to field measurements (Liu, 1992) the settlement in the foundation soil beneath the crest in the unreinforced section was 40 mm at the ground surface when the fill

height reached 12 m. For the Tensar SR-2 reinforced section the settlement profiles at the foundation soil beneath the crest were similar to the profiles in the unreinforced section, but the amount of the settlement varied between 8 mm at 6 m below the ground surface and 85 mm at the ground surface. However, the strains in the foundation soil based on the settlements reach the maximum of 1.4% for the reinforced section. It indicated that the foundation soil could be idealized as a linear elastic material under small strain conditions as shown in Figure 6.1. The soil parameters used in the finite element simulation are presented in Table 6.1.

6.2.2 Test Fill Soil

Triaxial tests were performed on fill soil materials to establish their stress-strain properties for the finite element analysis. The stress-strain curves and the effective frictional strength obtained from the consolidated drained triaxial tests would govern the long-term stability and deformation characteristics of the test fill. However, the stress path experienced by the test fill did not necessarily follow the consolidated drained triaxial test stress path. Construction of the test fill proceeded slowly, and there was sufficient time to allow excess pore pressure to dissipate. Therefore, it was extremely difficult to simulate the stress path of the field conditions in the laboratory tests. Hence, as an approximation, the stress-strain curves obtained from conventional consolidated drained triaxial tests were used for the finite element analysis. The stress-strain curves shown in Figure 6.2 appear to be hyperbolic in shape. The contribution of volume change, induced by shear stresses, to the horizontal and vertical strains in the fill soil has been included in the analysis. However, the volumetric strains due to consolidation of the test fill have not been considered.

These material parameters were based on laboratory test results which may not provide the best fit of field observations due to different stress paths, sample disturbance

and compaction effort. Therefore, one needs to calibrate the finite element model using field measurements. Preliminary material parameters were obtained from laboratory testing results and applied to the test fill analysis. Then, the material parameters were changed until the calculated values provide best fit of the field measurements. It was necessary to simulate the triaxial tests using selected material parameters in order to compare results with the experimental test results. Figure 6.2 and Figure 6.3 show the predicted stress-strain and volume change curves compared with the laboratory test results, respectively. The material parameters used in the simulation of triaxial tests are listed in Table 6.1. The predicted and measured stress-strain curves agree quite well at small strains. The observed volumetric strains are somewhat larger than those predicted. However, at a confining pressure of 80 kPa, volumetric strains are not significantly changed as shown in Figure 6.3. During the analysis the modulus number (K) of the hyperbolic model is varied to provide the best fit with the field measurements. Therefore, one needs to examine the sensitivity of the modulus number to the stress-strain curves. Figure 6.4 shows that the variation of the modulus number does not significantly affect the stress-strain behavior of the test fill.

6.2.3 Geogrid

Load-extension properties of reinforcement are obtained from unconfined tests such as the grab tensile test, the strip tensile test and the wide width tensile test. It has been recognized that soil confinement would not affect significantly the load-strain properties of the geogrid (McGown et al., 1984). The load-strain behavior of the geogrid was determined by the wide width tensile test under conditions of 20°C and a strain rate of 2% per minute. The strain rate of a reinforcement in an unconfined tensile test can affect the load-extension properties of the reinforcement. However, the load-strain properties of Tensar SR-2 was not affected by the strain rate (Liu, 1992). Tensar SR-2 does not become

brittle until a very low temperatures is reached, -50°C , and a service temperature range for SR-2 is considered to be -50°C to $+80^{\circ}\text{C}$.

The models developed for representing the load-strain behavior of polymer reinforcement were by curve fitting methods which included linear elastic, nonlinear quadratic and polynomial elastic behavior (Chalaturnyk, 1988). The results of short-term tests were not adequate because sustained loading of polymer materials would also induce creep. Hence, creep and constant strain rate tests must be performed. The results of constant strain rate tests on Tensar SR-2 at various temperatures indicate that the peak strength is a function of both temperature and rate of loading (McGown et al., 1984). These results also indicate that there is a tendency for load-strain behavior to change from ductile to brittle with decreasing temperature. For the long-term stability and deformation behavior of the test fill the creep, stress relaxation and temperature characteristics of the reinforcement should be considered in the analysis.

According to the field measurements lateral deformations of the fill soil in the reinforced slopes induced tensile strains of the geogrids in different layers, which varied between 1.0% and 2.5%, and mobilized tensile forces up to 35% of the peak tensile strengths (Liu, 1992). Creep data of the reinforcement may be plotted in the form of isochronous curves. Figure 6.5 shows that for Tensar SR-2 much of time-dependent deformation occurs in the first 100 hours to 1000 hours of loading. The creep effect at small strain such as 1.0 or 2.5% was not significantly based on the isochronous curves. Thus, the creep behavior of the reinforcement is excluded in this analysis.

The reinforcement was modeled using a non-linear quadratic relationship. Figure 6.6 shows the comparison of the load-strain curves between the observed data from tensile tests and the predicted data from simulation using the selected parameters listed in Table 6.1. As shown in Figure 6.6 the predicted behavior of the reinforcement is well matched at small strains of 1.0 or 2.5% which were mobilized in the reinforcement in the test fill.

6.3 Unreinforced Slope Analysis

In order to achieve a better understanding of the reinforcement mechanisms and to quantify the improved slope behavior due to reinforcing, the test fill had an unreinforced soil section. The behavior of the test fill was extensively monitored by a set of instruments installed in the embankment and on the geogrid (Liu, 1992). The data provided by these instruments provides a good basis for comparing the results of numerical studies with the measured performance of the test fill using the finite element techniques. In the analysis, the foundation soils are represented by eight node elements in two layers, and the fill soils are simulated using eight node isoparametric and six node triangle elements. A two dimensional plane strain idealization of the test fill is shown in Figure 6.7. A total of 453 soil elements with 1428 nodes was used in the simulation of the unreinforced slope. Because the fill soil is not saturated, analysis of the test fill behavior is carried out in terms of total stresses, i.e. no pore pressure was explicitly considered.

The construction of the test fill commenced in the summer of 1986, and the construction of the test fill was carried out in three stages. The fill was constructed to a height of 3 m by 23 October 1986, and the fill height reached 6 m at the end of the second construction season on 3 November 1987. The construction of the test fill continued during the following summer. The top 6m of soil was placed to reach the 12 m design height on 29 October 1988. Further details of the construction procedure and field instrumentation can be found in Liu (1992). Figure 6.8 shows the construction schedule of the test fill which was used in the analysis for the actual loading rate.

According to oedometer tests conducted on the foundation soil the preconsolidation stress was approximately 400 kPa. This was more than the increase in the stress the foundation soil will be subject to due to the weight of the test fill. Therefore, settlement of the foundation soil due to the weight of the overlying test fill would not be expected to be large. The development of the pore pressures in the fill was closely related to the height of

the fill. The pore pressures in the fill increased as the fill was placed during each construction season and dissipated when no fill was placed.

In the finite element analysis eleven construction layers were used to simulate the construction procedure of the test embankment. The first construction layer raises the embankment height to 2.0 m. The second layer was 1.0 m thick, and the remaining layers were also each 1.0 m thick. During the analysis, the incremental load was applied by assigning the gravity load of the fill elements layer by layer.

The calculated and measured settlement profiles at the ground level are compared in Figure 6.9 and 6.10. During the early stages of construction, the calculated and measured values agreed quite well. As the height of the embankment approached 6 m the total settlement increased from the toe to 9 m in the fill and remained approximately constant at about 23 mm. It was observed that the distribution and the variation of the vertical deformation of the foundation soil was uniform. Because no significant localization was observed in the foundation settlement the calculated vertical settlements agree quite well with the observed values. The calculated and measured settlements were in good agreement when the fill height reached 6m as shown in Figure 6.9.

Six months after the completion of a 12 m fill the settlement profile changed significantly; the vertical settlement of the foundation soil increased sharply from zero at the toe to 120 mm beneath the crest of the slope. The vertical settlement at the ground level represents the settlement of the foundation due to the placement of the fill. Therefore, this large increment of vertical settlement in the foundation soil may be due to consolidation in six months after the placement of the fill. However, the observed pore pressure in the foundation soil did not change significantly after the completion of the 12 m fill. The calculated vertical settlements after the completion of the test fill were smaller than those measured as shown in Figure 6.10.

A linear elastic model was selected for the foundation soil based on CU triaxial test results of a block sample. A large undisturbed block sample was removed from the floor

of a test pit at depth of 4.5 m below the ground surface. Two test pits were dug with a backhoe near the test fill site. As the fill height was increased the influence zone in the foundation soil would expand. Until 6m of fill the deformation modulus of the foundation soil can be obtained from the triaxial test results of the block sample. However, when the fill height reached 12 m the linear elastic model may not represent the foundation soil behavior. This implies that the calculated settlement in the foundation soil is underestimated.

The preconsolidation stress of the foundation soil was found to be 400 kPa based on oedometer test which was more than the maximum stress of approximately 240 kPa due to the test fill. However, if the preconsolidation stress of the foundation soil were in the range of 120 to 240 kPa, the overburden stress induced by the test fill up to 6 m high is less than the foundation soil's preconsolidation stress. Therefore, large settlements of the foundation soil would not be expected. When the fill height reached 12 m the overburden stress of the foundation soil is more than the foundation soil's preconsolidation. It indicates that the settlement of the foundation soil significantly increases because of a normal consolidated foundation soil. This assumption could provide an explanation for large settlement at the 12 m fill height.

Profiles of the settlement at the 2 m level in the unreinforced section are shown in Figure 6.11. A maximum total settlement of 56 mm had occurred at the 8 m location at the end of the second construction season. The settlement decreased gradually at locations approaching the slope surface and center of the test fill. The settlement profiles dramatically changed due to the placement of the 6m fill. The large increment of settlement at the foundation soil after the completion of the fill might affect the settlement profile. Agreement between the measured and calculated settlements at 2 m level is good as shown in Figure 6.11.

The calculated and the measured vertical settlements at 4 m level are compared in Figure 6.12. Usually the soil close to the center of a slope develops a large amount of

settlement as the fill is placed. The settlement profile after placement of the 6 m fill dramatically changed around the 6 m location from the slope face. Beyond the 7 m location, the rate of the increase of the settlement was much smaller. This localization of the vertical displacement would give an indication of a highly sheared area within the unreinforced slope or a non-uniform foundation soil formation. The vertical settlements at 4 m level in the unreinforced section distributed smoothly across the slope section, varying between 43 and 63 mm, when 2 m of fill was placed above the foundation level.

After the completion of the 12 m fill, the average amount of the settlement increased in the soil around the center part of the fill. It was observed that a total settlement of 237 mm occurred at the 12 m location from the slope surface; the largest incremental settlement appeared at the 5 m location where the increment of the vertical displacement varied from 26 to 90 mm within 2 m of soil. The excessive displacement of the soil within 1 m from the slope surface represented the shallow movement of the fill soil weakened by freeze-thaw cycles. But in finite element methods the freeze-thaw effect was not simulated. Therefore, in these analyses less agreement was obtained between the measured and calculated vertical settlement at the surface of the slopes.

The horizontal deflections of the foundation soils along vertical lines beneath the toe and the crest of each test section were monitored by using a vertical digital biaxial inclinometer operated in the casings installed. The results of the finite element analyses of the test fill are compared to the measured values of the horizontal deflections of the foundation soil in Figure 6.13 and 6.14. The calculated horizontal deflection by finite element analyses show outward movement which decreased towards the ground surface. As shown in Figures 6.13 and 6.14, the magnitudes of the calculated and measured horizontal deflections agreed quite well, especially when the fill reached a height of 6m. However, the measured horizontal deflection developed during the first construction season was of negligible magnitude. As the fill height increased, the horizontal movement increased from the bottom of the foundation to the ground surface in the analyses.

However, the profile of the deflection measured for the 3m fill and 6 m fill was almost identical from the bottom of the casing to the -3 m level.

The results of the analyses for the unreinforced section were in good agreement with the field conditions. This suggests that hyperbolic stress-strain relationships can be also used to model the behavior of reinforced soil embankment.

6.4 Reinforced Slope Analysis

The good agreement between calculated and measured settlement in the unreinforced section provided the confidence for the Tensar section analysis using the hyperbolic soil model. Three types of geogrids, Tensar SR-2, Signode TNX5001 and Paragrid 50S were used as reinforcing materials in the test fill. Unfortunately, the production of Signode geogrid was halted by the manufacturer after it was incorporated in the test fill. For Paragrid geogrid, it was found that during strip tensile tests that some of the high strength fibers in the tension member were broken or damaged at the intersections of the grids. Therefore, the load-strain properties of Paragrid geogrid was not completely obtained from laboratory. However, Tensar SR-2 geogrid has been widely used as a reinforcing material in reinforced soil structure. The load transfer mechanism between soil and Tensar geogrid has been studied by many researchers (Yogarajah and Yeo, 1994 ; Farrag et al., 1993). Additionally, SR-2 geogrid was used to simulate the pull-out test to study interface behavior (Chan et al., 1993 ; Yi et al., 1995). Therefore, the Tensar SR-2 reinforced section is chosen for the finite element analysis.

The input parameter used in the unreinforced slope analysis provided a guideline for the soil input parameters for the reinforced section. The foundation and fill soil were represented by eight node elements, while the SR-2 reinforcement was simulated by three nodes bar element which can not sustain compression forces. The reinforcement was modeled using a non-linear force-strain relationship based on a parabolic relationship between load and strain developed in the reinforcement (Chan et al., 1993).

The foundation soil profile was divided into two zones representing a dense sand beyond a depth of 6m from the ground surface and a stiff clay till between 6 and 10 m below the ground surface. The measured pore pressure response of the foundation did not show a response to the construction activities. The magnitude of the induced pore pressure in the foundation soils was of little significance for a total stress analysis. However, the development of pore pressures within the fill corresponded to the construction activities; pore pressure was built up during the construction period and dissipated in the subsequent consolidation period. However, there were no pore pressure measurements for the upper 6m of fill. To simulate the long term stress-strain behavior of the fill, consolidated drained triaxial tests were adopted for the long term condition of the test fill.

To simulate the interface between the soil and the reinforcement, zero thickness interface element was used. Wu (1993) suggested that if the value of the shear stiffness (Kn) is not large enough, penetration will occur at the contacting nodes between the soil and the reinforcement. If the value of Kn is too large, there will be a loss of accuracy and hence the resulting normal stress at the interface may be in error. The use of the interface element in the reinforced soil structure analyses causes some difficulties. Two input parameters for the interface element, shear stiffness (Ks) normal stiffness (Kn), was obtained from the pull-out test result. Usually, the normal stiffness (Kn) is assigned high values to prevent overlapping at the interface between the soil and the reinforcement. However, it was found that the normal stiffness of the interface element affected the analysis results. If, for example, the value of the normal stiffness which was less than 1×10^9 kN/cm³ or greater than 1×10^{16} kN/cm³, the numerical solution diverged in the nonlinear analyses at the third construction stage. Poor convergence of analysis was often found in non-linear problems involving the conventional joint elements (Rowe et al., 1978). Therefore, Wu (1993) suggested several points to simulate the interface behavior in the finite element analysis; in the case where the relative movement at the interface is judged unlikely or unimportant, the analysis should be performed using fixed interface condition,

i.e., no interface element should be used. Because small strain between the soil and the reinforcement would be expected, Chalaturnyk (1988) carried out the analysis of reinforced slope without an interface element because the strains were small between the soil and the reinforcement. The shear stiffness was obtained from the pull-out test conducted by Costalonga (1988).

The finite element mesh for the reinforced section is shown in Figure 6.15. It consists of 2464 nodes and 857 elements including 95 reinforcement elements and 170 interface elements. The foundation soils were represented by eight node elements in seven rows, and the fill was modeled using six and eight nodes elements. The soil-reinforcement interface was modeled using a 6 node interface element. The method of connecting the interface elements to the soil and the reinforcing elements is important, especially at the end of the reinforcement element end (Chan et al., 1993). In this analysis the B connection method was used. All input data used in the analyses can be found in Table 6.1.

6.4.1 Strain Distribution along the SR-2 reinforcement

Strains of the reinforcement were measured using electric wire resistance strain gauges and inductance transverse coils strain gauge for longitudinal members and for adjacent transverse members, respectively. Because the distribution of strains for transverse members of the reinforcement would be easily affected by the localization of strains of the fill. In this analysis strains in the longitudinal members of the reinforcement were chosen to compare with the calculated strains along the reinforcement. In the finite element modeling, SR-2 reinforcement is modeled using bar elements. Therefore, strains in the reinforcement measured along the longitudinal members are realistic to compare with the calculated values. As a matter of fact the measured strains distribution along longitudinal members of the SR-2 reinforcement were more consistent than the strain for the transverse members.

6.4.1.1 SR-2 Reinforcement Bottom Layer

Figure 6.16 shows the strains measured by the top and bottom gauges varying consistently throughout the observation period. The development of the strains were directly related to the construction stages. However, strain profiles one and two years after completion of construction were almost identical to that at the end of construction. Finite element analysis shows that the peak of the strain profile within the reinforcement layer tends to move into the slope as the embankment height increases as shown in Figure 6.17. Such a trend can be found in all three layers of the reinforcement.

According to the field measurement, strains due to the fill in the first and second construction season, when the fill height reached 3m and 6m, respectively, were almost identical until a distance 3m from the slope surface because of misadjustment on the initial sensor spacing. However, the development of strains in the second construction season was almost twice that of the first construction season in the finite element analysis. This was a more reasonable strain distribution. When the fill reached 12 m, a large amount of the strain increased was observed in the reinforcement around the location 3 m from the slope surface as shown in Figure 6.16. It indicates that the large settlements in the foundation soil causes the large strain in the bottom layer of the reinforcement. Therefore, the strains around the slope surface were underestimated. However, in these analyses good agreement was obtained between measured and calculated strains towards the center of slope.

The measured strains could be affected by variation of air-temperature on the readout indicator, which induced electric current and converted the electromagnetic coupling into an amplitude by means of an inductance bridge, even though the sensor itself might not be sensitive to temperature variation, as claimed by the manufacturer (Liu, 1992). It is thought that the apparent strains in the geogrid might be overestimated during summer

when the temperatures in the test fill was higher than that in winter, hence, this phenomenon might result in the decrease of strains in the spring. As shown in Figure 6.17, the location of the peak strain shifted into the slope as the fill height increased. Although the finite element analysis calculated the strain distribution around the slope center reasonably well, the prediction of the strain distribution around the slope surface was difficult. Usually the measured strains of the reinforcement were somewhat larger than those measured at the bottom layer of the reinforcement as shown in Figure 6.18.

6.4.1.2 SR-2 Reinforcement Middle Layer

Figure 6.19 illustrates the measured strain distribution of the middle of the primary reinforcing layer of the Tensar geogrid. When the fill height reached 6m, the strains increase from the slope surface into the fill and reached a peak value of 0.71% at 4 and 5 m locations; it decreased gradually further into the fill and dropped to 0.1% at the 10.5 m location. When the fill height reached 12 m, the location of the maximum strain remained the same, but its magnitude increased to 1.8%. The shape of the measured strains profile which showed the construction activities were more consistent and reasonable than those of the bottom layer of the Tensar geogrid. The strain profile after the completion of the test fill did not change near the slope surface. The development of the strains can be directly related to the construction activities.

Figure 6.19 shows the strains distribution for the fill height of 12 m. High localization of strains occurs at the peak location 5 m from the slope surface. It was observed that the development of the vertical settlement at the 2m fill level increased due to uniform consolidation settlement of the fill and the foundation soil. The settlement of the fill soil could cause the strain incremental in the reinforcement layer. It was also observed in the finite element analyses that the peak strains along the reinforcement moved towards the center of the slope as the embankment height increased. As shown in Figure 6.20 and

6.21, the calculated strains were in good agreement with measured strains except at the location from 4 to 5 m from the slope surface where there was development of a peak strain value. The measured strain profile was characterized by high strain localization at the peak location 5 m from the slope surface.

6.4.1.3 SR-2 Reinforcement Top layer

Figure 6.22 shows the observed strain distribution in the top layer of the reinforcement. A maximum strain of 0.24 % occurred at the 1 m location after placement of the 6 m fill. Almost one year after the completion of the 12 m fill, the peak strain moved to the 3m location with a maximum increase of 2.9%. The field measurements were consistent and reflected the construction activities.

When the fill height reached 6 m, the calculated strains distribution gave good agreement with those of the measured strains as shown in Figure 6.23. However, after the completion of the 12 m fill, the calculated strains distribution were underestimated near the slope surface, but the calculated values agree well towards the center of the slope as shown in Figure 6.24. As discussed before, the peak strain values of the reinforcement move into the slope, however the location of peak strain after a 6m fill height was around 2 m from the slope surface. When the fill height reached 12m, the location of peak strains moved slightly into the slope as shown in Figure 6.24. The peak strain occurred at the 3 m location, while in the case of the middle layer the location of the peak strain occurred at 5 m from the slope surface. Liu (1992) pointed out that the strains in the geogrid might be overestimated during summer when the temperature in the test fill is higher than that in winter. This thermal expansion of the geogrid might result in a decrease of strains during the spring.

6.4.2 Vertical Settlement of Fill and Foundation Soils

Relative vertical movements of the fill within the test fill at 0, 2, 4 and 6 m level above the ground were monitored using a horizontal inclinometer which operated in horizontally installed casings. The horizontal inclinometer measured vertical deflections of the casing relative to a certain datum point. When the settlement within the test fill was concerned, the absolute movement of the datum point was required. The sums of the relative displacement along the casing and absolute movement of the soil at the datum point provided the settlement profile at the instrumentation level.

6.2.1 Ground Level in Tensar section

Settlement profiles at the ground level in the Tensar section are shown in Figure 6.25. During the first construction season (3 m fill) a maximum settlement of 21 mm occurred at the center of the fill. Uniformly distributed settlements of 5 to 8 mm developed during the consolidation subsequent to the first construction season. The calculated settlements were compared with the measured settlements as shown in 6.25, which gave good agreement between the calculated and measured values. For a period of five months after the first construction season, the developed pore pressure in the fill and foundation soil due to the placement of the fill had completely dissipated. Because the drainage path in the fill was short, when the fill height reached 3 m, there was little development of pore pressure in the foundation soil. The distribution and the variation of the vertical deformation of the foundation soil was uniform

The fill was compacted with an average water content of 21 % which was about 1 % lower than its optimum water content. The void ratio of the fill varied between 0.62 and 0.81. This indicated that the fill was not saturated and the developed pore pressure in the fill due to the weight of the overlying fill was not expected to be large.

At the end of the second construction season, when the fill height reached 6m, the

settlement at the ground level increased gradually from 23 mm at the toe of the slope to 58 mm at the center of the fill. It increased between 15 and 25 mm due to consolidation and the placement of another 2 m of fill. The observed settlements around the toe of the fill was somewhat larger than those calculated, and as the location moved to the center of the slope, the observed settlements were less than those calculated. However, the agreement between calculated and measured settlement agreed quite well as shown in Figure 6.26.

During the final construction season and for a period of six months of consolidation, the settlement distribution at the ground level significantly changed. The total settlement increased rapidly from the toe and reached the maximum of around 200 mm at the center of the fill. As shown in Figure 6.27, the settlement at the toe of the fill reached 100 mm. Usually the settlement at an embankment increases gradually from the toe to the center of the slope as the calculated settlements in Figure 6.27. However, the magnitude of settlements at the ground level in the Tensar section was almost twice as large as those measured in the unreinforced section.

The profile of settlement at the Tensar section in September, 1990 increased rapidly from the toe to the center of the slope and the maximum of settlement reached 220 mm. Whereas, for the unreinforced section, the settlement characteristics at the same time increased rapidly from the toe to around the crest of the slope and remained almost constant at 138 mm at the center of the fill. However, when the settlements at the first two construction seasons were compared with the unreinforced section, the differences in the magnitude and characteristic of settlement at the two sections was small. Therefore, the agreement between calculated and measured settlements one year after the completion of the 12 m fill (September, 1990) was not as good as that for the first two construction seasons as shown in Figure 6.27.

The settlements at the ground level indicated that the settlement of the foundation soil was only due to the placement of the fill and the consolidation of the foundation soil. The pore pressure change was directly related to the construction of the test fill. Pore pressures

in the foundation soil in the Tensar and the unreinforced section had similar patterns and magnitudes (Liu, 1992). Small pore pressures in the foundation soils developed during the construction stages and it rapidly dissipated; the pore pressure measured in the fill were considerably larger than in the foundation soil. Therefore, it was expected that the consolidation settlements in the foundation soil in the two sections were not significantly different. Thus, it is likely that the significant difference of the foundation soil settlement between Tensar and unreinforced section may be explained by the variation of the foundation soil.

As the embankment height increased, an influence zone which is related to the settlement in the foundation soil would be deeper. Until the fill height reached 6 m, the formation of the influence zone in the foundation soil in the Tensar section would be similar to that of the unreinforced section. However, a weak soil strata might be in the influence zone of the Tensar section when the fill height reached 12 m. Signode reinforced slope which was located adjacent to the unreinforced slope section might have the same soil formations in the foundation soil. Therefore, it is very interesting to note that the variation and magnitude of the settlements in Signode reinforced section is quite similar to those of the unreinforced section after the final construction season as shown in Figure 6.28. Thus, it could be concluded that the weak soil strata located at a certain depth of the Tensar section of the foundation soil would cause some discrepancy between the measured and the calculated settlements when the fill height reached 12m. As discussed earlier, it is likely that the linear elastic model based on the triaxial test of the bulk soil sample can not represent the foundation soil behavior when the fill height reached 12 m. Another possibility of error could be from measuring the preconsolidation stress. The preconsolidation stress of the foundation soil may be less than 240 kPa, which cause the large settlement in the foundation soil at 12 m fill height.

The profile of the vertical deformation of the unreinforced section in the foundation soils were similar to those of the reinforced section. The vertical settlement in the

foundation soils increased gradually from the toe of the slope to the center of the fill as the load from the fill increased. However, there were significant differences in the magnitude of the settlement between the unreinforced section and SR-2 reinforced section as shown in Figures 6.29. It implied that the material properties used in the unreinforced section analysis could not be used in the reinforced section, especially deformation modulus. Therefore, elastic modulus of the foundation soil and the modulus number(K) of the fill in the reinforced section were changed as listed in Table 6.1.

6.4.2.2. 2 m Level in Tensar Section

The settlement due to the placement of the fill during the first construction season was rather uniformly distributed and varied from 22 mm at the toe to 30 mm at the center of the slope. The calculated and measured values of the vertical settlement at the 2 m level in the Tensar section were compared in Figure 6.30. The calculated and measured values are in very good agreement when the fill reached 3m high due to the change of the deformation modulus in the soil as discussed. After the second construction season, the total settlement increased gradually from 57 mm at the slope surface to 80 mm at the center of the fill. The increments of settlements were due to consolidation. The increments of vertical settlement due to consolidation and the placement of 2m of the fill increased slightly from the surface to the center of the fill without significant indications of localization. The calculated and measured values of vertical settlements are compared in Figure 6.31. The agreement is reasonably good with the measured values but somewhat greater than the calculated values.

Almost one year after the completion of the test fill, the measured settlements varied between 167 mm near the slope surface and 310 mm near the center of the slope, which shows considerable increase in the settlement. This large settlement might be caused by weaker soil strata in the foundation soil as discussed earlier. Therefore the difference in the settlements between the measured and calculated values became more pronounced as the fill

high was increased.

6.4.2.3 4 m Level in Tensar Section

The overall movements of the fill and foundation soils below the 4 m level is shown in Figure 6.32. When the fill height reached 6m, the measured settlement varied between 51 mm at the slope surface and 83 mm at the center of the fill. The difference between the measured and calculated values became larger at the surface of the slope.

The profile of settlements in May 1989 showed large differences in both shape and magnitude when compared to the profile of August 1988. The amount of the total vertical settlement increased to 166 mm near the slope surface and 304 mm at the center of the fill with an obvious localization at the location between 3 and 4 m from the slope surface. Therefore, it was expected that the calculated settlements provided less agreement between the measured and calculated settlement values after completion of the embankment.

Although the finite element analyses calculated the strains of the reinforcement reasonably well, settlement predictions are more difficult, especially as the fill height was increased.

6.4.3 Horizontal Deflection of Soils beneath Toe of Reinforced Slope

Horizontal movement of the fill and the foundation soil along the vertical lines beneath the toe was monitored. Calculated and measured horizontal deflections are compared in Figures 6.33. When the fill reached 3 m high, the foundation soils beneath the toe moved outward by a small amount, and the outward movement increased linearly with increase in the elevation. However, the calculated horizontal deflections increased linearly up to 2m below from the surface, and decreased around the upper part of the foundation soils. However, the lower part of the casing moved slightly inward to the

slope. The features of calculated horizontal deflections were similar throughout the analysis. Generally, the calculated values are larger than those measured in the analysis. However, it can be seen that the calculated and measured values are in relatively good agreement after the completion of the test fill.

The calculated profile of the horizontal deflections in the reinforced section and the unreinforced section were the same shape and had almost the same magnitude. It was believed that the reinforced fill soils did not affect the horizontal deformations in the foundation soils. However, the field measurements between the reinforced and the unreinforced slope were quite different. It might be explained that differential settlement of the foundation soils made the casing tilt into the fill or buckling of the casing by the settlement of the foundation soils. The development of horizontal deflection with the construction activities was obvious in the reinforced slope. Increments of 3 to 4 mm in the horizontal movement developed rather uniformly along the vertical alignment from 6m of fill height to 12 m of fill height. However, the displacement did not respond to the construction activities when 6 m of fill was placed.

6.4.4. Settlement beneath Crest of the Slope in Reinforced Section

Vertical movements of the fill and foundation soils along the vertical alignment beneath the crest of the reinforced section were monitored using extensometers. Magnets were installed in the foundation soils through a borehole, and in the fill soils. However, the access tube was blocked after placement of the 6 m of fill and no measurements were taken after the second construction season. Comparison of the measured and calculated settlement beneath the crest of the reinforced section is shown in Figures 6.34. The agreement was reasonably good, but the calculated values were somewhat greater than measured values in the fill. But the measured values were greater than the calculated values in the foundation soils. The settlement increased during the first construction season and

kept developing during subsequent consolidation seasons. The vertical settlement was small below the 2.5 m level from the ground surface, and above that level, the displacement increased approximately linearly to the ground surface and the fill as the elevation increased.

6.4.5. Horizontal Soil Strain in Reinforced Section

Horizontal soil strains of the fill at 0, 2 and 4 m above the ground level, were monitored using magnetic probe extensometers. The calculated horizontal strains of the soil at the ground level are compared with the measured values in Figures 6.35. The horizontal soil strains close to the toe are compressive, and developed extensive further into the fill. During the early stages of construction, the calculated and measured values agree quite well. As the fill height reached 12 m, the measured soil strains were larger than the calculated values, but the agreement between calculated and measured strain was reasonably well. Figure 6.36 compares the calculated horizontal soil strain in the reinforced section with those in the unreinforced section. Even though the deformation modulus for the foundation soil were changed for the reinforced section, the horizontal soil strains of the reinforced section are smaller than those of the unreinforced section as expected.

As the fill height increased, the compression of the soil strain close to the toe was not found at 2 and 4 m levels above the ground surface. The calculated maximum strain occurred in the area 4 to 6 m from the slope surface where the maximum strain was measured. Strain profile of the fill soil at the 4m level in the reinforced section are shown in Figure 6.37. It was seen that the measured strain of the soil developed due to overlaying of the 6 m fill was large, i.e., the development of horizontal strain did not correspond to the construction activities. Therefore, the calculated horizontal soil strain were somewhat larger than those measured when the fill height reached 12 m.

6.5 Conclusion

The behavior of grid reinforced embankment were predicted by plane strain finite element analysis. The comprehensive comparison was made in terms of settlements, lateral displacement and strains of the fill. The distribution of tensile strains along the reinforcement was also compared. The results of the finite element analyses were found to be in good agreement with the measured field behavior up to 6m fill. But the finite element method underestimated the vertical settlements after completion of the test fill. The deformation modulus of the foundation soil affected the settlement profiles when the fill height reached 12m. The results of the analyses performed suggest that the behavior of reinforced embankment can be modeled reasonably well using finite element methods.

6.6 References

- Chan, D.H, Yi, C.T. and Scott, J.D. (1993) "An Interpretation of the Pull-Out Test", Proc. Geosynthetics '93 Conference, Vancouver, Canada, Vol.2, pp.593-605.
- Chalaturnyk, R. (1988) **The Behavior of a Reinforced Soil Slope**, M.Sc. Thesis, The University of Alberta, Edmonton Alberta, Canada
- Costalonga, M.A.R. (1988) **Geogrid Pull-Out test in Clay**, M.Sc Thesis , The University of Alberta, Edmonton, Alberta, Canada, 211 p
- Farrag, K, Acar, Y.B.and Juran, I. (1993) 'Pull-out Resistance of Geogrid Reinforcements, " Geotextiles and Geomembrans No.12, pp.133-159.
- Hofmann, B.A.(1989) **Evaluation of The Soil Properties of The Devon Test Fill** ,M.Sc thesis, Department of Civil Engineering, University of Alberta, Edmonton, Alberta, 325 P.
- Holtz, W.G. and Kovacs, W.D. (1981) **An Introduction Geotechnical**

- Engineering**, Prentice-Hall Inc., Englewood Cliffs, N.J., 733p.
- Lambe, T.W. (1973) "Predictions in Soil Engineering", *Geotechnique*, Vol.23, pp. 149-202.
- Liu, Y. (1992) **Performance of Geogrid Reinforced Clay Slopes** Ph.D. thesis, Department of Civil Engineering, University of Alberta, Edmonton, Alberta, 406p.
- McGown, A., Andrawes, K.Z. and Kabir, M.H. (1982) "Load-Extension Testing of Geotextiles Confined In-soil," 2nd International Conference on Geotextiles, Las Vegas Vol.3, pp.793-798.
- McGown, A., Andrawes, K.Z. and Yoe, K.C. (1984) "Load-Strain-Time Behavior of Tensar Geogrids", *Pro. of Conference on Polymer Grid Reinforcement*, London, PP.31-36.
- Rowe, R.K., Booker, J.R. and Balaam, N.P. (1978) "Application of the initial stress method to soil-structure interaction", *International Journal for Numerical Methods in Engineering*, Vol.1
- Wu, J.T.H. (1992) "Discussion on the Use of Geogrids in Earth Reinforcement", *Pro. Int.Sympo.on Earth Reinforcement*, Vol 2, pp. 928-929.
- Yi, C.T., Chan, D. A "A Slipping Finite Element Model for Geosynthetics", *Geosynthetics '95 Conference* (in press)
- Yogarajah, I. and Yeo, "Finite Element Modelling of Pull-out Tests with Load and Strain Measurements", *Geotextiles and Geomembranes* 13, pp. 43-54.

Table 6. Material Parameters Used in Devon Test Fill Analysis

Parameter	Symbol	Foundation soil		Fill	Fill Reinforced	Reinforcement: Tensar SR-2	Interface
		Silty clay	Till				
Cohesion, kPa	C			30*, 50	50		9
Friction angle	ϕ			25*, 23	23		15
Modulus number	K			125*, 178	87		
Modulus exponent	n			0.26*, 0.22	0.23		
Failure ratio	Rf			0.85*, 0.84	0.84		
Volume change parameter	D			9.5	4.5		
	F			0	0		
	G			0.45	0.45		
Unit weight, kN/m ³	γ	19.8	20.5	18.8	18.8		
Elastic Modulus, kPa	E	23500*	35000 (Unre.)				
		25000 (Unre.)	25000(Rein.)				
Poisson's ratio	ν	0.3	0.3	0.42	0.42		
Tensile Strength, kN/m						87.8	
Load modulus, kN/m						840	
Failure strain, %	ϵ					20	
Normal stiffness, kN/m ³	Kn						1.00E+10
Shear stiffness, kN/m ³	Ks						1530

Rein : Reinforced Section

Unre : Unreinforced Section

* : Material Properties Obtained from Laboratory Testings (before Calibration)

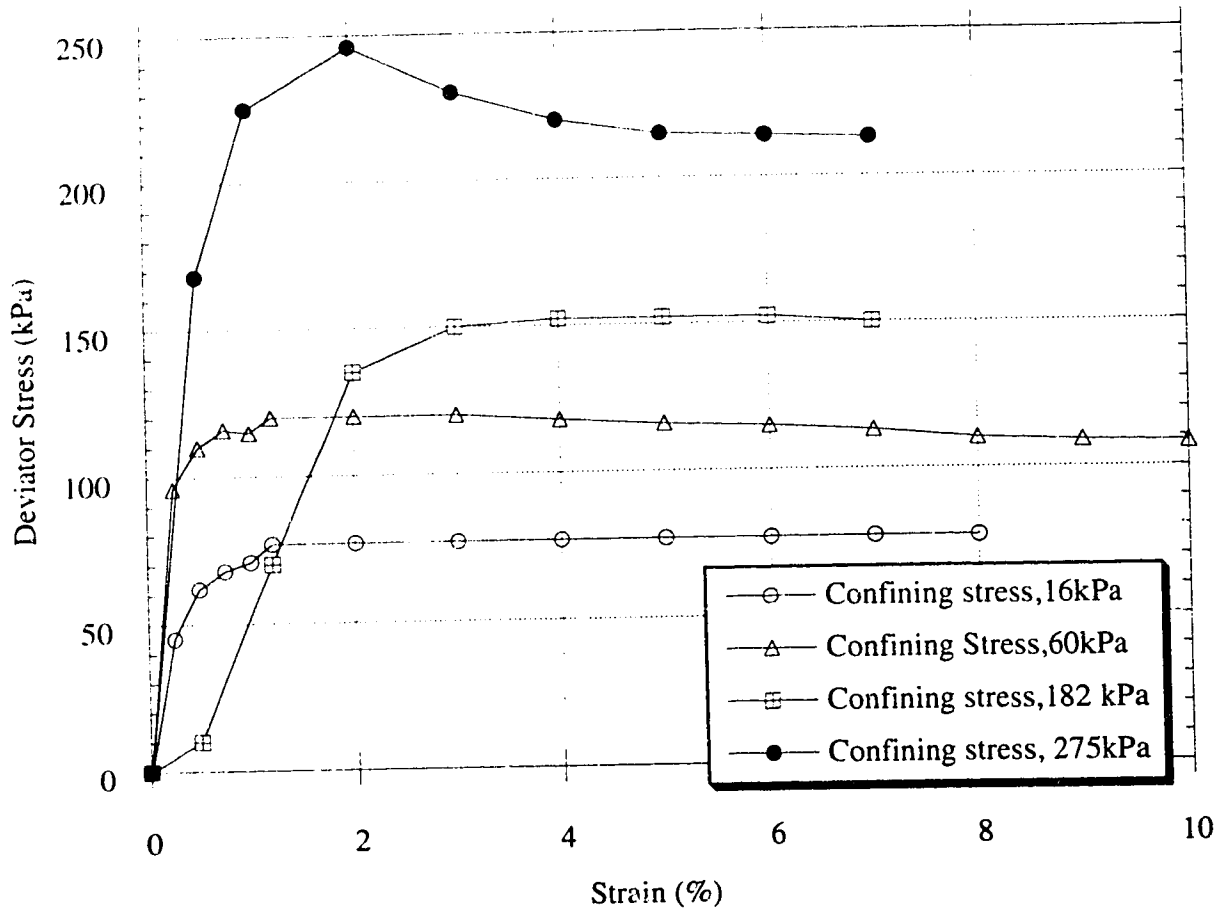


Figure 6.1 Consolidated Undrained Triaxial Tests on Foundation Soil
(after Hofmann, 1989)

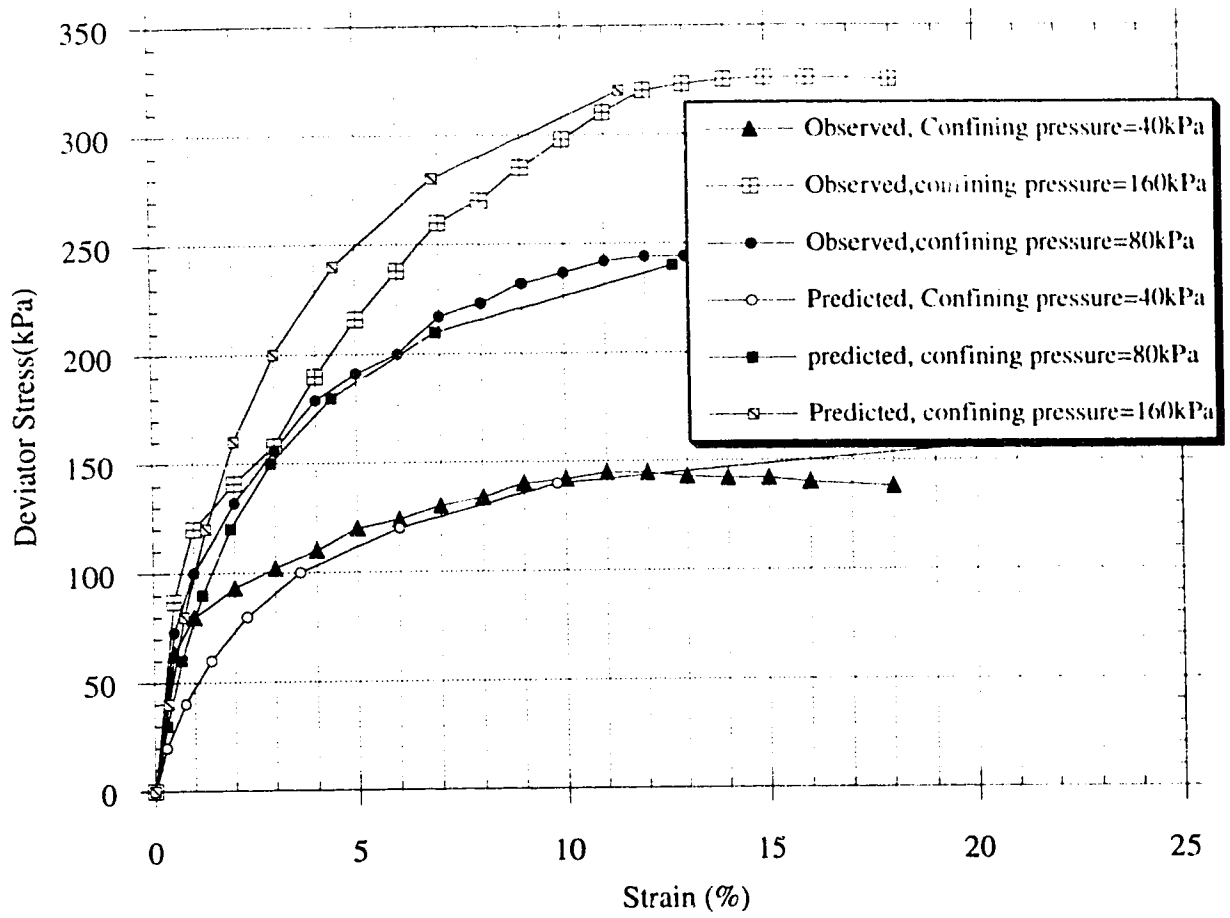


Figure 6.2 Predicted Stress-Strain Curves Compared with Observed Stress-Strain Curves

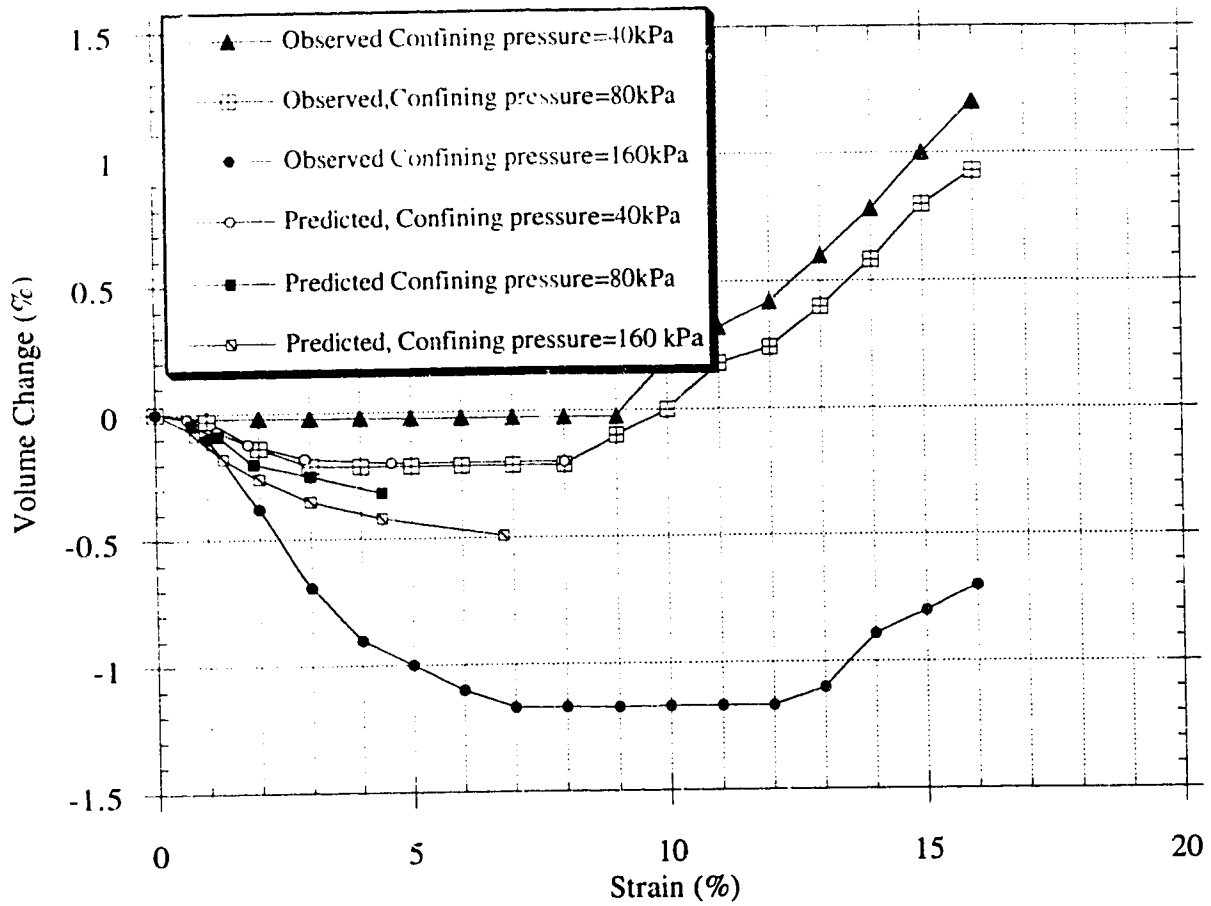


Figure 6.3 Predicted Volume Change Curves Compared with Observed Volume Change Curves

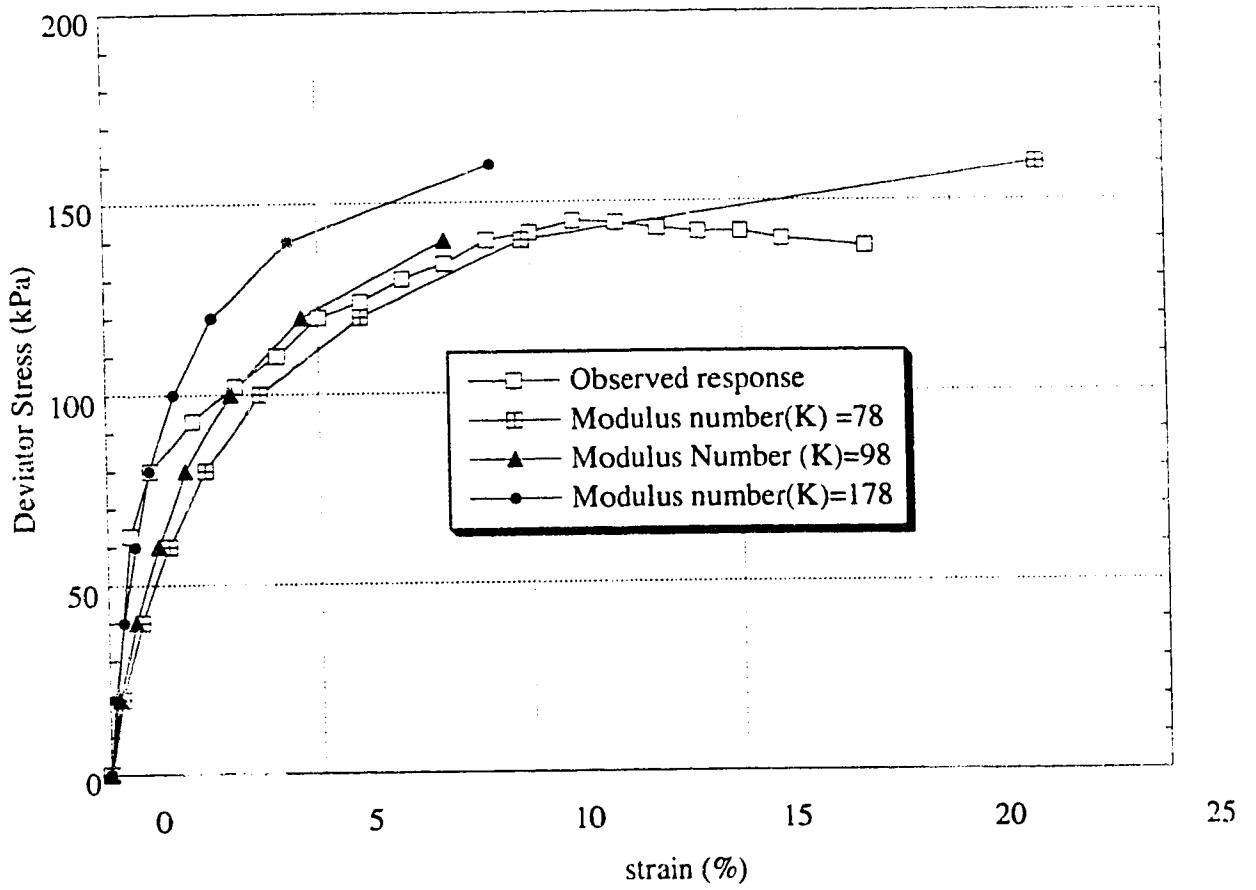


Figure 6.4 Effect of Modulus Number(K) on Stress-Strain Curves
(Confining Pressure=40 KPa, $n=0.23$, $R_f=0.84$)

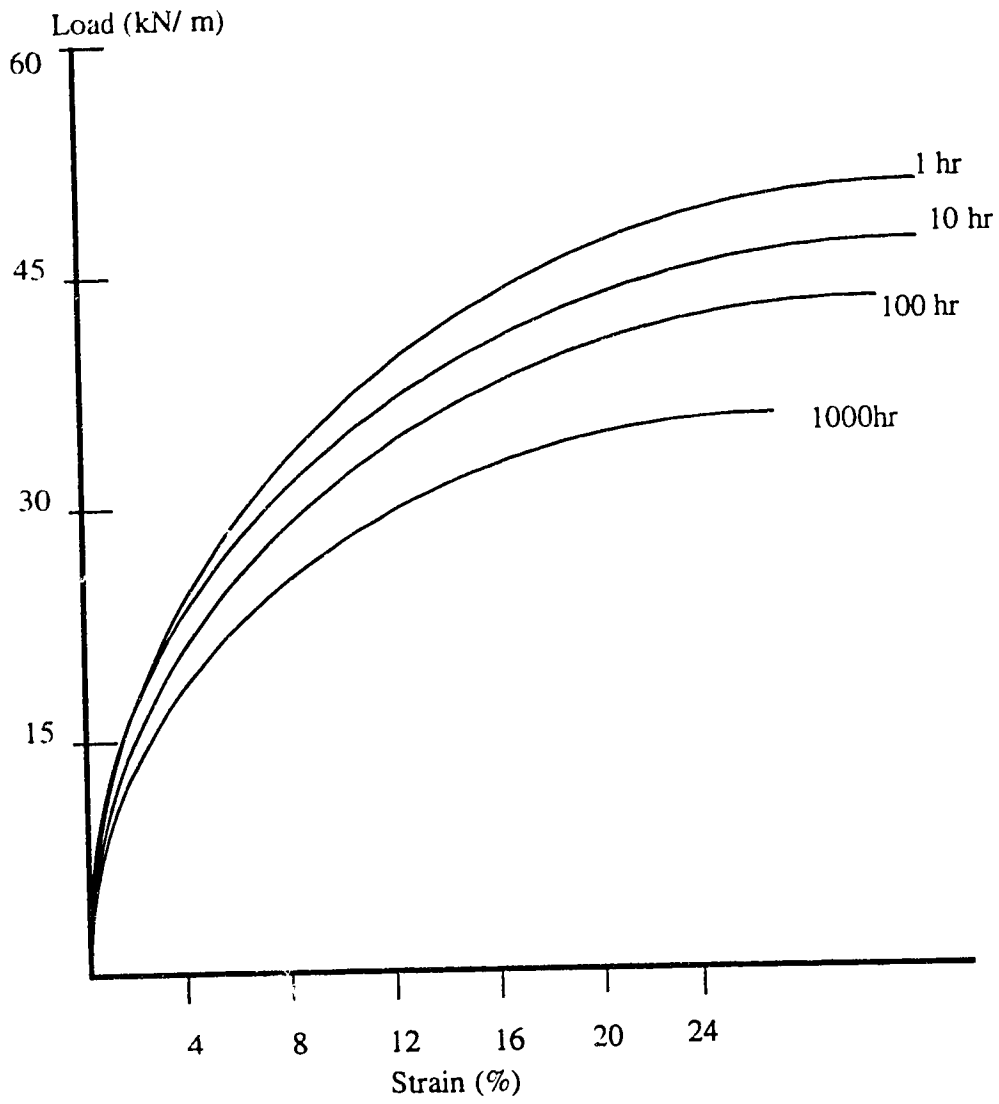


Figure 6.5 Isochronous Load-strain Curves for SR-2 (McGown et al. ,1984)

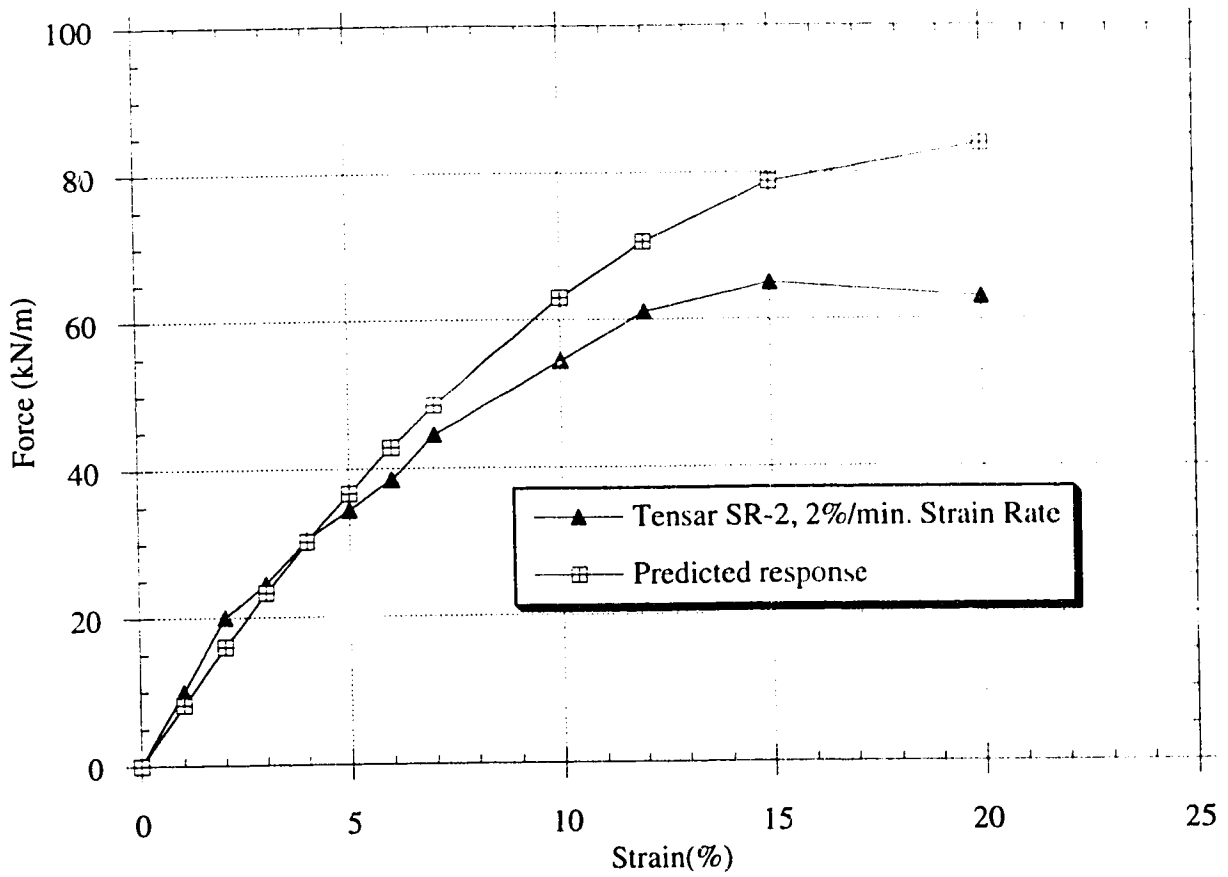


Figure 6.6 Tensile Test of Tensar SR-2 Compared with Predicted Response

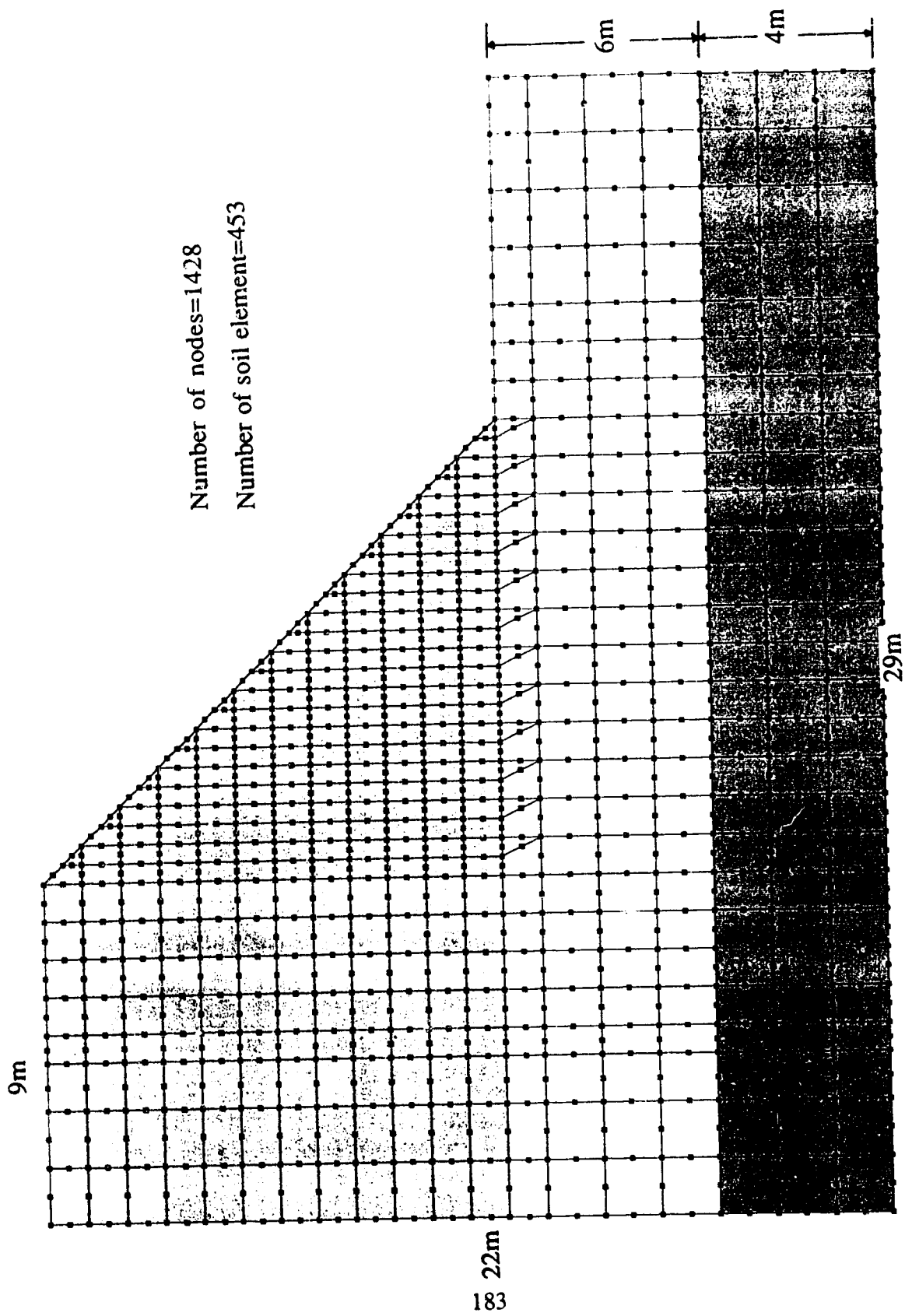
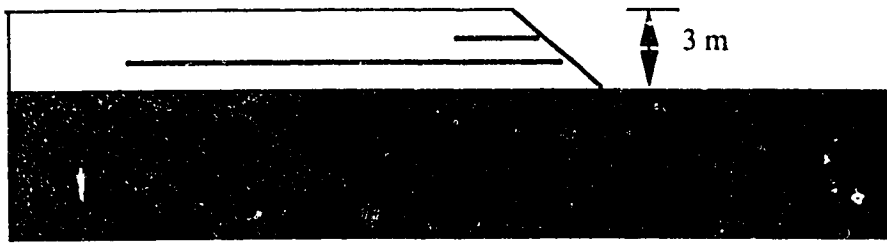
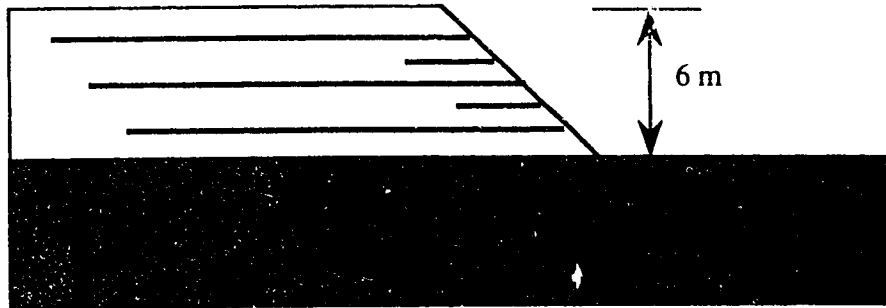


Figure 6.7 Two Dimensional Plane Strain Idealization of Unreinforce Section

1st construction step (Oct.23.86)



2nd construction step (Nov. 3,87)



3th construction step (Oct.29,88)

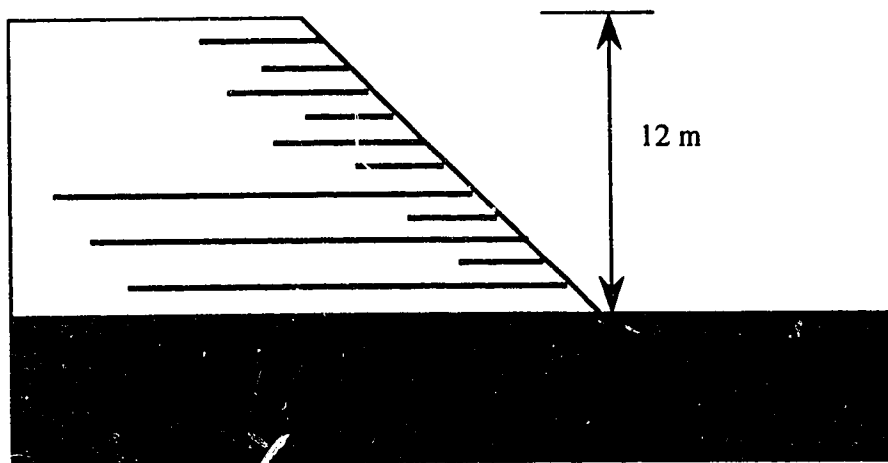


Figure 6.8 Embankment Construction Sequences

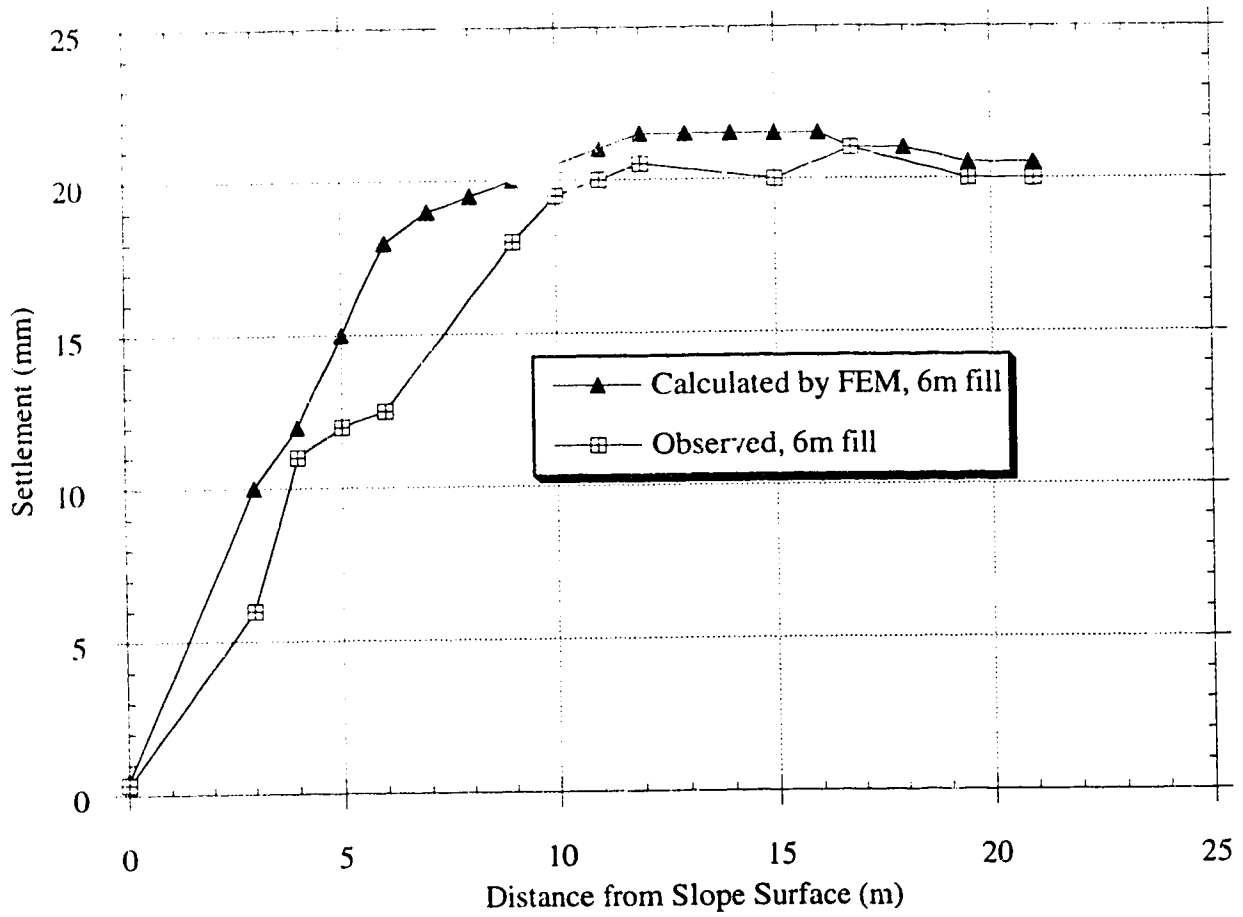


Figure 6.9 Settlement at Ground Level in Unreinforced Section at 6m Fill

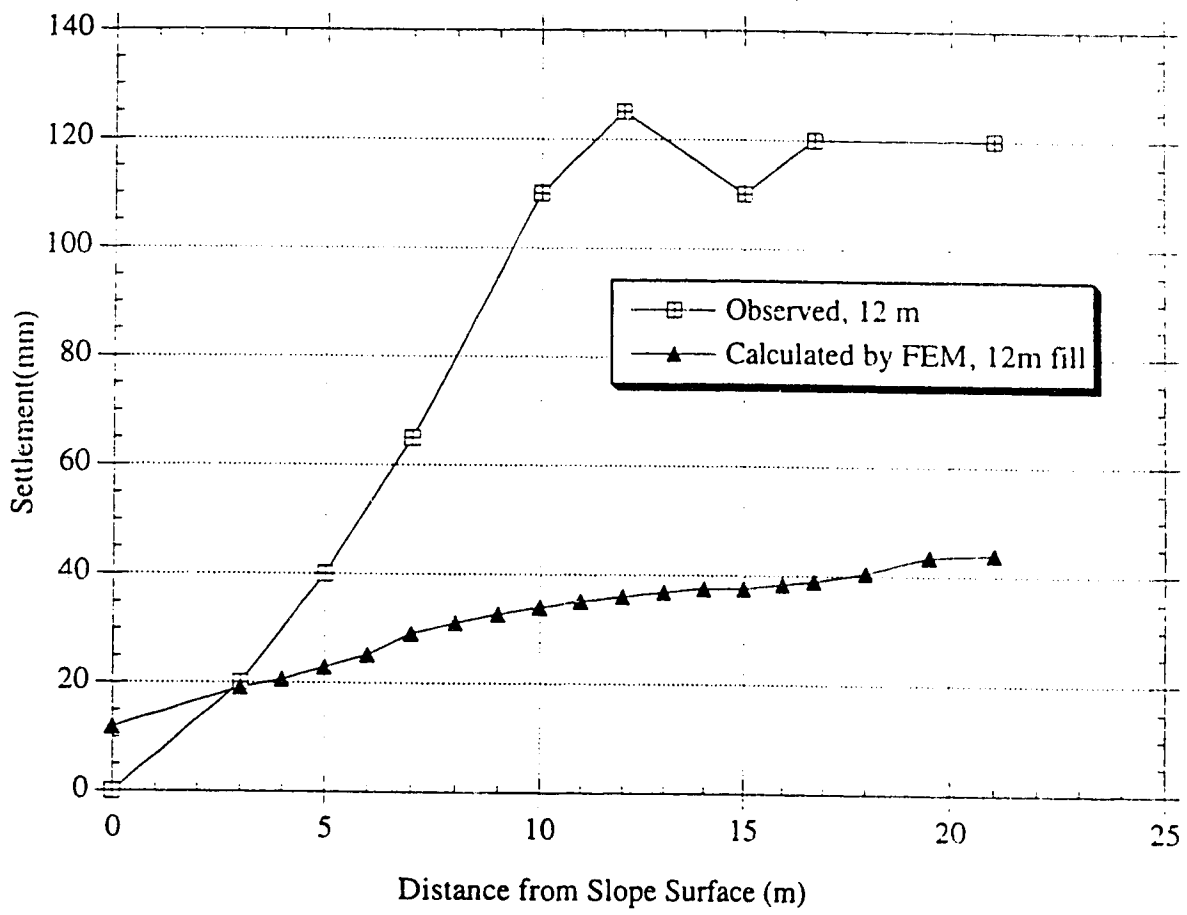


Figure 6. 10 Settlement at Ground Level in Unreinforced Section at 12 m Fill

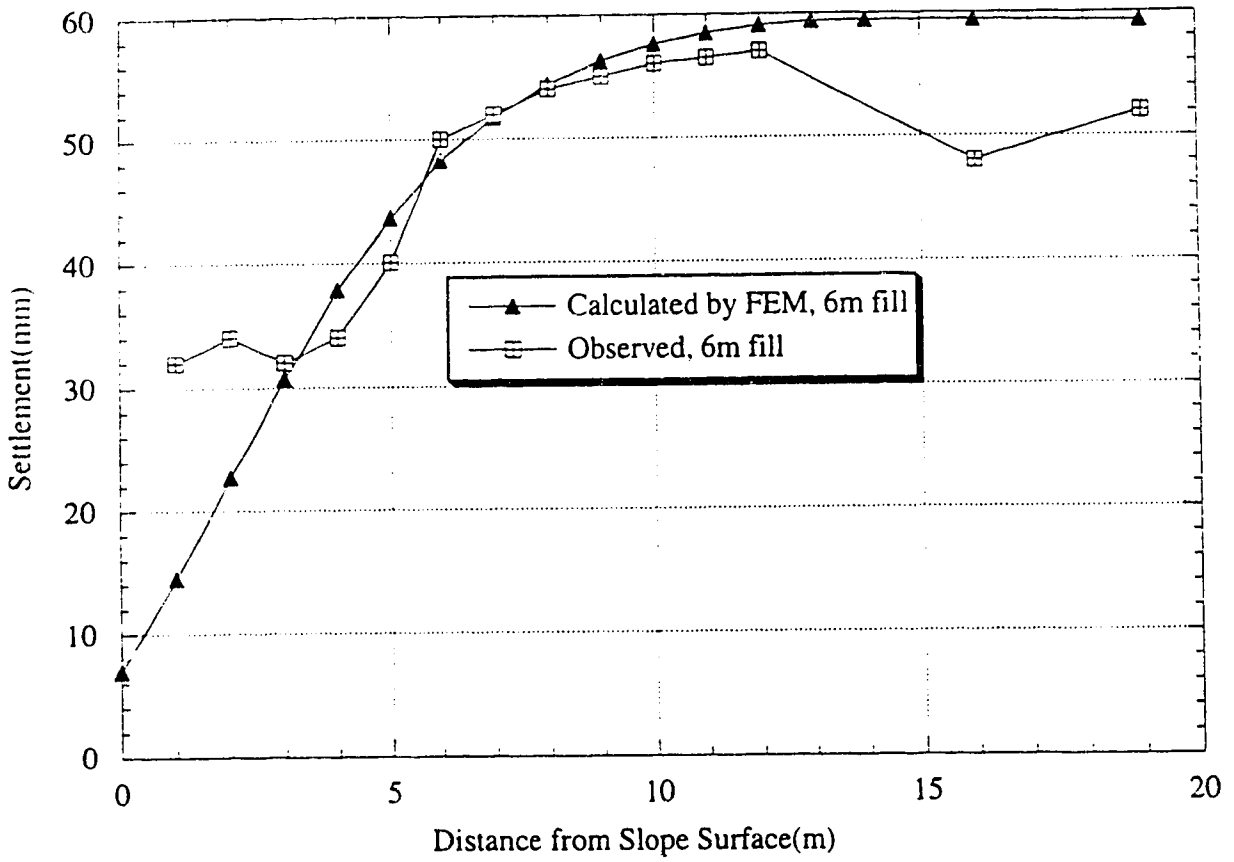


Figure 6.11 Settlement at 2m Level in Unreinforced Section at 6m Fill

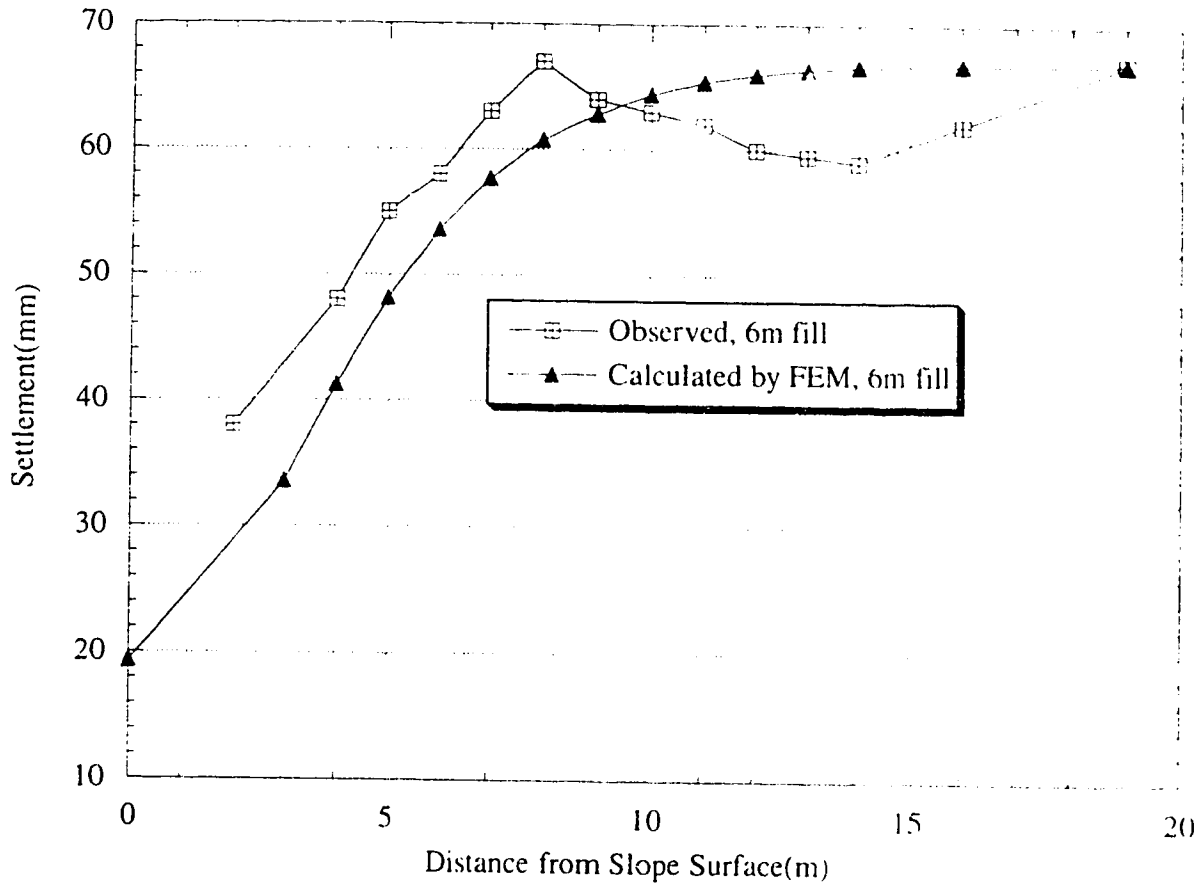


Figure 6.12 Settlement at 4m Level in Unreinforced Section at 6m Fill

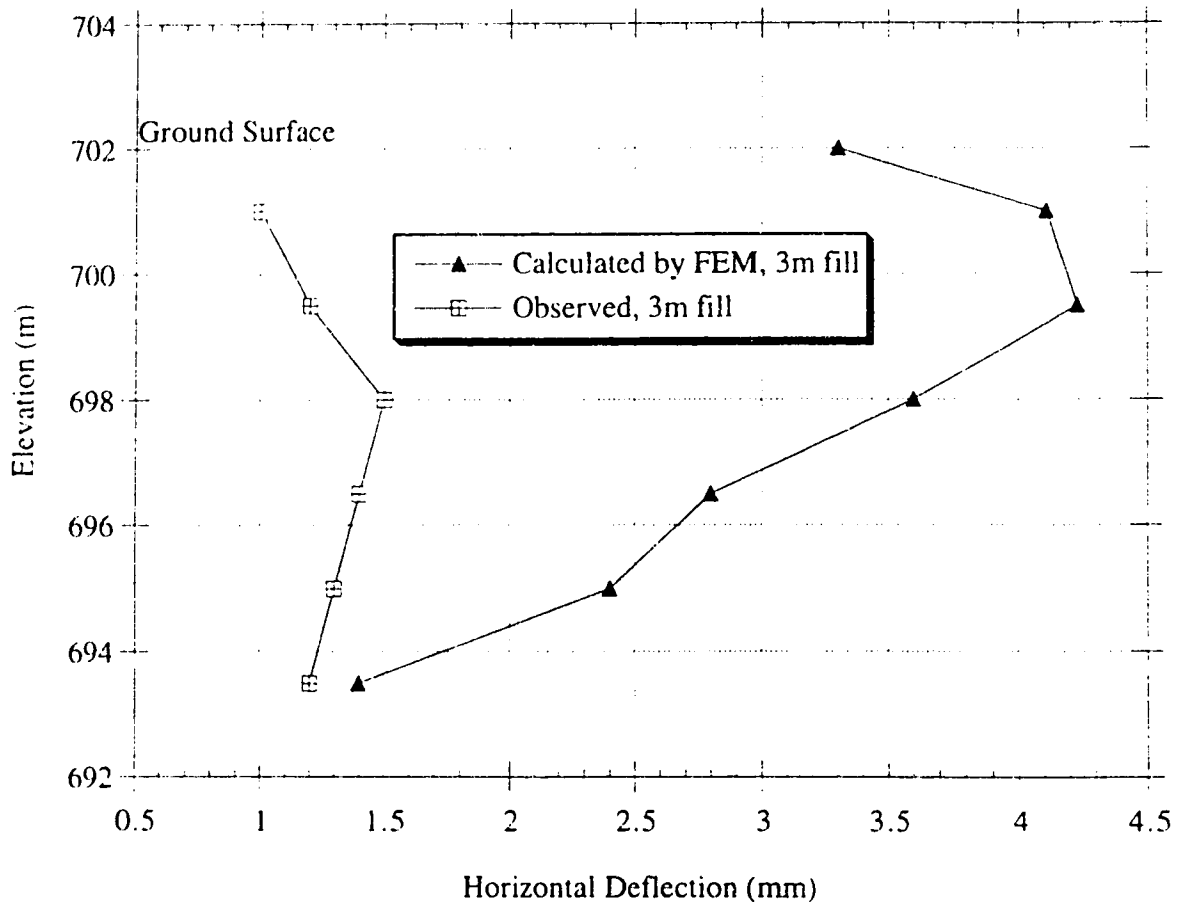


Figure 6.13 Horizontal Deflection of Soil beneath Toe of Slope in Unreinforced Section at 3m Fill

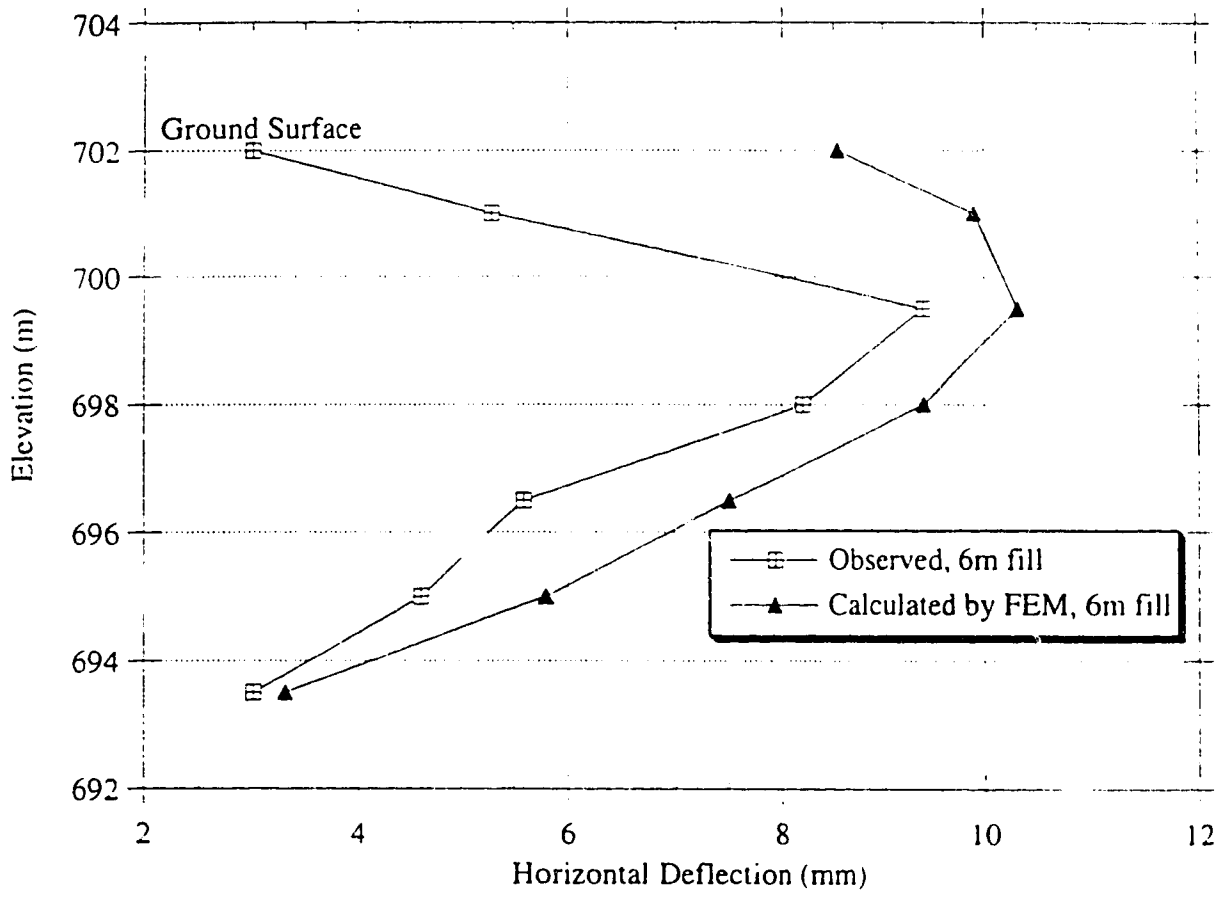


Figure 6.14 Horizontal Deflection of Soil beneath Toe of Slope in Unreinforced Section at 6m Fill

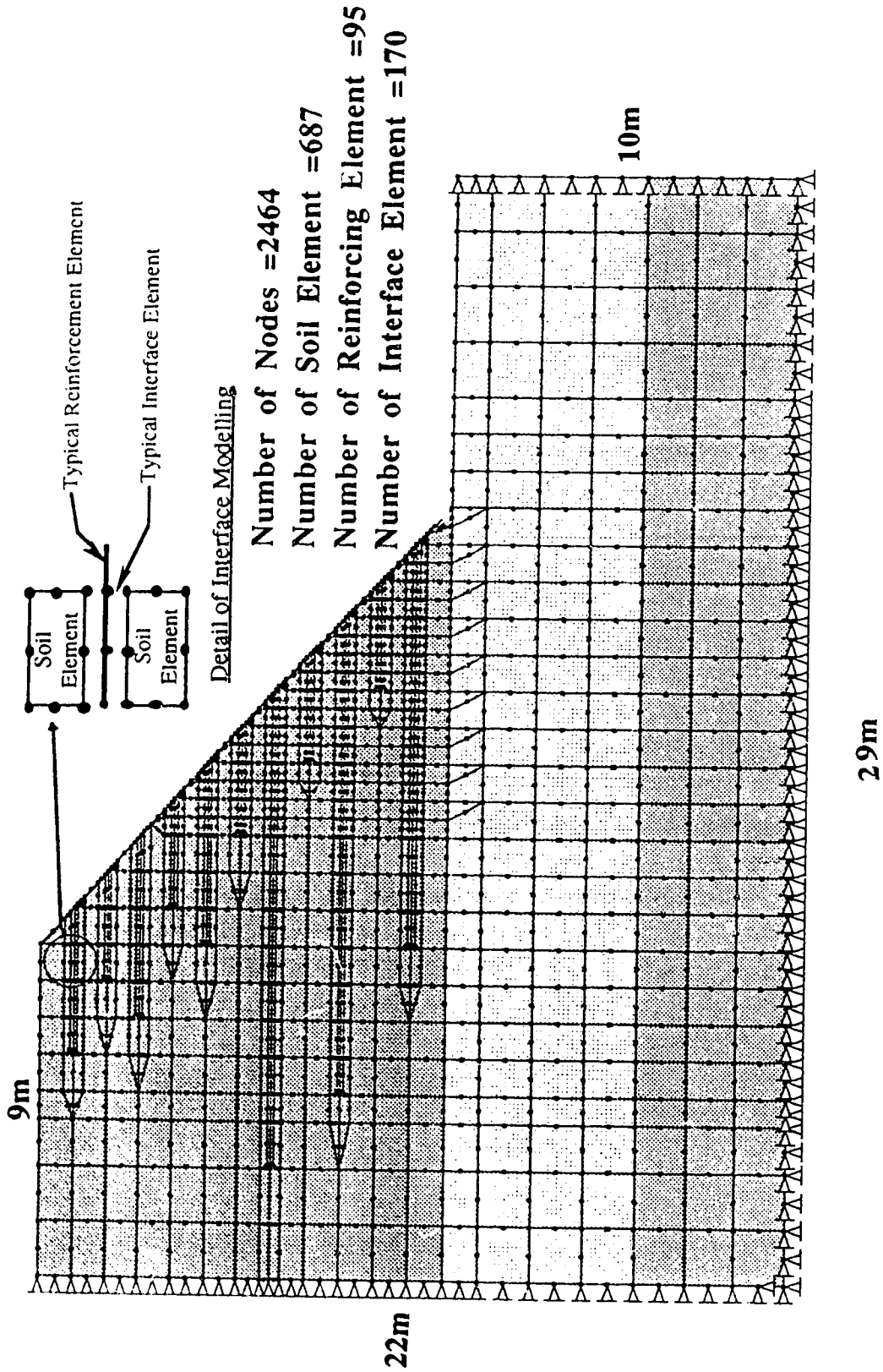


Figure 6.15 Finite Element Idealization of Soil and Reinforcement for Devon Test Fill

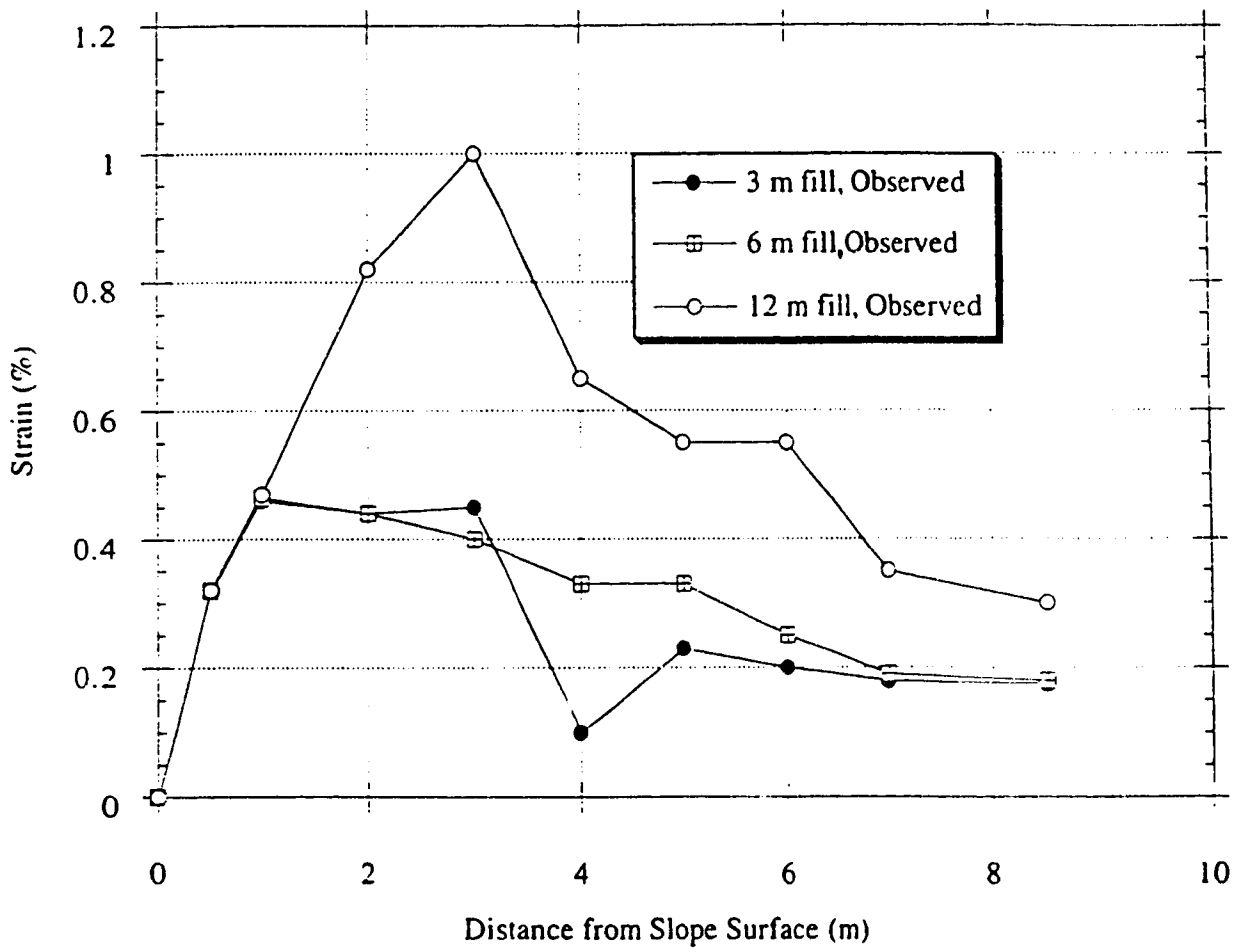


Figure 6.16 Observed Strain Distribution in Tensar Bottom Layer (modified from Liu, 1992)

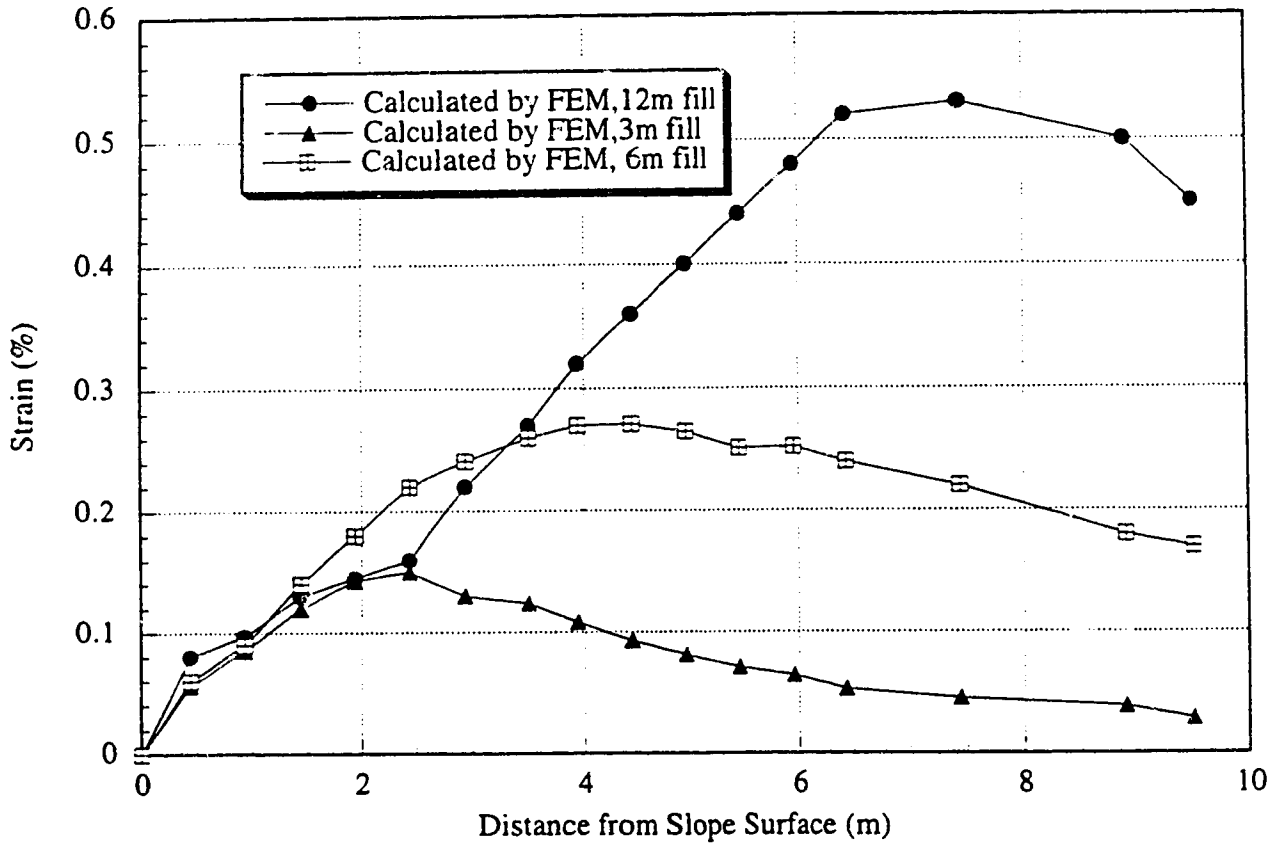


Figure 6.17 Calculated Strain Distribution in Tensar Bottom Layer

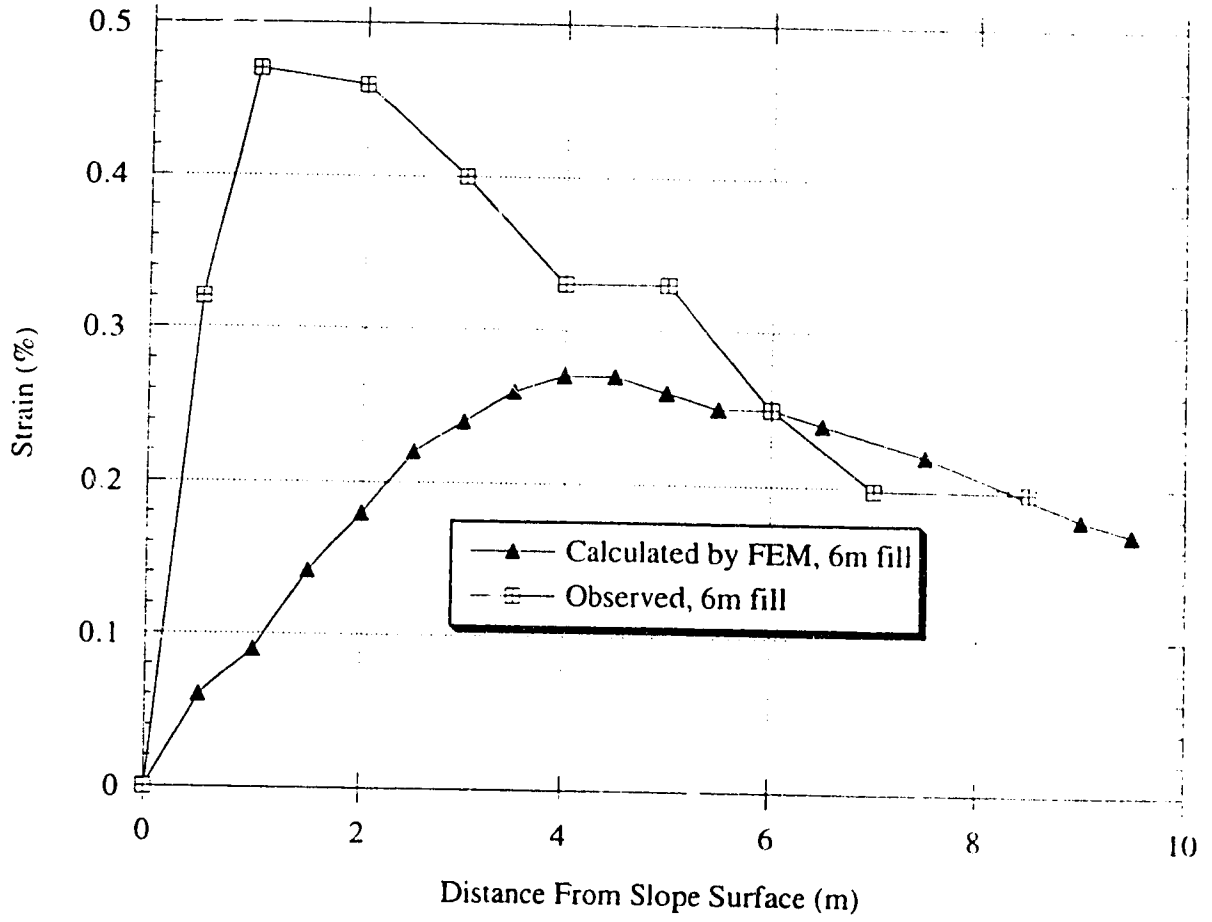


Figure 6.18 Strain Distribution along Tensar Reinforcement of Bottom Layer at 6m Fill

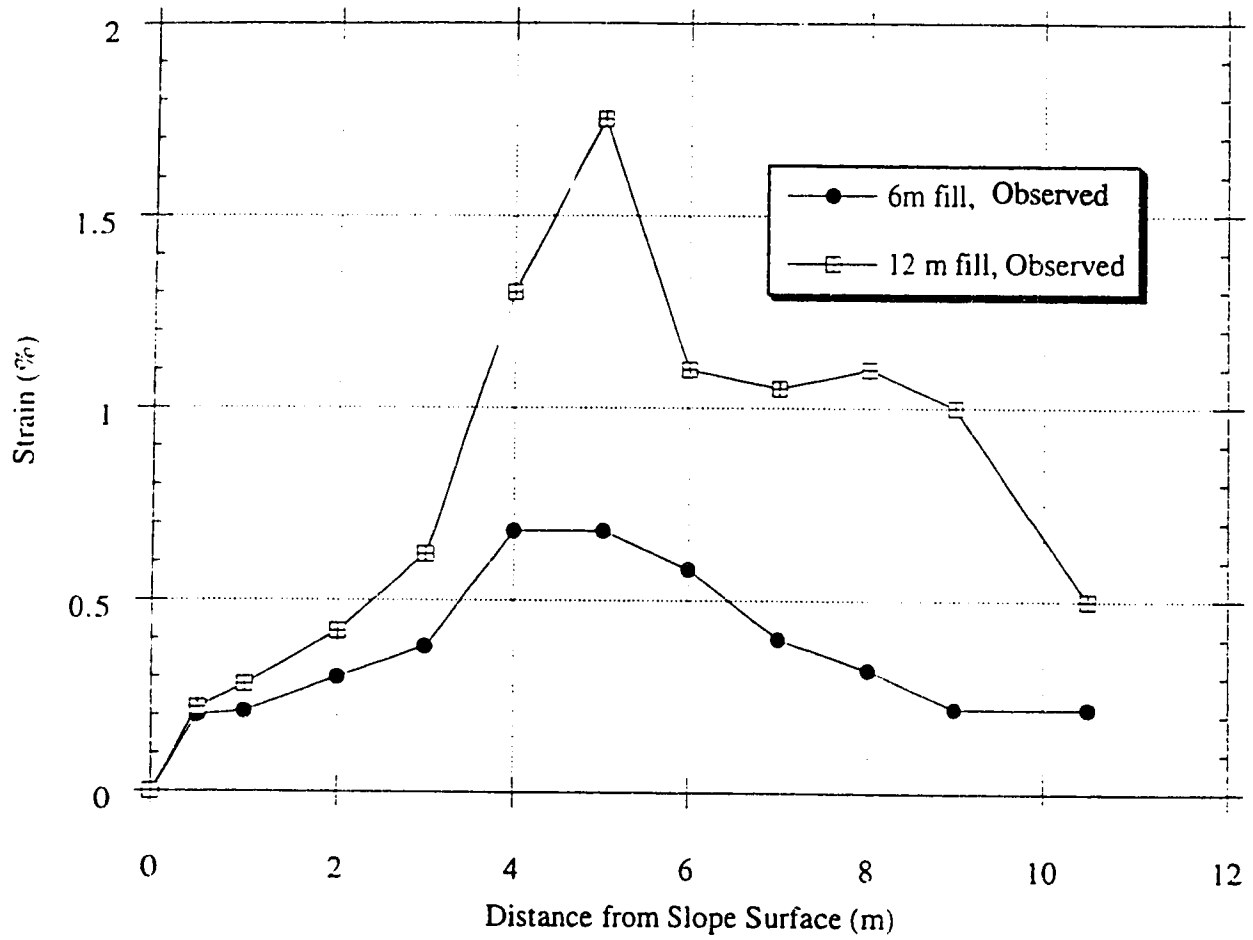


Figure 6.19 Measured Strain Distribution in Tensar Middle Layer (modified from Liu,1992)

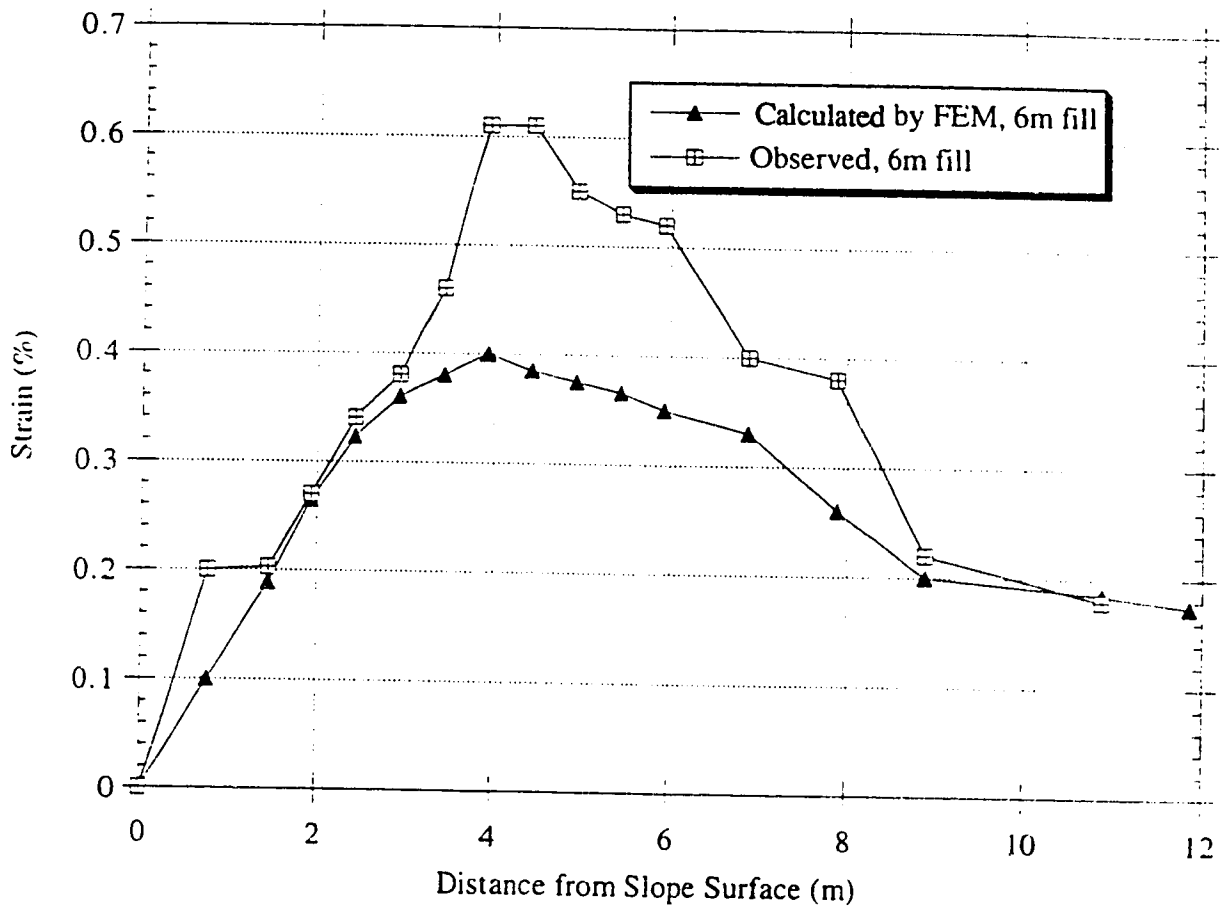


Figure 6.20 Strain Distribution in Tensar Middle Layer at 6m Fill

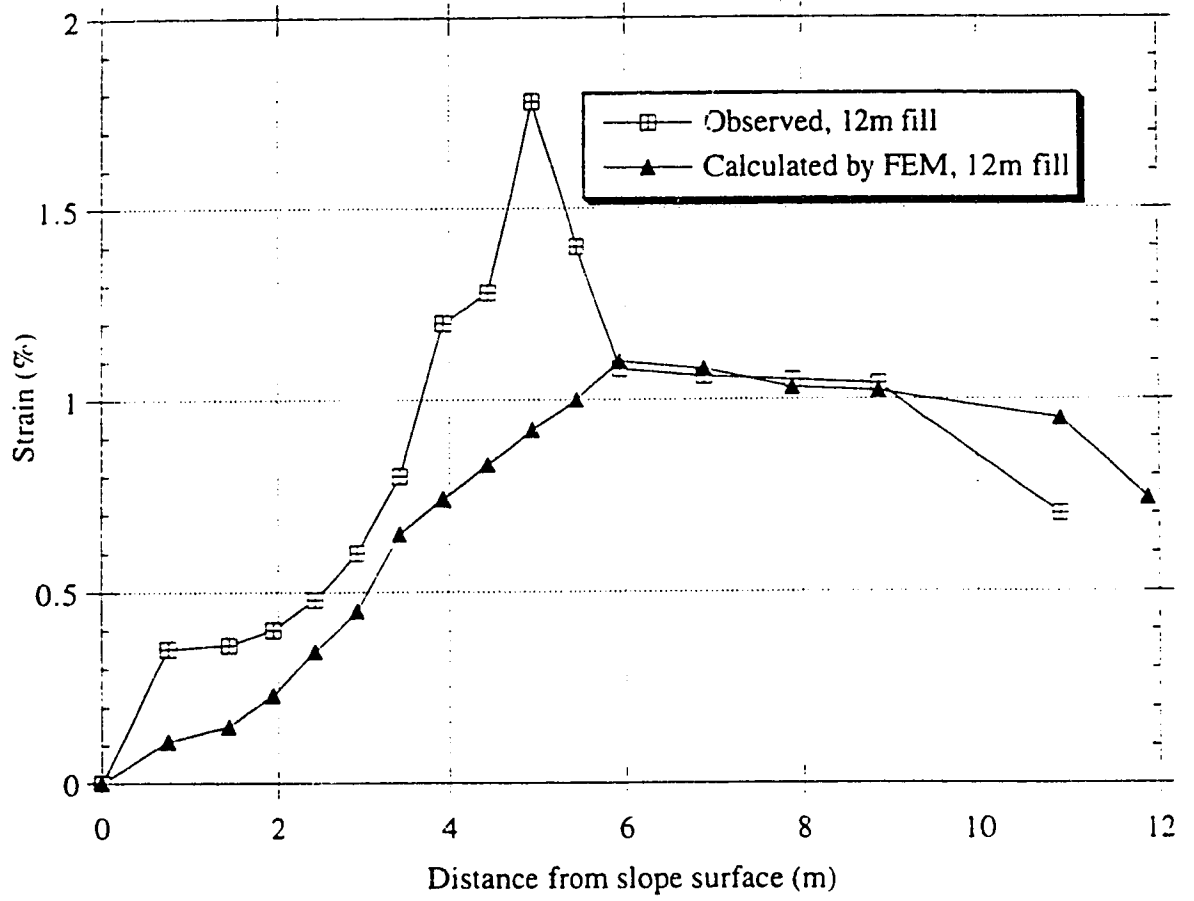


Figure 6.21 Strain Distribution in Tensar Middle Layer at 12 m Fill

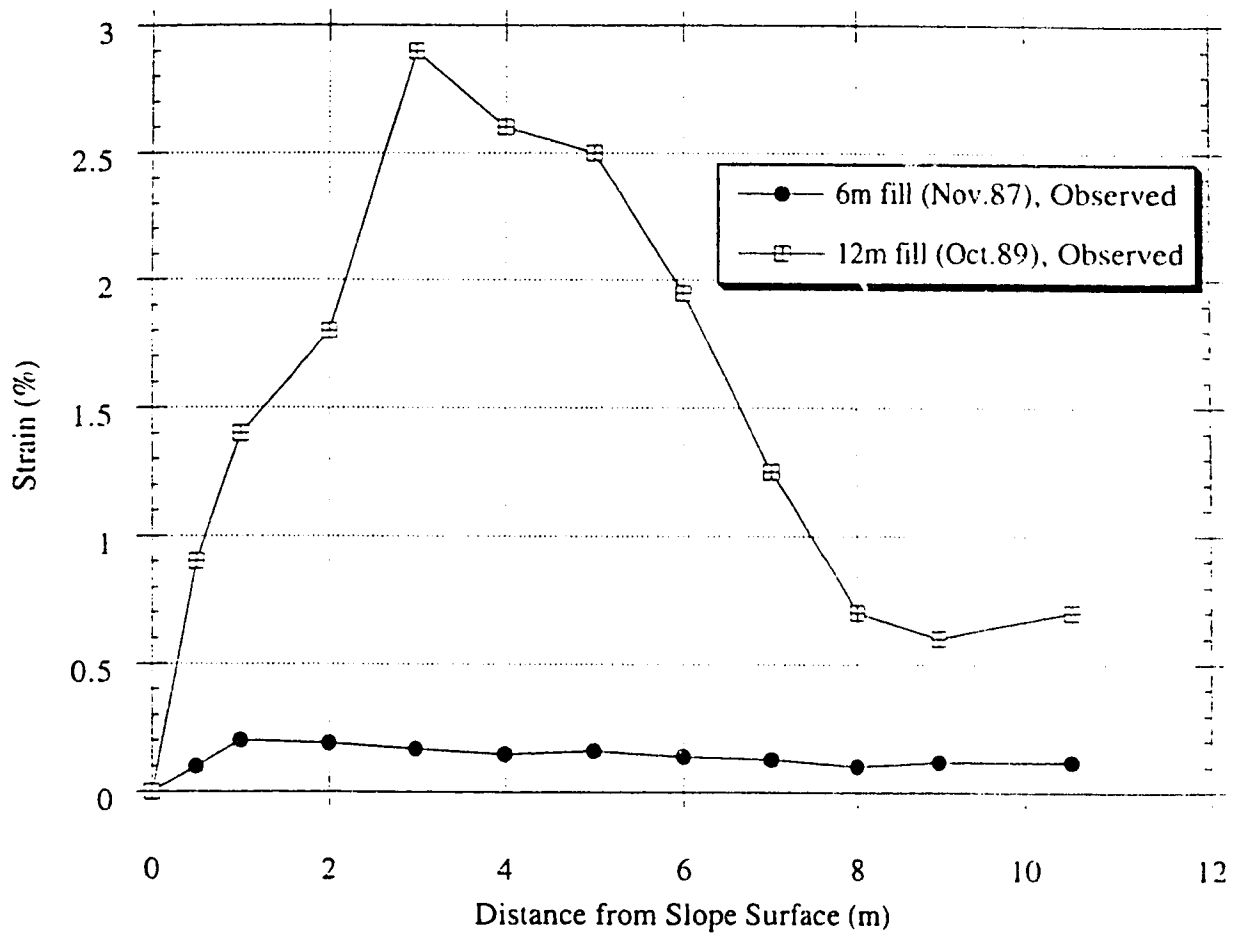


Figure 6.22 Measured Strain Distribution in Tensor Top Layer (modified from Liu, 1992)

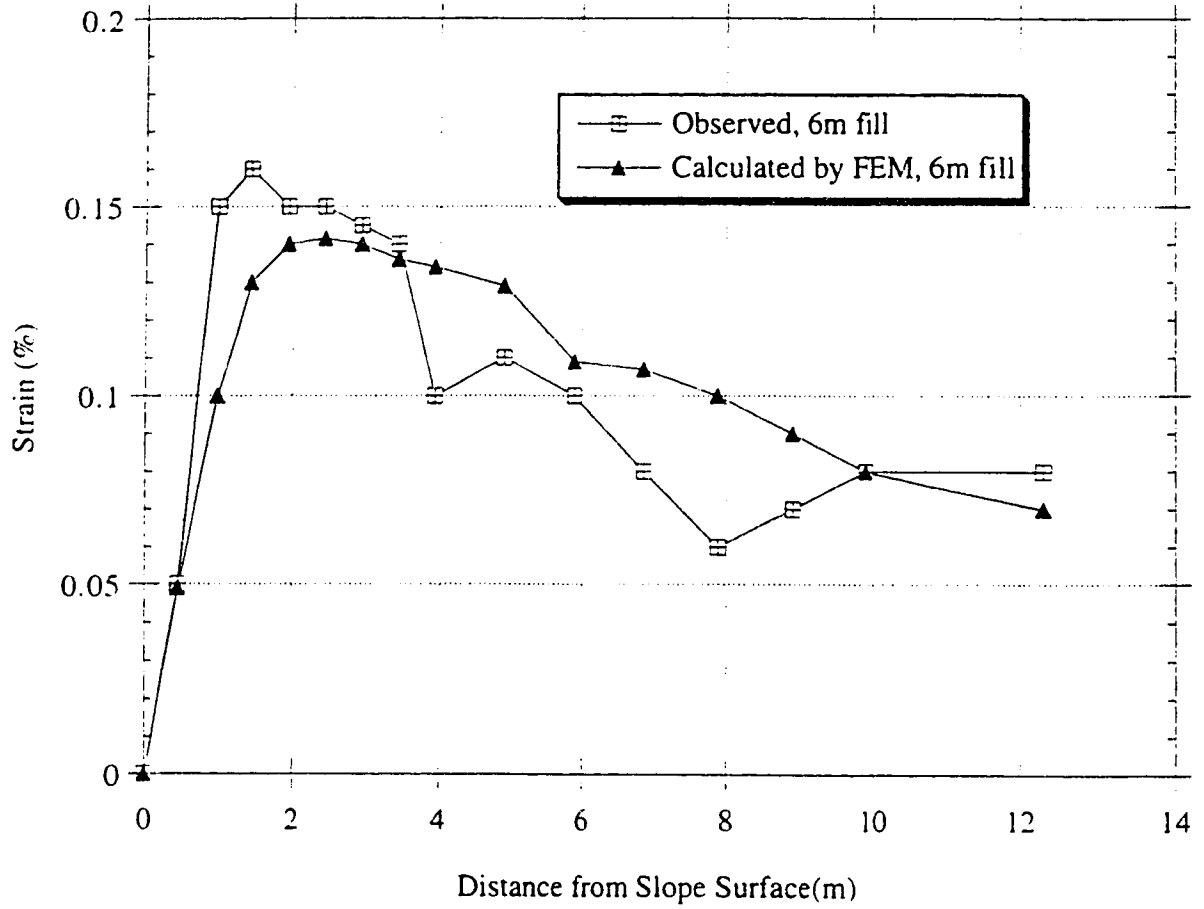


Figure 6.23 Strain Distribution in Tensor Top Layer at 6m Fill

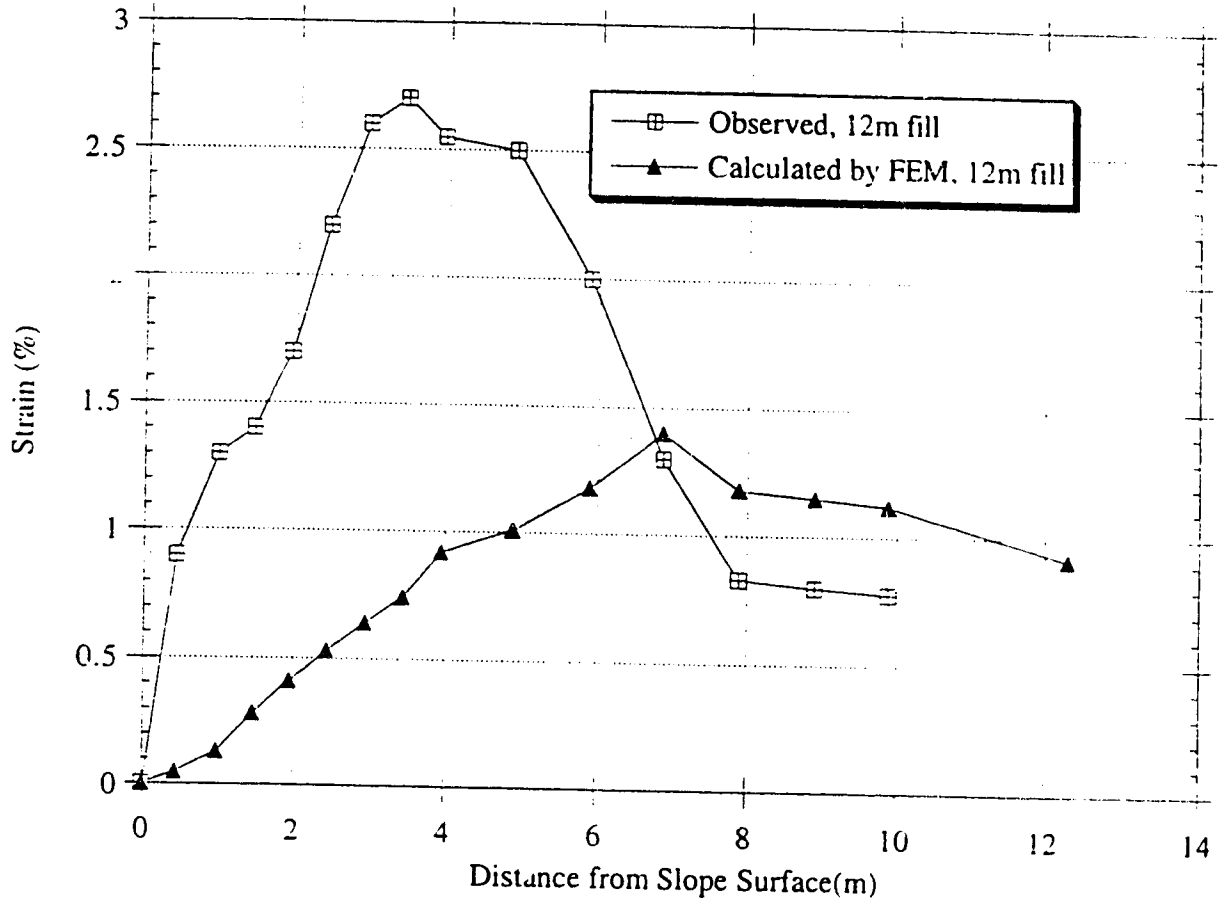


Figure 6.24 Strain Distribution in Tensar Top Layer at 12 m Fill

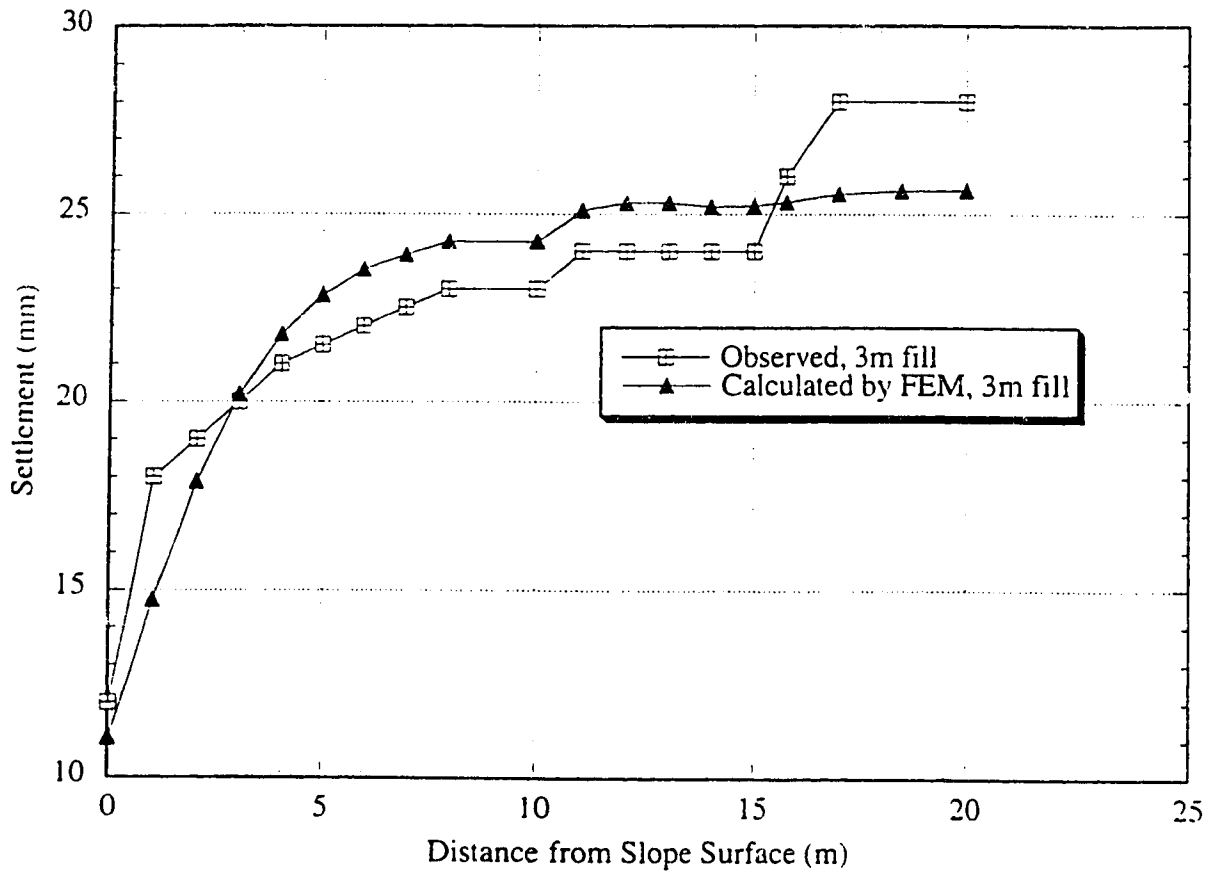


Figure 6.25 Settlement at Ground Level in Tensar Section at 3m Fill

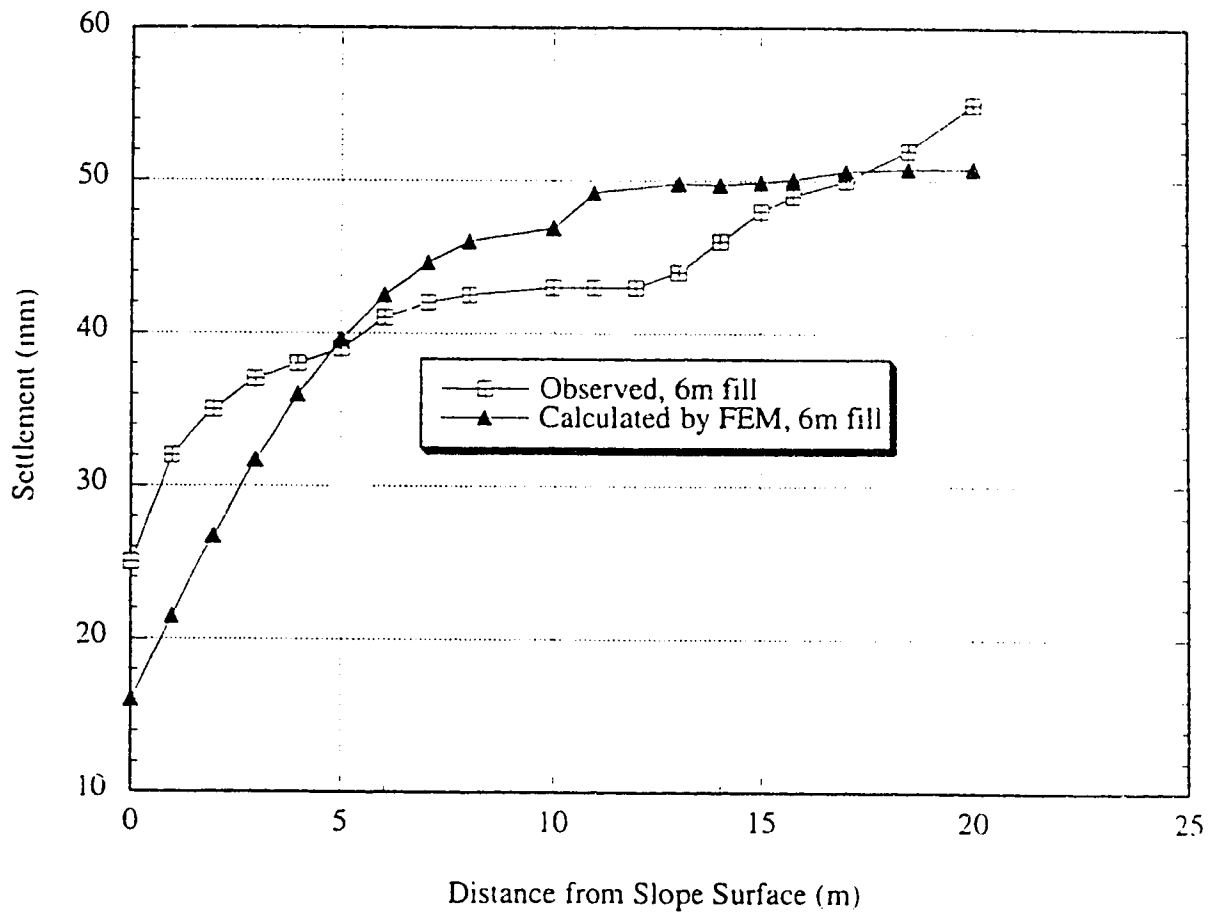


Figure 6.26 Settlement at Ground Level in Tensar Section at 6m Fill

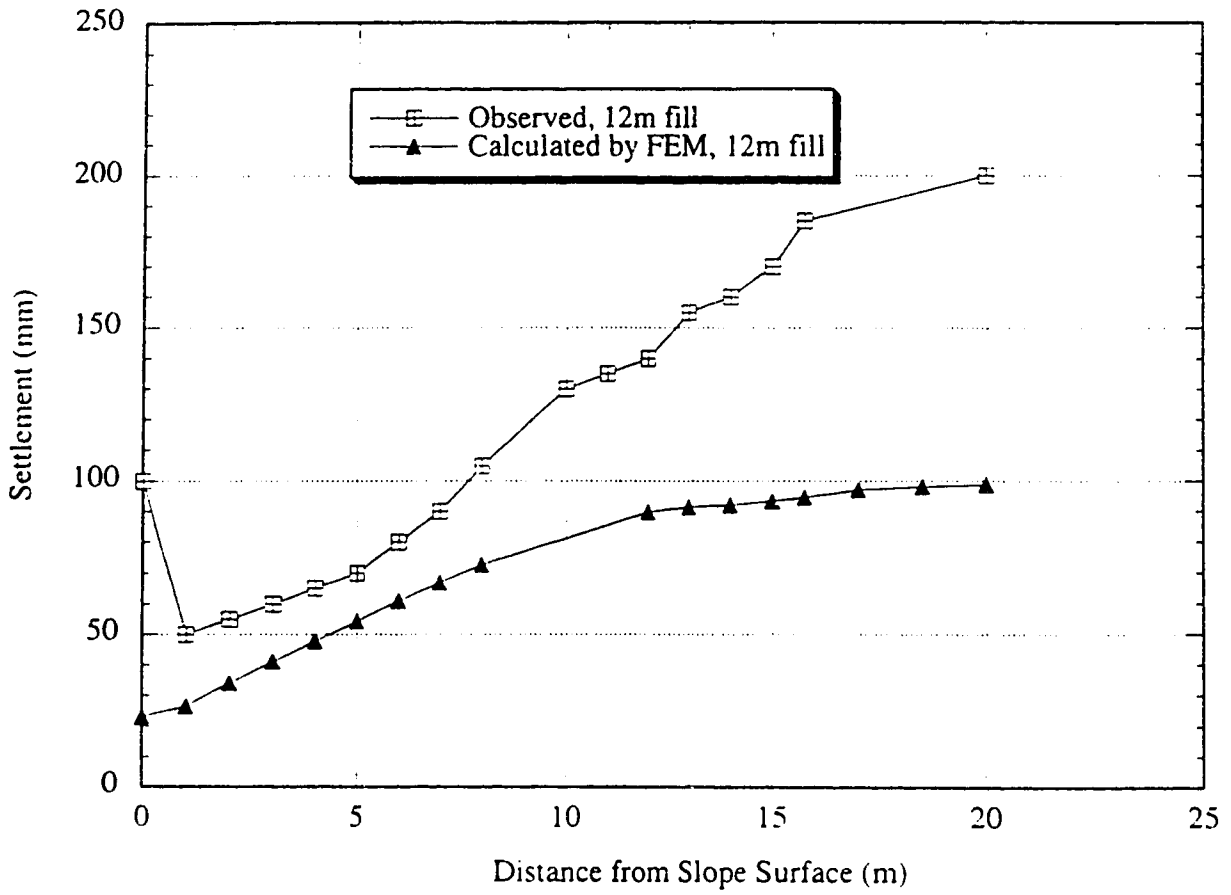


Figure 6.27 Settlement at Ground Level in Tensar Section at 12m Fill

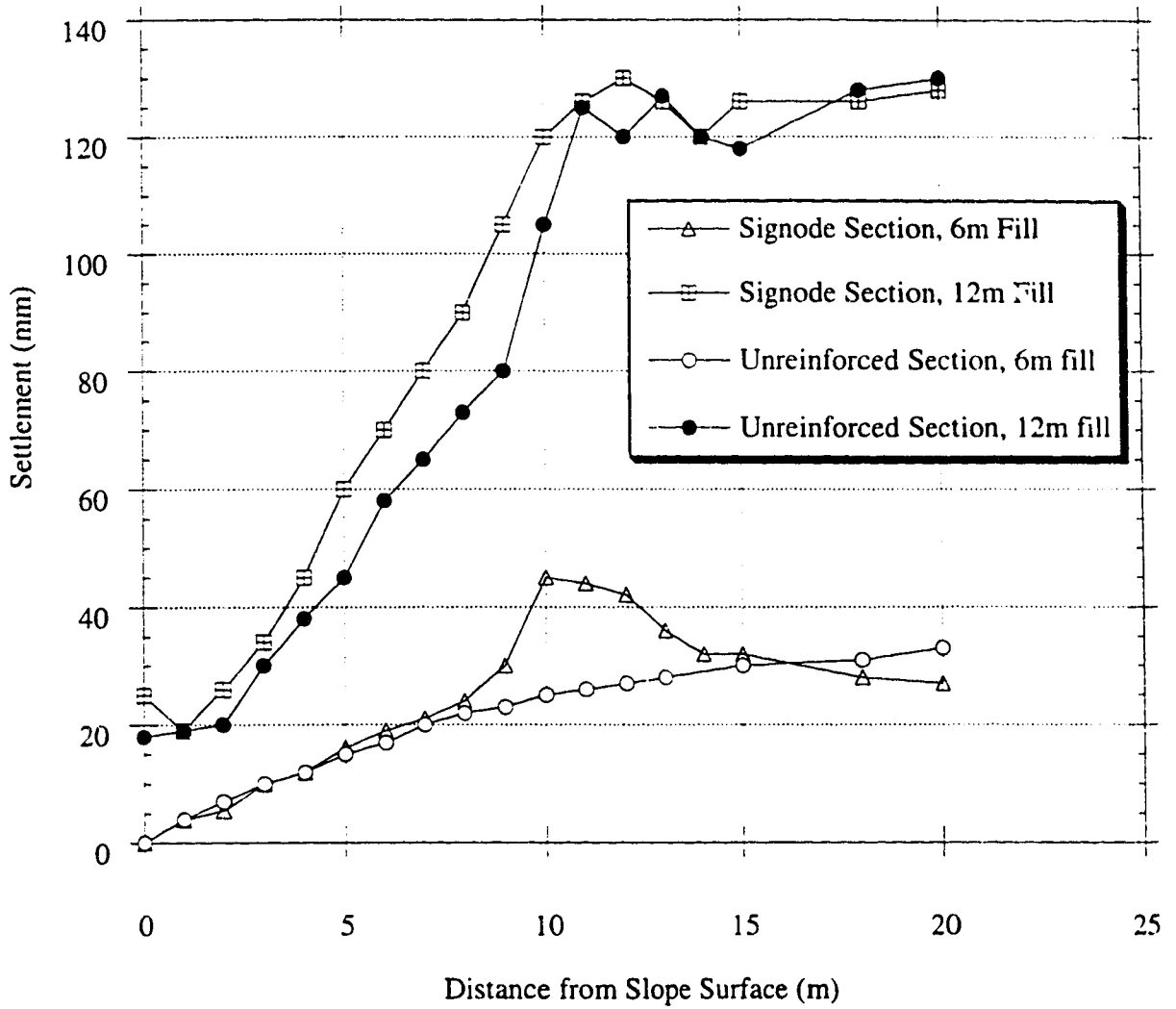


Figure 6.28 Settlement at Ground Level in Unreinforced Section Compared with Signode Section (modified from Liu,1992)

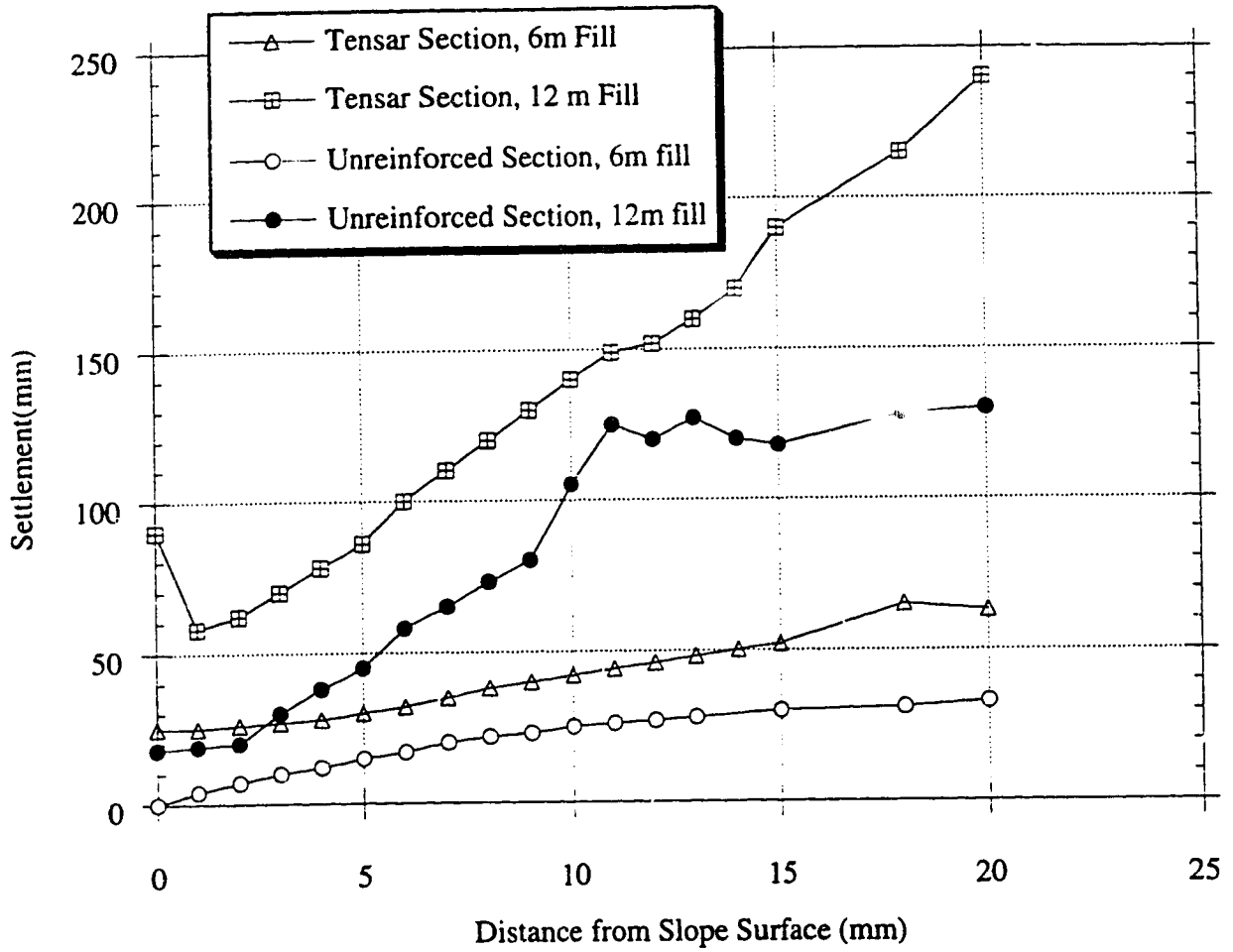


Figure 6.29 Settlement at Ground Level in Tensar Section Compared with Unreinforced Section (modified from Liu,1992)

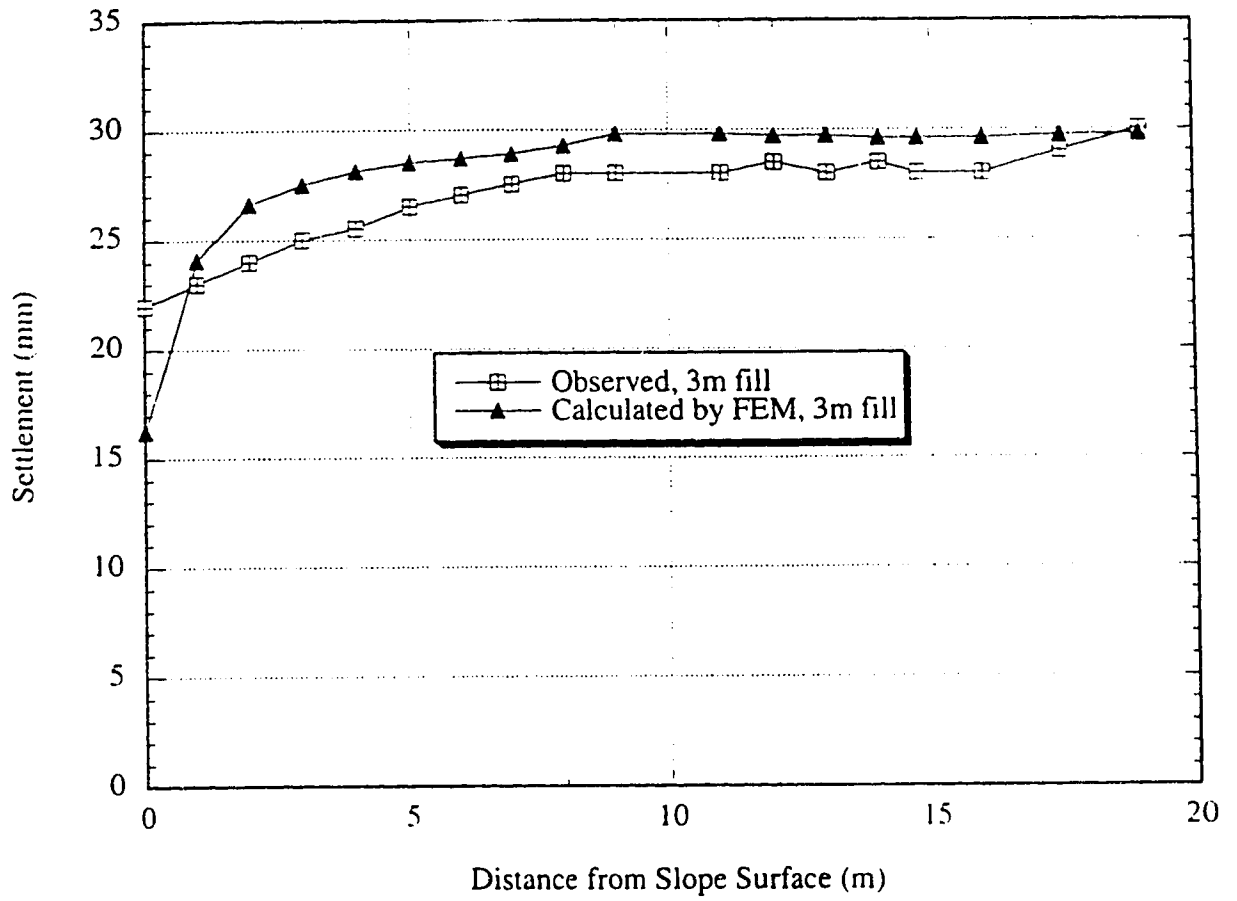


Figure 6.30 Settlement at 2m Level in Tensar Section at 3m Fill

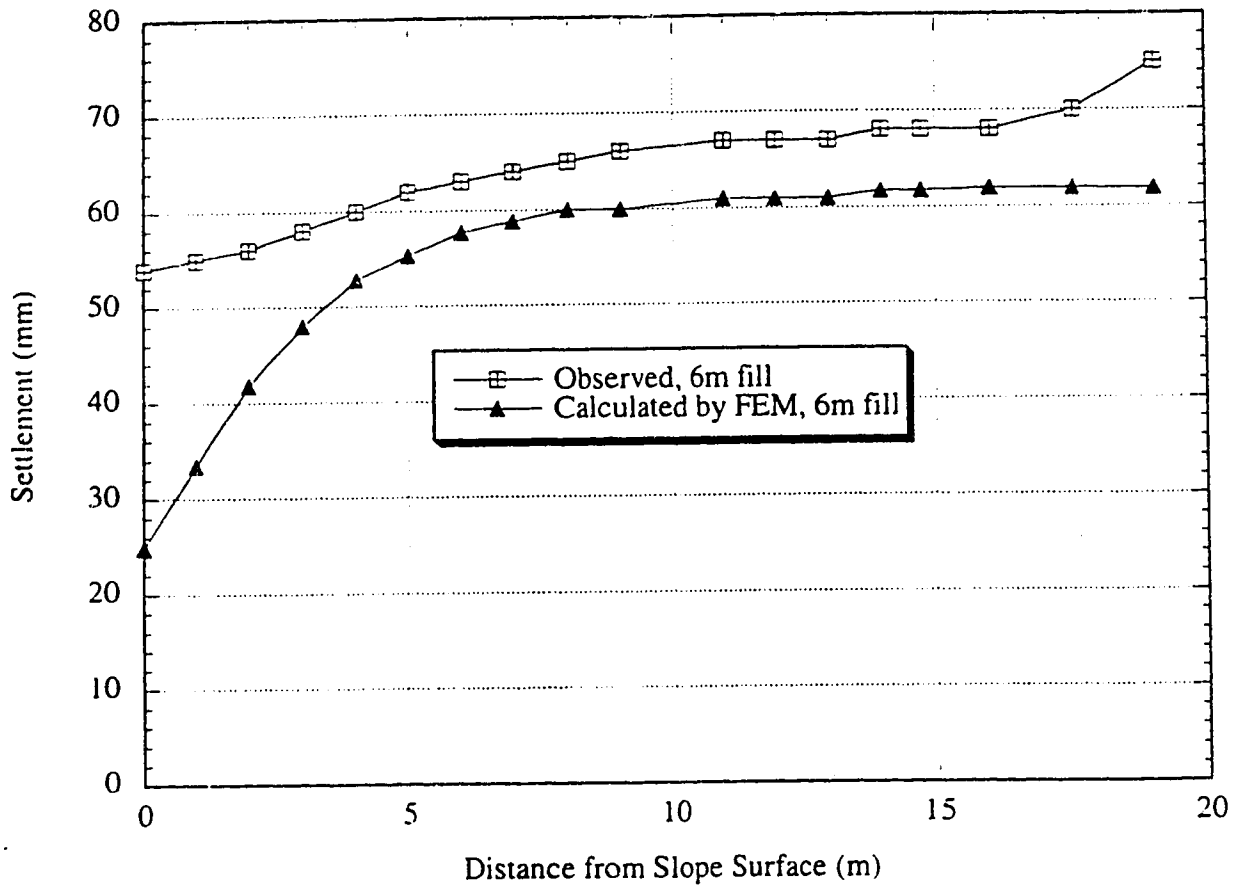


Figure 6.31 Settlement at 2m Level in Tensar Section at 6m Fill

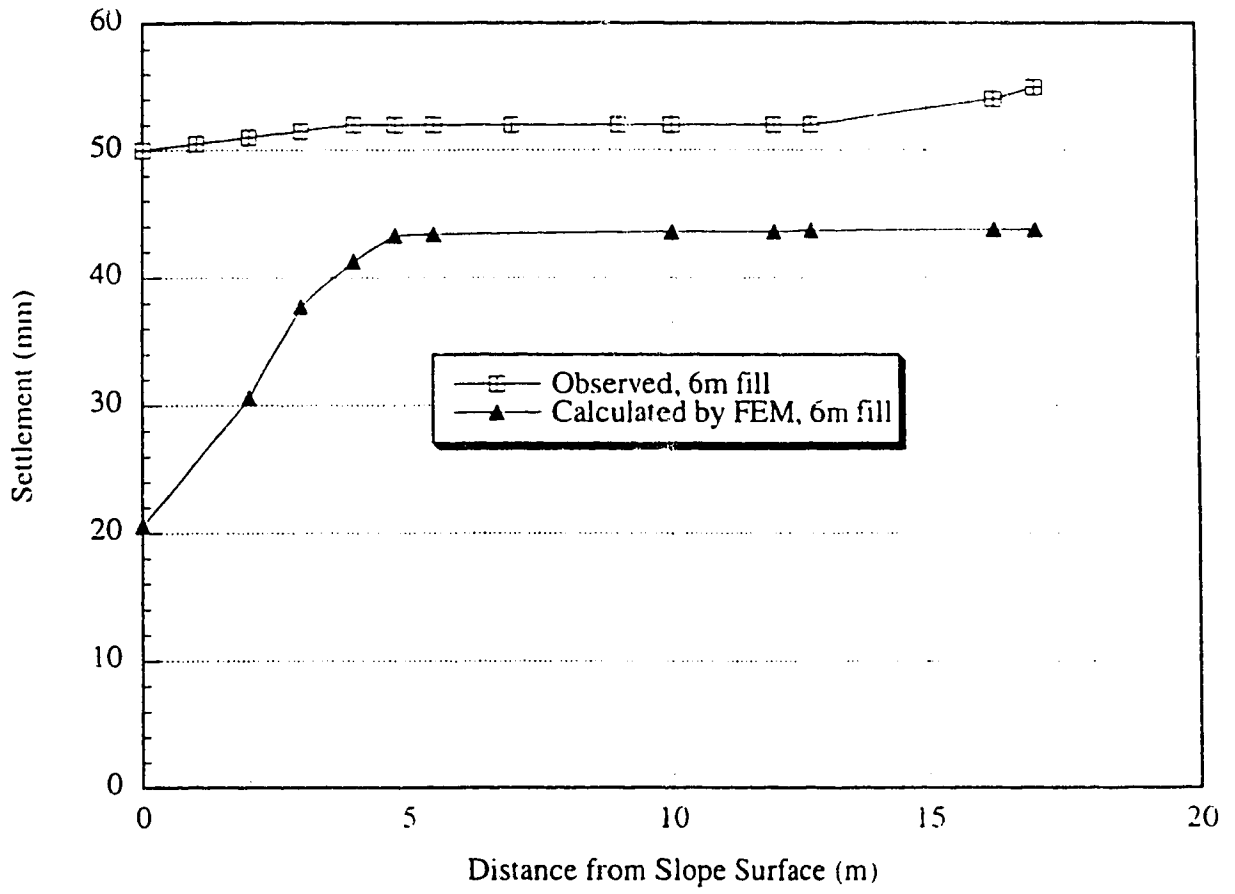


Figure 6.32 Settlement at 4m Level in Tensar Section at 6m Fill

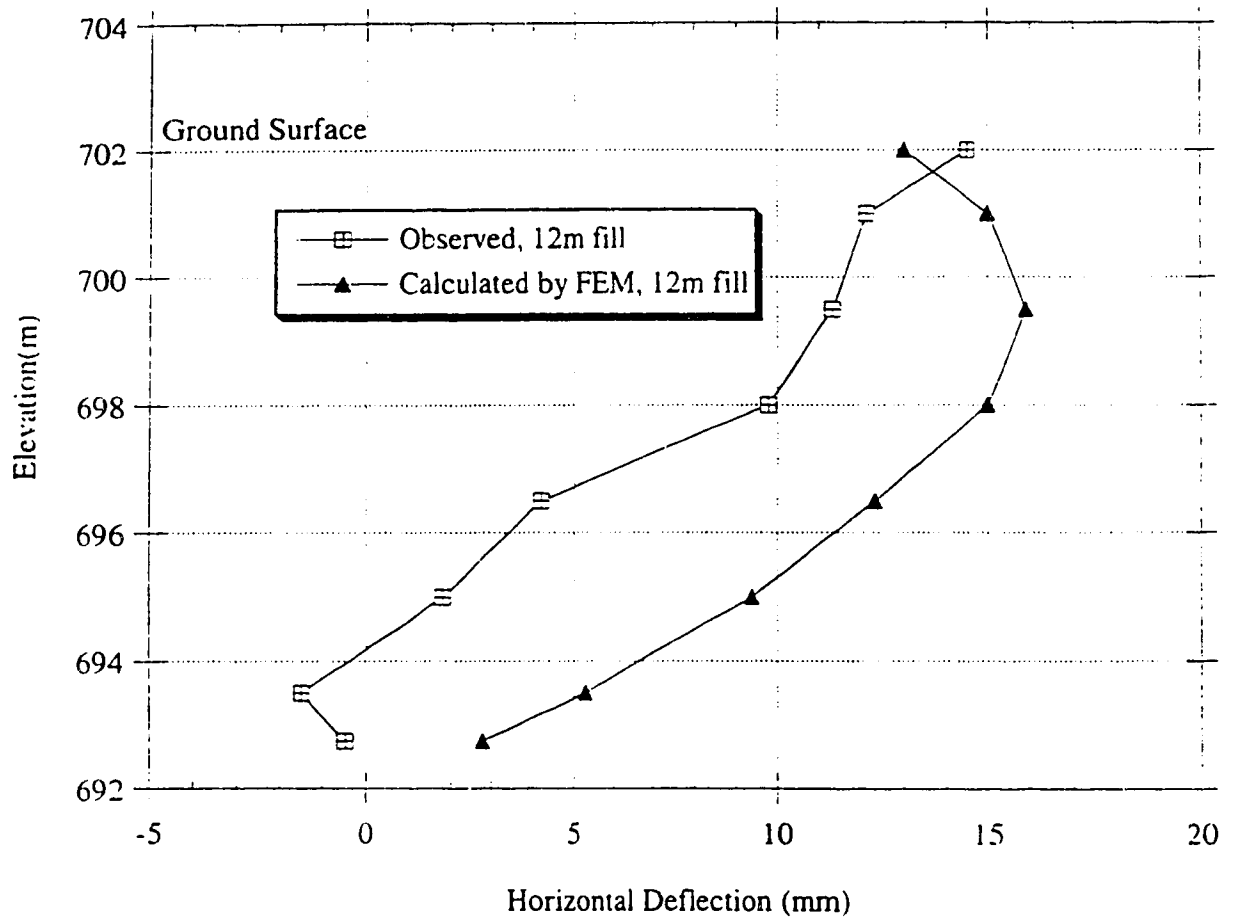


Figure 6.33 Horizontal Deflection of Soil beneath Toe of Slope in Tensar Section at 12 m Fill

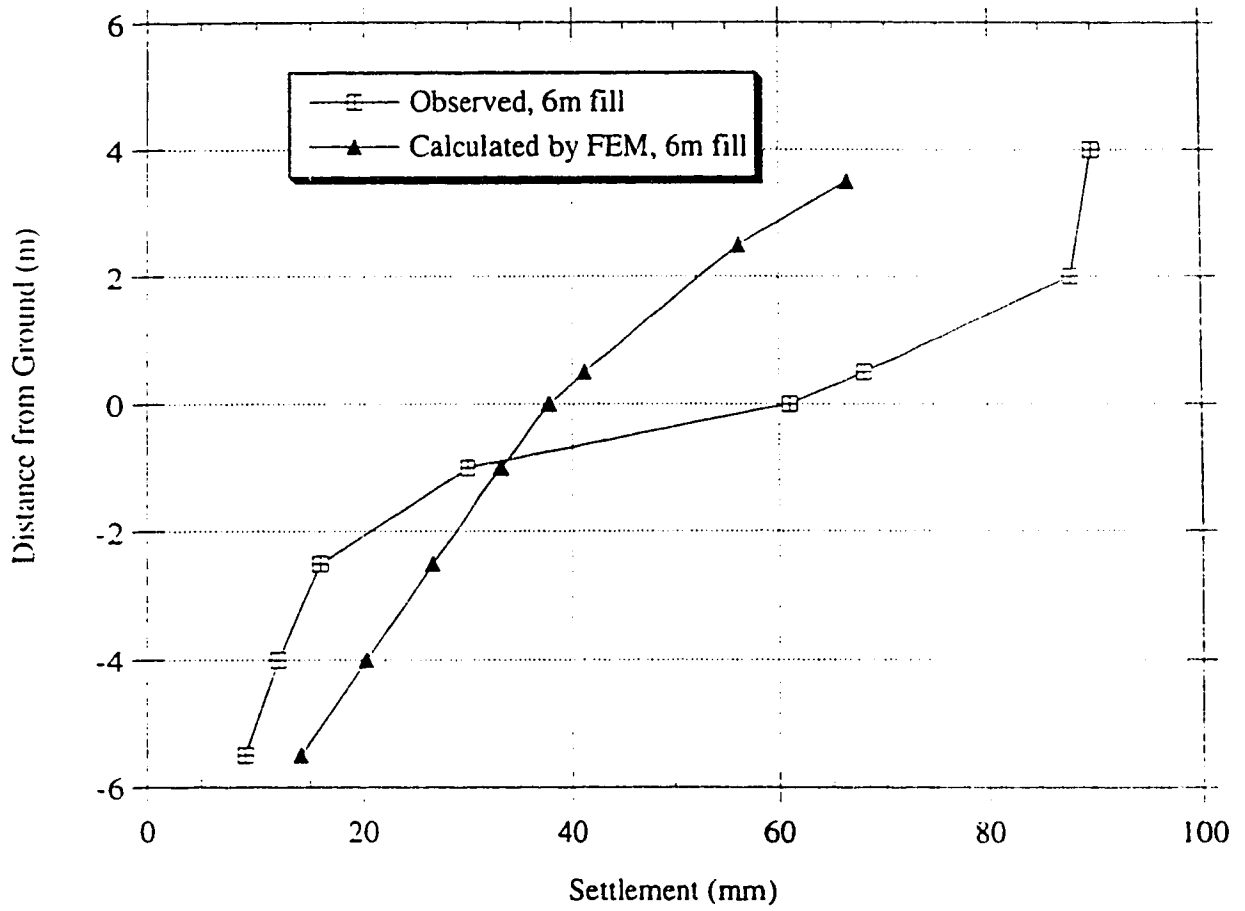


Figure 6.34 Settlement beneath Crest of Slope in Tensar Section at 6m Fill

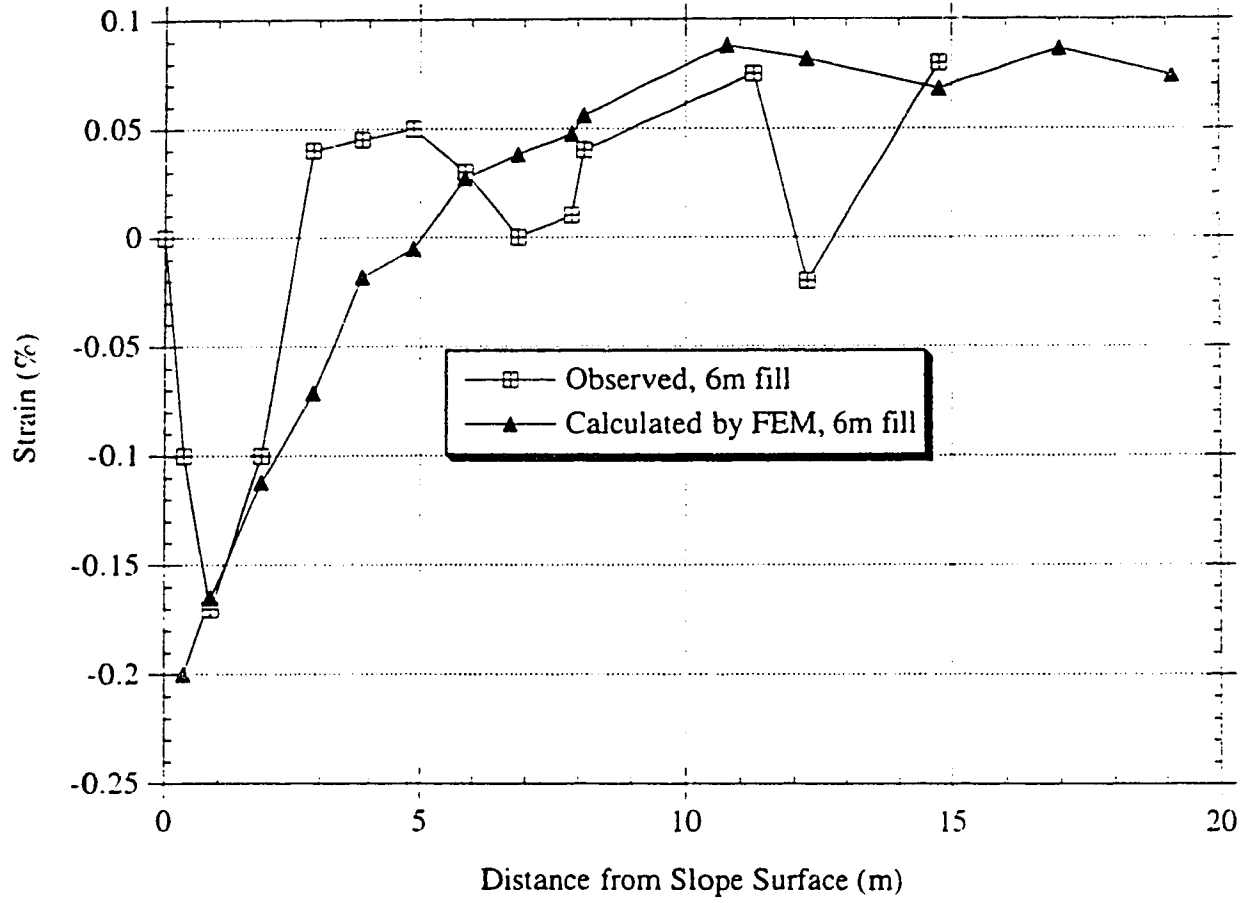


Figure 6.35 Distribution of Horizontal Soil Strain at Ground Level in Tensar Section at 6m Fill

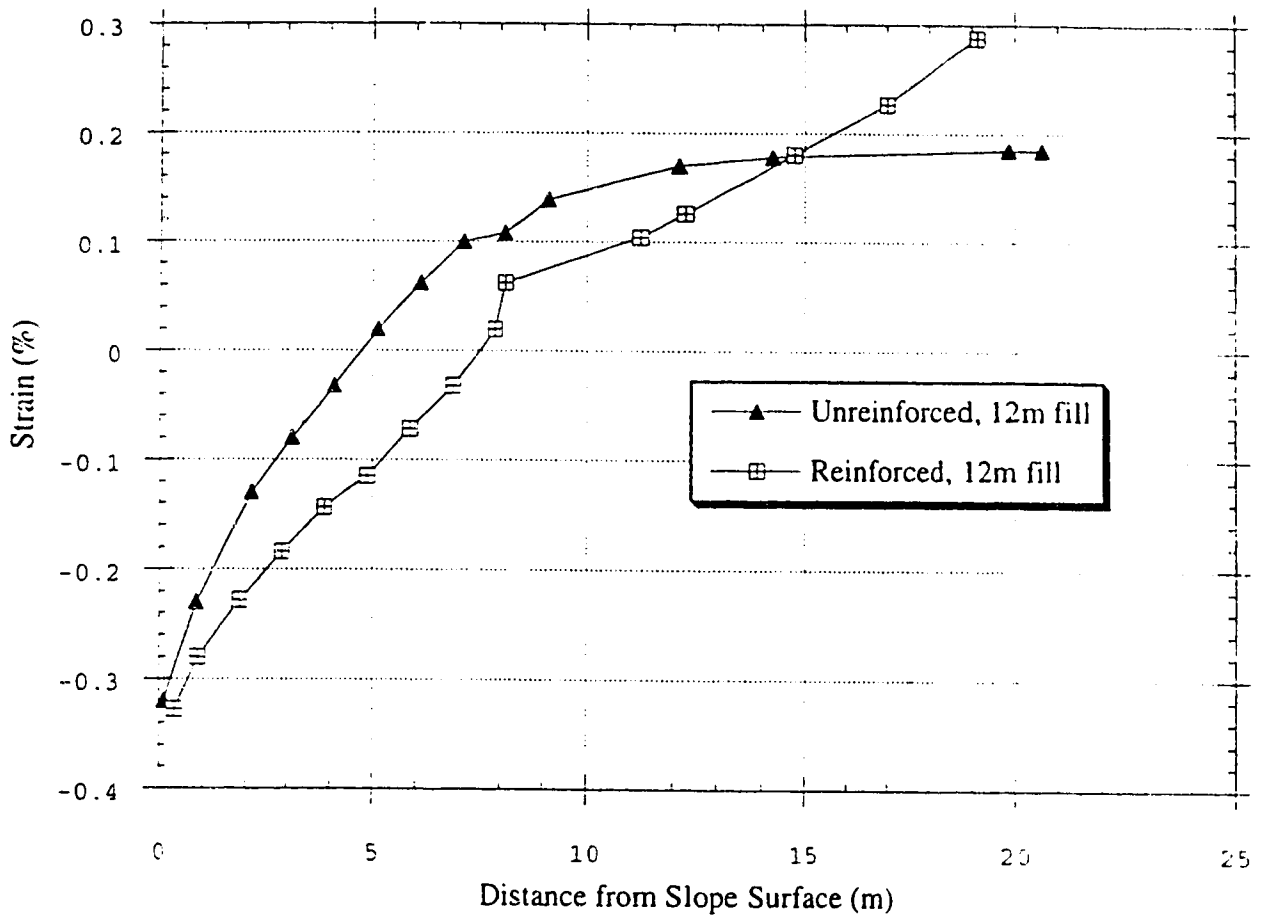


Figure 6.36 Comparison of Calculated Horizontal Soil Strain at Ground Level between Unreinforced and Reinforced Section

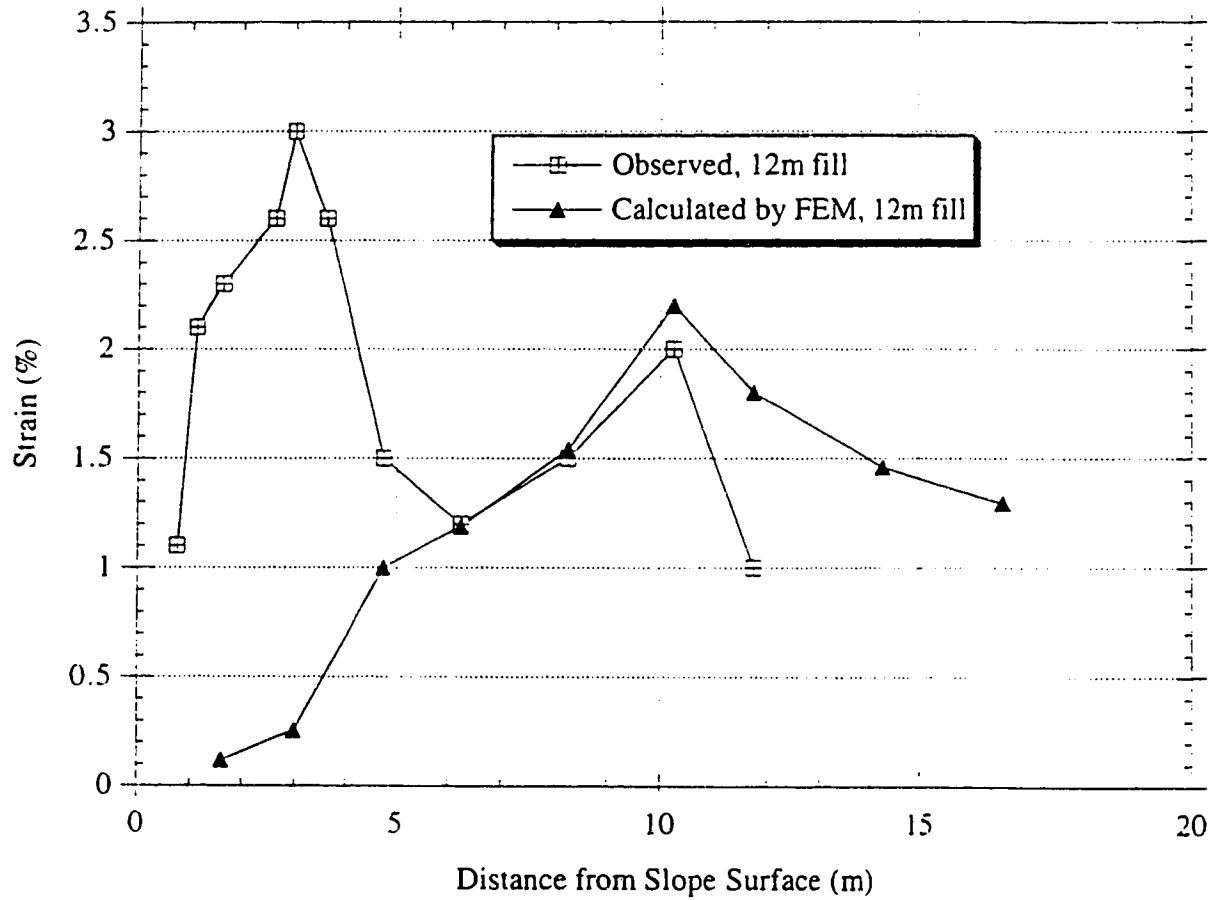


Figure 6.37 Distribution of Horizontal Soil Strain at 4 m Level in Tensar Section at 12 m Fill

CHAPTER 7. SUMMARY AND CONCLUSIONS

7.1 General

The safe and economical design of reinforced soil structures requires the knowledge of the mechanical behavior of composite materials and the behavior at the soil-reinforcement interface. During the last decade the interaction behavior at the soil-reinforcement interface has been investigated extensively using various types of geosynthetics by conducting large scale laboratory pull-out and direct shear tests.

The application of finite element analysis to geotechnical engineering has rapidly developed during the last two decades. Since there are some difficulties in simulating the interaction between soil and reinforcement, the finite element method is being used presently to verify existing semiempirical design methods. This research was focused on applying the finite element method in modeling the interaction behavior between soil and reinforcement. Pull-out and direct shear tests were analyzed using the finite element method in order to investigate the progressive shearing of the reinforcement, the failure modes and the interaction behavior between soil and reinforcement. A new interface element was proposed to simulate the large amount of slippage between soil and reinforcement. Finite element analysis of a reinforced slope was also carried out to compare the analysis results with field measurements and observations.

7.2 Summary of Results

a) Mobilization of shear stress along a reinforcement is highly non-uniform during the initial stage of the pull-out test. To investigate the effect of progressive shearing on the calculation of the shear stiffness of the soil-reinforcement interface, the finite element

method was used to simulate the pull-out test. The reinforcement, soil and interface behaviors were modeled using linear and non-linear constitutive models. Shear stiffnesses were calculated using conventional methods. It was found that there are considerable discrepancies between the calculated shear stiffnesses and the corrected stiffnesses which were used in the finite element analysis. The amount of error depends on the relative stiffness between reinforcement and soil and the size of the specimen being analyzed. The finite element results were also compared with the observed response from laboratory experiments.

b) The contribution of passive resistance to the total shearing resistance is a function of the rib spacing. As the spacing of the ribs decreases, shear resistance consists mainly of the frictional resistance due to soil-soil friction. There might be a optimum spacing of the transverse member of a geogrid reinforcement at which the passive resistance can be fully developed.

c) The presence of the ribs of the reinforcement was shown to increase the shear resistance and to alter the behavior of particles which cause shear failure to form within the sand mass. Instead of sliding along the contact surface of the reinforcement. A passive zone can develop with the ribs thereby increasing the shear resistance. However, the movement of soil particles can not be modeled well by the hyperbolic soil model.

d) A new interface finite element model is proposed to simulate the large amount of slippage between soil and reinforcement. The interaction between soil and reinforcement is considered to be a contact problem between two bodies and a contact approach is used by applying the Lagrange multiplier technique. A bi-linear stress-strain relationship for the interface using the Mohr-Coulomb failure criterion is adopted. The proposed method eliminates the need to assign arbitrary high values for the normal stiffness of the interface in order to maintain compatibility in the conventional joint element approach.

e) Limit equilibrium analysis deals with the stability of a structure under ultimate failure conditions. This method has been used for the design of soil structures which

involves small displacement problems. Therefore, a new interface element can deal with small displacement problems as well as ultimate failure conditions. The analysis of the large amount of slippage between soil and reinforcement mainly depends on the finite element mesh.

f) The material parameters for the test fill analysis were mainly obtained from laboratory test results which may not provide the best fit of field observations due to different stress paths, sample disturbance and compaction efforts. Triaxial tests are simulated by the finite element method using the calibrated material parameters and these results are compared with the laboratory test results.

g) For the long-term stability and deformation behavior of a reinforced soil structure, the creep characteristics of the reinforcement should be considered in the analysis. According to the field measurements, tensile strains of Tensar SR-2 in different layers varied between 1.0% and 2.5%. Creep data of the reinforcement may be plotted in the form of isochronous curves for design purposes. These curves show that for Tensar SR-2 much of time-dependent deformation occurs in the first 100 hours to 1000 hours of loading. However, the creep effect at small strains such as 1.0% or 2.5% is not significant, as shown by the isochronous curves.

h) The preconsolidation stress of the foundation soil was approximately 400 kPa, which was more than the increase of stress in the foundation soil due to the weight of the test fill. Therefore settlement of the foundation soil would not be expected to be large. However, after placement of 12 m of fill the settlement in the foundation soil increased significantly. It may indicate that the preconsolidation stress of the foundation soil is less than 240 kPa which is approximately the maximum overburden stress due to the weight of the test fill.

7.3 Conclusions

a) If the force-displacement response of the pull-out test was used to obtain shear stiffness for modeling the interface between the soil and reinforcement, the assumption of uniform stress distribution can result in considerable error between the values of apparent shear stiffness and the true shear stiffness. This discrepancy depends on the relative stiffness between the interface and the reinforcement. It was illustrated that stiffer reinforcement results in a lesser degree of progressive shearing and, therefore, results in less discrepancy between the true and apparent stiffness values. True stiffness can be estimated from the results of the pull-out test by using an appropriate stiffness correction. The calculated force-displacement response using true stiffness values gives better agreement with the experimental observations

b) The failure mode of the ribbed reinforcement in Ottawa sand was quite similar to the local failure mode of the foundation. For cohesive soil, the shear failure surface is close to the punching shear failure mode rather than the local shear failure mode, and it needs a large relative displacement of 0.6 cm to be completely formed.

c) The thickness of shear zone is affected by soil types. The shear zone thickness of Ottawa sand and cohesive soil are about 2.0 and 1.5 times the rib height respectively, based on the shear stress and strain distributions around the ribs.

d) The results of the finite element analyses for the Devon test fill are found to be in good agreement with the measured field behavior during early stages of construction, when the fill reached 6 m high. In the later stages of construction, as the embankment approached 12 m high, the agreement between the finite element analyses and the field measurements was not as good, especially with settlements. However, the results of the analyses performed suggest that the behavior of reinforced embankments using the cohesive soil can be modeled reasonably well using the finite element method.

e) In modelling the interface between soil and reinforcement usually the normal stiffness (K_n) of the interface element is assigned high values to prevent overlapping at the interface between soil and reinforcement. However, it is found that the normal stiffness of

the interface element can affect the analysis results. A new large slipping finite element model for geosynthetic interface models has been introduced. The Lagrange multiplier method is used to satisfy compatibility between the soil and the reinforcement, and the shear stiffness (K_s) is used to apply horizontal resistance along the reinforcement, thus, it is possible to account for both frictional and passive soil resistance of the geogrid reinforcement. Using a simple reinforced soil structure example and the analysis of a pull-out test it was demonstrated that this model can easily simulate a large amount of slipping between the soil and the reinforcement. It is also expected that the new model can deal with any soil-structure interaction problem which involves a large amount of slipping.

7.4 Recommendations for Further Research

a) Actual movements of grain displacements can not be properly simulated by the finite element method. Since a discrete element model can simulate each grain particle movement, the discrete element model will be a useful tool to predict the interface behavior between soil and ribbed reinforcement such as the shear failure surface and the shear zone.

b) Waste-containment lining systems commonly contain both soil and geosynthetics. These components can undergo a large amount of stretching as a result of the loading of waste. Determination of tensile loads in the geosynthetic components is important to ensure adequate safety against rupture of the geosynthetics. The interface behavior of lining systems can be successfully simulated by the large slippage interface model.

c) The construction of the Devon test fill began in the summer of 1986. The field measurements were taken until the summer of 1991. Those field measurements should be taken for the long term performance of the reinforced slopes in the Devon test fill. The finite element method included the creep effect of the cohesive soil can be used for the long term analysis. Those field measurements and analysis results will provide the information of the long term behavior of the reinforced slope.

APPENDIX A: Material Properties of the Devon Test Fill

The mechanical properties of the Devon test fill and foundation soil were studied by Hofmann (1989). The properties of fill, foundation soil and geogrid were determined by the laboratory tests at The University of Alberta. Laboratory testing results for the finite element analysis are presented in Appendix A.

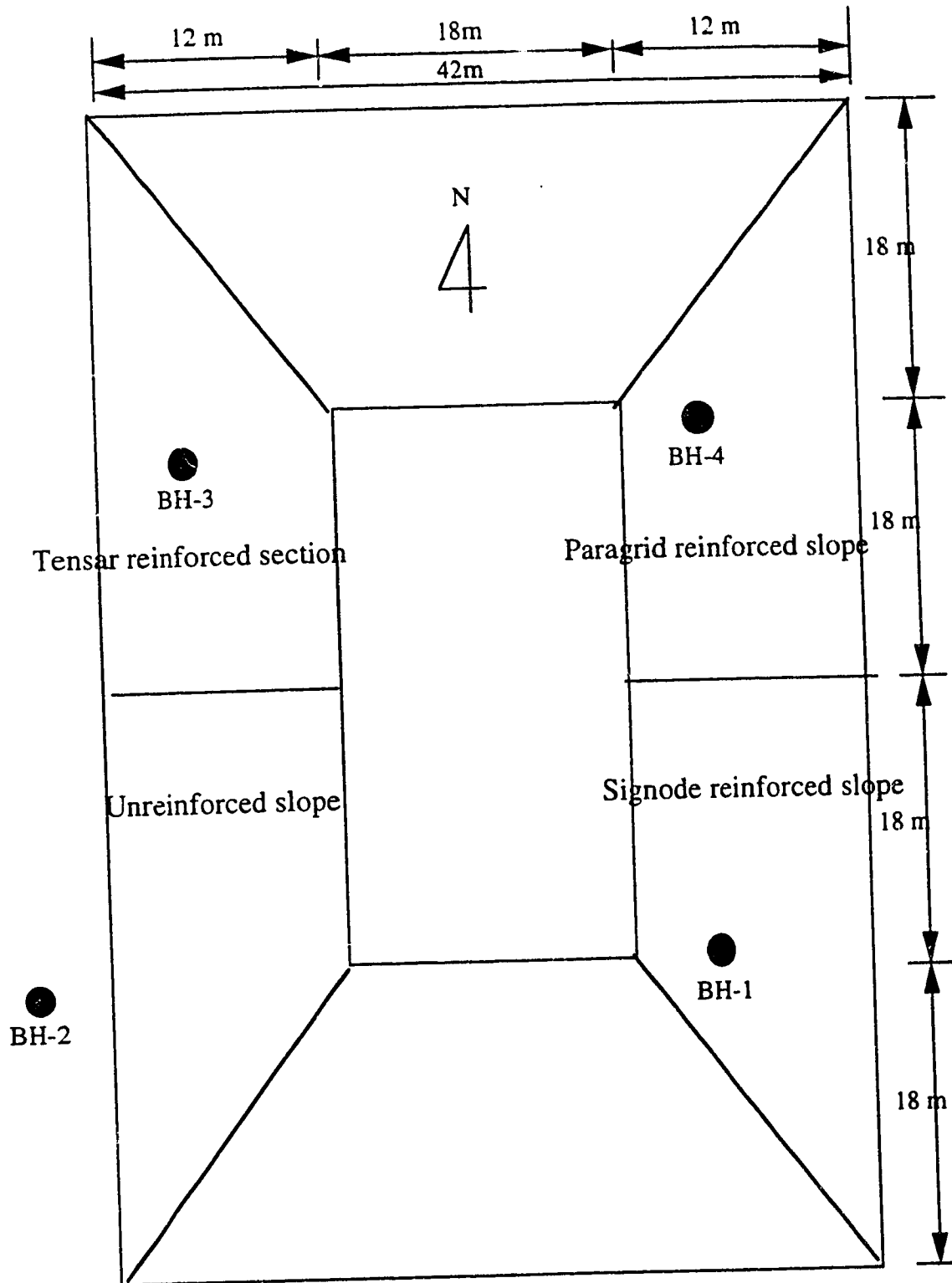


Figure A1. Plan View of Devon Test Fill

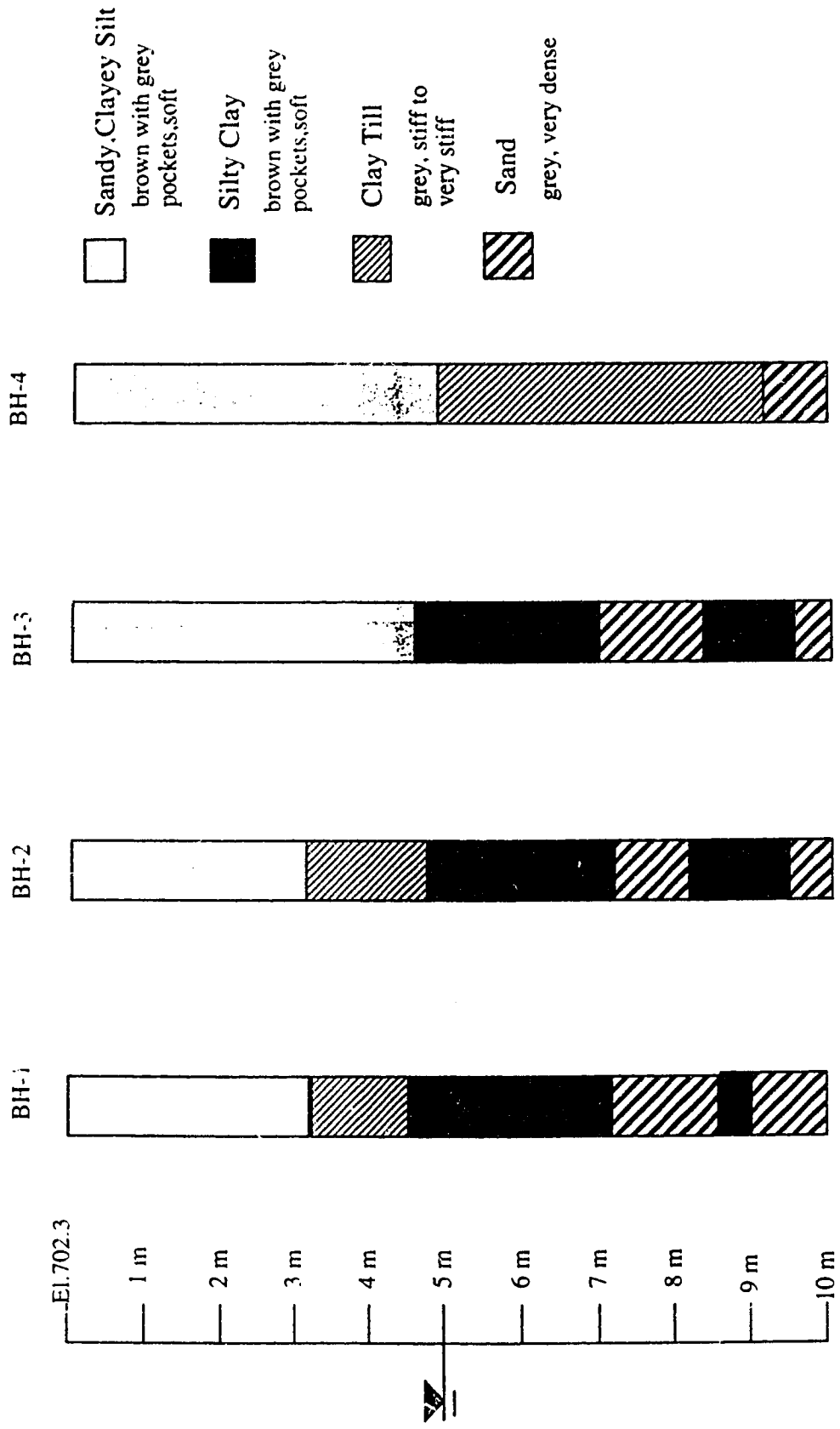


Figure A2. Soil Profile of Fill Foundation (modified from Hofmann, 1989)

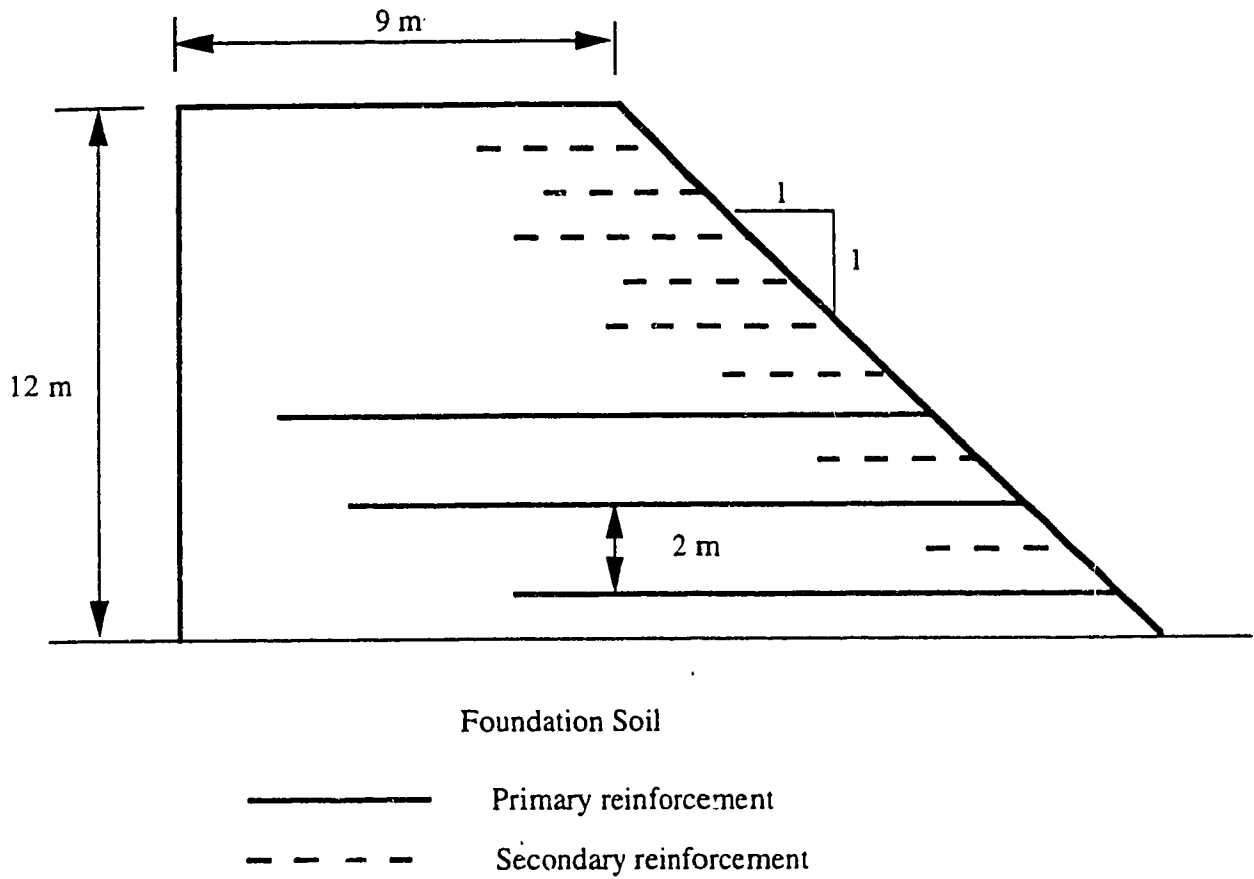


Figure A3. Cross Section and Reinforcement Layout of Reinforced Slope

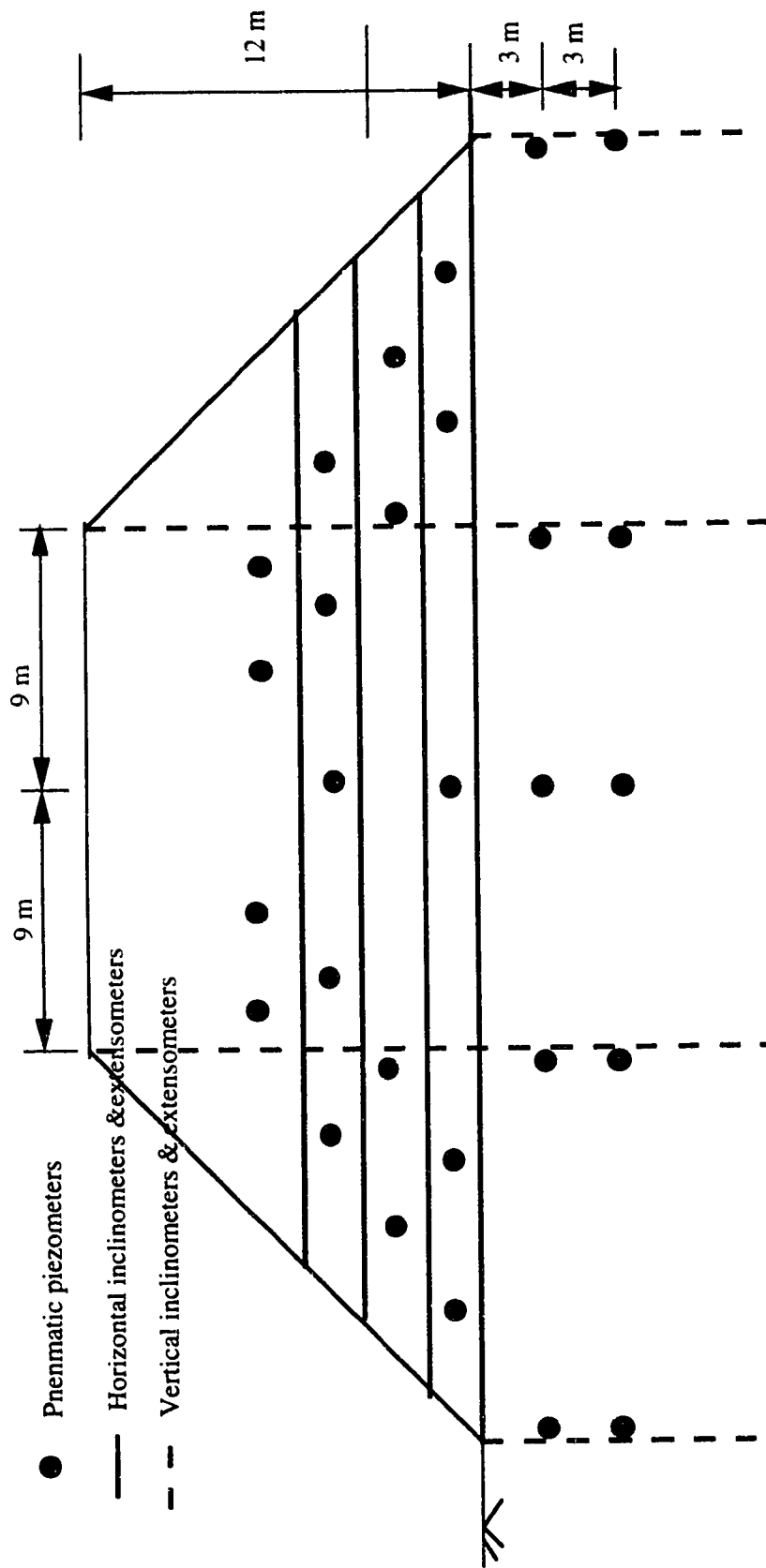


Figure A4. Layout of Soil Instrumentations in Test Fill

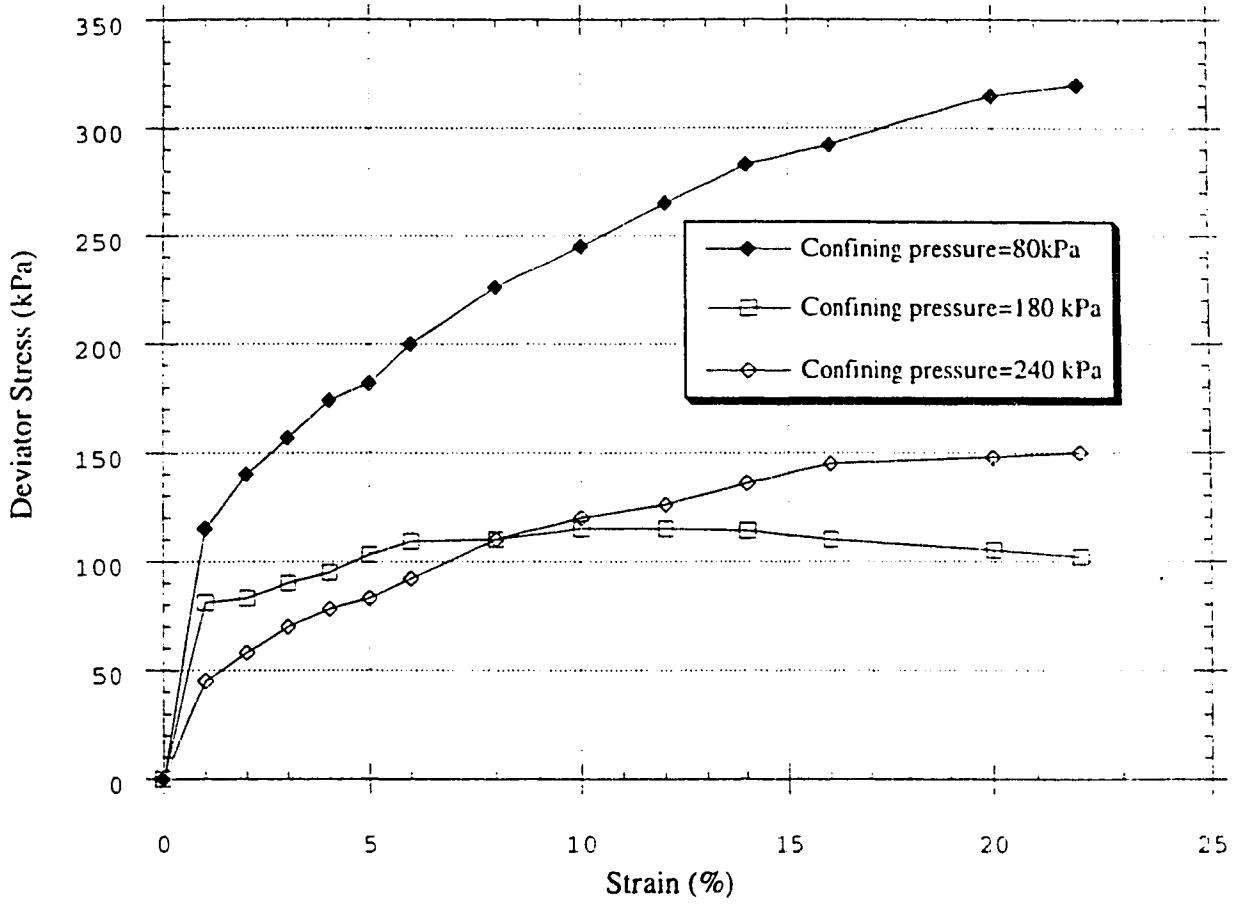


Figure A.5. UU Triaxial Tests on Fill Soil (modified from Hofmann, 1989)

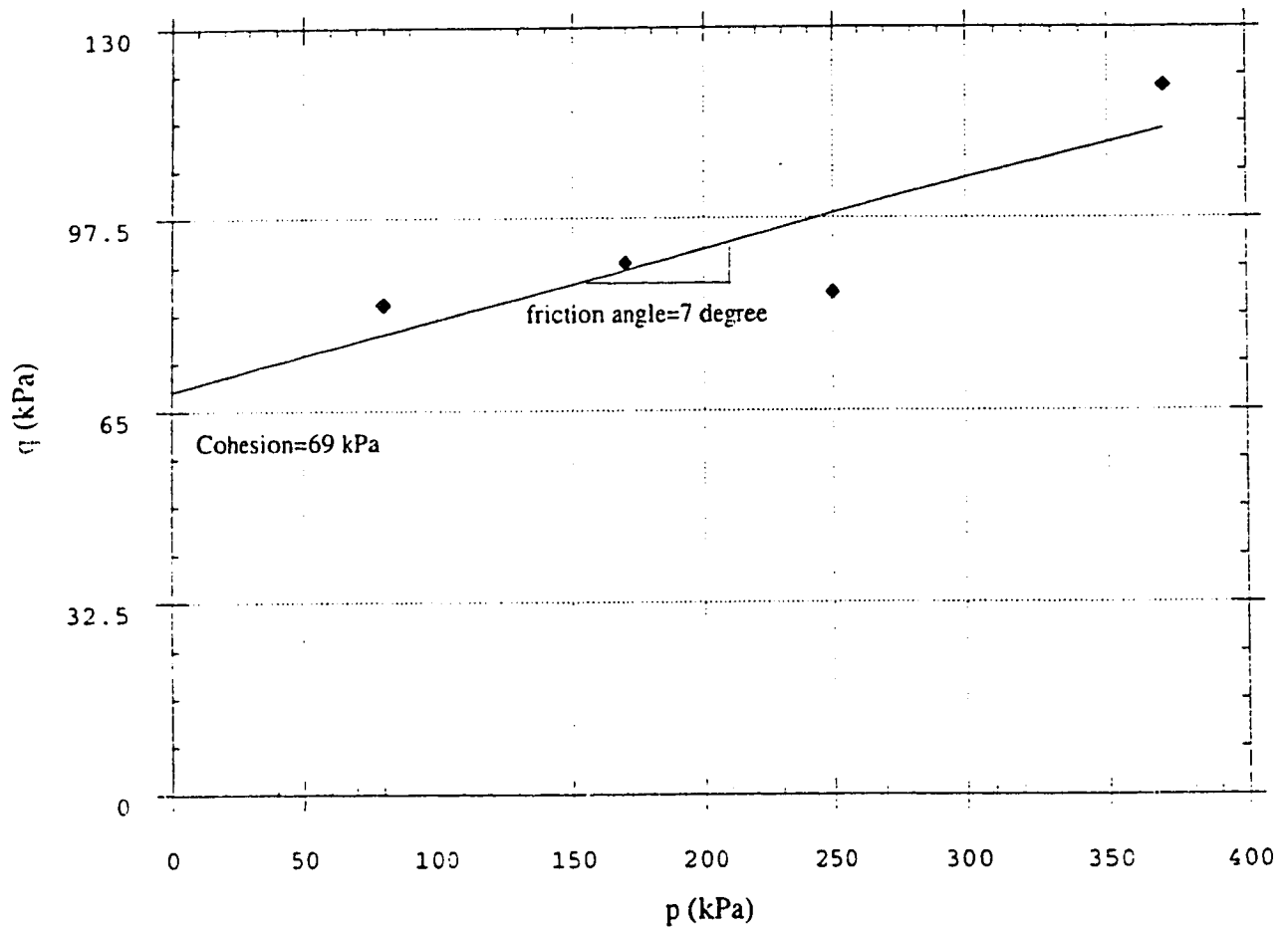


Figure A6. Total Stress p-q Plot for Fill Soil from UU Triaxial Tests
(modified from Hofmann, 1989)

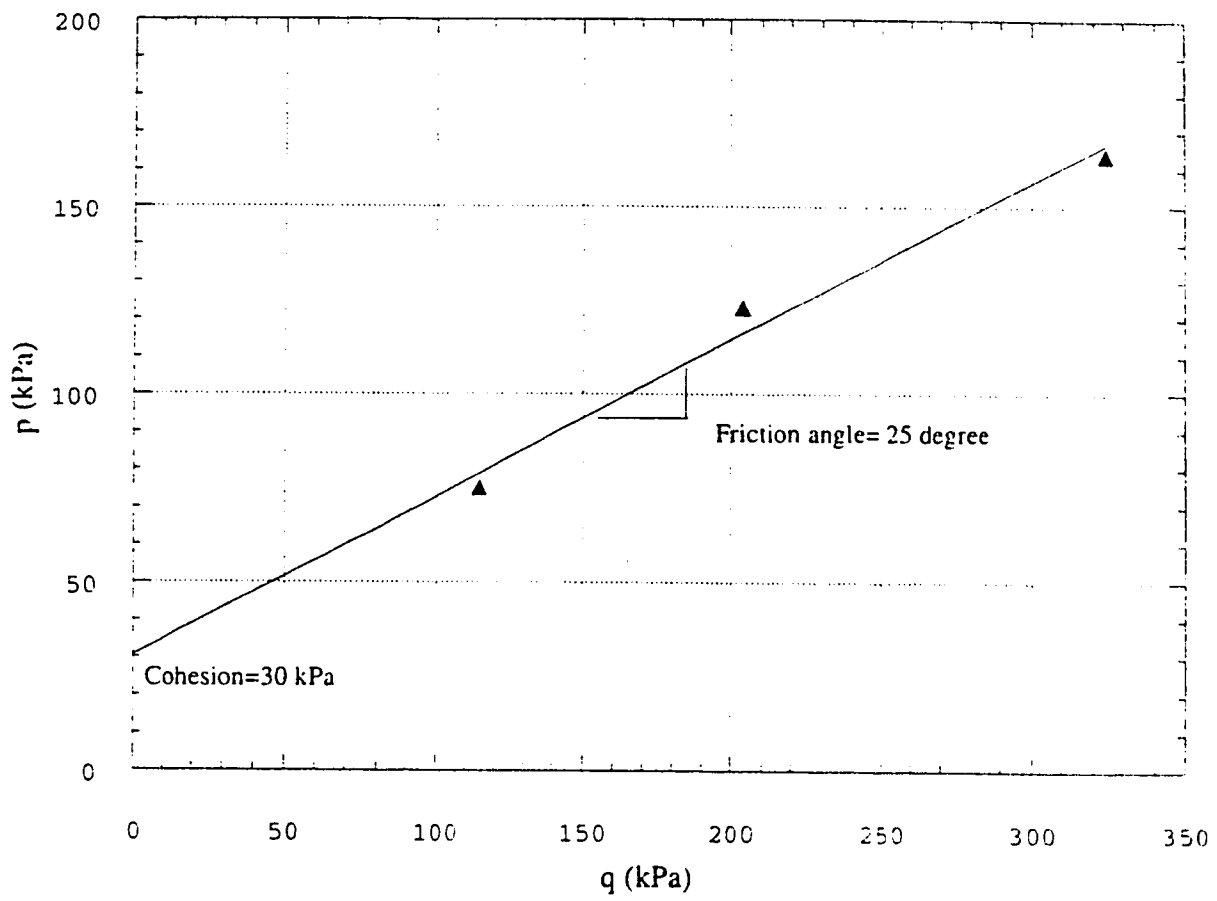


Figure A7. Effective Stress p - q Plot for Fill Soil (modified from Hofmann, 1989)

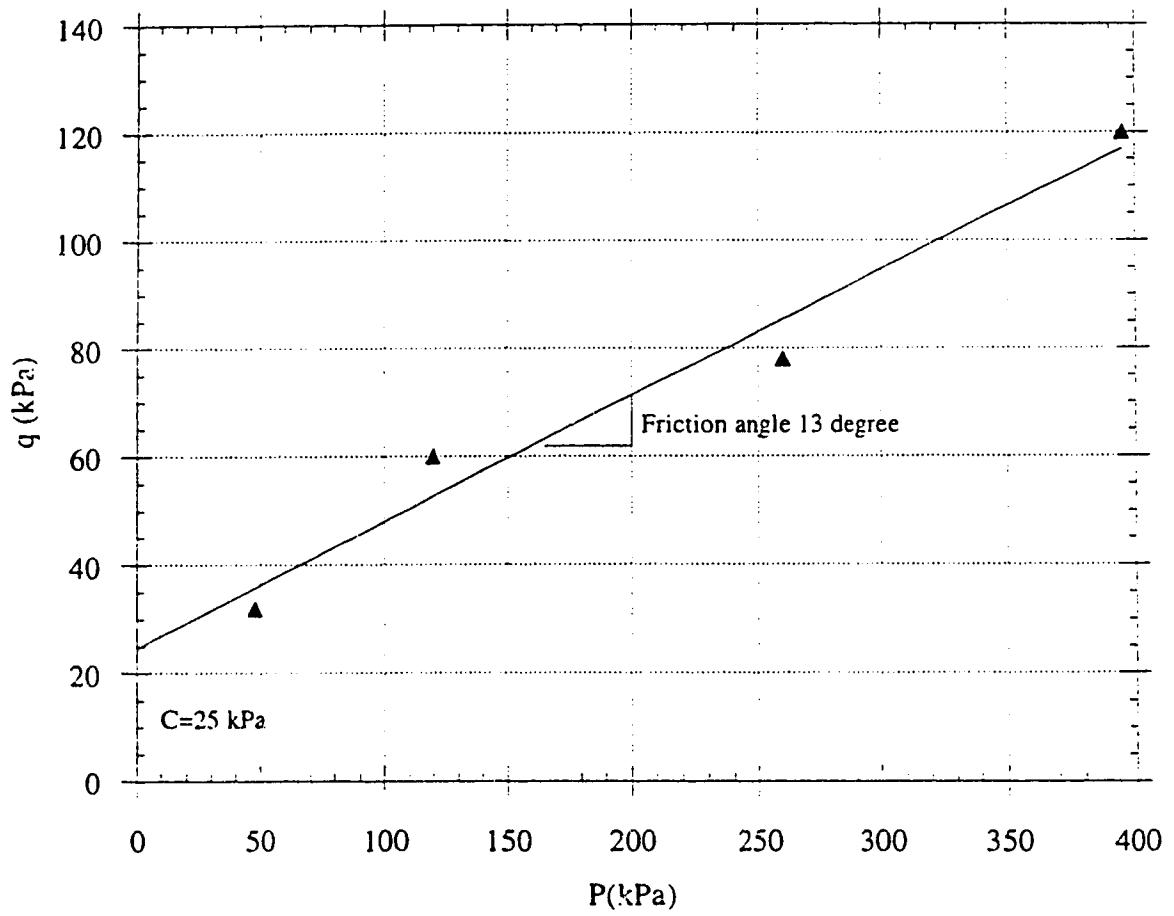


Figure A 8 . Total Stress p-q Plot for Foundation Soil
(modified from Hofmann, 1989)

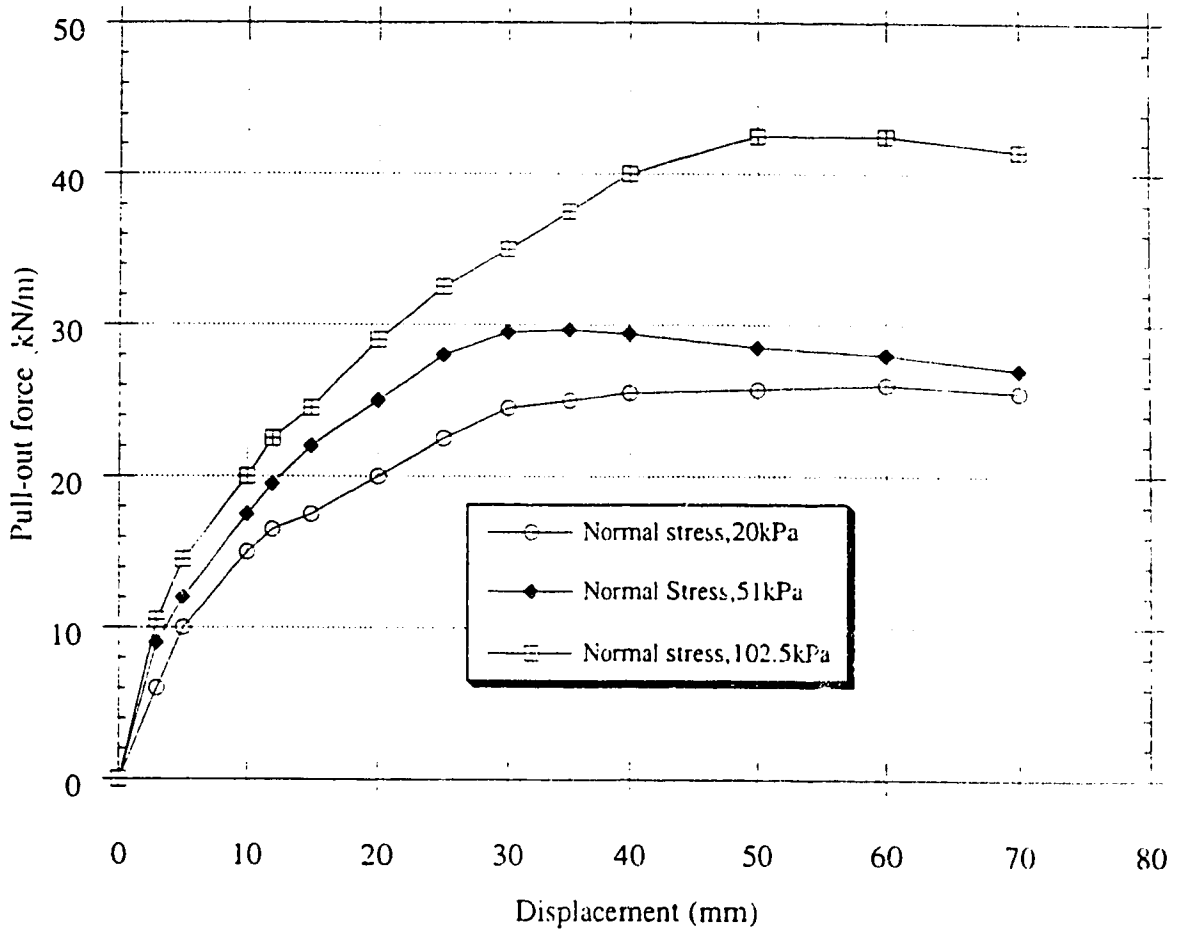


Figure A9 . Pull-out Tests for Tensar SR-2 geogrid (after Costalonga, 1988)

APPENDIX B: Finite Element Analysis of the Devon Test Fill

Additional analysis results of the Devon test fill are illustrated on the following figures.

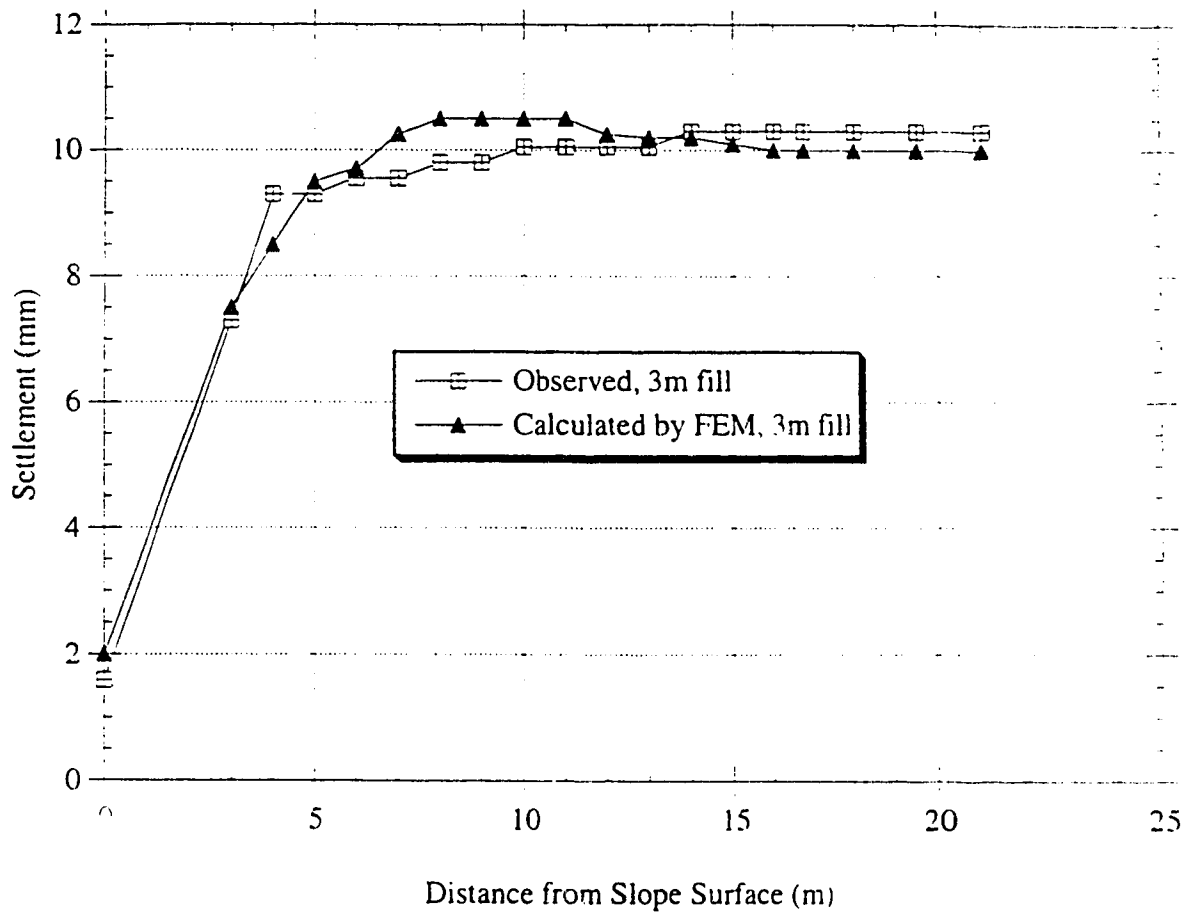


Figure B1. Settlement at Ground Level in Unreinforced Section at 3m Fill

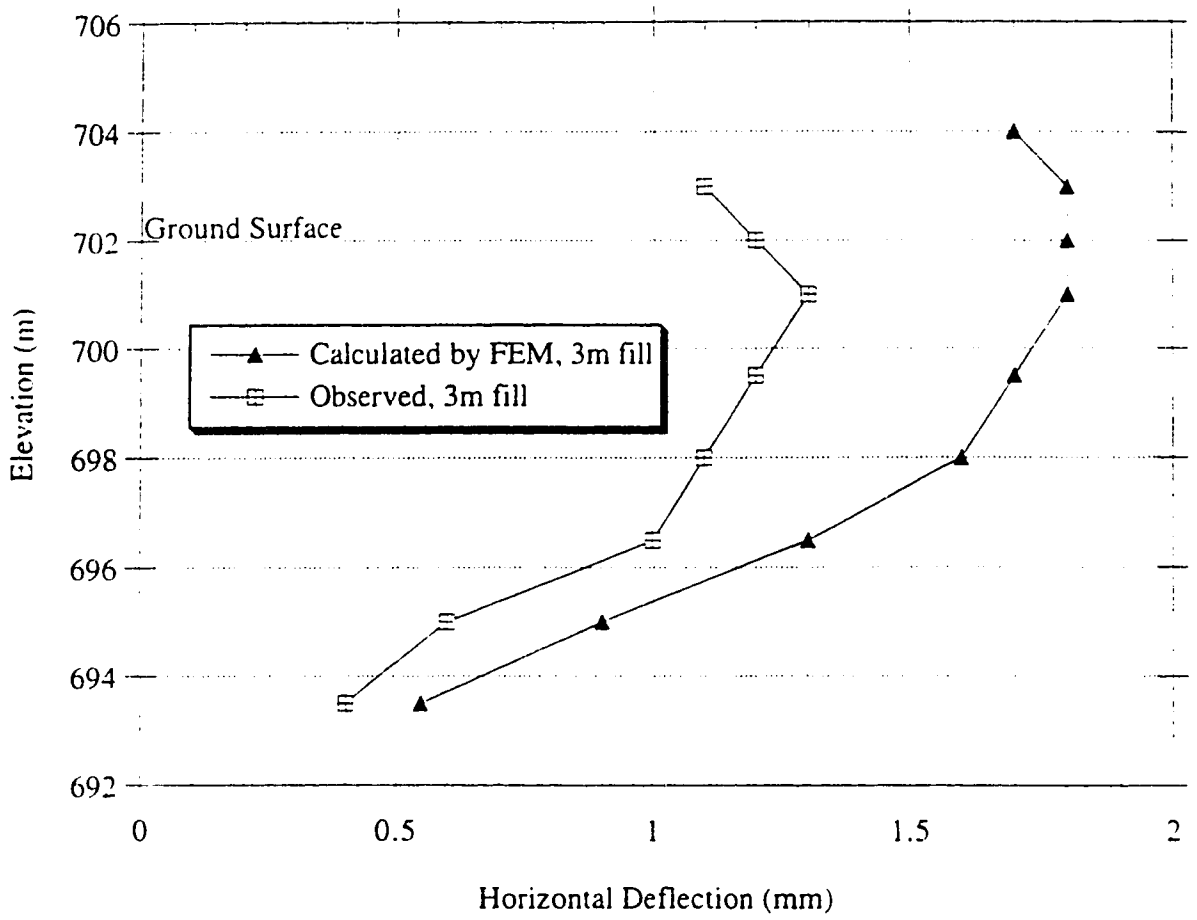


Figure B2. Horizontal Deflection of Soil beneath Crest of Slope in Unreinforced Section at 3m Fill

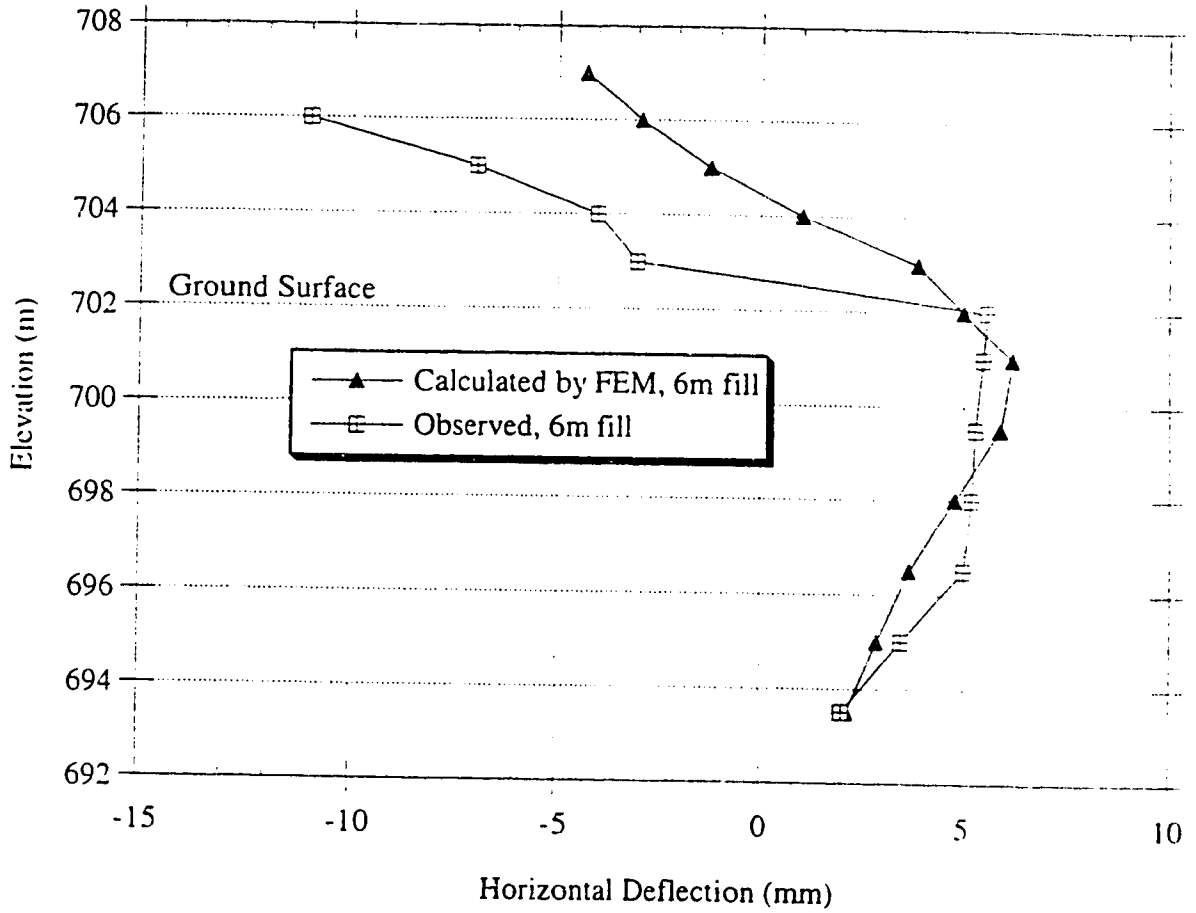


Figure B3. Horizontal Deflection of Soils beneath Crest of Slope in Unreinforced Section at 6m Fill

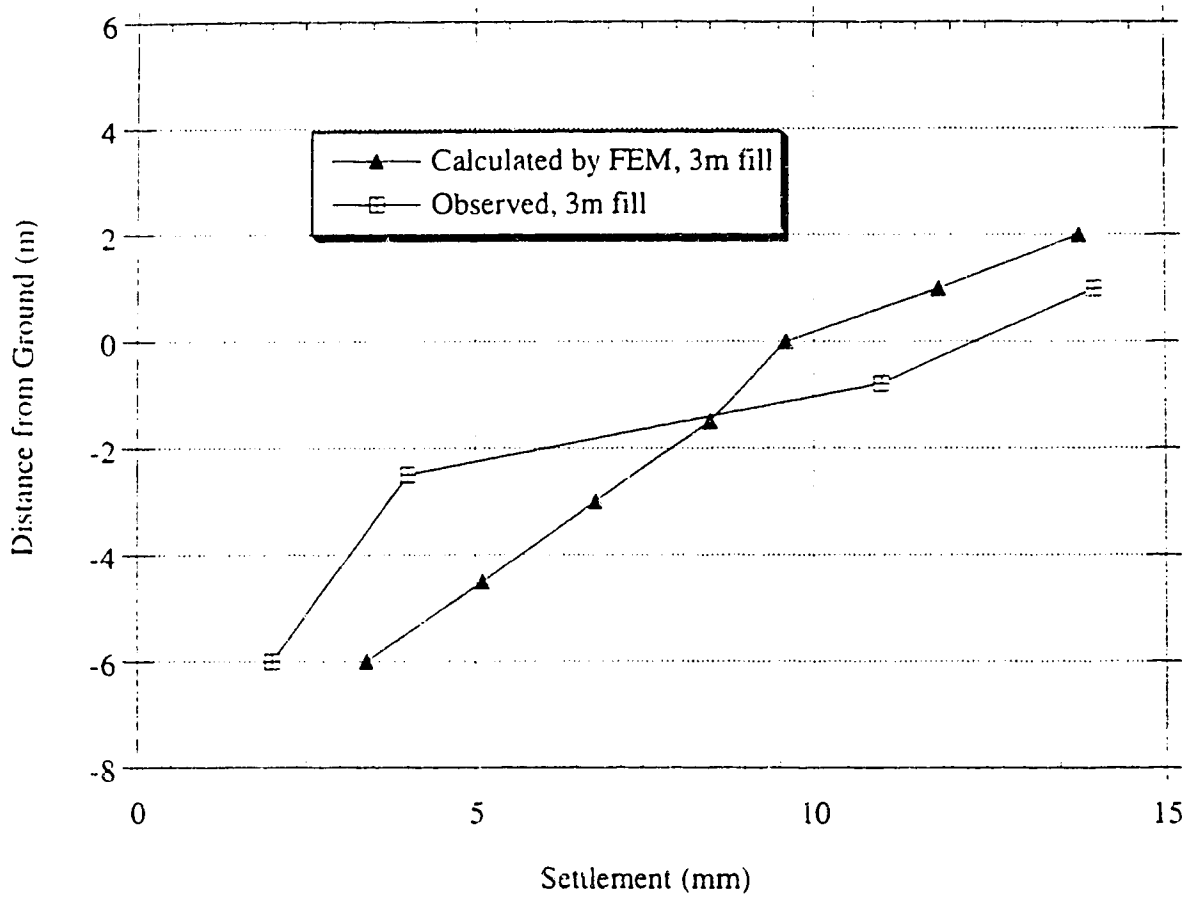


Figure B4. Settlement beneath Crest of Slope in Unreinforced Section at 3m Fill

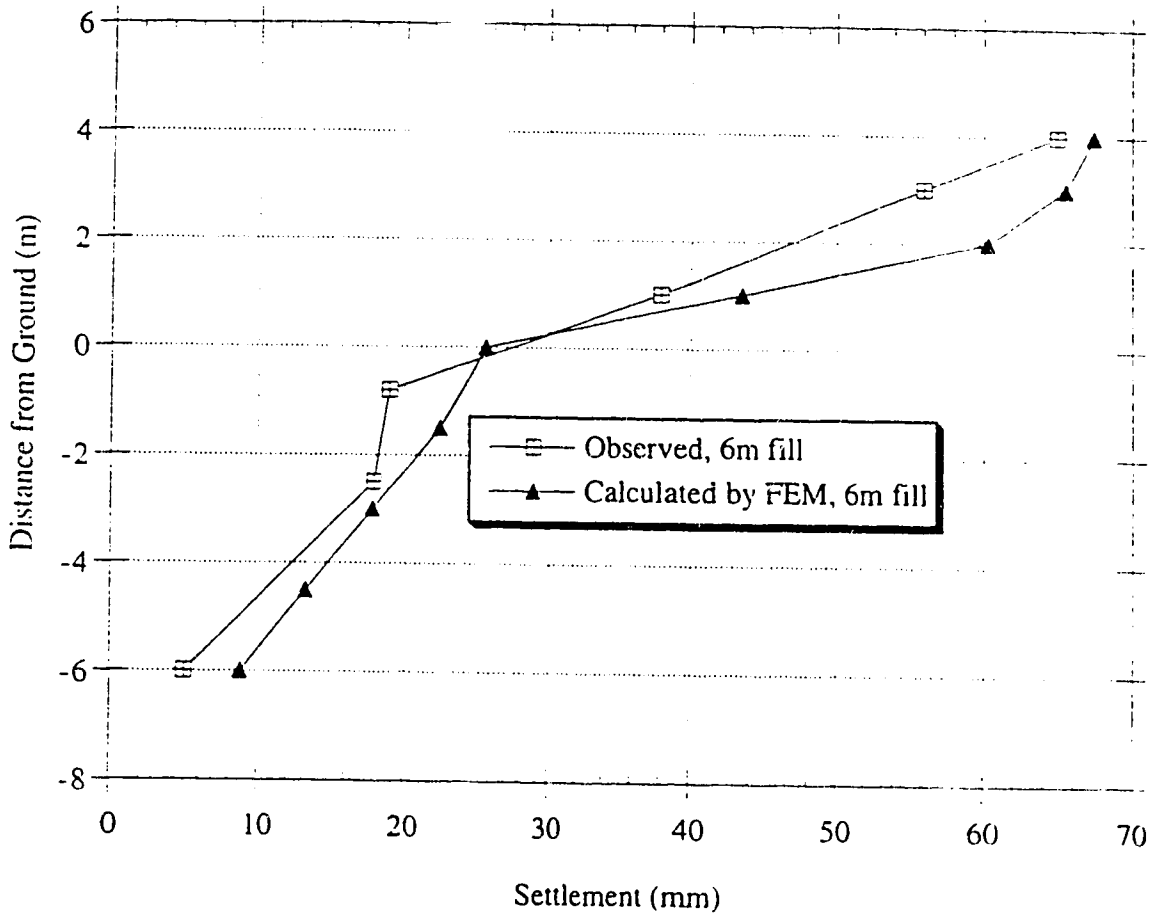


Figure B5. Settlement beneath Crest of Slope in Unreinforced Section at 6m Fill

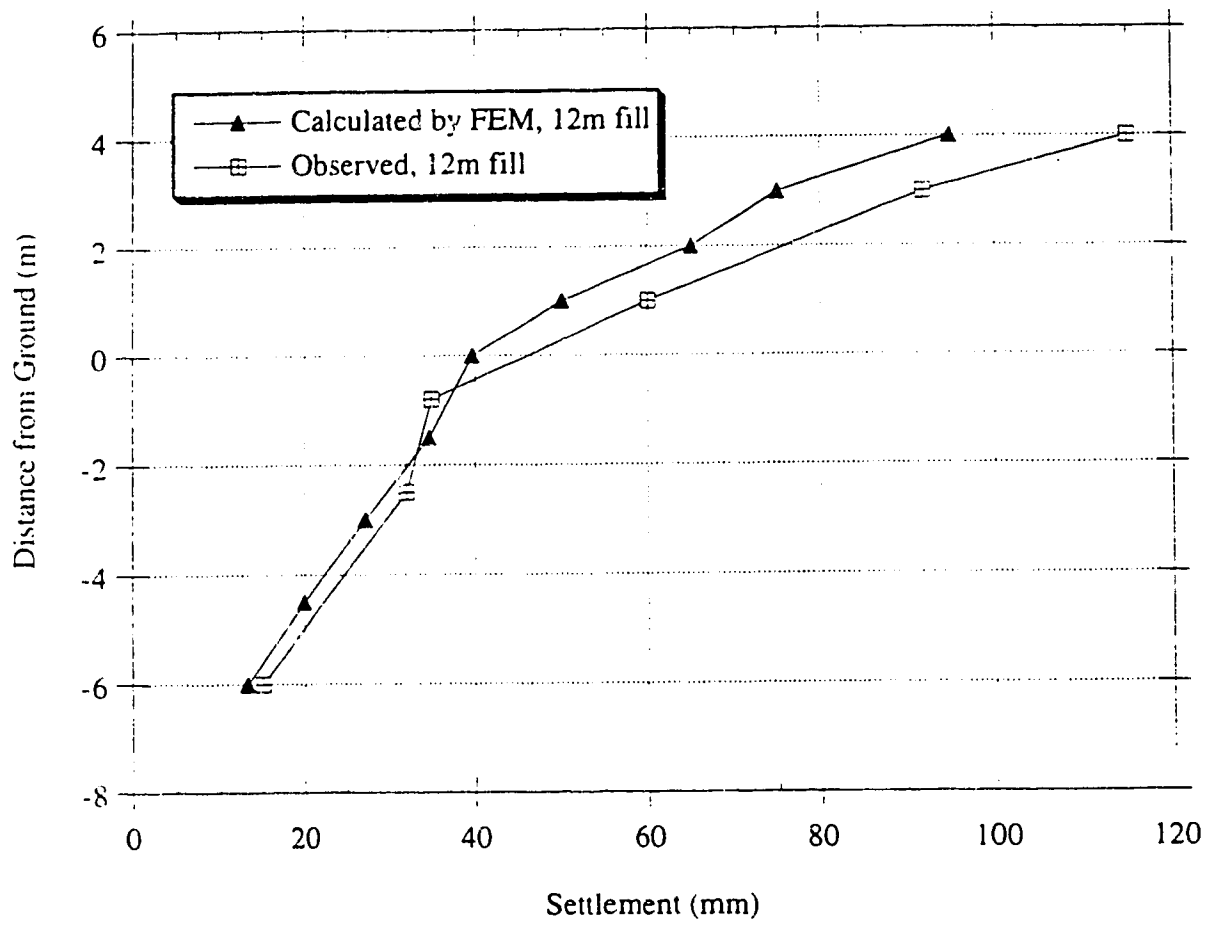


Figure B6. Settlement beneath Crest of Slope in Unreinforced Section at 12 m Fill

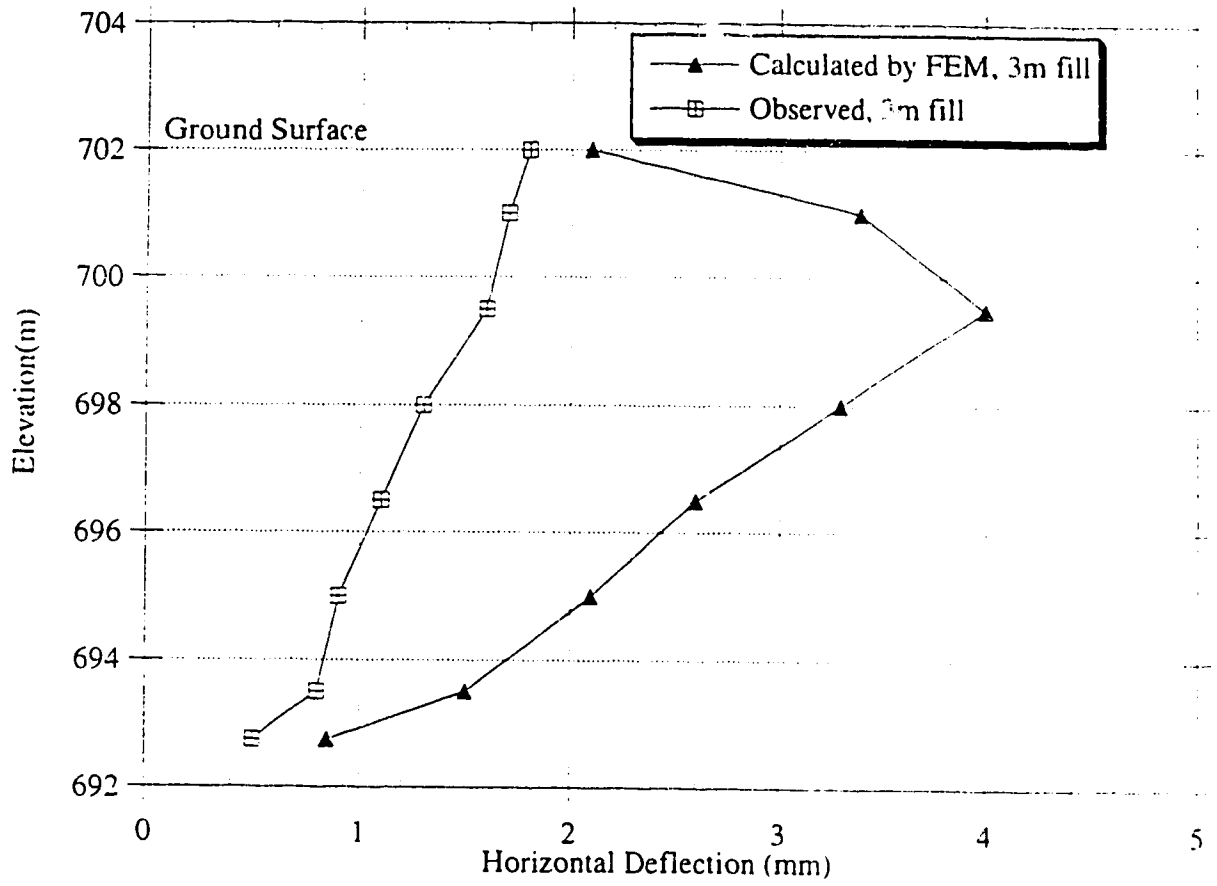


Figure B7. Horizontal Deflection of Soils beneath Toe in Tensar Section at 3m Fill

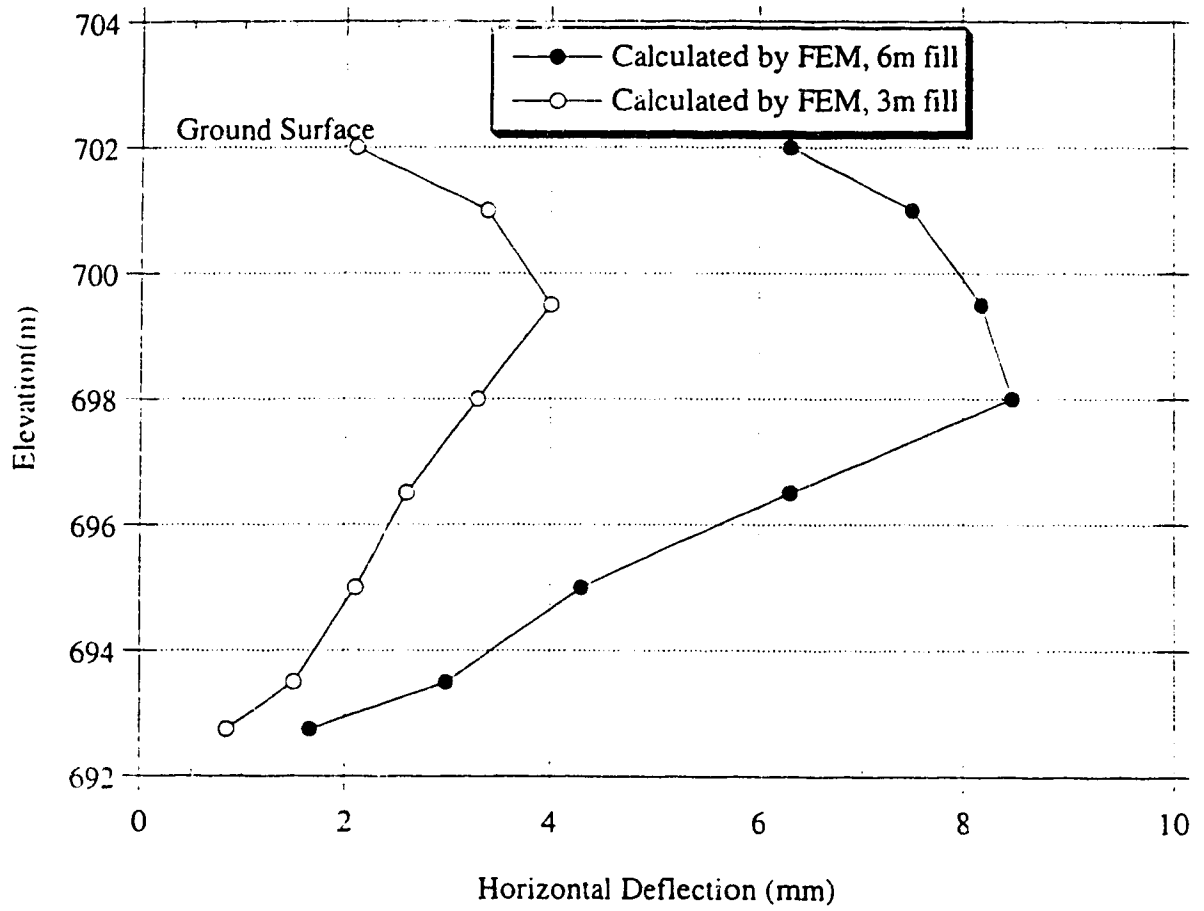


Figure B8. Calculated Horizontal Deflection of Soil beneath Toe of Slope in Tensar Section

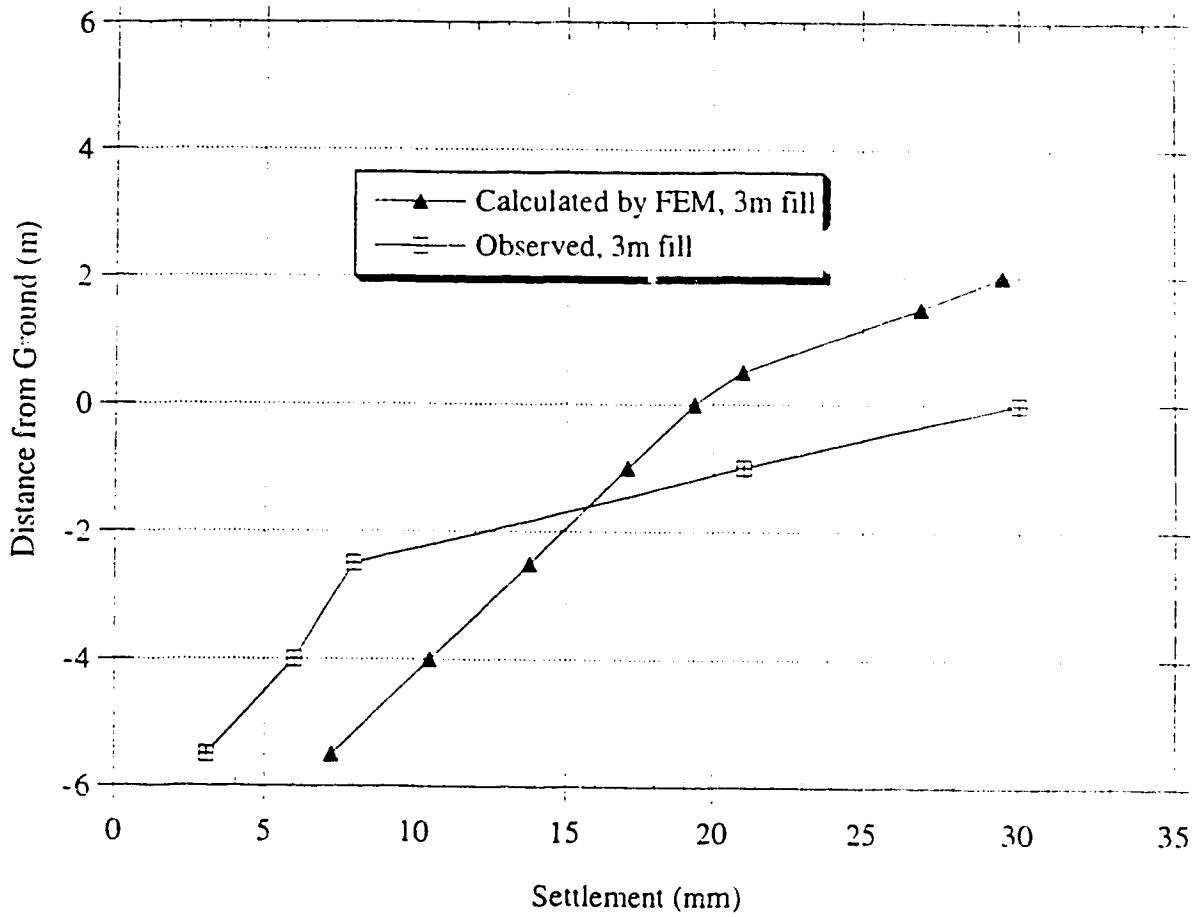


Figure B9. Settlement beneath Crest of Slope in Tensar Section at 3m Fill

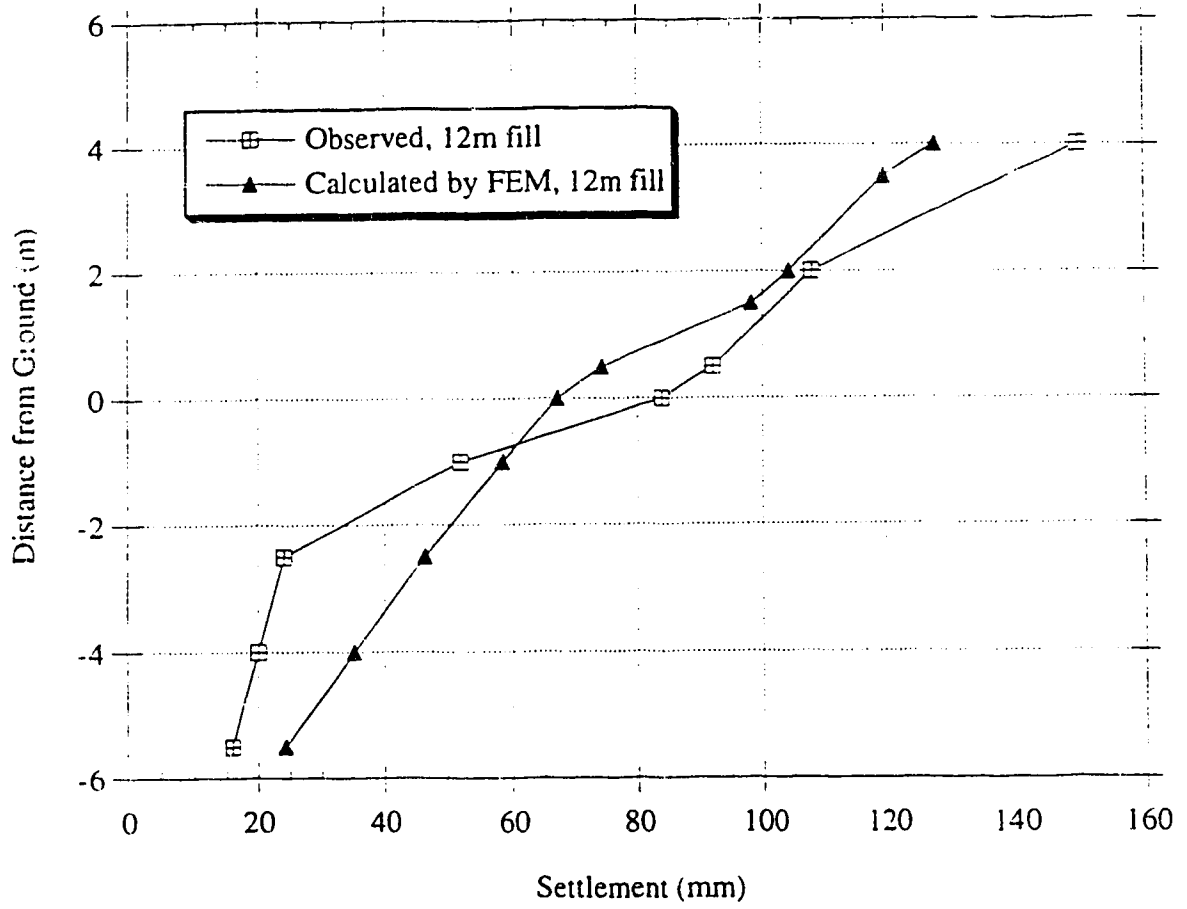


Figure B10. Settlement beneath Crest of Slope in Tensar Section at 12 m Fill

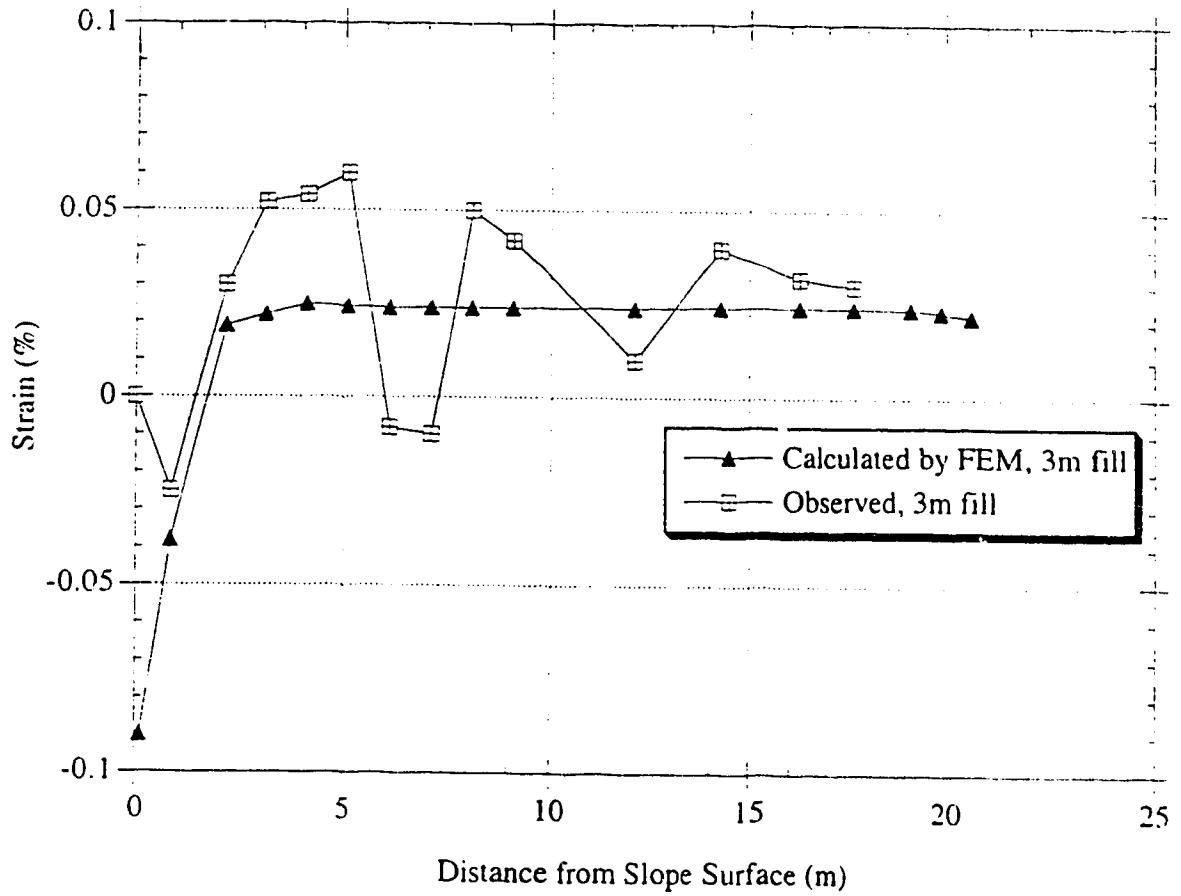


Figure B11. Distribution of Horizontal Soil Strain at Ground Level in Unreinforced Section at 3m Fill

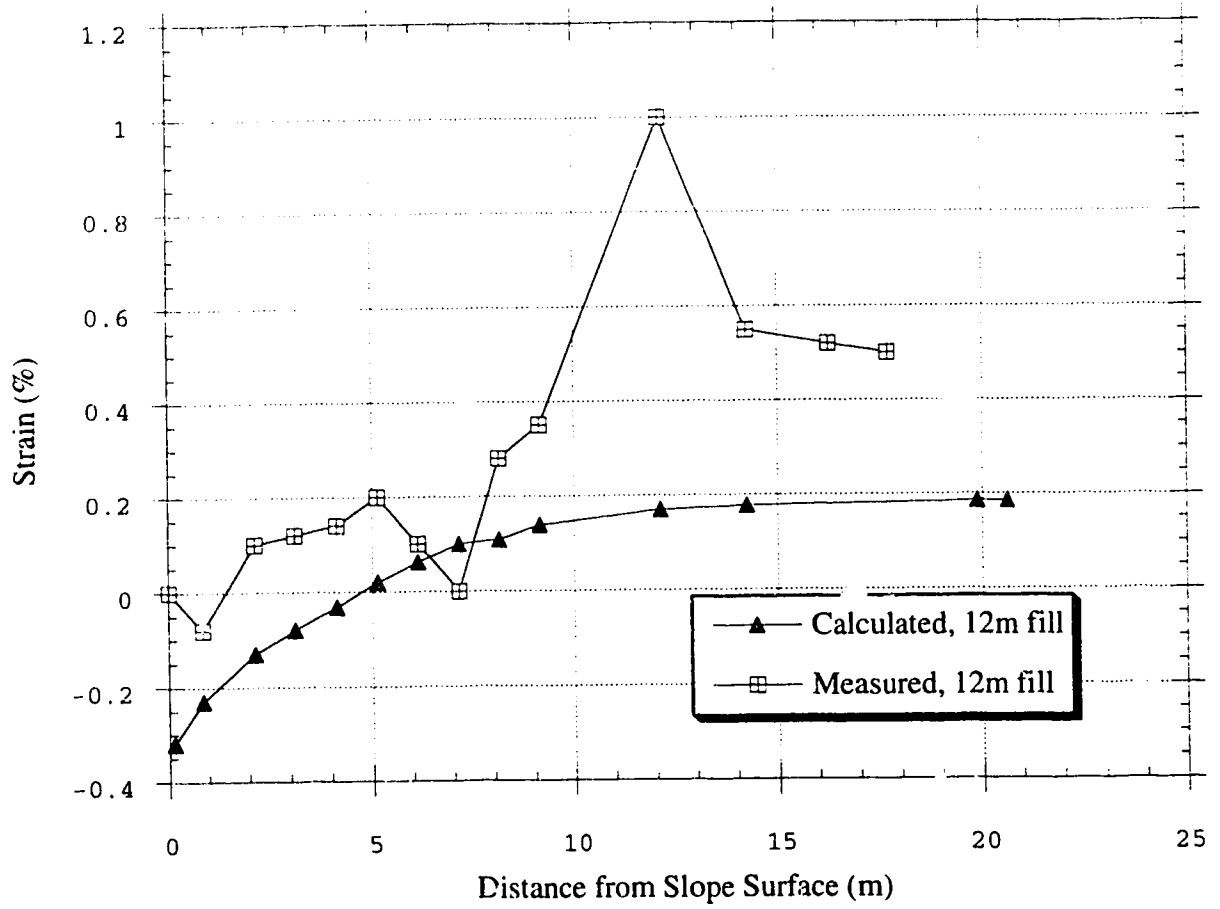


Figure B12. Distribution of Horizontal Soil Strain at Ground Level in Unreinforced Section at 12 m Fill

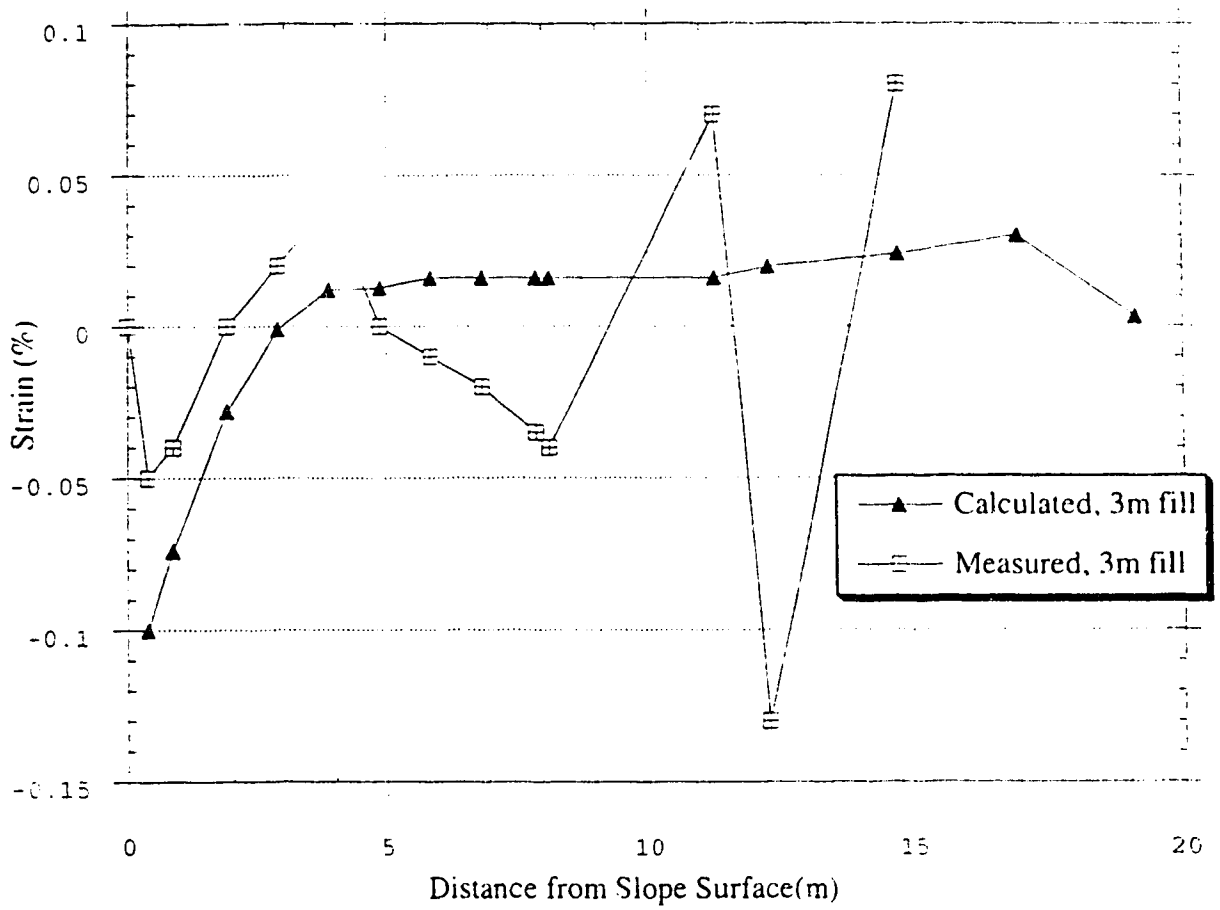


Figure B13. Distribution of Horizontal Soil Strain at Ground Level in Tensar Section at 3 m Fill

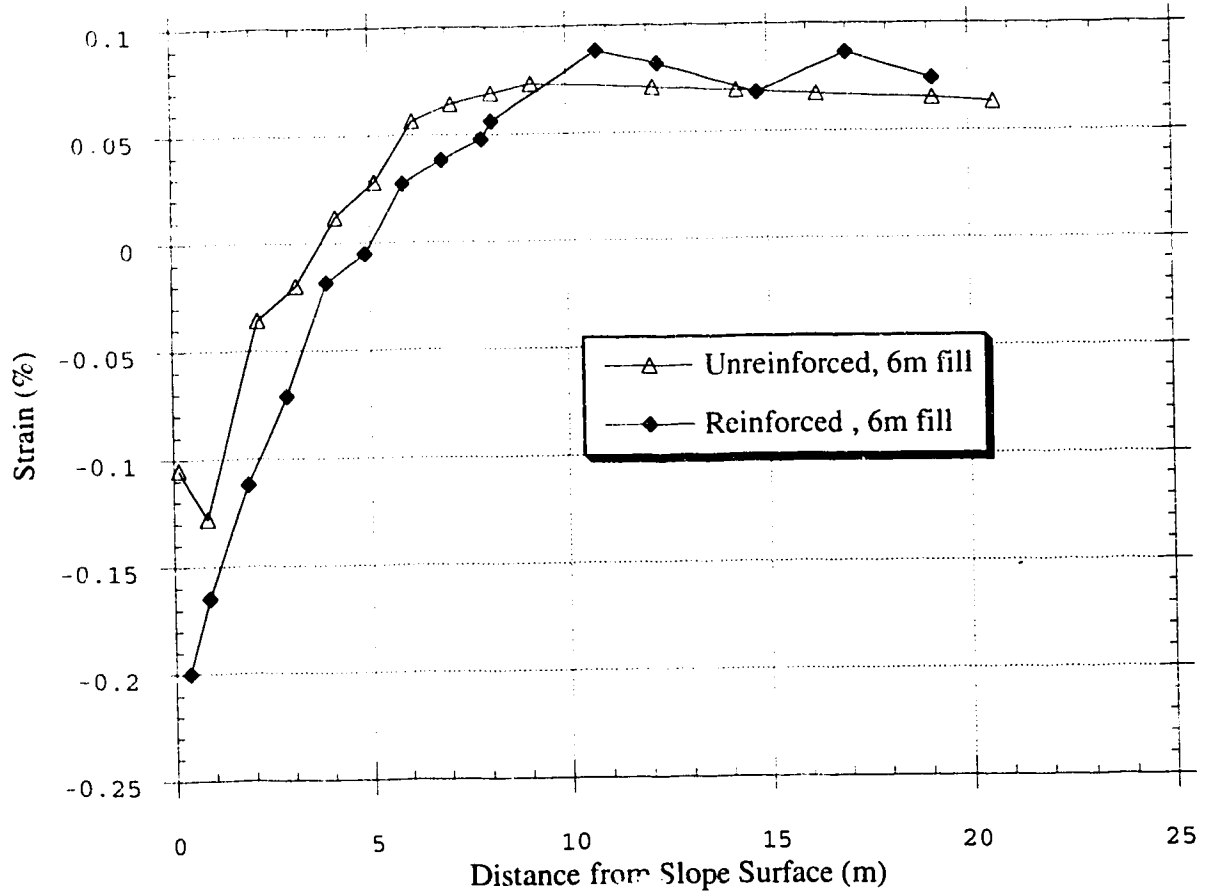


Figure B14. Comparison of Calculated Horizontal Soil Strain at Ground Level between Tensar and Unreinforced Section

